NOTE TO USERS

Page(s) not included in the original manuscript and are unavailable from the author or university. The manuscript was scanned as received.

218-236

This reproduction is the best copy available.

UMI®

DISSERTATION

APPLICATION OF PHYSIOLOGICALLY BASED PHARMACOKINETIC/ PHARMACODYNAMIC (PBPK/PD) MODEL IN STUDYING THE CARCINOGENIC POTENTIAL OF HEXACHLOROBENZENE, PCB 126, AND THEIR MIXTURE

Submitted by

Yasong Lu

Department of Environmental and Radiological Health Sciences

In partial fulfillment of the requirements

For the Degree of Doctor of Philosophy

Colorado State University

Fort Collins, Colorado

Fall 2006

COLORADO STATE UNIVERSITY

October 26, 2006

WE HEREBY RECOMMEND THAT THE DISSERTATION PREPARED UNDER OUR SUPERVISION BY YASONG LU ENTITLED APPLICATION OF PHYSIOLOGICALLY BASED PHARMACOKINETIC/PHARMACODYNAMIC (PBPK/PD) MODEL IN STUDYING THE CARCINOGENIC POTENTIAL OF HEXACHLOROBENZENE, PCB 126, AND THEIR MIXTURE BE ACCEPTED AS FULFILLING IN PART REQUIREMENTS FOR THE DEGREE OF DOCTOR OF PHILOSOPHY.

Committee on Graduate Work

Stephen A. Benjamin, Ph.D.

Rory B. Conolly, Sc.D.

Kenneth F. Reardon, Ph.D.

Brad Reisfeld, Ph.D.

Adviser Raymond S.H. Yang, Ph.D.

Department Head John D. Zimbrick, Ph.D.

ABSTRACT OF DISSERTATION

APPLICATION OF PHYSIOLOGICALLY BASED PHARMACOKINETIC/PHARMACODYNAMIC (PBPK/PD) MODEL IN STUDYING THE CARCINOGENIC POTENTIAL OF HEXACHLOROBENZENE, PCB 126, AND THEIR MIXTURE

This dissertation research studied the carcinogenic potential of hexachlorobenzene (HCB), 3,3',4,4',5-pentachlorobiphenyl (PCB 126), and their mixture (HCB+PCB 126) based on the integration of experimental bioassay and physiologically based modeling. It included collecting pharmacokinetic and preneoplastic foci (glutathione S-transferase placental-form, GST-P) data of the individual chemicals and the mixture in the context of an established medium-term liver foci bioassay, and then developing PBPK and clonal growth models based on the data generated. The foci bioassay involved a series of treatments, including a single injection of an initiating agent, a two-thirds partial hepatectomy, and daily oral gavage of a chemical solution in male Fischer 344 rats. The animals were sacrificed at five time points for time-course data. All bioassays were conducted at two doses: HCB 8.55 and 28.5 mg/kg, PCB 126 3.3 and 9.8 μg/kg, and HCB+PCB 126 8.55 mg/kg + 3.3 μg/kg and 28.5 mg/kg + 9.8 μg/kg.

HCB was mainly distributed in the fat, followed by the liver and other tissues, in accordance with its lipophilicity. When HCB was co-administrated with PCB 126, its disposition was remarkably affected in two aspects. First, the amount of HCB accumulated in the body was reduced before partial hepatectomy and dramatically increased afterwards. The reason, we believe, is attributed to the alterations in HCB

absorption and exsorption processes by PCB 126. Second, the partitioning of HCB into the fat, liver, and muscle was altered by PCB 126, which can be resulted from the severe fat mobilization under the conditions of partial hepatectomy and the treatment of HCB+PCB 126. A PBPK model was developed for HCB. This model included two special features: division of the blood compartment into plasma and erythrocytes due to the binding of HCB to erythrocytes, and the exsorption process (*i.e.*, the plasma-to-gut lumen passive diffusion – a reversal of the absorption process).

HCB, PCB 126, and their mixture displayed their carcinogenic potential in the liver foci bioassays by increasing the foci number and/or foci size. The comparisons of the foci data from the three bioassays suggested that there appeared to be a greater-than-additivity interaction at the low doses and a less-than-additivity interaction at the high doses between HCB and PCB 126 in terms of the size and number of foci at the last time point (day 56).

A clonal growth model was developed for simulating the foci data from the HCB+PCB 126 bioassay, and then modified to simulate the foci data for the individual chemicals, HCB and PCB 126. The concept of negative selection and two-cell (types A and B; the latter with growth advantage) hypothesis were incorporated in the model. Furthermore, we explored the size-dependent growth kinetics of the initiated cells by grouping the foci into four categories according to their size. Each category was assumed to have distinct growth kinetics. The model was parameterized with the information from the literature as well as from our own study. The simulations were in good agreement with three pieces of data: relative foci volume, foci number/cm^3 of liver, and size distribution, which were derived from the bioassays. The interaction between HCB and

PCB 126 was also examined by comparing the growth kinetic parameters of type B initiated cells/foci under HCB, PCB 126, and the mixture treatment. At the low doses, a greater-than-additivity interaction occurred in promoting mini- (2-11 cells) and medium-foci (12-399 cells), and at the high doses, a less-than-additivity interaction took place in promoting large-foci (>399 cells).

This research improved our understanding in the pharmacokinetics and the pharmacodynamics regarding carcinogenic potential of HCB, PCB 126, and their mixture in the context of a medium-term liver foci bioassay. Continuing on the earlier contribution in PBPK and clonal growth modeling from our laboratory, the present work added the unique perspectives of considering the pharmacokinetics and pharmacodynamics of a chemical mixture, as well as the refinement of clonal growth modeling by categorizing liver GST-P foci into different classes. Once again, we were able to illustrate how the biologically based computational modeling facilitated our study on chemical carcinogenesis.

Yasong Lu

Department of Environmental and Radiological Health Sciences

Colorado State University

Fort Collins, CO 80523

Fall 2006

ACKNOWLEDGEMENTS

During my pursuit of the Ph.D. degree, I am indebted to many persons. I have been benefiting from the valuable scientific advice, ranging from animal study and data interpretation to modeling techniques, from my Committee, Drs. Raymond S.H. Yang, Brad Reisfeld, Stephen A. Benjamin, Rory B. Conolly, and Kenneth F. Reardon, and the former committee member Dr. Julie Campain. Dr. Reisfeld kindly serves in my Committee in the place of Dr. Campain when she left Colorado State University when I was half way through the training.

Special thank you to my adviser Dr. Yang. He offered me the great opportunity of being a member of his Quantitative and Computational Toxicology Group, where I have been enjoying the study of PBPK/PD modeling as well as other techniques. Dr. Yang's scientific and financial support makes my pursuit possible. His advice, kindness, and encouragement shall always be on my mind.

I highly appreciate the help from and the friendship with my fellow graduate students, Mr. and Mrs. Manupat and Ornrat Lohitnavy (Noon and Som). When I had trouble in oral communication in English during the early days, they helped me understand and abide by the Departmental and Graduate School requirements. They are the major contributors to all of my animal studies; we had spent numerous hours side by side in the necropsy room at the former CETT building and in the surgery room at the Painter Center. As experienced users of gas chromatography, they helped me overcome the frustrations that I suffered when I was new to this technique.

I was mentored by Dr. Micaela B. Reddy in PBPK and clonal growth modeling. Dr. Reddy nicely and patiently introduced me the skills of PBPK model coding,

troubleshooting, and the simulation software Berkeley Madonna. She took hours and hours to walk me through the lengthy code of the clonal growth model for hexachlorobenzene written by Dr. Ying C. Ou. In addition, I learned a lot from her in writing when we were repetitively revising the chapter I prepared on reviewing the dioxin PBPK models.

Many thanks to Dr. Arthur Mayeno, who for a long time has been a friend, a travel supporter, an academic consultant, an English polisher, and an all-purpose helper. I am particularly grateful to his help with my preliminary exam.

I appreciate my wife, Dongmei Xu, for her love and continuous support. She gave up her "modern city life" in Shanghai and came to stay with me at this "remote" small town, she marked up tubes for me for tissue collection, she kept me accompanied at late night in the lab... I also appreciate my parents and the other family members for their firm support and encouragement throughout the years.

Many more individuals have contributed to my dissertation research from various aspects. A comprehensive list may not be possible. Here I try to recall as many as I can:

Those who participated in animal studies: Ms. Amanda Ashley, Ms. Christine Battaglia, Ms. Laura Chubb, Dr. Charles Dean, Ms. Elizabeth Eickman, Ms. Lisa Gerjevic, Ms. Corrie Lane, Dr. Sun Ku Lee, Dr. Ken Liao, Ms. Tracy Nichols, Dr. Todd Painter, Dr. Damon Perez, Dr. Micaela Reddy, Ms. Caroline Yang, Dr. Ying Zhang, and Laboratory Animal Research personnel (Ms. Sheryl Carter, Ms. Elisa French, Ms. Kim Olson, *et al.*) at the Painter Center at Colorado State University;

Those who assisted statistical analysis: Dr. Thomas J. Keefe, Mr. Yingchang Lu, Mr. Xiaohui Xu;

Those who provided support in modeling: Dr. Melvin E. Andersen, Mr. Harvey Clewell, Dr. Rory Conolly, Dr. James Dennison, Dr. Ying C. Ou;

Stereology program provider: Dr. Yihua Xu;

Magnetic resonance image supporter: Dr. Susan Kraft;

All-purpose helper: Ms. Linda Monum.

This research is supported by the NIOSH/CDC grant 1 RO1 OH07556 and NIEHS Training Grant 1 T32 ES 07321.

DEDICATION

To my wife and parents.

TABLE OF CONTENTS

CHAPTER 1

Application of Biologically Based Computational Modeling in Chemical Carcinogenesis Research and Cancer Risk Assessment: A Literature Review

Yasong Lu

OUTLINE

1. Basics of chemical carcinogenesis[1]
   - *1.1. Stages in carcinogenesis*
   - *1.2. Modes of action of chemical carcinogenesis*
2. Methods of chemical carcinogenesis research
   - *2.1. Epidemiologic methods*
   - *2.2. Laboratory methods*
     - *2.2.1. In vivo study*
       - *2.2.1.1. Long-term bioassays*
       - *2.2.1.2. Alternative shorter-term animal bioassays*
     - *2.2.2. In vitro study*
   - *2.3. Theoretic methods*
3. Cancer risk assessment
4. PBPK modeling – describing internal dosimetry
   - *4.1. Basics of PBPK modeling*

---

[1] Although the terms *cancer/carcinogenesis* and *tumor/tumorigenesis* are distinct in pathology, they are not strictly differentiated and are used interchangeably in this dissertation.

1. Basics of chemical carcinogenesis

Cancer has been widely recognized as a disease resulting from environmental or genetic factors, or the interactions of both. In modern society, environmental factors, including lifestyle (e.g., tobacco, alcohol, diet) (Doll and Peto 1981; Kolonel *et al.* 2004) and chemical pollutants (Howard and Newby 2004; Novogradec and Ali 2004), substantially contribute to the cancer incidence in humans. The observation of carcinogenesis associated with chemical exposure has a long history (Pitot and Dragan 2001a). In 1775, Sir Percivall Pott, an English physician and surgeon, first established a causal relationship between exposure to soot and occurrence of cancer at the scrotal skin in the patients who were chimney sweeps (Pitot and Dragan 2001b). The experimental

study of chemical carcinogenesis began in 1915 when two Japanese pathologists, Katsusaburo Yamagiwa and Koichi Ichikawa, successfully produced malignant epithelial tumors by applying coal tar to the ears of rabbits (Pitot and Dragan 2001b). A brief history of the understanding in chemical carcinogenesis, including the timeline of the critical experimental achievements in the 20th century, has been summarized recently (Luch 2005).

With the expansion of human activities and advances in technologies, many chemicals have been introduced, either intentionally or non-intentionally, into the environment. As such, humans are extensively exposed to chemicals although the exposures are variable in relation to occupations or living conditions. Elevated incidences or relative risks of cancers in humans have been observed attributable to exposure to chemicals; some examples are beryllium (Sanderson *et al.* 2001), arsenic (Chen *et al.* 1992; Wu *et al.* 1989), benzene (Hayes *et al.* 2001; Rinsky *et al.* 1987), vinyl chloride (Bosetti *et al.* 2003), benzo(a)pyrene (BaP) (Sinha *et al.* 2005), and 2,3,7,8-tetrachlorodibenzo-*p*-dioxin (TCDD) (Johnson 1991; Steenland *et al.* 2001). Therefore, to protect human health, it is essential to study every aspect of chemical carcinogenesis and to characterize the cancer risk in humans induced by chemical exposure. Indeed, a great deal of research in this field is underway.

1.1. Stages in carcinogenesis

From the experimental work on mouse skin carcinogenesis in the 1940's, the researchers learned that carcinogenesis is a multi-step process. Armitage and Doll (1954; 2004a; 2004b) later supported this multi-step nature from mathematical modeling of the human cancer incidence data. Although the real number of stages and the molecular

changes in each stage are not completely understood, it is known that genetic alteration (usually known as mutation) and cell proliferation are the two critical events on the pathway toward cancer formation (Cohen and Ellwein 1990a, b, 1995a; Moolgavkar 1980; Moolgavkar 1978, 1988).

Today, a three-stage carcinogenesis model is well recognized; that is, carcinogenesis can be divided into at least three consecutive stages: initiation, promotion, and progression (Hasegawa and Ito 1994; Pitot 2001; Pitot and Dragan 2001b; Trosko *et al.* 2005). Initiation refers to the irreversible change in the genome in a cell. It may occur spontaneously due to DNA replication error(s) or attacks of reactive agents (e.g., reactive oxygen/nitrogen species, ROS/RNS), or be induced by exposure to exogenous chemicals that can interact, directly or after metabolic activation, with DNA. The initiated cells may be killed by apoptosis or escape from the monitoring mechanisms. The surviving initiated cells need to undergo one or more rounds of proliferation to fix the genetic change in the tissue. This process, designated as promotion, is reversible; withdrawal of a promotion stimulus slows down this process. The progression stage is characterized by karyotypic instability and the development of neoplasms. The genetic and phenotypic changes become increasingly severe; malignant characteristics, e.g., autonomous growth, invasiveness, metastasis, morphologic abnormality, may emerge.

Conventionally, chemical carcinogens are classified according to the stage where they exert their carcinogenic effects in the animal study settings (Pitot and Dragan 1991). Those that act in initiation are termed initiators; diethylnitrosamine (DEN) is a potent initiator used in some animal bioassays (Ito *et al.* 1988; Ito *et al.* 2003). The chemicals that act in promotion are called promoters. TCDD and 3,3',4,4',5-pentachlorobiphenyl

(PCB 126) are well-known promoters. Some chemicals may act in both initiation and promotion and are referred to as complete carcinogens. 2-Acetylaminofluorene (2-AAF) is a complete carcinogen in inducing urinary bladder cancer in mice (Cohen and Ellwein 1990b). Moolgavkar (1983) and Cohen and Ellwein (1990b) further clarified these definitions in a quantitative sense using biologically based carcinogenesis modeling.

1.2. Modes of action of chemical carcinogenesis

The modes of action of chemical carcinogenesis fall into two broad categories: genotoxic (DNA-reactive) and non-genotoxic (epigenetic) (Luch 2005; Weisburger and Williams 1981, 2000; Williams 2001). In the former, electrophilic chemical moieties or ROS/RNS induced by chemical treatment interact with DNA and hence alter the structure of DNA. Consequently, they may cause mutations, such as point mutation, frameshift mutation, strand break, DNA-protein cross-link, chromosomal aberration. The mutated cells may get growth advantages and develop into neoplastic lesions. It is noteworthy, however, that chemical-DNA interactions do not necessarily lead to mutagenesis (Pitot and Dragan 2001b) and mutagenesis does not always result in carcinogenesis (Sakai *et al.* 2002). Thus, the concepts of electrophilic chemical moieties, mutagens, and carcinogens should be distinguished (Cohen and Ellwein 1995a; Pitot and Dragan 2001b; Sakai *et al.* 2002).

The majority of genotoxic carcinogens, e.g., 2-AAF (Verna *et al.* 1996a), DEN (Lai and Arcos 1980; Verna *et al.* 1996b), BaP (Gelboin 1980; Luch 2005), aflatoxin B1 (McLean and Dutton 1995), need to be metabolically activated prior to the reaction with DNA. The cytochrome P450 (CYP450) family has been recognized as the most important enzymes for the activations (Eaton *et al.* 1995; Gonzalez and Kimura 2001; Lang and

Pelkonen 1999). The carcinogenic susceptibility of individuals is therefore somewhat dependent on their CYP450 activities.

The non-genotoxic modes of action involve the cellular responses to carcinogens independent of chemical reaction with DNA. This category includes the types discussed below. Note that this list is not meant to be comprehensive; rather, it only covers those modes of action suggested by or associated with the current carcinogenesis modeling considerations (see Section 5).

(1) *Cytotoxicity and compensatory cell proliferation*: Some chemicals may kill cells via cytotoxicity when the dose is sufficiently high and/or the microenvironment is appropriate. The cells surrounding the lesions are then signaled to proliferate to counterbalance the cell loss as a homeostatic mechanism. If the cytotoxic agent remains operative, the compensatory proliferation may be sustained. Moreover, during this process, genetic errors in DNA replication can take place and be fixed with a higher probability. Consequently, preneoplastic and neoplastic lesions may follow. Two well-understood examples of this mode of action are the urinary bladder cancer induced by sodium saccharin and the renal tumor induced by d-limonene in the male rat (Olin *et al.* 1995). In the long-term animal carcinogenesis bioassay, the cancers observed at the highest dose (maximum tolerated dose, MTD) are presumably recognized as a result of this mode of action by some researchers (Ames and Gold 1990; Gaylor 2005; Lutz 1998). Interestingly, although apoptosis is usually recognized as an anticarcinogenic mechanism (Grasl-Kraupp *et al.* 2000; Schulte-Hermann *et al.* 1990), it sometimes elicits compensatory proliferation and induces carcinogenesis (Dragan *et al.* 2001).

(2) *Mitogenesis and inhibition of apoptosis*: Under normal physiologic conditions, cell proliferation is properly balanced by cell loss, *i.e.*, apoptosis. Disruption of this balance in favor of proliferation brings forth an undesirable buildup of cells. A chemical may induce mitogenesis, inhibit apoptosis, or do both (Butterworth *et al.* 1991; Conolly and Andersen 1997; Hadjiolov and Bitsch 1997; Marsman and Barrett 1994; Tharappel *et al.* 2002). In this regard, Andersen *et al.* (1995) proposed a general mechanistic model for liver tumor promoters. Upon exposure to a promoter, the liver cells are stimulated to proliferate, which activates the homeostatic mitoinhibition. The growth of the normal cells is inhibited by the homeostatic control, but the initiated cells are resistant to the control and thus gain growth advantages. As such, the mutated cells expand to clones, preneoplastic lesions, or go even further. Various signaling pathways are often involved in this process. For example, the modulation of transforming growth factor α (TGF-α) and β (TGF-β) pathways was observed in PCB 126-promoted preneoplastic foci development in the rat (Dean 2003; Painter 2005). The insulin and insulin-like growth factor (IGF) pathways were altered in a rat mammary tumor bioassay on hexachlorobenzene (HCB)(Randi *et al.* 2006), a chemical being classified as "reasonably anticipated to be a human carcinogen" by the US National Toxicology Program (NTP) (2001).

(3) *Inhibition of gap junctional intercellular communication (GJIC)*: The GJIC is a homeostatic mechanism that organizes cells in a society and places each cell under effective monitoring by all the neighboring cells (Krutovskikh 2002; Omori *et al.* 2001). When an initiated cell appears, it is monitored by its neighbors and its proliferation is checked by receiving growth-controlling signals through gap junctions (Krutovskikh

2002). If the expression of the GJIC between an initiated and the surrounding normal cells is inhibited, the initiated cell is not adequately monitored and thus has the possibility to replicate and eventually advance to malignancy. HCB (Plante *et al.* 2002), TCDD (Bager *et al.* 1997), and PCB 126 (Bager *et al.* 1997) have been reported to inhibit GJIC expression in the rat.

The modes of action of chemical carcinogenesis are generally identified from *in vitro* tests and animal studies. During cancer risk assessment, it is necessary to evaluate qualitatively and quantitatively the relevance of the modes of action *in vitro* and in animals to in humans; omission of this process may result in misclassification of a chemical in terms of its carcinogenicity in humans. Cohen (2004) illustrated the importance of mode of action in chemical cancer risk assessment using examples of some rodent-specific tumors. In the latest USEPA guidelines for carcinogen risk assessment (USEPA 2005b), the importance of mode of action is particularly stressed.

2. Methods of chemical carcinogenesis research

From the regulatory perspective, chemical carcinogenesis research should determine the carcinogenicity/carcinogenic potential, the dose-cancer incidence (or carcinogenesis-related effect biomarkers) relationship, and the mode of action of a chemical. Currently, three different kinds of methods, *i.e.*, epidemiologic, laboratory, and theoretic, are being actively employed in carcinogenesis research. The epidemiologic methods date back to the 18th century when the European medical doctors cast their attention to human cancers. The laboratory methods in animals were introduced in the early 20th century. At present, laboratory methods are essential for screening chemicals for their carcinogenicity and

establishing dose-response relationships. The theoretic methods involve mathematic modeling and biologically based modeling. They are instrumental for performing various extrapolations that are necessary for risk assessment. Each of these methods has pros and cons; the utilization and integration of them in the risk assessment process help uncover the mystery of carcinogenesis and shape the strategy and policy for cancer prevention and human health protection (Franco *et al.* 2004).

2.1. Epidemiologic methods

Epidemiology is a subject that studies the distribution and determinants of disease frequency in humans and animals; similarly, cancer epidemiology studies the distribution and determinants of cancer frequency in humans and animals. More specifically, cancer epidemiology investigates the distributions, examines the etiologic factors (e.g., lifestyle, occupation, chemical exposure, etc.) of cancers, identifies the strength of links between etiologic factors and cancer incidences, and evaluates the effects of intervention strategies on cancer occurrence. In this arena, researchers observe what happens in humans, which is in sharp contrast with animal studies where researchers observe what happens in animals upon intentional treatments. Human cancer epidemiology has two basic types of studies distinguished by their designs and purposes: descriptive and analytic (Bourke and Daly 1983; Clayson 2001a). The former looks at the distribution patterns of cancer occurrence with age, gender, ethnicity, nationality, and geography at a certain time point. It helps form a hypothesis of the etiology of a cancer. An analytic study examines etiologic hypotheses and defines how strong the links are between factors and cancers of concern. Analytic studies can be either retrospective, *i.e.*, looking backward for the differences in factors between two pre-determined groups with and without a certain

cancer (case-control study), or prospective, *i.e.*, following up two groups with and without exposure to selected factors for cancer occurrence (cohort study) (Bourke and Daly 1983; Clayson 2001a). Because of various, usually inevitable, biases, confounding factors, and information errors in an epidemiologic study, interpretation of the results is often difficult. Even though a significant link between a factor and cancer occurrence is identified, the link is not guaranteed to be a causal relationship. Nevertheless, criteria were suggested to determine whether or not a link can be recognized as a causal relationship (Franco *et al.* 2004; Hill 1965).

The importance of epidemiologic data in cancer risk assessment has been stressed by USEPA (1996). Thus far, some chemicals (e.g., arsenic, benzene, ethylene oxide, vinyl chloride, TCDD) have been defined as human carcinogens based on epidemiologic studies (IARC 2003; Pitot and Dragan 2001b). In addition, cancer epidemiology identifies genetic polymorphism and susceptibility biomarkers in human populations, valuable information for human risk assessment (Duell *et al.* 2001; Santella *et al.* 2005; Stucker *et al.* 1999). It may also produce clues of modes of action of exposure-induced cancers, which are subjected to laboratory studies to explore more details at the cellular and molecular levels.

2.2. Laboratory methods

Because of the limitations in cancer epidemiology and the reality that it is not ethical to test chemicals in humans, laboratory study is the primary means for determining carcinogenicity, along with other toxicities, of chemicals. Laboratory study can be conducted *in vivo* (whole animals in long term or shorter term) or *in vitro* (bacteria, cultured cells, etc.)

2.2.1. In vivo study

2.2.1.1. Long-term bioassays

According to USEPA (1996), "[t]he objective of long-term carcinogenesis bioassays is to determine the carcinogenic potential and dose response relationships of the test agent." The current standard long-term carcinogenesis bioassays employ both sexes of rats (Fischer 344/N, F344/N) and mice (B6C3F1 hybrid) with three exposure levels plus untreated controls in groups of 50 animals for two years (NTP 2006; USEPA 1996). The high dose used in a long-term bioassay is usually the MTD, which sufficiently challenges the animals but does not cause any apparent adverse effect on their longevity or clinical condition (Bucher *et al.* 1996; Clayson 2001b). The MTD is determined from the results of prior shorter term studies (14 days and/or 13 weeks), and the rationale for how the doses are selected in a long-term bioassay was presented by J. R. Bucher earlier (Bucher *et al.* 1996).

The utility of the long-term animal bioassay relies on the assumption that "positive effects in animal cancer studies indicate that the agent under study can have carcinogenic potential in humans." (USEPA 1996) This assumption is supported by the fact that nearly all of the agents known to induce cancer in humans are carcinogenic in animals in adequately designed tests (Huff 1994). Up to date, a great body of information has been accumulated from long-term bioassays. Over 500 agents have been tested by the National Cancer Institute (NCI)/NTP, and even more by various research agencies around the world. The results of 1485 chemicals subjected to long-term bioassays, selected according to a set of criteria, have been analyzed and compiled into a Carcinogenic Potency Database, which is accessible at http://potency.berkeley.edu.

Although the long-term bioassay remains a "gold standard" for carcinogenicity testing, its limitations are well appreciated. Such a bioassay is very expensive (up to several millions dollars per chemical), uses a large number of animals (about 2000 animals per chemical), and takes long time (5-12 years per chemical) (Yang *et al.* 2004). Moreover, its specificity is being questioned: some tumors induced in animals by test agents may not be relevant to humans (Bucher and Portier 2004; Cohen 2004; MacDonald 2004). The use of a dose as high as an MTD renders the possibility that the tumors developed in animals may be a result of regenerative cell replication triggered by the cytotoxicity at the MTD level, which is obviously not relevant to human exposure at a much lower dose (Ames and Gold 1990; Gaylor 2005; Lutz 1998). Therefore, great efforts have been made to design, optimize, and evaluate alternative shorter-term (generally less than a year) animal bioassays which may hopefully overcome some, if not all, of the limitations of the long-term bioassay and are more flexible for accommodating various data needs.

2.2.1.2. Alternative shorter-term animal bioassays

The value of shorter-term animal bioassays in risk assessment has been discussed by Clayson and Iverson (1996) and Cohen (2004). Since carcinogenesis is currently recognized as a consequence of mutation and cell proliferation (Cohen and Ellwein 1990a, b; Moolgavkar 1988, 1991), Cohen (2004) proposed a mechanism-based conceptual framework for cancer risk assessment. Within this framework, a chemical will be examined for its DNA reactivity and proliferative potential and the relevance of these effects to humans. The proliferative potential can be identified in four- and/or thirteen-week bioassays in rodents. This concept is scientifically reasonable and practically

attractive. However, intensive investigations are needed to realize them and to evaluate their usefulness.

Multiple shorter-term animal bioassays have been proposed to test chemical carcinogenicity. A comprehensive collection of these bioassays was compiled by the International Agency for Research on Cancer (IARC) (1999). Some examples are micronucleus test in mice, genetically engineered mouse bioassays, and initiation-promotion bioassays. The micronucleus test examines the mutagenicity of chemicals at the level of chromosome using the endpoint of micronucleus formation in the immature erythrocytes in mouse bone marrow (USEPA 1998). The genetically engineered mouse bioassays employ several genetically engineered mouse lines; those of the greatest potential usefulness are the Tg.AC (carrying a v-Ha-ras oncogene fused to the promoter of the ζ-globin gene), p53+/- (heterozygous p53 tumor suppressor gene), and TgHras2 (carrying the human protooncogene c-Ha-ras) mouse lines, as reviewed by Tennant *et al.* (1999). The initiation-promotion shorter-term bioassays typically involve a combination of treatment of an initiator and a promoter (*i.e.*, test chemicals); some bioassays include mitogenic stimuli (e.g., two-thirds partial hepatectomy, carbon tetrachloride exposure) to expedite the development of endpoint markers (e.g., altered hepatic foci). These bioassays have been reviewed by several groups (Goldsworthy *et al.* 1986; Pitot and Dragan 2001b; Shirai *et al.* 1999; Tsuda *et al.* 1999). Despite the advantages of the shorter-term bioassays, the interpretation of the results is still a debatable issue because the animals and/or the treatments are even more different, compared to those in long-term bioassays, from humans and/or human exposure conditions. Some evaluation data of the

concordance between shorter-term and long-term bioassays have been reported (Ito *et al.* 2003; Jacobs 2005; Tennant *et al.* 1990; Thompson *et al.* 2003).

One of the well-recognized initiation-promotion bioassays was developed by Ito and colleagues (Ito *et al.* 1988; Ito *et al.* 2003; Shirai *et al.* 1999), which is referred to as Ito's bioassay or protocol henceforth and is explained in detail as follows. The optimized procedure (Fig. 1.1) (Ito *et al.* 2003; Shirai *et al.* 1999) of this bioassay is: Male F344 rats, about 6-weeks old, are divided into groups 1, 2, and 3. Within the 8-week time frame, at week 0, groups 1 and 2 are initiated with DEN (intraperitoneally, i.p.) in 0.9% saline at a necrotic dose of 200 mg/kg; group 3 is injected with saline to serve as a saline control. At week 2, groups 1 and 3 are administered a test agent (usually a chemical); group 2 is treated with the vehicle free of the agent to serve as a DEN control. At week 3, all rats are subjected to a two-thirds partial hepatectomy which serves as a mitotic stimulation to the hepatocytes. The rats are sacrificed at 8 weeks. The livers are fixed and sectioned for detecting the hepatic foci immunohistochemically positive for placental-form glutathione S-transferase (GST-P; see Section 5.3 for the biologic significance of GST-P foci). The numbers and areas of GST-P foci larger than 0.2 mm in diameter are recorded. At the level of $\alpha = 0.05$, an increase or decrease in either the number or the area of foci in group 1 relative to those in group 2 is considered a "positive" result. Up to year 2002, 313 compounds had been tested using this protocol within about 25 years; these compounds include mutagens, nonmutagens, hepatocarcinogens, carcinogens targeting organ(s) other than the liver, and noncarcinogens (Ito *et al.* 2003). The analysis on the results of 113 hepatocarcinogens and non-carcinogens against their corresponding long-term bioassay data indicated that the sensitivity (the probability that a chemical is identified as a

carcinogen in the Ito's bioassay given it is carcinogenic in the long-term bioassay), specificity (the probability that a chemical is identified as a noncarcinogen in the Ito's bioassay given it is not carcinogenic in the long-term bioassay), positive predictivity (the probability that a chemical identified as a carcinogen in the Ito's bioassay is indeed carcinogenic in the long-term bioassay), and negative predictivity (the probability that a chemical identified as a noncarcinogen in the Ito's bioassay is indeed noncarcinogenic in the long-term bioassay) of the Ito's protocol were 92.3% (60/65), 97.9% (47/48), 98.4% (60/61), and 90.4% (47/52), respectively (Ito *et al.* 2003). This result suggests excellent suitability of this protocol for hepatocarcinogen screening. When the carcinogens targeting organ(s) other than the liver are included in the analysis, the sensitivity is reduced to 65%. However, because more than 60% of the environmental carcinogens target the liver (Ito *et al.* 2003), this protocol is of practical use.

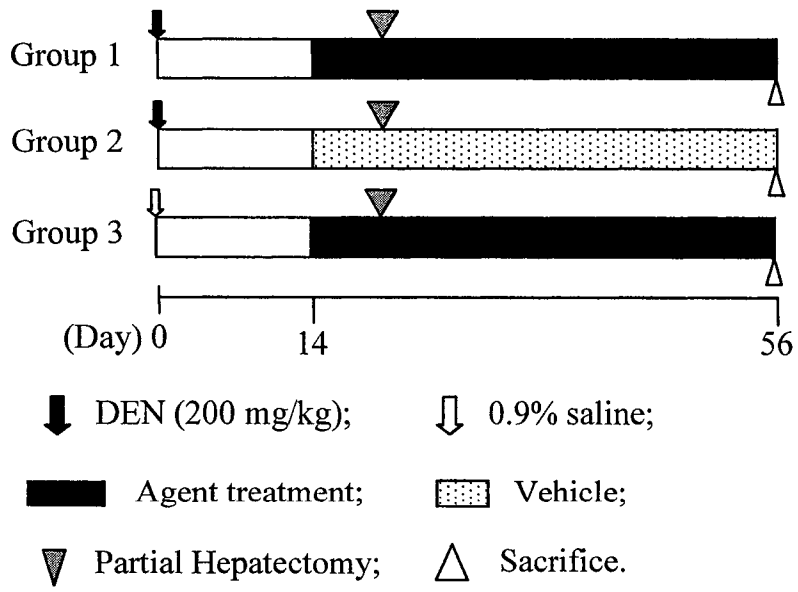

Fig. 1.1. Experimental protocol of the Ito's medium-term initiation-promotion liver foci bioassay (Ito *et al.* 2003; Shirai *et al.* 1999).

In our laboratory, the Ito's bioassay has been modified by incorporating a series of sacrifice points to collect time-course data on chemical pharmacokinetics and GST-P foci development. With such a modified version, the pharmacokinetics of and GST-P foci promoted by 1,2,4,5-tetra-, penta-, and hexachlorobenzene, PCB 126, and some chemical mixtures have been studied (Dean *et al.* 2002; Lu *et al.* 2006b; Ou *et al.* 2003; Ou *et al.* 2001; Painter 2005; Thomas 1998; Thomas *et al.* 2000)(Lohitnavy, M., *et al.*, unpublished data).

2.2.2. In vitro study

The *in vitro* studies in chemical carcinogenesis research are usually conducted using bacteria or cultured cells and devoted primarily to the detection of chemical genotoxicity. Some well-known classic *in vitro* studies include *Salmonella* reverse mutation test, comet assay, unscheduled DNA synthesis assay, hypoxanthine-guanine phosphoribosyltransferase (hprt) gene mutation test. The principles, underlying assumptions, and usefulness of these assays were discussed and analyzed in the 1999 IARC compilation (McGregor and Anderson 1999; Quillardet and McGregor 1999; van Zeeland and Vrieling 1999).

Another *in vitro* assay worthy discussion is the cell transformation assay. This assay covers the process of the transformation from phenotypically normal cells to malignant cells *in vitro*, recapitulating the multi-stage process of tumor formation in the body (LeBoeuf *et al.* 1999). Thus, it can be used to screen chemicals for carcinogenic potentials and study mode of action of chemical carcinogenesis. LeBoeuf *et al.* (1999) found that this assay, using BALB/c 3T3 immortal cell line or Syrian hamster embryo cell line, has satisfactory sensitivity (the probability that a chemical is identified as a

carcinogen in the cell transformation assay given it is carcinogenic in the long-term bioassay), specificity (the probability that a chemical is identified as a noncarcinogen in the cell transformation assay given it is not carcinogenic in the long-term bioassay), positive predictivity (the probability that a chemical identified as a carcinogen in the cell transformation assay is indeed carcinogenic in the long-term bioassay), negative predictivity (the probability that a chemical identified as a noncarcinogen in the cell transformation assay is indeed noncarcinogenic in the long-term bioassay), and overall concordance with the animal carcinogenesis bioassay. More impressively, the overall concordance of this assay is higher than that of the *Salmonella* test or the battery of *Salmonella* test, mouse lymphoma test, and *in vitro* cytogenicity assay.

2.3. Theoretic methods

The theoretic methods refer to mathematic modeling, which is a valuable tool for organizing data in a system, inferring potential mechanism(s) of the interactions among the components in the system, and predicting the behaviors of the system under certain conditions. Thus, mathematic modeling is complementary to experimental studies. A close interaction between modeling and experimentation may expedite our understanding in a problem. Mathematic modeling has been utilized in many biology-related fields, from the population level (animal migration, spread of HIV) to the tissue and cell level (pharmacokinetics, cellular kinetics) and even down to the molecular level (signal transduction pathway, gene network). In chemical carcinogenesis research, the most important applications of mathematic modeling are (1) to understand chemical disposition process in the body, and determine the internal dosimetry of a chemical that is closely related to its carcinogenic effect(s) (Andersen 2003; Clewell *et al.* 2002); (2) to

uncover the mode of action in a carcinogenic process (Andersen *et al.* 1987); and (3) to facilitate various extrapolations that are inevitably involved in cancer risk assessment (Andersen 2003; Clewell *et al.* 2002; Conolly and Andersen 1991; Conolly *et al.* 2003; Krishnan and Johanson 2005). In addition, modeling can identify data needs and direct experimental design and thus improve the effectiveness of the experiment, as pointed out by multiple investigators (Bucher *et al.* 1996; Eickman 2005; Kopp-Schneider and Portier 1991; Liao *et al.* 2001; Ou *et al.* 2003; Ou *et al.* 2001; Portier 1987; Thomas 1998; Thomas *et al.* 2000).

According to the way it is developed, a model in chemical carcinogenesis can be either data-based or biology/physiology/mechanism-based. The former is a data-fitting exercise and the model formulation is not sufficiently directed by biological reality. Such models include (quantitative) structure-activity relationship (SAR/QSAR), compartmental pharmacokinetic model, and linearized multistage carcinogenesis model. To the contrary, the latter, e.g., physiologically based pharmacokinetic (PBPK) model, biologically based dose-response (BBDR) model, takes into account biologic, physiologic, or mechanistic determinants governing the biological processes related to the endpoints of our interest. A shift from the former to the latter took place with the improvement in the computational capability, accumulation of biologic knowledge, and the infusion of concepts and tools from chemical engineers. In the past three decades, great achievements have been obtained in biologically based modeling, which are discussed in detail later (Sections 4 and 5). It is noteworthy that models by no means can exactly reproduce a system under investigation. Thus, "all models are wrong; but some are useful." (Box 1976)

3. Cancer risk assessment

Cancer risk assessment is integrated by four crucial parts, hazard assessment, dose-response assessment, exposure assessment, and risk characterization. The last two parts are not covered in this review. The first part addresses two questions: "whether an agent may pose a carcinogenic hazard to human beings" and "under what circumstances an identified hazard may be expressed" (USEPA 1996, 2005b). The second part estimates potential risks to humans at exposure levels of concern through a two-step procedure. The relationship of dose to the degree of response (cancer incidence) is first determined at the range observable from experimentation, and then an extrapolation down to the unobservable low-dose range is performed (USEPA 1996, 2005b). The data necessary to the hazard and dose-response assessment are generally obtained from SAR/QSAR, *in vitro* assays, short-term and long-term animal bioassays, and epidemiologic studies. Epidemiologic data are highly desirable because they are obtained directly from humans, but such data are very scarce. Thus, practically, the long-term bioassay often represents the most important source of data. When utilizing long-term bioassay data to estimate human risk, animal-to-human and high-to-low-dose extrapolations are essential. Uncertainties exist in these extrapolations; with increasing understanding in modes of action of carcinogenesis, uncertainties can be reduced by the application of biologically based computer models, *i.e.*, PBPK and two-stage carcinogenesis models as discussed below.

4. PBPK modeling – describing internal dosimetry

4.1. Basics of PBPK modeling

The concept of PBPK (also know as PBTK where TK stands for toxicokinetics) modeling dates back to 1920's and 1930's when the effects of physical, chemical, and physiologic factors on the dispositions of drugs and anesthetics were quantitatively studied (Andersen 2003). Due to the limitation in computational capacity, however, the early PBPK modeling was simplified and led to the development of the compartmental modeling. The structure of a compartmental model is determined by the data set to be described (thus known as data-based model), and the compartment(s) and parameters therein lack physiologic meaning. Since 1970's, the advances in computer technology, computational methods, and modeling techniques (especially in chemical engineering) have been propelling the evolution and maturation of PBPK modeling. In toxicology, among the pioneering publications on PBPK modeling are Andersen (1981), Angelo *et al.* (1984; 1984), Bungay *et al.* (1979; 1981), Caperos *et al.* (1982), Fernandez *et al.* (1977), King *et al.* (1983), Lutz *et al.* (1977), Nolan *et al.* (1984), Ramsey and Andersen (1984), and Tuey and Matthews (1980a; 1980b). At present, PBPK modeling is an essential technique in toxicological research and risk assessment. The current status of PBPK application has been thoroughly reviewed in a book (Reddy *et al.* 2005b). Readers who are interested in the detailed history of PBPK can refer to Andersen and Andersen *et al.* (Andersen 2003; Andersen *et al.* 2005).

A PBPK model describes the disposition of a chemical in the body by taking into account physiologic, physicochemical, and biochemical determinants. In a PBPK model, the body of an organism, usually mouse, rat, or human, is divided into several compartments that represent anatomic organs or groups of tissues/organs connected by the blood circulation. A hypothetic PBPK model structure is shown in Fig. 1.2. The liver,

fat, and blood are separate tissue compartments, the remaining organs/tissues are lumped into a rapidly and a slowly perfused compartment, and the lung and gastrointestinal (GI) lumen compartments are included to accommodate exposure routes. How to compartmentalize a body in PBPK model construction is determined by the modeling purposes, data (including parameters and pharmacokinetics) availability, and pharmacokinetic characteristics of the chemical of interest and is under the guidance of the Principle of Parsimony. Regardless of this general rule, model formulation is often a tricky task (Bailer and Dankovic 1997; Bois *et al.* 1991; Nestorov *et al.* 1998); improper formulation results in model misspecification (Nestorov *et al.* 1998) and may have considerable impacts on model performance and utility (Bailer and Dankovic 1997).

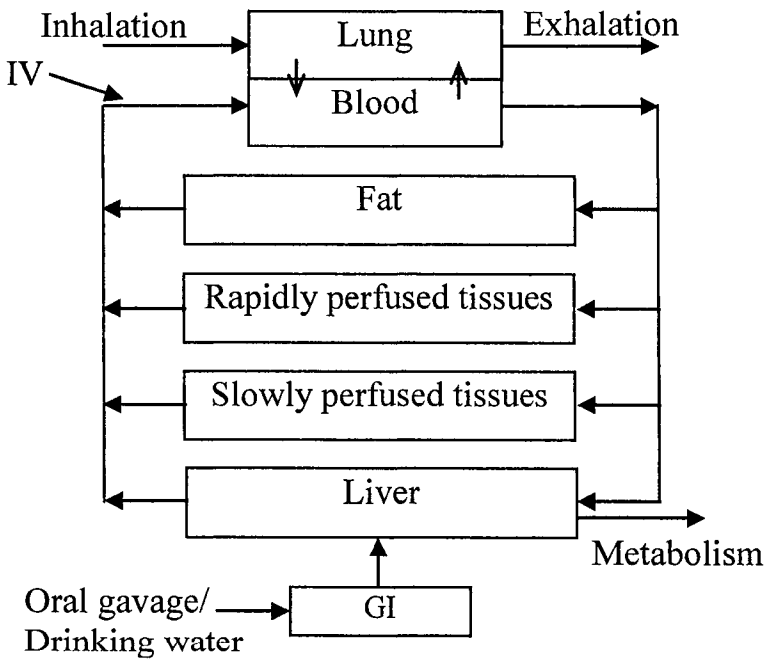

Fig. 1.2. A hypothetic PBPK model structure for a volatile and lipophilic chemical that is metabolized in the liver.

The uptake of a chemical into a compartment is governed by partitioning, and sometimes macromolecular binding (Andersen *et al.* 1997; Leung *et al.* 1989) as well. The uptake process falls into two types: perfusion-limited (also known as flow-limited) and diffusion-limited. The former refers to the scenario where the partitioning of the chemical into the compartment is rapid and the blood flow into the compartment is the rate-limiting factor. With the usual assumption of chemical homogeneous distribution in a compartment (X), the concentration in the compartment (CX) is in equilibrium with the concentration in the efflux venous blood (CVX) by a factor of partition coefficient (PX), *i.e.*, CVX = CX/PX. The diffusion-limited uptake is a process where the partitioning is slow and diffusion, in turn, becomes a rate-limiting factor. The uptake is controlled by a permeability coefficient (volume/time). Although the type of uptake may be inferred from experimental data, such inference is often not certain. For simplicity, perfusion-limited uptake is frequently assumed. The importance of the selection of an uptake type in PBPK modeling has been demonstrated (Kohn 1997).

The rate of change of chemical amount in a compartment (dAX/dt) can be calculated by a mass balance differential equation:

$$\frac{dAX}{dt} = QX \times (CA - CVX) - RMetabolism \quad \text{(Eq-1)}$$

where QX is the blood flow rate to this compartment, CA is the arterial blood concentration, CVX is the efflux venous blood concentration, and RMetabolism is the rate of metabolism in the compartment. Collectively, a PBPK model is translated into a group of coupled differential as well as algebraic equations. With the aid of computational software, e.g., ACSL (Advanced Continuous Simulation Language), Berkeley Madonna, the equations can be solved and generate time courses of chemical

amounts and/or concentrations in all compartments, including the internal dose metrics of interest [see (Krishnan and Andersen 1994) and (Yang and Lu 2006) for detailed examples].

PBPK models are generally rich in parameters; a simple model may involve 10-20 parameters. Three kinds of parameters are required for PBPK models: physiologic (e.g., body weight, cardiac output, ventilation rate, volume of and blood flow to each compartment), physicochemical (e.g., partition coefficient, permeability coefficient), and biochemical (e.g., metabolism rate, protein binding). In animals, the majority of physiologic parameters are experimentally available; an excellent compilation has been published (Brown *et al.* 1997). The other parameters are either measured through *in vivo* or *in vitro* experimentation or optimized by model fitting. In humans, the parameters are generally sparse. Except the physicochemical parameters, the others are usually allometrically scaled from animal parameters by body weight (Dedrick 1973; Fiserova-Bergerova 1995; Krishnan and Andersen 1994; Luebeck *et al.* 1999). An allometric scaling equation is as follows:

$$Y = a \times BW^{b} \quad \text{(Eq-2)}$$

where Y is a parameter of interest, BW is the body weight of an organism, and a and b are parameter-specific constants obtained from regression analysis of data in multiple species.

After a PBPK model is developed, it should be subjected to validation. This process tests whether or not the model can simulate data sets that are not involved in the model development. If the model simulates these data sets successfully, its validity and utility

are substantiated; otherwise, the model needs to be refined and then tested again. It is noteworthy that PBPK model development is an iterative process.

4.2. Statistical issues in PBPK modeling

4.2.1. Optimization

PBPK models describe chemical pharmacokinetics using *a priori* information. In reality, however, some parameters, e.g., the rate constants of metabolism and gastrointestinal absorption, permeability coefficient constant, are difficult to obtain experimentally. Such parameters are calibrated using available pharmacokinetic data; this process is termed parameter optimization. In the early years of PBPK evolution, optimization was generally performed by visual fitting, which does not require statistical calculation and is easy to fulfill. Nevertheless, visual optimization cannot elude subjectivity. Therefore, more emphasis has been placed upon statistical optimization, which is based on statistical measurements such as least square of residual or maximum likelihood that define how well model predictions agree with corresponding data.

It is often desirable to couple visual and statistical optimization to take advantage of both methods. Using visual optimization, one can manually adjust a parameter and check its effect on model outputs. As such, one can capture a rough idea of the effects of parameters (either known or unknown) on model performance and pharmacokinetics of concern. Furthermore, this process obtains a set of values of best visual fit that serves as the starting values for statistical optimization. It is recommended to set a constraint range for an unknown parameter during statistical optimization so that the statistically best but biologically unrealistic values can be excluded. According to the experience in PBPK

modeling of ours and other investigators (Conolly and Kimbell 1994), visual optimizations yield similar parameter estimates as statistical optimizations.

4.2.2. Sensitivity analysis

For various reasons, it is valuable to identify the sensitivity of PBPK model outputs to parameters. Here "sensitivity" means the magnitude(s) of change(s) in output(s) in response to the perturbation in a parameter, which is determined by sensitivity analysis. Conceptually, there are two kinds of sensitivity analyses in mathematic modeling: local and global (Blower and Dowlatabadi 1994; Nestorov *et al.* 1997; Saltelli *et al.* 1999). The local sensitivity refers to the response of model outputs to the perturbation of a single parameter, whereas the global sensitivity refers to the response of outputs to the simultaneous alterations in all parameters. The sensitivity analysis in the PBPK community is currently predominated by the local sensitivity (Clewell *et al.* 1994; Easterling *et al.* 2000; Emond *et al.* 2004; Evans and Andersen 2000; Evans *et al.* 1994; Lu *et al.* 2006b; Sweeney *et al.* 2003) despite the existence of exceptions (Hetrick *et al.* 1991; Woodruff and Bois 1993).

The sensitivity of an output to a parameter can be quantitatively reflected by a sensitivity coefficient (SC) (Clewell *et al.* 1994). Considering an output R is a function of a parameter x, *i.e.*, R = F(x), then

$$SC = \frac{F(x + \Delta x) - F(x)}{\Delta x} \quad \text{(Eq-3)}$$

where Δx is a perturbation in x. When the Δx is sufficiently small, the SC is a partial derivative of R with respect to x, thus Eq-3 can be reformulated into

$$SC = \frac{\partial R}{\partial x} \quad \text{(Eq-4).}$$

Since parameters and outputs have distinct units and magnitudes, the SC should be properly normalized for inter-parameter or inter-output comparisons. Thus,

$$SC = \frac{\frac{\partial R}{R}}{\frac{\partial x}{x}} = \frac{\partial \ln R}{\partial \ln x} \quad \text{(Eq-5)}$$

where SC can be recognized as the sensitivity of the logarithm of an output R (lnR) to the logarithm of a parameter x (lnx), hence it is also known as log-normalized sensitivity coefficient (LSC). An LSC identifies the percentage change in an output due to a percentage change in a parameter. It has been suggested that LSCs should be in the range of -1 to 1. A value substantially beyond the range indicates that the error in a parameter is greatly amplified in the output, and hence implies undesirable feature(s) in the model (Clewell *et al.* 1994).

The utilities of sensitivity analysis include: (1) to identify the most sensitive parameters for an output, which helps understand a pharmacokinetic behavior (Emond *et al.* 2004; Evans and Andersen 2000; Lu *et al.* 2006b); (2) to evaluate the necessity of accurately measuring unknown parameters. If the output of interest is sensitive to an unknown parameter, accurate measurement of this parameter is required; and (3) to direct targeted experimentation and improve study design. For example, sensitivity analysis may suggest optimal exposure conditions, necessary data to be collected, and the frequency of data collection (Evans *et al.* 1994; Schlosser 1994).

4.2.3. Uncertainty analysis

The term "uncertainty" is often used along with, and sometimes mistaken for, "variability" although they are totally different concepts. Uncertainty is defined as the possible error in estimating a true value of a parameter; it is a defect in knowledge and

can be reduced by improving experimental methods (Clewell and Andersen 1996). Variability, however, refers to the difference of a parameter among individuals; it is a fact that can be measured but not be changed (Clewell and Andersen 1996). For the purpose of risk assessment, average pharmacokinetic information as obtained from many PBPK exercises is of limited use because it does not take into account the uncertainty and variability in the parameters (Clewell and Andersen 1996). Thus, quantitative exploration of uncertainty and variability in a PBPK model is necessary.

Uncertainty analysis provides the impacts of uncertainty and variability in model parameters on predicted pharmacokinetics. Monte Carlo simulation is a common technique for uncertainty analysis. Prior to PBPK simulation, the statistical distributions of all parameters are determined. A set of the parameters is sampled from those distributions using Monte Carlo simulation. These parameters are then input into a PBPK model, which is executed and generates a set of outputs. Then another set of parameters is sampled, the PBPK model is re-executed, and the outputs are recorded. This process is repeated for many times (*e.g.*, 1000). The many sets of outputs are statistically analyzed to get the distribution characteristics and means, variances, as well as other statistics. As such, the effects of the uncertainty and variability in parameters on outputs are measured (Blower and Dowlatabadi 1994; Clewell and Andersen 1996; El-Masri *et al.* 1999; Thomas *et al.* 1996).

It has been a difficult task to quantitatively differentiate the effects of uncertainty and variability. Fortunately, the difficulty has been greatly alleviated thanks to the application of a more advanced statistical approach, Bayesian analysis, in PBPK modeling advocated by Bois and co-workers (Bois 1999, 2001; Bois *et al.* 1996; Jonsson 2001) since late

1990's. This approach has found its great utility in supporting chemical risk assessment (Bois 1999, 2001; David *et al.* 2006; Jonsson and Johanson 2001a, b, 2003; Marino *et al.* 2006).

4.2.4. Bayesian analysis

Information is gradually acquired; newly acquired information helps us update our existing belief on a certain problem so that the belief becomes compatible with both old and new information. Bayesian analysis, based on probabilistics and Bayesian Theorem, is a widely used tool for updating a belief. Take an example of metabolism rate constant (K_m). Assuming in an earlier study, the measurement (K_{m1}) can be expressed using a likelihood function $p(K_{m1})$, which is named as prior probability, or simply prior. In a present study, the new measurement K_{m2} has a likelihood function $p(K_{m2})$. In the case that $p(K_{m2})$ is different from $p(K_{m1})$, it is not wise to just take one of them to represent K_m. Rather, a likelihood function of K_{m2} conditional on the earlier information of K_{m1}, $p(K_{m2}|K_{m1})$, would be a better choice. According to the Bayesian Theorem,

$$p(K_{m2} \mid K_{m1}) = \frac{p(K_{m2}) \bullet p(K_{m1} \mid K_{m2})}{p(K_{m1})} \qquad \text{(Eq-6).}$$

Thus, our previous knowledge in Km [p(Km1)] is updated with the new information [p(Km2)]. The $p(K_{m2}|K_{m1})$ is referred to as posterior probability or posterior.

The principle of Bayesian analysis in the context of PBPK modeling has been explained at large by Bernillon and Bois (2000). To analyze the variability in parameters, a PBPK model is necessarily structured at both an individual level and a population level. At the individual level, the pharmacokinetic parameters (Ψ_i), along with other factors (including time and exposure conditions), are organized to describe the individual pharmacokinetic data (y, with experimental error of σ^2). At the population level, the

individual pharmacokinetic parameters are pooled to form a population distribution with a mean of μ and a variance of Σ. As pharmacokinetic data are collected conditional on multiple factors (Ψ, μ, Σ, and σ^2, collectively represented by θ), the data likelihood can be expressed by $p(y|\theta)$. Since in this analysis the multiple factors are of much more concern than the data likelihood, the variable $p(\theta|y)$ is the focus. According to the Bayesian Theorem, $p(\theta|y)$ is proportional to the product of $p(y|\theta)$ and $p(\theta)$; *i.e.*,

$$p(\theta \mid y) \propto p(y \mid \theta) \times p(\theta) \quad \text{(Eq-7)}.$$

Since θ is a collection of Ψ, μ, Σ, and σ^2, Eq-7 can be re-written as

$$p(\Psi, \mu, \Sigma, \sigma^2 \mid y) \propto p(y \mid \Psi, \mu, \Sigma, \sigma^2) \times p(\Psi, \mu, \Sigma, \sigma^2) \quad \text{(Eq-8)}.$$

With some reasonable assumptions (Bernillon and Bois 2000), Eq-8 is reformulated into

$$p(\Psi, \mu, \Sigma, \sigma^2 \mid y) \propto p(y \mid \Psi, \sigma^2) \times p(\Psi \mid \mu, \Sigma) \times p(\mu) \times p(\Sigma) \times p(\sigma^2) \quad \text{(Eq-9)}.$$

Resultantly, $p(\theta|y)$ is decomposed to data likelihood, population parameter distribution, and priors of population parameter mean and variance and of experimental errors. The priors are determined based on information available from the literature. The $p(\mu)$ is a function of the real population mean (usually not obtainable) and the standard error (deviation of the measured value away from the real mean due to experimental limitations). This standard error is a measure of the uncertainty in the parameters. The $p(\Sigma)$ is a function of variability among individuals. As such, the uncertainty and variability are distinguished.

The Bayesian analysis is performed with the aid of computational tools. At present, the main tool in the PBPK community is Markov chain Monte Carlo (MCMC) simulation, which is an extension of the regular Monte Carlo simulation. By sampling from predetermined priors of the parameters to be updated with new information, MCMC

simulation generates a joint posterior for these parameters. Sampled using regular Monte Carlo simulation, the posteriors are then fed to a PBPK model to obtain the distributions of outputs of interest. In addition, the correlation between parameters and the sensitivity of posteriors or model outputs to priors can also be easily acquired.

4.3. Applications of PBPK modeling

Because PBPK models can calculate internal dose metrics based on physiologic, physicochemical, and biochemical information, they have various applications (Andersen *et al.* 2005; Krishnan and Johanson 2005; Yang and Andersen 1994): (1) Store and organize available pharmacokinetic knowledge of chemicals; (2) Test hypotheses related to the mechanisms underlying chemical dispositions; (3) Determine the values of pharmacokinetic parameters that are not readily measurable; (4) Help identify modes of action of chemicals; (5) Predict internal dose metrics in humans and thus facilitate risk assessment; (6) Direct experimental studies, optimize experimental design, and save resources and animals; (7) Assess and reconstruct human exposure in cancer epidemiologic studies using tissue concentration-to-exposure back calculation; and (8) Investigate and predict the pharmacokinetic interaction among components in a mixture. The applications of 2, 4, and 5 are further discussed below.

4.3.1. Test hypotheses related to the mechanisms underlying chemical dispositions

Some chemicals may have complex pharmacokinetics in the body and the disposition mechanisms may not be easily understood through experimentation. Once a hypothesis of a disposition mechanism is formed, it can be tested using a PBPK model. If the model by no means replicates available data, the hypothesis should be discarded. Otherwise, the hypothesis might be of some value. Manipulations of the hypothesis-related parameters

may provide a better picture of how the disposition process is controlled by the hypothetical mechanism, and hence direct further experimentation. The evolving study on TCDD pharmacokinetics successfully exemplifies how PBPK plays its role in this regard. Lu (2005) has thoroughly summarized this case. Here a brief discussion is presented.

TCDD is a lipophilic and metabolically resistant organic pollutant and has various adverse effects. TCDD binds to the cytosolic aryl hydrocarbon receptor (AhR), and the complex is subsequently translocated into the nucleus and interacts with a specific DNA response element, *i.e.*, a dioxin response element (DRE) or xenobiotic response element (XRE), which leads to gene (e.g., CYP 1A1, 1A2) expression modulation and downstream responses (e.g., induction of CYP 1A1 and 1A2) (Birnbaum 1994; DeVito and Birnbaum 1994). This mode of action was supported by the resistance of AhR knockout mice to TCDD-induced toxicity (Fernandez-Salguero *et al.* 1996; Vasquez *et al.* 2003).

Given its high lipophilicity, TCDD is expected to be mainly distributed in the adipose tissue and other fat-rich tissues. However, earlier studies found that the concentration of TCDD in the liver may be higher than in the fat (Gasiewicz *et al.* 1983). Abraham *et al.* (1988) clearly showed that the pattern of TCDD tissue distribution was dose- and time-dependent. The female Wistar rats were given a single dose of TCDD subcutaneously. The liver-to-fat TCDD concentration ratio increased (from 0.74 to 7.7) with the level (from 3 to 3000 ng/kg) of the dose, and decreased roughly exponentially during the 91 days after a given dosing. In addition, binding of TCDD with microsomal protein was observed (Teitelbaum 1978). Therefore, these questions followed: Why is TCDD sequestered in the liver? Does AhR play a role in the sequestration? What is the

contribution of the microsomal protein to the disposition? Does the content of fat in a body affect TCDD distribution in the liver? How doen one quantitatively differentiate the roles of fat content, AhR, and microsomal protein in TCDD disposition? How do other factors impact upon TCDD disposition?

Leung *et al.* (1988; 1989) developed the first TCDD PBPK model in two strains of mice (C57BL/6J, AhR responsive with low body fat content, and DBA/2J, AhR non-responsive with high body fat content) to explore the importance of fat content, AhR, and microsomal protein in TCDD disposition. The uptake of TCDD into the liver was considered a result of solubility and two protein bindings (with AhR and micorsomal protein). Their model exercises suggested that in the C57BL/6J mouse, the binding with microsomal protein was the most important factor; the binding with AhR and fat content had only relatively minor effects. In this model, an unreasonably low rate constant was necessary for the absorption of an intraperitoneal dose, which could be attributed to the omission of induction of microsomal protein. Thus, Leung *et al.* (1990b) conducted an animal study focusing on the impacts of micorsomal protein induction, and they observed that TCDD was indeed sequestered into the liver in the induced rats, but not in the naïve rats. Then Leung *et al.* (1990a) updated their earlier model (Leung *et al.* 1988; Leung *et al.* 1989) by incorporating microsomal protein induction. This updated model simulated successfully not only several sets of liver and fat concentrations but also the data of microsomal protein enzymatic activity. Thereafter, Kohn *et al.* (1993) and Andersen *et al.* (1993) further extended the framework of the Leung *et al.* model (1990a) by including the interaction between TCDD-AhR complex and DREs/XREs.

The microsomal protein was later identified to be CYP 1A2 by experiments (Diliberto *et al.* 1997; Santostefano *et al.* 1996). Based on the experimental and PBPK modeling findings, the mechanism of TCDD disposition in the body can be put together as follows: Once TCDD partitions into a liver cell, it binds with AhR, and the resultant complex is translocated into the nucleus and binds with DREs/XREs. The TCDD-AhR-DRE/XRE complex up-regulates CYP 1A2 gene expression and enlarges the pool of CYP 1A2 protein, which, in turn, binds and sequesters TCDD in the liver. Within a certain range of dose, the expression of CYP 1A2 protein elevates with TCDD dose, and thus the dose-dependent increase in the liver-to-fat concentration ratio follows. As CYP 1A2 protein is degraded over time, the time-dependent decline in the liver-to-fat concentration ratio is also perceptible.

4.3.2. Help identify modes of action of chemicals

PBPK models can provide internal dose metric time courses in the body. The comparison between internal dose metrics with toxic endpoints may help identify modes of action of chemicals. The earlier work by Andersen *et al.* (1987) on methylene chloride convincingly illustrates this point. Methylene chloride is a solvent used in industrial processes. The chronic bioassays on methylene chloride showed remarkable dependence of tumorigenicity on species and exposure route. Significant increases in lung and liver tumors were observed in B6C3F1 mice after chronic inhalation exposure to 2000 or 4000 ppm of methylene chloride (NTP 1986), but not after chronic exposure to 250 mg/kg/day in drinking water (Serota *et al.* 1984). Two metabolic pathways were recognized to be able to generate reactive species. The first is a low affinity, high capacity process

mediated by GST, and the second is a high affinity, low capacity process mediated by CYP450 (primarily CYP 2E1).

Three possible modes of action of the tumorigenicity were speculated: (1) the presence of the parent chemical at the target tissues, (2) the generation of metabolites via the CYP450 pathway, and (3) the generation of metabolites via the GST pathway. The first was rejected because this chemical has a low reactivity. The other two were tested by Andersen *et al.* (1987) using a PBPK model. They selected six potential dose surrogates: the area-under-concentration of the parent compound vs time curve (AUC) in the liver and lung, the metabolite concentration of the CYP450 pathway in the liver and lung, and the metabolite concentration of the GST pathway in the liver and lung. The model-calculated AUCs of the parent chemical and metabolite concentrations of the GST pathway in the liver and lung were correlated well with the tumor incidence data in two mouse bioassays (NTP 1986; Serota *et al.* 1984). Since the parent chemical is not likely to be the active moiety, the reactive product in the GST pathway could be the actual culprit. This conclusion was in line with the contemporary and the later experimental findings.

4.3.3. Facilitate risk assessment

The utility of PBPK modeling in risk assessment relies on its powerful extrapolation across multiple scenarios based on internal dosimetry. Figure 1.3 outlines a generic framework how a PBPK model is applied in risk assessment. Instead of direct extrapolation from animal exposure to human exposure by a body weight-based default method (dashed arrow), a PBPK model calculates the internal dose following exposure in animals. With the critical level of animal internal dose known, the critical level of human

internal dose can be determined (pharmacodynamic extrapolation, beyond the scope of the discussion here). Then the acceptable human exposure can be back calculated from the critical human internal dose level using a human PBPK model. Since the seminal publication on styrene by Ramsey and Andersen (1984), PBPK modeling has been progressively incorporated in the process of risk assessment (Andersen 2003; Bruckner *et al.* 2004; Clewell and Andersen 2004; Clewell *et al.* 2000; Kim *et al.* 2002; Krishnan and Johanson 2005; Reitz *et al.* 1996; Sielken *et al.* 1996; Simmons *et al.* 2005; USEPA 2005a). Indeed, the PBPK models of some chemicals, such as methylene chloride, vinyl chloride, and 2-butoxyethanol, have been used by USEPA in their risk assessment (Clewell *et al.* 2002).

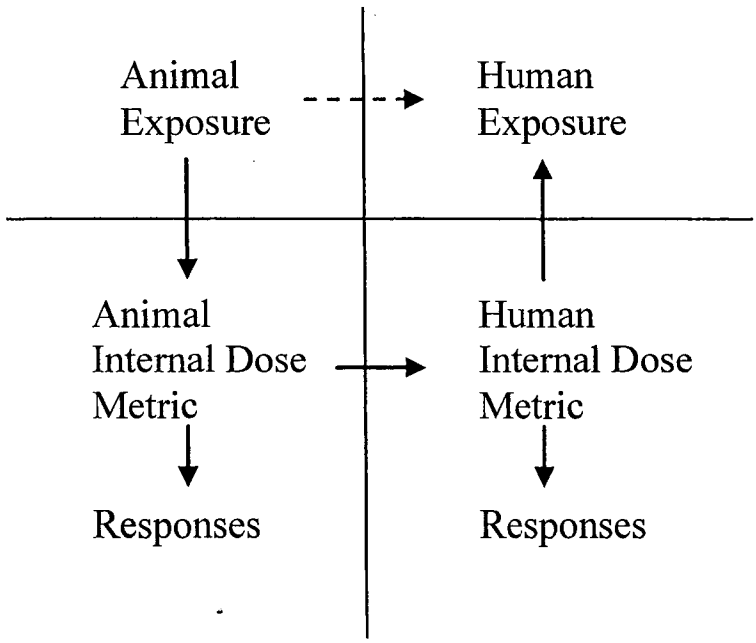

Fig. 1.3. A framework of using PBPK modeling in chemical risk assessment. Instead of direct extrapolation from animal exposure to human exposure based on the default method (dashed arrow), a PBPK model calculates the internal dose following exposure in animals. With the critical level of animal internal dose known, the critical level of human internal dose can be determined. Then the acceptable human exposure can be back calculated from the critical human internal dose level using a human PBPK model.

Although the framework of PBPK application in risk assessment remains consistent over time, for a particular chemical, the PBPK model, along with the model-aided assessment result, may be gradually improved with the acquisition of new data and new techniques in PBPK modeling. One of the notable examples is PBPK-aided risk assessment of methylene chloride. The first model for this chemical was constructed by Andersen *et al.* (1987) which was based on limited information on some parameter values. On the basis of this model, Clewell (1995) and Portier and Kaplan (1989) then explored the distribution of human tumor risk by considering parameter variability using Monte Carlo simulation. El-Marsi *et al.* (1999) updated the dosimetry [DNA-protein cross-link (Casanova *et al.* 1996) instead of GST-mediated metabolite production or amount of the parent compound metabolized] and incorporated the frequencies of GST genotypes in the human population. Jonsson and co-workers (Jonsson 2001; Jonsson and Johanson 2001a, 2003) modified the structures and parameters of the earlier models based on human pharmacokinetic data with the aid of Bayesian analysis. They also included the frequencies of human GST genotypes in their analysis of tumor risk. David *et al.* (2006) later implemented an analysis similar to Jonsson *et al.* (Jonsson 2001; Jonsson and Johanson 2001a, 2003) using a different model structure initially proposed by Sweeney *et al.* (2004). The features of these analyses are listed in Table 1.1. Note that Table 1.1 does not include all the available publications on methylene chloride PBPK modeling. A more comprehensive list, along with the history of PBPK modeling for methylene chloride, up to 2001 has been presented by Reddy *et al.* (2005a).

Table 1.1. Evolution of PBPK-Aided Cancer Risk Assessment for Methylene Chloride

Reference	Analysis features
(Andersen *et al.* 1987)	PBPK models in the mouse, rat, hamster, and human. Structure: fat, rapidly and slowly perfused tissues, gas exchange, liver, and lung, with metabolism pathways in the last two compartments; Appropriate dose surrogates (metabolite concentrations of the GST pathway in the liver and lung) identified; Rough comparison between the conventionally derived and PBPK-aided tumor risks based on the appropriate dose surrogates.
(Portier and Kaplan 1989)	Model structure same as Andersen *et al.* (1987); Monte Carlo simulation performed to understand the effects of variability in parameters on model outputs; Tumor risk estimated by coupling PBPK model with a carcinogenesis model.
(El-Masri *et al.* 1999)	Mouse and human PBPK structure: fat, rapidly and slowly perfused tissues, arterial and venous blood, liver, and lung, with metabolism pathways in the last two compartments; Cancer potency determined in the mouse using PBPK model (internal dosimetry DNA-protein cross-link) and cancer incidence data; Human DNA-protein cross-link production determined by PBPK model with Monte Carlo simulation and consideration of genotypic frequencies of -/- and +/+; Human risk distribution calculated based on the distribution of DNA-protein cross-link production and the cancer potency in the mouse.
(Jonsson 2001; Jonsson and Johanson 2001a, 2003)	Human PBPK structure: adipose tissue, well-perfused tissue, working muscle, resting muscle, liver, and blood & lung, with metabolism pathways in the last two compartments; PBPK model parameters improved by Bayesian analysis and inter- and intraindividual variability in parameters analyzed; Frequencies of GST genotypes (-/-, -/+, and +/+) in the Swedish population incorporated in the Monte Carlo simulation of the PBPK

	model coupled with a cancer risk model.
(Marino *et al.* 2006)	Mouse PBPK structure same as Andersen *et al.* (1987); PBPK model improved by Bayesian analysis updating a limited number of parameters; Internal dose metric in the mouse calculated using the means of the posteriors; Internal dosimetry-cancer incidence modeling formulated for the mouse.
(David *et al.* 2006)	Human PBPK structure: fat, gas exchange, slowly and rapidly perfused tissues, liver, and lung, with metabolism pathways in the last three compartments; a metabolite (carbon monoxide) submodel; PBPK model improved by Bayesian analysis updating a limited number of parameters; Frequencies of GST genotypes (-/-, -/+, and +/+) in the US population incorporated in the Monte Carlo simulation of the PBPK model coupled with a cancer risk model.

Note: This table selectively lists the methylene chloride PBPK model papers where tumor risk in either animals or humans is estimated. It does not include all the available publications on methylene chloride PBPK modeling; such a list, along with the history of PBPK modeling for this chemical, up to 2001 has been presented by Reddy *et al.* (2005a).

5. Two-stage carcinogenesis modeling[2] – describing carcinogenic process

In 1970's, carcinogenesis research was at such a stage that a series of mutations were recognized crucial for tumor development; cell division was found related to carcinogenesis; initiation-promotion experiments had been performed on animals; a great body of epidemiologic data on cancer incidence had been accumulated; and mathematic

[2] There are various carcinogenesis models describing the carcinogenic processes in multiple tissues (e.g., skin, colon, liver) due to several factors. Because of our research interests, the carcinogenesis models and their derivatives reviewed in this section is primarily concentrating on hepatocarcinogenesis and hepatic preneoplastic lesions induced or promoted by exogenous chemicals.

modeling (Armitage and Doll 1954; Cook *et al.* 1969; Day and Brown 1980; Doll and Peto 1978; Hethcote and Knudson 1978; Knudson *et al.* 1975; Knudson and Strong 1972; Manton and Stallard 1980) had been acknowledged as a promising tool for exploring the underlying dynamics of tumorigenesis. Among the then existing mathematic cancer models, the most notable one was established by Armitage and Doll (1954). This model has been widely cited, and is thoroughly reviewed recently (Cogliano *et al.* 1999). In general, the available cancer models at the time had two notable features: (1) the cellular kinetics of the normal susceptible cells and genetically altered cells were not considered; and (2) they were termed "two-stage" or "multistage" models since a tumor was seen as a result of two or more successive, irreversible changes or mutations. A review of all those carcinogenesis models is outside of our intention; a reader who is interested in such reviews may refer to van Leeuwen and Zonneveld (2001), Tan (1991), Kopp-Schneider (Kopp-Schneider 1997), and Cogliano *et al.* (Cogliano *et al.* 1999).

5.1. Moolgavkar-Venzon-Knudson (MVK) model

Given the then understanding in carcinogenesis, Moolgavkar and colleagues in 1970s and 1980s felt that a biologically reasonable cancer model should explicitly incorporate cellular kinetics and contain no more than two stages. The beauty of a model with such features was that it could clarify how cell kinetics affect carcinogenic processes; moreover, the two-stage concept was in line with the postulation of homozygosity development of mutation at a gene locus critical to tumor formation (Moolgavkar 1986). Therefore, Moolgavkar *et al.* proposed their two-stage carcinogenesis model (Fig. 1.4) with consideration of the kinetics of the normal and genetically transited (mutated) cells (Moolgavkar 1983; Moolgavkar *et al.* 1980; Moolgavkar and Knudson 1981;

Moolgavkar and Venzon 1979). This model is referred to as Moolgavkar-Venzon-Knudson (MVK) model in the literature to attribute the credit to Drs. Moolgavkar SH, Venzon DJ, and Knudson AG, Jr.

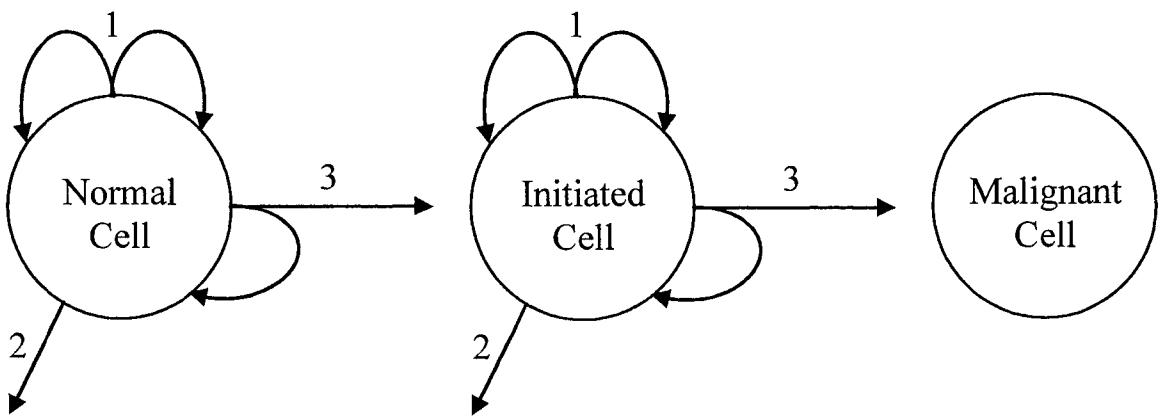

Fig. 1.4. Diagram representation of the Moolgavkar-Venzon-Knudson (MVK) model. A susceptible cell (also termed "stem cell") was at one of three states: normal, initiated, and malignant. A normal or initiated cell was subjected to division into two stem cells without mutation (Event 1), death/differentiation (Event 2), division into two stem cells with one being mutated (Event 3) and the other no change. A malignant cell was committed to develop into a tumor in a fixed time.

The MVK model involves several assumptions that (1) only a subpopulation of cells, termed susceptible cells or stem cells, in a target organ or tissue can give rise to tumors; (2) all susceptible cells behave independently; (3) two successive, irreversible genetic transitions (mutations), generating initiated and malignant cells[3], respectively, are required to form a tumor; (4) mutations only occur during mitosis in a probabilistic fashion (Poisson process); (5) once transformed to the malignant state, a cell gives rise to

[3] Please note that the terms normal, initiated, and malignant cells used in the two-stage carcinogenesis modeling in this review cannot be equated with those in cancer pathology or clinical oncology. In this review, these terms simply describe the three distinct states of cells in the pathway of carcinogenesis.

a tumor with a probability of 1; and (6) the time of a malignant cell reaching clinically detectable size is a constant. The last two assumptions were later lifted in some modified versions of the MVK model by explicitly considering the stochastic growth kinetics of malignant cells (Dewanji *et al.* 1991; Luebeck and Moolgavkar 1994).

In the MVK models, a susceptible cell was in one of three states: normal, initiated, and malignant (or transformed) (Fig. 1.4). A normal cell could divide into two normal cells with a rate of α_1, die or differentiate (these two pathways not distinguished because both left the pool of susceptible cells) with a rate of β_1, or divide into a normal and an initiated cell with a mutation rate of μ_1. The generation of initiated cells followed a Poisson process. An initiated cell underwent the same pathways except that the mutation during mitosis produced a malignant cell; the corresponding parameters were α_2, β_2, and μ_2. Once generated, a malignant cell was to develop into a tumor with a probability of 1 in a certain time. For the ease of mathematic computation, the behaviors of normal cells were described deterministically because the number of normal cells was large and under homeostatic control; the growth of initiated cells were treated as a stochastic birth-and-death process.

The mathematic derivation of the MVK model, as well as the others discussed below, involved profound knowledge of probability that is usually beyond the statistical expertise of biologists. Thus, the details of the probabilistic derivation are not elaborated here. It is assumed that the numbers of normal, initiated, and malignant cells at time t are X(t), Z(t), and W(t), and that μ_1, μ_2, α_2, and β_2 remain constant over time. Through probabilistic reasoning, the incidence (or hazard) function I(t), representing the instantaneous rate at which tumors appear in a previously tumor-free tissue, is obtained:

$$I(t) = \mu_2 E[Z(t) \mid W(t) = 0] \qquad \text{(Eq-10)}$$

where E[Z(t)|W(t)=0] is the expected number of initiated cells conditional on no malignant cell at time t. Since cancer is a rare disease in a young and healthy human population, it is reasonable to assume that μ_2 is close to zero (*i.e.*, the probability of there being a malignant cell at time t is near zero). Then $E[Z(t)|W(t)=0] \approx E[Z(t)]$, and Eq-10 is approximated to

$$I(t) = \mu_1 \mu_2 \int_0^t X(s) \exp[(\alpha_2 - \beta_2)(t-s)] ds \qquad \text{(Eq-11)}$$

where s is a variable representing time. Therefore, the age-specific incidence rate at age t per 10^5 individuals in a human population predicted by the model is $I(t) \times 10^5$. At a certain age, the magnitude of the incidence function is dependent on μ_1, μ_2, α_2, β_2, and the number of normal stem cells. As the latter is assumed to be a constant or is calculated by a deterministic function, it is not included in parameter estimation. During the model exercises, Moolgavkar *et al.* determined the product $\mu_1\mu_2$ and the net growth rate of initiated cells (α_2-β_2) instead of the individual parameters (Moolgavkar *et al.* 1980; Moolgavkar and Knudson 1981) for convenience. Given constant μ_1 and μ_2, the shape of the predicted incidence rate is entirely governed by the growth curve of normal cells [X(s)] and the kinetics of the initiated cells (α_2-β_2) (Moolgavkar *et al.* 1980). It should be reiterated here that the parameters μ_1, μ_2, α_2, and β_2 are constant over time. In order to accommodate the effects of environmental factors that influence those parameters, Eq-11 has to be adjusted (Moolgavkar *et al.* 1980).

From Eq-11, one can envision how an internal or external factor affects the magnitude and shape of the age-specific incidence rate. Moolgavkar *et al.* (Moolgavkar 1986; Moolgavkar and Knudson 1981) suggested that a carcinogenic factor can increase

the incidence rate by either or both of two ways: (1) induction of mutation (*i.e.*, increase in μ_1); (2) increase in proliferation of normal or initiated cells [*i.e.*, increase in X(s) or $(\alpha_2-\beta_2)$]. The modes of action of experimentally defined "initiators" and "promoters" are readily explained here (Moolgavkar 1983). An initiator, usually genotoxic, causes mutation in a gene locus critical to cancer development, and thus increases μ_1. This effect influences the incidence rate in magnitude only. In a population exposed to a given dose of an initiator, the cancer risk is higher than that in the nonexposed by a constant fold regardless of time as long as μ_1 is linear with dose. Termination of the initiator exposure leads to a risk between the exposed and the nonexposed because initiated cells are already built up during initiation. A promoter, however, increases α_2, decreases β_2, or does both, resulting in net increase in $(\alpha_2-\beta_2)$, which causes proliferation of the initiated cells and hence a higher probability of the occurrence of malignant cells. As $(\alpha_2-\beta_2)$ is strongly modified by time, a small change in $(\alpha_2-\beta_2)$ may bring forth a dramatic change in the incidence rate as time goes on (Moolgavkar and Knudson 1981). If the exposure to a promoter is stopped, the resultant risk is also between the risks of the exposed and the nonexposed. As for the physiologic factors (e.g., hormones) that affect normal cell growth curves of tissues or organs [X(s)], their impacts on the incidence rate are also perceivable.

The MVK models satisfactorily simulated multiple epidemiologic data sets of lung cancer (Moolgavkar and Knudson 1981) and female breast cancer (Moolgavkar *et al.* 1980; Moolgavkar and Knudson 1981) with reasonable parameter adjustments. Furthermore, they provided biologically plausible explanations to the modifying effects of menarche, menopause, and pregnancy on female breast cancer incidence, and of

smoking and smoking abstinence on lung cancer. The model also suggested pathogenetic similarity between hereditary and sporadic tumors (Moolgavkar and Knudson 1981). In essence, the MVK model serves as a unifying tool for interpreting carcinogenic processes under various circumstances.

The incidence function I(t) in Eq-11 holds the assumption that μ_2 is very small. In some cases, e.g., animal cancer studies, this assumption is likely invalid. The inadequacy of the approximation based on this assumption was examined (Moolgavkar *et al.* 1988). To relax this assumption, Moolgavkar *et al.* (Moolgavkar *et al.* 1988; Moolgavkar and Luebeck 1990) presented the exact solution of I(t)

$$I(t) = \mu_2 \int_0^t \mu_1(s) X(s) \times \left(\exp\{ \int_0^{t-s} [2\alpha_2 \Phi(1,0;u) - (\alpha_2 + \beta_2 + \mu_2)] du \} \right) ds \quad \text{(Eq-12)}$$

where $\Phi(1,0;u)$ represents the probability that there is no malignant cell at time u starting with one initiated cell at time 0. Note that here μ_1 varies with time and hence the original assumption of constant μ_1 is relaxed. Eq-12 clearly indicates that α_2 and β_2, rather than their difference, are both important. By holding (α_2-β_2) and μ_2/α_2 (approximate rate of mutation to malignancy per division of initiated cell) constant, the incidence rate increases quickly with increasing α_2; but eventually the magnitude of the rate is reversely related to α_2 (Moolgavkar *et al.* 1988). The latter statement is somewhat contrary to intuition because β_2 increases concurrently with α_2 thereby provided a constant (α_2-β_2). In other words, while the initiated cells are stimulated to proliferation, they are also prone to extinction. In the same paper (Moolgavkar *et al.* 1988), the authors also pointed out computational difficulty in incorporating time-dependency of α_2 and β_2.

5.2. Cohen-Ellwein-Greenfield (CEG) model

Drs. Cohen, SM, Ellwein, LB, and Greenfield, RE (Cohen and Ellwein 1990a, b, 1995a; Ellwein and Cohen 1992; Greenfield *et al.* 1984) constructed another carcinogenesis model (Fig. 1.5), also based on the two-stage theory, henceforth called Cohen-Ellwein-Greenfield (CEG) model for convenience. With the aid of the CEG model, Cohen *et al.* intended to enhance the understanding of the carcinogenic process and to provide insights into the issue - how cell proliferation and genotoxic effects are related to tumor formation. The major assumptions of the CEG model were that (1) only a subpopulation of cells, *i.e.*, stem cells, in a target organ can give rise to tumors; (2) all the susceptible cells behave independently; (3) two successive irreversible mutations are required to form a tumor; and (4) the mutations only occur during mitosis in a probabilistic fashion (Cohen and Ellwein 1988; Greenfield *et al.* 1984).

In the CEG model, the stem cells could be in one of three states, normal, initiated (intermediate), and transformed (malignant), with the cellular kinetics of each state being considered. During a small time interval, the stem cells in the first two states were subjected to one of six events: death, mitosis forming two genetically unchanged stem cells, mitosis forming a mutated stem cell and an unchanged stem cell, mitosis forming an unchanged stem cell and a committed (differentiated) cell, mitosis forming a committed cell and a mutated stem cell, and no change (Fig. 1.5). As the transformed stem cells would not have further mutation, they could divide with or without differentiation, die, or stay unchanged. Note that here death was separated from differentiation.

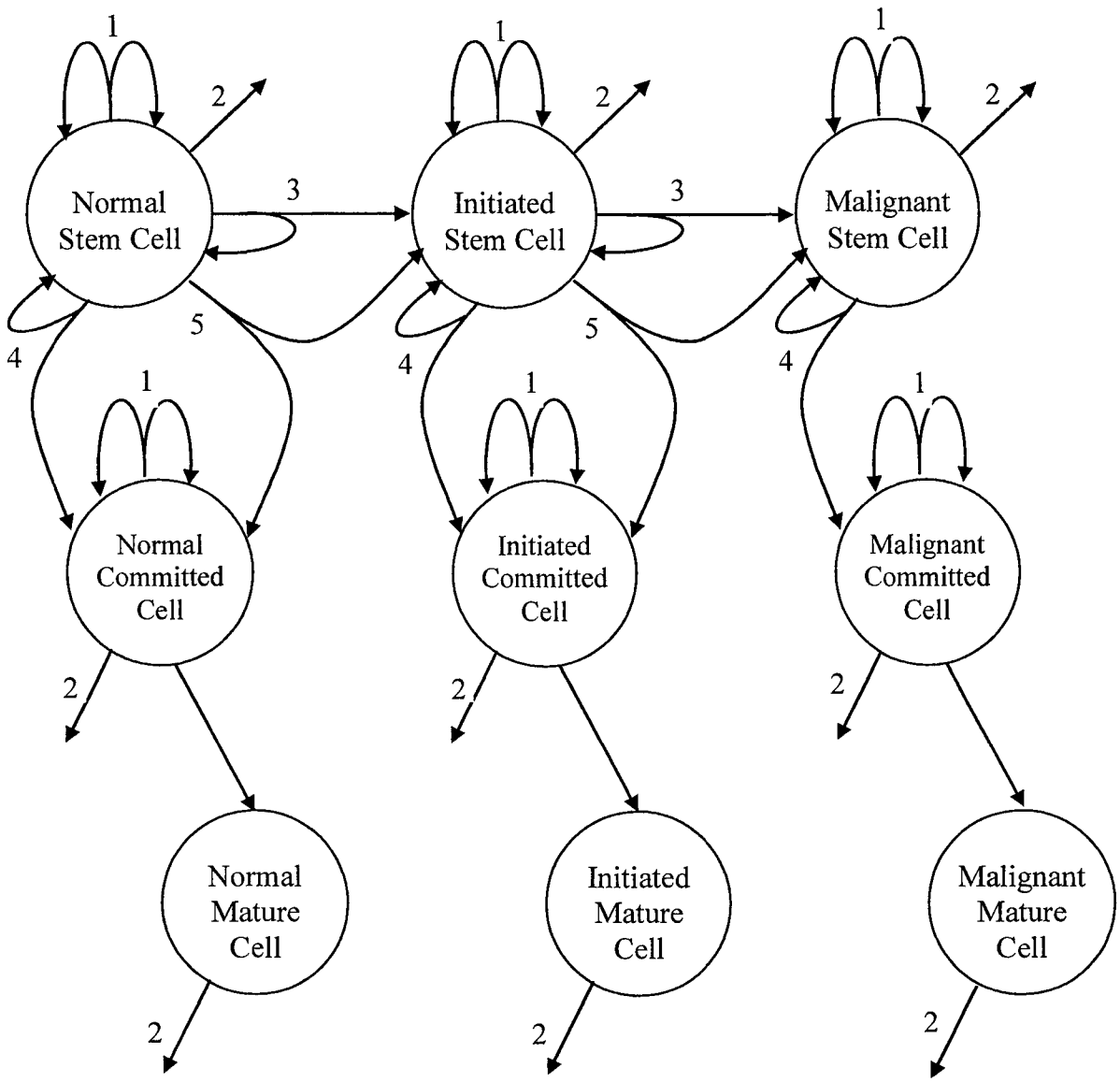

Fig. 1.5. Diagram representation of the Cohen-Ellwein-Greenfield (CEG) model. A stem cell was at one of three states: normal, initiated, and malignant. A normal or initiated cell is subjected to division into two stem cells without mutation (Event 1), death (Event 2), division into two stem cells with one being mutated (Event 3), division into one stem cell and one committed cell (Event 4), division into one mutated stem cell and one committed cell (Event 5), and no change. A malignant stem cell is subjected to the same events except 3 and 5 (*i.e.*, no further mutation). A stem cell at any state may be differentiated into a committed and then a mature cell. This model is distinct from the MVK model in two aspects: (1) the differentiation is separated from death, and (2) the kinetics of the malignant stem cells is described.

With the parameters of mitotic rate, mutation probabilities, death rate, and stem cell birth probability being assigned with appropriate values, the probability of the occurrence of each event was calculable. Through probabilistic derivations different from those in the MVK model (Moolgavkar 1983; Moolgavkar *et al.* 1980; Moolgavkar and Knudson 1981; Moolgavkar and Venzon 1979), the mean time of the occurrence of the first transformed stem cell, the expected number of foci, the probability of tumor formation, and the incidence of visible tumors in a group of animals at a given time point could be obtained. The derivation indicated that the relationship between tumor incidence and pertinent parameters was apparently non-linear (Greenfield *et al.* 1984). This model only predicted the average behavior of a carcinogenic process; the stochasticity was not considered. As Moolgavkar noted (1993), "[Cohen *et al.*] approach does not take into account the stochastic nature of clonal growth but substitutes for the stochastic birth-and-death process a deterministic recursion formula that computes the expected clones size."

Due to animal growth, chemical treatments, suspensions of chemical exposures, or other external manipulations (e.g., two-thirds partial hepatectomy), the critical model parameters, mainly tissue stem cell number, rates of stem cell mitosis, differentiation, and death, and mutation probability, inevitably fluctuate over time. The incorporation of these fluctuations in the modeling is necessary to reflect the biological and/or experimental reality; however, it considerably complicates the computation of the analytic derivations, which was noted by Moolgavkar *et al.* (Moolgavkar 1983; Moolgavkar *et al.* 1980; Moolgavkar and Knudson 1981; Moolgavkar and Venzon 1979). Therefore, Cohen and Ellwein (1990a) characterized the tumorigenic continuum as a discrete-time Markov process where the time axis was divided into a series of small time intervals. The

simulation was implemented recursively. At the very beginning, the simulation program started calculating the numbers of stem cells in all three states until the end of the first time interval; these results were then utilized as the variable inputs for the calculations in the second interval, and likewise the results of the second interval became the inputs of the third interval, and so on. Meanwhile, model parameters were allowed to change, if necessary, between but not within the intervals. With such a manner, the simulation advanced to a desired time point such as experimental termination or animal death. This strategy was later adapted by Conolly and Kimbell (1994) and Ou *et al.* (2003; 2001).

While the total number and mitotic rate of stem cells are typically available from animal studies, numerous parameters, such as probabilities of mutations from normal to intermediate and from intermediate to transformed stem cells and rates of stem cell birth and death, have to be inferred from comparison of model predictions with experimental data. The procedure of this model calibration was detailed by Ellwein and Cohen (1992). With simulation onset at a week or more prior to birth when all stem cells were assumed normal, the calibration started in the control group with a reproduction of the development of the target organ, which determined the rates of stem cell birth and death. Then the mutation probabilities and the rates of birth and death of the mutated cells were adjusted to match the predicted tumor probability with the observed cumulative tumor incidence in the control group. The calibration in the treated groups followed the similar procedure with parameters being adjusted according to biological hypotheses. As the particular recursive simulation approach precluded statistical optimization, the model calibration relied on biological plausibility, scientific judgments, and subjective comparisons (Ellwein and Cohen 1992).

Utilizing this model, Cohen, Ellwein, and Greenfield have quantitatively analyzed the tumorigenesis data in the laboratory rodents induced by multiple regimens of genotoxic chemicals, N-[4-(5-nitro-2-furyl)-2-thiazolyl]formamide (FANFT) (Cohen and Ellwein 1988; Greenfield *et al.* 1984) and 2-AAF (Cohen and Ellwein 1990a, b), and a non-genotoxic chemical, sodium saccharin (Cohen and Ellwein 1988, 1990a, 1995a; Ellwein and Cohen 1988; Greenfield *et al.* 1984). The distinct time-dose-response (tumor incidence) relationships of those chemicals (Arnold *et al.* 1980; Cohen *et al.* 1979; Frith *et al.* 1980a; Frith *et al.* 1986; Frith *et al.* 1980b; Gaylor 1980; Jacobs *et al.* 1977; Littlefield *et al.* 1980; Nakanishi *et al.* 1980; Schoenig *et al.* 1985) could not be explained by experimental data *per se*; however, they were amenably explained by the modeling exercises that suggested potential modes of action by which the chemicals exert their tumorigenic effects. Here we briefly introduce the cases of 2-AAF and sodium saccharin.

5.2.1. Exploring the modes of action of 2-AAF induced liver and urinary bladder tumors in mice

In the ED_{01} study (Frith *et al.* 1980a; Frith *et al.* 1980b; Gaylor 1980; Littlefield *et al.* 1980) performed at the National Center for Toxicology Research, 2-AAF (30-150 ppm in diet) was administered in multiple regimens to over 24,000 female BALB/c mice up to 33 months. The two major endpoints were liver and urinary bladder neoplasms. The dose-tumor response relationship in the liver was apparently linear, whereas that in the urinary bladder was obviously nonlinear with a "no-observed effect level". When time was taken into account, the bladder tumors appeared earlier and depended on the continuous presence of the exposure; the liver tumors, however, appeared very late and did not

require the continuous presence of the exposure (Cohen and Ellwein 1990b; Littlefield *et al.* 1980).

These interesting observations were not explainable from only the perspective of metabolism saturation or DNA adduct formation (Cohen and Ellwein 1995b). Cohen and Ellwein (1990b) reproduced these observations using the CEG model by manipulating some mutation and cell kinetics-related parameters. Their quantitative analyses suggested that at the given doses, 2-AAF in the liver only elevates the initiation probability and does not affect the cell kinetic parameters and transformation probability. Since the effect of 2-AAF on the initiation probability is linear with dose, the predicted liver tumor incidence was also linear with dose as observed. In contrast, in the urinary bladder, 2-AAF affects not only initiation and transformation probabilities, but also the bladder cell kinetic parameters given the dose higher than 60 ppm. Thus, the bladder tumor occurrence is a result of the interaction between the linear effects on mutations and the nonlinear effects on cell kinetics. Consequently a nonlinear dose-response relationship is warranted. Furthermore, Cohen and Ellwein (1990b) explored how tumor incidence was influenced by the effects of 2-AAF on mutations and cell kinetics individually, independently and interactively. They pointed out that there is strong synergism between the two kinds of effects during urinary bladder tumorigenesis.

5.2.2. Exploring the mode of action of sodium saccharin induced urinary bladder tumors in rats

Sodium saccharin increased the incidence of urinary bladder tumors in the rats when administered at a high dose (5% in diet) to rats starting prior to or at birth and continuing for a lifetime (Schoenig *et al.* 1985). If sodium saccharin was given at 6 weeks of age or

later, such an effect was not observed (Schoenig *et al.* 1985). But if the sodium saccharin exposure was preceded with treatment of initiators (e.g. FANFT) or freeze ulceration at 5-10 weeks of age, there was also increased incidence of urinary bladder tumors (Cohen *et al.* 1979; Cohen and Ellwein 1995a). In all studies, male rats were more susceptible than female rats, and the effect was not evident in other species (Fukushima *et al.* 1983). Sodium saccharin is not genotoxic (Kramers 1975), is not metabolized to a reactive form, and does not interact with DNA (Lutz and Schlatter 1977). However, it does cause bladder cell proliferation (Fukushima and Cohen 1980). Thus it is likely that sodium saccharin elicits tumorigenesis through its proliferative effects. The simulations of the CEG model supported this hypothesis (Cohen and Ellwein 1990a; Ellwein and Cohen 1988). From the modeling exercise, along with existing biologic evidence, Cohen and Ellwein put forth the mode of action of sodium saccharin: the increased concentration of sodium ion in urine and the elevated pH of urine facilitate saccharin precipitation in the urinary bladder, and the precipitate damages epithelial cells and causes regenerative proliferation. The abundance of protein in male rat urine further enhances the precipitation, explaining the remarkable susceptibility of male rats. This mode of action is not likely to occur in humans at the normal uptake level, and thus the tumorigenic risk in humans due to exposure to sodium saccharin is minimal (Olin *et al.* 1995).

5.3. Preneoplastic foci (clonal growth) model – a derivative of the MVK model

5.3.1. Values of preneoplastic foci in carcinogenesis

Focal cellular alterations in the liver were observed experimentally as early as 1960's (Pitot 1990). The foci were identified and classified according to various markers, including morphologic features (e.g., basophilic-cell foci, clear-cell foci) (Squire and

Levitt 1975; Ward 1981) and enzymatic alterations manifested by histochemical staining [e.g., ATPase-deficient foci (Laib *et al.* 1982), glucose-6-phosphate dehydrogenase (Moore *et al.* 1986), γ-glutamylpeptidase foci (Pitot *et al.* 1978), GST-P foci (Tatematsu *et al.* 1987)]. Among all the markers, GST-P has been recognized as the ideal one because of its sharp demarcation and persistence (Tatematsu *et al.* 1988). The role of preneoplastic foci as potential precursors of tumors has been firmly established (Bannasch 1986; Ito *et al.* 2003; Kitagawa and Sugano 1978; Ogiso *et al.* 1990; Pitot *et al.* 1978; Tsuda *et al.* 2003; Watanabe and Williams 1978). A certain portion of foci could eventually become tumors given enough time.

Due to the value of preneoplastic foci as markers of carcinogenesis, various short- and medium-term experimental protocols have been proposed to study the evolution of chemically induced and/or promoted foci (Goldsworthy *et al.* 1986; Shirai *et al.* 1999; Tsuda *et al.* 1999). With the intensive utilization of these protocols, a plethora of data has been accumulated. A set of foci formation data generally includes the number, size, and size distribution of foci. Different from dichotomous data of tumor occurrence (*i.e.*, whether or not tumors are present), foci data contain more information (Kopp-Schneider 2003) and provide insights into modes of action of carcinogens. Therefore, foci data should be subjected to thorough examination.

5.3.2. Issues related to preneoplastic foci modeling

A preneoplastic foci model describes foci formation in a tissue (liver in many cases) by continuously updating the number of initiated cells in each focus and yields 3-dimensional (3D) data over time. Experimental data on foci formation are obtained from microscopic examination of tissue slides. This method has a detection limit (*i.e.*, a

threshold size below which foci can not be identified reliably) and generates only 2-dimensional (2D) data. To transform these laboratory data into useful modeling data, three issues must be addressed:

(1) *2D-3D conversion.* This conversion involves stereologic methods. Two methods, based on different rationales, have been applied in preneoplastic foci modeling. One was developed by Xu *et al.* (Campbell *et al.* 1986; Xu *et al.* 1998; Xu and Pitot 2003) at the McArdle Laboratory for Cancer Research at the University of Wisconsin at Madison, and the other by Moolgavkar, Luebeck, and their colleagues (De Gunst and Luebeck 1994; de Gunst and Luebeck 1998; Luebeck and Moolgavkar 1991; Moolgavkar *et al.* 1990) at the Fred Hutchinson Cancer Research Center, Seattle, Washington. The underlying theories of these methods have been introduced in the publications by the two groups;

(2) *Detection limit.* A preneoplastic focus can be reliably detected no less than a certain size (e.g., 2 cells for GST-P staining in our laboratory); depending on foci markers, the detection limit may vary. Upon slide examination, a detection limit should be defined and converted into an appropriate measure during modeling;

(3) *Cell number-volume conversion.* The preneoplastic foci model algorithm tracks each focus in terms of its cell number. When a 2D measure is expressed in terms of area and then transformed into volume, a conversion between cell number and volume is necessary for comparison of these two kinds of data. Approximately, cell number can be related to volume through a factor of hepatocyte numerical density, *i.e.*, number of cell per unit volume.

5.3.3. Simulating preneoplastic foci

To interpret and utilize the foci data, several models have been developed. Within the framework of the two-stage MVK model, these foci models are particularly focused on the first stage, from normal to initiated cells. They will be named clonal growth models henceforth, acknowledging the fact that foci are the result of the clonal growth/expansion of single initiated cells. Note that, in a clonal growth model, an initiated cell is not necessarily equivalent to a mutated cell. Rather, it may be a result of epigenic changes (Higashi *et al.* 2004; Satoh and Hatayama 2002). Therefore, in this section, the term *initiation* or *mutation* shall carry the meaning of *any alterations, either genetic or epigenetic, that lead to a detectable phenotype.*

5.3.3.1. Early clonal growth modeling by Moolgavkar et al.

One of the earliest clonal growth models was reported by Dewanji *et al.* (1989). They derived variables characterizing the growth of foci based on analytical solutions for both nonextinct (including nondetectable and detectable) foci and detectable foci. The "detectable foci" is differentiated from the "nonextinct foci" here because only the development of the former is experimentally measurable.

5.3.3.1.1. Variables characterizing nonextinct foci formation

Among all quantities generated by Dewanji *et al.* (1989), the probability of extinction, the expected number and size, and the distribution of sizes of foci are of special interest. The first quantity gives a sense of the destiny of initiated cells. The other three outline growth characteristics of the initiated cells.

With the same denotations for the parameters in the MVK model discussed earlier (Section 5.1) and the assumption that α_2 and β_2 are time independent, the extinction

probability at time t starting from time s with one initiated cell [p(t,s)] can be expressed as

$$p(t,s) = p(t-s) = \begin{cases} \dfrac{\beta_2 - \beta_2 e^{-(\alpha_2-\beta_2)(t-s)}}{\alpha_2 - \beta_2 e^{-(\alpha_2-\beta_2)(t-s)}}, & if\ \alpha_2 \neq \beta_2 \\ \dfrac{\alpha_2(t-s)}{1+\alpha_2(t-s)}, & if\ \alpha_2 = \beta_2 \end{cases} \qquad \text{(Eq-13)}$$

When t approaches ∞, the extinction probability converges to β_2/α_2 or 1 depending on $\alpha_2 > \beta_2$ or $\alpha_2 \leq \beta_2$. In other words, in an infinite time, if the division rate is higher than the death rate, the extinction probability approaches to an asymptote β_2/α_2; if the division rate is equal to or less than the death rate, initiated cells are certainly to become extinct.

The expected total number of initiated cells in all nonextinct foci at time t, E(t), is

$$E(t) = \int_0^t \mu_1(s)X(s)\exp[(\alpha_2 - \beta_2)(t-s)]ds \qquad \text{(Eq-14).}$$

Eq-14 shows that E(t), also representing the total size of all foci, is controlled only by $(\alpha_2-\beta_2)$ at a given time. If $(\alpha_2-\beta_2)$ is held constant, the total size of all foci remains fixed regardless of the value of α_2.

The expected number of nonextinct foci, N(t), is a function of α_2 and β_2 where both parameters, instead of their difference, are important. When time approaches ∞, N(t) diverges to infinity with $\alpha_2 \geq \beta_2$; if $\alpha_2 < \beta_2$, then N(t) approaches to an asymptote. At a given time if $(\alpha_2-\beta_2)$ is fixed, N(t) decreases with increasing α_2. The reason is that when α_2 increases, β_2 also does so due to the constant difference, which leads to higher extinction.

The distribution of sizes of all nonextinct foci is determined by a geometric function. The expected size, in terms of cell number, of a focus equals the expected number of cells in all nonextinct foci divided by the expected number of all nonextinct foci, E(t)/N(t).

When (α_2-β_2) is constant at a given time, an increase in α_2 causes larger expected size of a focus because N(t) is reduced and E(t) is fixed anyway. From these deductions, promoters can be categorized into two groups by their effects on α_2 and β_2 even if they do not alter (α_2-β_2). Exposure to a promoter that strongly elevates α_2 yields a small number of large foci, whereas exposure to a promoter that reduces β_2 but has minimal effect on α_2 yields a large number of small foci. These two scenarios have been observed experimentally (Schwarz *et al.* 1984).

5.3.3.1.2. Variables characterizing detectable foci formation

For detectable foci formation, Dewanji *et al.* (1989) derived such quantities as the probability of being undetectable and the expected number and size of detectable foci, following a similar method as that for nonextinct foci. Different from the extinction probability, the probability of being undetectable is a function increasing or decreasing with time, depending on the threshold size. However, this probability always converges to the limit of the extinction probability. The relationships between α_2 and the number and size of nonextinct foci discussed above also hold for detectable foci. Through the number, size, and distribution of sizes of detectable foci, the model can be tested against experimental observations.

The Dewanji *et al.* (1989) paper is a pure theoretic presentation. Based on that work, Moolgavkar *et al.* (1990) simulated the result of hepatic ATPase-deficient foci in the rats following continuous exposure to N-nitrosomorpholine at various doses via drinking water. The main parameters in the model were μ_1, α_2, and β_2. They were assumed to be time independent and dose-related. Besides, β_2/α_2 was assumed constant in all dose groups. As long as the size of a focus is in the range of 60 to 500 μm in radii, α_2 and β_2

were presumably not affected by the size of a focus. Using the maximum likelihood method, Moolgavkar *et al.* estimated $\mu_1 X$, α_2-β_2, and β_2/α_2 rather than the individual parameters for ease of parameterization. The calculation was performed for a volume of 1 mm^3 rather than the whole liver, and hence the X here represents the number of normal susceptible cells in 1 mm^3 liver. In addition to reproducing the data, the modeling of Moolgavkar *et al.* indicated that only a small fraction (less than 10%) of initiated cells could develop into foci and that the foci shifted to larger sizes with increasing dose. Their results confirm the importance of apoptosis in the kinetics of initiated cells (Columbano *et al.* 1984; Schulte-Hermann *et al.* 1990). Assuming $\mu_1 X$ and (α_2-β_2) being linearly related to dose, Moolgavkar *et al.* (1990) proposed these indices as potencies for carcinogen initiation and promotion. In the same paper (Moolgavkar *et al.* 1990), the limitations in the indices as well as the issues in parameterization were discussed. Luebeck *et al.* (1991) analyzed the data from a different experiment using a similar method and presented similar findings.

5.3.3.2. Clonal growth modeling incorporating more biologic information

5.3.3.2.1. Less-than-exponential growth kinetics of initiated cells

In the early clonal growth models, the growth of initiated cells was assumed to be exponential (Dewanji *et al.* 1989; Moolgavkar *et al.* 1990). This assumption was found not biologically plausible (Bogen 1989; Buchmann *et al.* 1994; Schulte-Hermann *et al.* 1990); rather, a less-than-exponential growth is considered more likely due to heterogeneity in cellular kinetics. This heterogeneity is reflected in two aspects: (1) The growth rate of a focus is dependent on its size, and (2) The growth rate within a focus is heterogeneous with the highest growth at the focal surface (Buchmann *et al.* 1994). These

points were demonstrated by a number of laboratories. Buchmann *et al.* (1994) found that 5-bromo-2'-deoxyuridine (BrdU) incorporation, an index of DNA replication, in focal nuclei in both control and TCDD-treated rats, was dependent on focal size. Grasl-Kraupp *et al.* (2000) reported that GST-P single cells induced by N-nitrosomorpholine had lower replication than the cells in multicellular foci. Krutovskikh (2002) proposed a GJIC-mediated mechanism in the cellular kinetic heterogeneity. Further, Bogen (1989) argued that initiated cells were likely to grow in a much more restricted fashion due to direct or indirect controls on proliferation by surrounding cells, as well as by intraclonal gradients of growth factor molecules. Based on the above discussion, it appears that a geometric function is more desirable than an exponential one for describing the proliferation of initiated cells (Bogen 1989).

Luebeck *et al.* (1991) incorporated the idea of less-than-exponential growth in his modeling of foci promoted by polychlorinated biphenyls (PCBs) or other chemicals. The parameters α_2 and β_2 were modified by time so that the mean growth of foci was Gompertz-like (subexponential) rather than exponential. Moolgavkar *et al.* (Luebeck *et al.* 1995; Moolgavkar *et al.* 1996) further tested the effect of size on foci expansion using their model. Two kinetic scenarios were considered:

(a) Volume growth: All cells in a focus were kinetically homogeneous and actively undergoing mitosis; and

(b) Surface growth: Only a fraction of cells, preferentially on the surface, in a focus, was actively undergoing mitosis.

Quantitative analyses on the data of foci promoted by phenobarbital, α-hexachlorocyclohexane (Luebeck *et al.* 1995), TCDD, and 1,2,3,4,6,7,8-

heptachlorodibenzo-*p*-dioxin (Moolgavkar *et al.* 1996) indicated that the surface growth postulation described the data better than the volume growth postulation; this conclusion lent support to the less-than-exponential assumption.

Inspired by the foregoing discussion on focal size- and cell kinetics-related clonal growth, we (Lu *et al.* 2006a) categorized GST-P foci, promoted by the mixture of HCB and PCB 126 in the rat, into single cells, mini- (2-11 cells), medium- (12-399 cells), and large-foci (>399 cells), and assigned distinct division and death rate constants to each group of foci. This strategy turns out to be a good one as the modeling results simulated the number, total size, and size distribution data well. We also found that the effects of the mixture dose on the division and death rate constants were not always consistent and apparently dependent on focal size and time.

5.3.3.2.2. Two-cell hypothesis

The cells initiated by genotoxic agents were assumed to have the same phenotypic characteristics (hence the name *one-cell*) in the early clonal growth models (Conolly and Kimbell 1994; Luebeck *et al.* 1995; Moolgavkar *et al.* 1990; Portier *et al.* 1994). One of the consequences of this assumption is the speculation (Portier *et al.* 1994) that TCDD might have initiation activity. This speculation is not supported by experimental evidence (Conolly and Andersen 1997). Several other lines of evidence against the one-cell assumption have been accumulated. More than one form of DNA adducts with different persistence were identified in the initiated cell pool induced by DEN (O^6-alkylguanine adduct with short half life, O^2- and O^4-ethylthimidine adduct with longer half lives) (Dragan *et al.* 1994; Swenberg *et al.* 1984). Yusuf (1999) observed discrepant responses of foci to the same chemical selective pressures. Moreover, the multiple studies (Lu *et al.*

2006a; Ou *et al.* 2001; Thomas *et al.* 2000) using the modified Ito's protocol in our laboratory consistently revealed a pattern of divergent evolution in foci number and volume (*i.e.*, decrease in foci number vs increase in volume in the late period of the protocol). These studies imply that there could be more than one type of initiated cells. Conolly and Andersen (1997) first incorporated in their model the hypothesis that the initiated cell pool could be composed of two types of subpopulations with different phenotypes (hence the name *two-cell*). They labeled the subpopulations as A and B cells, with A cells being responsive to and B cells resistant to homeostatic controls or chemical mitoinhibitory selective pressures. With the inclusion of this hypothesis, Conolly and Andersen (1997) satisfactorily simulated the data of foci promoted by TCDD without presuming TCDD initiation activity. This hypothesis was later substantiated by more modeling work (Haag-Gronlund *et al.* 2000; Lu *et al.* 2006a; Ou *et al.* 2003; Ou *et al.* 2001; Thomas *et al.* 2000).

5.4. Statistical issues in the two-stage carcinogenesis modeling

Some critical parameters in biologically based two-stage carcinogenesis models are not readily measured and have to be estimated through statistical optimization against tumor incidence or prevalence data from long-term animal experiments or epidemiologic studies. Although adequate fitting of available data has been repeatedly obtained, statistical issues in the modeling and parameter estimation deserve attentions, especially when the model is applied in cancer risk assessment. Wosniok *et al.* (1999) and Portier *et al.* (Portier and el Masri 1997; Portier 1987; Portier 1995), along with other investigators, have explored in this field. According to their analyses, the statistical issues identified thus far are as follows:

(1) Problem in experimental data.

In long-term studies, some animals may die before the end of the studies due to reasons either related or not related to tumor occurrence. This problem affects tumor data interpretation and parameterization in a model using the data;

(2) Parameter nonidentifiability.

If a model has the form of Eq-11 in Section 5.1, the parameters μ_1, μ_2, α_2, and β_2 cannot be defined separately; rather, only $\mu_1 \times \mu_2$ and $\alpha_2 - \beta_2$ can be determined. Thus, there could be infinite combinations of these four parameters that fit data equally well, which is known as parameter nonidentifiability;

(3) Parameter nonestimability.

Portier and El-Masri (1997) found that a maximum likelihood function may have multiple peaks or an extremely flat region that prevents a computer algorithm from converging at the optimal point, which results in the situation that statistically best parameters cannot be estimated;

(4) Model nondifferentiability.

Model selection is typically based on goodness-of-fit testing; the better a model fits the data, the higher preference the model receives. In comparing the two-stage model to the Armitage-Doll multistage model, it has been observed that the same data can be simulated by these two kinds of models equally well, or by neither. Hence, the preference of either model cannot be differentiated. To solve these issues, sound statistical methods must be developed. The promising applications of biologically based carcinogenesis models in risk assessment warrant further study on these issues.

6. Integration of PBPK and carcinogenesis modeling in cancer risk assessment

In risk assessment, dose-response relationship is a crucial piece of information. Earlier, the dose-response relationship was usually analyzed solely based on information on exposure and response without knowing the modes of action/mechanisms of chemical pharmacokinetic behaviors and the toxic effects. Lying between the "dose" and "response" were two black boxes related to pharmacokinetic and pharmacodynamic modes of action/mechanisms. The research and applications of PBPK and carcinogenesis modeling have been shedding light on the two black boxes. Thus, integration of these two models builds a mechanistic foundation for the conventional statistical dose-response relationship. The dose-response relationship, once developed upon the foundation, may be considered as a BBDR model. A simple way for the integration of the two models is to link internal dose metric (output of a PBPK model) with critical pharmacodynamic parameters in a carcinogenesis model since a carcinogen exerts its effects likely through modulation of those parameters. The internal dose metric-parameter linkages can be expressed with linear or nonlinear functions (Portier 1987). The function selection is based on mode(s) of action of the chemical of concern or scientific guess and it is therefore liable to investigators' subjectivity. In the low-dose region (below experimental region), the selection of the function is difficult because its validity cannot be experimentally tested. This selection decides the nature of the overall dose-response curve in the low-dose region and has great impact on the risk assessment.

The value of BBDR model in cancer risk assessment has been recognized by USEPA (1996; 2005b). In the Guidelines for Carcinogen Risk assessment published in March 2005, USEPA (2005b) states:

> "[i]f there are sufficient quantitative data and adequate understanding of the carcinogenic process, a biologically based model may be developed to relate dose and response data on an agent-specific basis. Otherwise, as a default procedure, a standard model can be used to curve-fit the data."

It also states that the low-dose "extrapolation is based on extension of a biologically based model if supported by substantial data. Otherwise, default approaches can be applied ..." An excellent example of the application of BBDR model in risk assessment was provided by Conolly and colleagues on formaldehyde, a chemical causing nasal squamous cell carcinoma in both sexes of F344 rats that are chronically exposed through inhalation to 6 ppm or higher levels (Conolly and Andersen 1993; Conolly *et al.* 2003, 2004; Conolly *et al.* 2000; Kimbell *et al.* 1997; Kimbell *et al.* 2001). They developed a 3D computational fluid dynamics model (Kimbell *et al.* 1997; Kimbell *et al.* 2001) to predict the disposition and dosimetry of formaldehyde in the respiratory tract in rodents and humans. The uptake of formaldehyde in the respiratory tract cells leads to two key events that are considered to be the modes of action of the carcinoma: formation of DNA-protein cross-link at low concentration and cytotoxicity followed by regenerative cell proliferation at higher concentration. The dose-response submodels for the two modes of action were then determined (Conolly *et al.* 2004). The submodel for DNA-protein cross-link formation was linear, and for cytotoxicity and regenerative cell proliferation the submodel was derived from the labeling index measured at multiple doses. These submodels, along with other information, were input into a two-stage carcinogenesis model. As a result, the additional risks due to exposure to formaldehyde in humans were estimated. These results were compared with the earlier ones from a different method by USEPA (Conolly *et al.* 2004).

7. Cancer risk assessment and biological modeling – the future

7.1. Present issue in cancer risk assessment

Current cancer risk assessment relies heavily on the long-term animal bioassay. As discussed in Section 2.2.1.1, the long-term bioassay has various limitations. Some of the most notable are its enormous requirements in dollars, animals, time, and other resources. While only over 500 agents have been tested using long-term bioassays by the NTP during the past three decades, there are more than 80,000 chemicals registered for use in the US, and each year an additional 2,000 new chemicals are introduced for various purposes (NTP 2004). It is obviously impossible to characterize the carcinogenicity, along with other toxic effects, of all chemicals, let alone the astronomical number of mixtures derived from these chemicals (Yang 1997; Yang *et al.* 2004; Yang *et al.* 1998). Thus, scientifically sound predictive tools must be developed to evaluate carcinogenic potentials, among other toxicities, for chemicals and chemical mixtures.

7.2. What is our strategy?

It is well known that reliable risk assessment requires experimental data on chemical pharmacokinetics and toxic effects. Also, it is known that computer modeling is a valuable means complementary to experimentation. An integration of experimentation and modeling in risk assessment may take advantage of both methods. Yang *et al.* (1998) proposed approaches of integrating computer modeling, including PBPK, carcinognenesis/clonal growth modeling, SAR/QSAR, with *in vitro* biological systems and *in vivo* shorter-term bioassays. As the Ito's protocol has been recognized to be a reliable substitute for the long-term bioassay, our laboratory has intensively used this protocol, with the incorporation of pharmacokinetics and pharmacodynamics, in studying

chlorobenzenes, PCBs, and other chemicals (see Section 2.2.1.2). It is possible that, by studying a series of congeners, QSAR can be utilized to couple with PBPK and clonal growth modeling for predictive purposes. It is also possible that the carcinogenic potential of chemical mixtures could be predicted using computer modeling based on the understanding in the components and their interactions. As such, the risk assessment on chemicals or chemical mixtures could be expedited.

8. Dissertation research

8.1. Purposes

This dissertation research is a part of a larger project, Physiologically-based Pharmacokinetic and Clonal Growth Modeling: Predicting Cancer Potential of Chemical Mixtures, funded by CDC/NIOSH. The project involves collecting pharmacokinetic and GST-P foci data of HCB, PCB 126, arsenic, and their binary and ternary mixtures in the context of a medium-term liver foci bioassay, analyzing the data using PBPK and clonal growth modeling, and making predictions of carcinogenic potential of higher level mixtures based on the acquired understanding in the individuals and lower level mixtures. This project embodies the strategy discussed in Section 7.2. The dissertation presented here is focused on HCB, PCB 126, and their mixture.

8.2. Main contents

The main contents in this dissertation are organized around the theme "What happens pharmacokinetically and pharmacodynamically if HCB and PCB 126 are co-administered to rats?" The disposition of HCB in the context of the liver foci bioassay is explored using PBPK modeling in Chapter 2. Whether or not HCB disposition is altered

by PCB 126 coexposure in the liver foci bioassay is reported in Chapter 3. The effect of the mixture of HCB and PCB 126, with the end point of liver foci development, is analyzed using a clonal growth model in Chapter 4. In Chapter 5, we report the cross-utilization of the clonal growth model built for the HCB+PCB126 mixture to component chemicals, HCB and PCB 126. The overall summary of the research and the future directions are presented in Chapter 6. The computer codes of the PBPK model for HCB and the clonal growth model for the mixture of HCB and PCB 126 are attached as appendices.

REFERENCES

Abraham, K., Krowke, R., and Neubert, D. (1988). Pharmacokinetics and biological activity of 2,3,7,8-tetrachlorodibenzo-p-dioxin. 1. Dose-dependent tissue distribution and induction of hepatic ethoxyresorufin O-deethylase in rats following a single injection. *Arch Toxicol* **62**, 359-68.

Ames, B. N., and Gold, L. S. (1990). Too many rodent carcinogens: mitogenesis increases mutagenesis. *Science* **249**, 970-1.

Andersen, M. E. (1981). A Physiologically Based Toxicokinetic Description of the Metabolism of Inhaled Gases and Vapors - Analysis at Steady- State. *Toxicol Appl Pharmacol* **60**, 509-526.

Andersen, M. E. (2003). Toxicokinetic modeling and its applications in chemical risk assessment. *Toxicol Lett* **138**, 9-27.

Andersen, M. E., Birnbaum, L. S., Barton, H. A., and Eklund, C. R. (1997). Regional hepatic CYP1A1 and CYP1A2 induction with 2,3,7,8- tetrachlorodibenzo-p-dioxin evaluated with a multicompartment geometric model of hepatic zonation. *Toxicol Appl Pharmacol* **144**, 145-155.

Andersen, M. E., Clewell, H. J., 3rd, Gargas, M. L., Smith, F. A., and Reitz, R. H. (1987). Physiologically based pharmacokinetics and the risk assessment process for methylene chloride. *Toxicol Appl Pharmacol* **87**, 185-205.

Andersen, M. E., Mills, J. J., Gargas, M. L., Kedderis, L., Birnbaum, L. S., Neubert, D., and Greenlee, W. F. (1993). Modeling receptor-mediated processes with dioxin: implications for pharmacokinetics and risk assessment. *Risk Anal* **13**, 25-36.

Andersen, M. E., Mills, J. J., Jirtle, R. L., and Greenlee, W. F. (1995). Negative selection in hepatic tumor promotion in relation to cancer risk assessment. *Toxicology* **102**, 223-37.

Andersen, M. E., Yang, R. S. H., Clewell, H., 3rd, and Reddy, M. B. (2005). Introduction: A historical perspective of the development and applications of PBPK models. In Physiologically Based Pharmacokinetic Modeling: Science and Applications (M. B. Reddy, R. S. H. Yang, M. E. Andersen and H. Clewell, 3rd, eds.), pp. 1-18. John Wiley & Sons, Hoboken.

Angelo, M. J., Bischoff, K. B., Pritchard, A. B., and Presser, M. A. (1984). A physiological model for the pharmacokinetics of methylene chloride in $B_6C_3F_1$ mice following i.v. administrations. *J Pharmacokinet Biopharm* **12**, 413-436.

Angelo, M. J., and Pritchard, A. B. (1984). Simulations of methylene chloride pharmacokinetics using a physiologically based model. *Regul Toxicol Pharmacol* **4**, 329-339.

Armitage, P., and Doll, R. (1954). The age distribution of cancer and a multi-stage theory of carcinogenesis. *Br J Cancer* **8**, 1-12.

Armitage, P., and Doll, R. (2004a). The age distribution of cancer and a multi-stage theory of carcinogenesis [Reprint]. *Int J Epidemiol* **33**, 1174-9.

Armitage, P., and Doll, R. (2004b). The age distribution of cancer and a multi-stage theory of carcinogenesis [Reprint]. *Br J Cancer* **91**, 1983-9.

Arnold, D. L., Moodie, C. A., Grice, H. C., Charbonneau, S. M., Stavric, B., Collins, B. T., McGuire, P. F., Zawidzka, Z. Z., and Munro, I. C. (1980). Long-term toxicity of ortho-touenesulfonamide and sodium saccharin in the rat. *Toxicol Appl Pharmacol* **52**, 113-52.

Bager, Y., Kato, Y., Kenne, K., and Warngard, L. (1997). The ability to alter the gap junction protein expression outside GST-P positive foci in liver of rats was associated to the tumour promotion potency of different polychlorinated biphenyls. *Chem Biol Interact* **103**, 199-212.

Bailer, A. J., and Dankovic, D. A. (1997). An introduction to the use of physiologically based pharmacokinetic models in risk assessment. *Stat Methods Med Res* **6**, 341-358.

Bannasch, P. (1986). Preneoplastic lesions as end points in carcinogenicity testing. I. Hepatic preneoplasia. *Carcinogenesis* **7**, 689-95.

Bernillon, P., and Bois, F. Y. (2000). Statistical issues in toxicokinetic modeling: a bayesian perspective. *Environ Health Perspect* **108 Suppl 5**, 883-93.

Birnbaum, L. S. (1994). Evidence for the role of the Ah receptor in response to dioxin. *Prog Clin Biol Res* **387**, 139-54.

Blower, S. M., and Dowlatabadi, H. (1994). Sensitivity and uncertainty analysis of complex models of disease transmission: an HIV model, as an example. *Int Stat Rev* **62**, 229-243.

Bogen, K. T. (1989). Cell proliferation kinetics and multistage cancer risk models. *J Natl Cancer Inst* **81**, 267-77.

Bois, F. Y. (1999). Analysis of PBPK models for risk characterization. *Ann N Y Acad Sci* **895**, 317-37.

Bois, F. Y. (2001). Applications of population approaches in toxicology. *Toxicol Lett* **120**, 385-94.

Bois, F. Y., Jackson, E. T., Pekari, K., and Smith, M. T. (1996). Population toxicokinetics of benzene. *Environ Health Perspect* **104 Suppl 6**, 1405-11.

Bois, F. Y., Woodruff, T. J., and Spear, R. C. (1991). Comparison of 3 physiologically based pharmacokinetic models of benzene disposition. *Toxicol. Appl. Pharmacol.* **110**, 79-88.

Bosetti, C., La Vecchia, C., Lipworth, L., and McLaughlin, J. K. (2003). Occupational exposure to vinyl chloride and cancer risk: a review of the epidemiologic literature. *Eur J Cancer Prev* **12**, 427-30.

Bourke, G. J., and Daly, L. (1983). Epidemiology and cancer. In The epidemiology of cancer (G.J. Bourke, ed), pp. 5-16. Charles Press, Philadelphia.

Box, G. E. P. (1976). Science and statistics. *J Am Stat Assoc* **71**, 791-802.

Brown, R. P., Delp, M. D., Lindstedt, S. L., Rhomberg, L. R., and Beliles, R. P. (1997). Physiological parameter values for physiologically based pharmacokinetic models. *Toxicol. Ind. Health* **13**, 407-484.

Bruckner, J. V., Keys, D. A., and Fisher, J. W. (2004). The Acute Exposure Guideline Level (AEGL) program: applications of physiologically based pharmacokinetic modeling. *J Toxicol Environ Health A* **67**, 621-34.

Bucher, J. R., and Portier, C. (2004). Human carcinogenic risk evaluation, Part V: The national toxicology program vision for assessing the human carcinogenic hazard of chemicals. *Toxicol Sci* **82**, 363-6.

Bucher, J. R., Portier, C. J., Goodman, J. I., Faustman, E. M., and Lucier, G. W. (1996). Workshop overview. National Toxicology Program Studies: principles of dose selection and applications to mechanistic based risk assessment. *Fundam Appl Toxicol* **31**, 1-8.

Buchmann, A., Stinchcombe, S., Korner, W., Hagenmaier, H., and Bock, K. W. (1994). Effects of 2,3,7,8-tetrachloro- and 1,2,3,4,6,7,8-heptachlorodibenzo-p-dioxin on the proliferation of preneoplastic liver cells in the rat. *Carcinogenesis* **15**, 1143-50.

Bungay, P. M., Dedrick, R. L., and Matthews, H. B. (1979). Pharmacokinetics of halogenated hydrocarbons. *Ann N Y Acad Sci* **320**, 257-70.

Bungay, P. M., Dedrick, R. L., and Matthews, H. B. (1981). Enteric transport of chlordecone (Kepone) in the rat. *J Pharmacokinet Biopharm* **9**, 309-41.

Butterworth, B. E., Slaga, T. J., Farland, W., and McClain, M. (1991). *Chemically induced cell proliferation: Implications for risk assessment.* Wiley-Liss, Inc., New York.

Campbell, H. A., Xu, Y. D., Hanigan, M. H., and Pitot, H. C. (1986). Application of quantitative stereology to the evaluation of phenotypically heterogeneous enzyme-altered foci in the rat liver. *J Natl Cancer Inst* **76**, 751-67.

Caperos, J. R., Droz, P. O., Hake, C. L., Humbert, B. E., and Jacot-Guillarmod, A. (1982). 1,1,1-Trichloroethane exposure, biologic monitoring by breath and urine analyses. *Int Arch Occup Environ Health* **49**, 293-303.

Casanova, M., Conolly, R. B., and Heck, H. d. A. (1996). DNA-protein cross-links (DPX) and cell proliferation in B6C3F1 mice but not Syrian golden hamsters exposed to dichloromethane: pharmacokinetics and risk assessment with DPX as dosimeter. *Fundam Appl Toxicol* **31**, 103-16.

Chen, C. J., Chen, C. W., Wu, M. M., and Kuo, T. L. (1992). Cancer potential in liver, lung, bladder and kidney due to ingested inorganic arsenic in drinking water. *Br J Cancer* **66**, 888-92.

Clayson, D. B. (2001a). Epidemiology - Studies of cancer causes in humans. In Toxicological carcinogenesis, pp. 9-18. Lewis Publishers, Boca Raton.

Clayson, D. B. (2001b). Standard animal bioassays for carcinogens. In Toxicological carcinogenesis, pp. 19-30. Lewis Publishers, Boca Raton.

Clayson, D. B., and Iverson, F. (1996). Cancer risk assessment at the crossroads: the need to turn to a biological approach. *Regul Toxicol Pharmacol* **24**, 45-59.

Clewell, H. J., 3rd (1995). The use of physiologically based pharmacokinetic modeling in risk assessment: A case study with methylene chloride. In Low dose extraplolation of cancer risks: Issues and perspectives (S. Olin, W. Farland, C. Park, L. Rhomberg, R. Scheuplein, T. Starr and J. Wilson, eds.), pp. 199-221. ILSI press, Washington, D.C.

Clewell, H. J., 3rd, and Andersen, M. E. (1996). Use of physiologically based pharmacokinetic modeling to investigate individual versus population risk. *Toxicology* **111**, 315-29.

Clewell, H. J., 3rd, and Andersen, M. E. (2004). Applying mode-of-action and pharmacokinetic considerations in contemporary cancer risk assessments: an example with trichloroethylene. *Crit Rev Toxicol* **34**, 385-445.

Clewell, H. J., 3rd, Andersen, M. E., and Barton, H. A. (2002). A consistent approach for the application of pharmacokinetic modeling in cancer and noncancer risk assessment. *Environ Health Perspect* **110**, 85-93.

Clewell, H. J., 3rd, Gentry, P. R., Covington, T. R., and Gearhart, J. M. (2000). Development of a physiologically based pharmacokinetic model of trichloroethylene and its metabolites for use in risk assessment. *Environ Health Perspect* **108 Suppl 2**, 283-305.

Clewell, H. J., 3rd, Lee, T. S., and Carpenter, R. L. (1994). Sensitivity of physiologically based pharmacokinetic models to variation in model parameters: methylene chloride. *Risk Anal* **14**, 521-31.

Cogliano, V. J., Luebeck, E. G., and Zapponi, G. A. (1999). The multistage model of carcinogenesis: A critical review of its use. In Perspectives on biologically based cancer risk assessment (V. J. Cogliano, E. G. Luebeck and G. A. Zapponi, eds.), pp. 183-204. Kluwer Academic/Plenum Publishers, New York.

Cohen, S. M. (2004). Human carcinogenic risk evaluation: an alternative approach to the two-year rodent bioassay. *Toxicol Sci* **80**, 225-9.

Cohen, S. M., Arai, M., Jacobs, J. B., and Friedell, G. H. (1979). Promoting effect of saccharin and DL-tryptophan in urinary bladder carcinogenesis. *Cancer Res* **39**, 1207-17.

Cohen, S. M., and Ellwein, L. B. (1988). Cell growth dynamics in long-term bladder carcinogenesis. *Toxicol Lett* **43**, 151-73.

Cohen, S. M., and Ellwein, L. B. (1990a). Cell proliferation in carcinogenesis. *Science* **249**, 1007-11.

Cohen, S. M., and Ellwein, L. B. (1990b). Proliferative and genotoxic cellular effects in 2-acetylaminofluorene bladder and liver carcinogenesis: biological modeling of the ED01 study. *Toxicol Appl Pharmacol* **104**, 79-93.

Cohen, S. M., and Ellwein, L. B. (1995a). Biological theory of carcinogenesis: Implications for risk assessment. In Low dose extraplolation of cancer risks: Issues and perspectives (S. Olin, W. Farland, C. Park, L. Rhomberg, R. Scheuplein, T. Starr and J. Wilson, eds.), pp. 145-161. ILSI Press, Washington, D.C.

Cohen, S. M., and Ellwein, L. B. (1995b). Relationship of DNA adducts derived from 2-acetylaminofluorene to cell proliferation and the induction of rodent liver and bladder tumors. *Toxicol Pathol* **23**, 136-42.

Columbano, A., Ledda-Columbano, G. M., Rao, P. M., Rajalakshmi, S., and Sarma, D. S. (1984). Occurrence of cell death (apoptosis) in preneoplastic and neoplastic liver cells. A sequential study. *Am J Pathol* **116**, 441-6.

Conolly, R. B., and Andersen, M. E. (1991). Biologically based pharmacodynamic models: tools for toxicological research and risk assessment. *Annu Rev Pharmacol Toxicol* **31**, 503-23.

Conolly, R. B., and Andersen, M. E. (1993). An approach to mechanism-based cancer risk assessment for formaldehyde. *Environ Health Perspect* **101 Suppl 6**, 169-76.

Conolly, R. B., and Andersen, M. E. (1997). Hepatic foci in rats after diethylnitrosamine initiation and 2,3,7,8-tetrachlorodibenzo-p-dioxin promotion: evaluation of a quantitative two-cell model and of CYP 1A1/1A2 as a dosimeter. *Toxicol Appl Pharmacol* **146**, 281-93.

Conolly, R. B., and Kimbell, J. S. (1994). Computer simulation of cell growth governed by stochastic processes: application to clonal growth cancer models. *Toxicol Appl Pharmacol* **124**, 284-95.

Conolly, R. B., Kimbell, J. S., Janszen, D., Schlosser, P. M., Kalisak, D., Preston, J., and Miller, F. J. (2003). Biologically motivated computational modeling of formaldehyde carcinogenicity in the F344 rat. *Toxicol Sci* **75**, 432-47.

Conolly, R. B., Kimbell, J. S., Janszen, D., Schlosser, P. M., Kalisak, D., Preston, J., and Miller, F. J. (2004). Human respiratory tract cancer risks of inhaled formaldehyde: dose-response predictions derived from biologically-motivated computational modeling of a combined rodent and human dataset. *Toxicol Sci* **82**, 279-96.

Conolly, R. B., Lilly, P. D., and Kimbell, J. S. (2000). Simulation modeling of the tissue disposition of formaldehyde to predict nasal DNA-protein cross-links in Fischer 344 rats, rhesus monkeys, and humans. *Environ Health Perspect* **108 Suppl 5**, 919-24.

Cook, P. J., Doll, R., and Fellingham, S. A. (1969). A mathematical model for the age distribution of cancer in man. *Int J Cancer* **4**, 93-112.

David, R. M., Clewell, H. J., 3rd, Gentry, P. R., Covington, T. R., Morgott, D. A., and Marino, D. J. (2006). Revised assessment of cancer risk to dichloromethane II. Application of probabilistic methods to cancer risk determinations. *Regul Toxicol Pharmacol.*

Day, N. E., and Brown, C. C. (1980). Multistage models and primary prevention of cancer. *J Natl Cancer Inst* **64**, 977-89.

De Gunst, M. C., and Luebeck, E. G. (1994). Quantitative analysis of two-dimensional observations of premalignant clones in the presence or absence of malignant tumors. *Math Biosci* **119**, 5-34.

de Gunst, M. C., and Luebeck, E. G. (1998). A method for parametric estimation of the number and size distribution of cell clusters from observations in a section plane. *Biometrics* **54**, 100-12.

Dean, C. E., Jr. (2003). Mechanisms of hepatic tumor promotion by polychlorinated biphenyl mixtures. Ph.D. dissertation. Department of Microbiology, Immunology and Pathology. Colorado State University, Fort Collins.

Dean, C. E., Jr., Benjamin, S. A., Chubb, L. S., Tessari, J. D., and Keefe, T. J. (2002). Nonadditive hepatic tumor promoting effects by a mixture of two structurally different polychlorinated biphenyls in female rat livers. *Toxicol Sci* **66**, 54-61.

Dedrick, R. L. (1973). Animal scale-up. *J Pharmacokinet Biopharm* **1**, 435-61.

DeVito, M. J., and Birnbaum, L. S. (1994). Toxicology of dioxins and related chemicals. In Dioxin and Health (A. Schecter, ed), pp. 139-162. Plenum Press, New York and London.

Dewanji, A., Moolgavkar, S. H., and Luebeck, E. G. (1991). Two-mutation model for carcinogenesis: joint analysis of premalignant and malignant lesions. *Math Biosci* **104**, 97-109.

Dewanji, A., Venzon, D. J., and Moolgavkar, S. H. (1989). A stochastic two-stage model for cancer risk assessment. II. The number and size of premalignant clones. *Risk Anal* **9**, 179-87.

Diliberto, J. J., Burgin, D., and Birnbaum, L. S. (1997). Role of CYP1A2 in hepatic sequestration of dioxin: studies using CYP1A2 knock-out mice. *Biochem Biophys Res Commun* **236**, 431-3.

Doll, R., and Peto, R. (1978). Cigarette smoking and bronchial carcinoma: dose and time relationships among regular smokers and lifelong non-smokers. *J Epidemiol Community Health* **32**, 303-13.

Doll, R., and Peto, R. (1981). The causes of cancer: quantitative estimates of avoidable risks of cancer in the United States today. *J Natl Cancer Inst* **66**, 1191-308.

Dragan, Y. P., Bidlack, W. R., Cohen, S. M., Goldsworthy, T. L., Hard, G. C., Howard, P. C., Riley, R. T., and Voss, K. A. (2001). Implications of apoptosis for toxicity, carcinogenicity, and risk assessment: fumonisin B(1) as an example. *Toxicol Sci* **61**, 6-17.

Dragan, Y. P., Hully, J. R., Nakamura, J., Mass, M. J., Swenberg, J. A., and Pitot, H. C. (1994). Biochemical events during initiation of rat hepatocarcinogenesis. *Carcinogenesis* **15**, 1451-8.

Duell, E. J., Millikan, R. C., Pittman, G. S., Winkel, S., Lunn, R. M., Tse, C. K., Eaton, A., Mohrenweiser, H. W., Newman, B., and Bell, D. A. (2001). Polymorphisms in the DNA repair gene XRCC1 and breast cancer. *Cancer Epidemiol Biomarkers Prev* **10**, 217-22.

Easterling, M. R., Evans, M. V., and Kenyon, E. M. (2000). Comparative analysis of software for physiologically based pharmacokinetic modeling: Simulation, optimization, and sensitivity analysis. *Toxicol Method* **10**, 203-229.

Eaton, D. L., Gallagher, E. P., Bammler, T. K., and Kunze, K. L. (1995). Role of cytochrome P4501A2 in chemical carcinogenesis: implications for human variability in expression and enzyme activity. *Pharmacogenetics* **5**, 259-74.

Eickman, E. (2005). Development of a biologically-based model describing spontaneous neoplastic transformation with incorporation of experimental data from RHEK-1 human keratinocytes. Master Thesis. Department of Environmental and Radiological Health Sciences, Colorado State University, Fort Collins, CO.

Ellwein, L. B., and Cohen, S. M. (1988). A cellular dynamics model of experimental bladder cancer: analysis of the effect of sodium saccharin in the rat. *Risk Anal* **8**, 215-21.

Ellwein, L. B., and Cohen, S. M. (1992). Simulation modeling of carcinogenesis. *Toxicol Appl Pharmacol* **113**, 98-108.

El-Masri, H. A., Bell, D. A., and Portier, C. J. (1999). Effects of glutathione transferase theta polymorphism on the risk estimates of dichloromethane to humans. *Toxicol Appl Pharmacol* **158**, 221-30.

Emond, C., Birnbaum, L. S., and DeVito, M. J. (2004). Physiologically based pharmacokinetic model for developmental exposures to TCDD in the rat. *Toxicol Sci* **80**, 115-33.

Evans, M. V., and Andersen, M. E. (2000). Sensitivity analysis of a physiological model for 2,3,7,8-tetrachlorodibenzo-p-dioxin (TCDD): assessing the impact of specific model parameters on sequestration in liver and fat in the rat. *Toxicol Sci* **54**, 71-80.

Evans, M. V., Crank, W. D., Yang, H. M., and Simmons, J. E. (1994). Applications of sensitivity analysis to a physiologically based pharmacokinetic model for carbon tetrachloride in rats. *Toxicol Appl Pharmacol* **128**, 36-44.

Fernandez, J. G., Droz, P. O., Humbert, B. E., and Caperos, J. R. (1977). Trichloroethylene exposure. Simulation of uptake, excretion, and metabolism using a mathematical model. *Br J Ind Med* **34**, 43-55.

Fernandez-Salguero, P. M., Hilbert, D. M., Rudikoff, S., Ward, J. M., and Gonzalez, F. J. (1996). Aryl-hydrocarbon receptor-deficient mice are resistant to 2,3,7,8-tetrachlorodibenzo-p-dioxin-induced toxicity. *Toxicol Appl Pharmacol* **140**, 173-9.

Fiserova-Bergerova, V. (1995). Extrapolation of physiological parameters for physiologically based simulation models. *Toxicol Lett* **79**, 77-86.

Franco, E. L., Correa, P., Santella, R. M., Wu, X., Goodman, S. N., and Petersen, G. M. (2004). Role and limitations of epidemiology in establishing a causal association. *Semin Cancer Biol* **14**, 413-26.

Frith, C. H., Farmer, J. H., Greenman, D. L., and Shaw, G. W. (1980a). Biologic and morphologic characteristics of urinary bladder neoplasms induced in BALB/c female mice with 2-acetylaminofluorene. *J Environ Pathol Toxicol* **3**, 103-19.

Frith, C. H., Kodell, R. L., and Farmer, J. H. (1986). The effects of continued versus discontinued administration of 2-acetylaminofluorene on the morphology and behavior of hepatocellular and urinary bladder tumors in mice. *J Environ Pathol Toxicol Oncol* **7**, 17-23.

Frith, C. H., Kodell, R. L., and Littlefield, N. A. (1980b). Biologic and morphologic characteristics of hepatocellular lesions in BALB/c female mice fed 2-acetylaminofluorene. *J Environ Pathol Toxicol* **3**, 121-38.

Fukushima, S., Arai, M., Nakanowatari, J., Hibino, T., Okuda, M., and Ito, N. (1983). Differences in susceptibility to sodium saccharin among various strains of rats and other animal species. *Gann* **74**, 8-20.

Fukushima, S., and Cohen, S. M. (1980). Saccharin-induced hyperplasia of the rat urinary bladder. *Cancer Res* **40**, 734-6.

Gasiewicz, T. A., Geiger, L. E., Rucci, G., and Neal, R. A. (1983). Distribution, excretion, and metabolism of 2,3,7,8-tetrachlorodibenzo-p-dioxin in C57BL/6J, DBA/2J, and B6D2F1/J mice. *Drug Metab Dispos* **11**, 397-403.

Gaylor, D. W. (1980). The ED01 study: summary and conclusions. *J Environ Pathol Toxicol* **3**, 179-83.

Gaylor, D. W. (2005). Are tumor incidence rates from chronic bioassays telling us what we need to know about carcinogens? *Regul Toxicol Pharmacol* **41**, 128-33.

Gelboin, H. V. (1980). Benzo[alpha]pyrene metabolism, activation and carcinogenesis: role and regulation of mixed-function oxidases and related enzymes. *Physiol Rev* **60**, 1107-66.

Goldsworthy, T. L., Hanigan, M. H., and Pitot, H. C. (1986). Models of hepatocarcinogenesis in the rat--contrasts and comparisons. *Crit Rev Toxicol* **17**, 61-89.

Gonzalez, F. J., and Kimura, S. (2001). Understanding the role of xenobiotic-metabolism in chemical carcinogenesis using gene knockout mice. *Mutat Res* **477**, 79-87.

Grasl-Kraupp, B., Luebeck, G., Wagner, A., Low-Baselli, A., de Gunst, M., Waldhor, T., Moolgavkar, S., and Schulte-Hermann, R. (2000). Quantitative analysis of tumor initiation in rat liver: role of cell replication and cell death (apoptosis). *Carcinogenesis* **21**, 1411-21.

Greenfield, R. E., Ellwein, L. B., and Cohen, S. M. (1984). A general probabilistic model of carcinogenesis: analysis of experimental urinary bladder cancer. *Carcinogenesis* **5**, 437-45.

Haag-Gronlund, M., Conolly, R., Scheu, G., Warngard, L., and Fransson-Steen, R. (2000). Analysis of rat liver foci growth with a quantitative two-cell model after treatment with 2,4,5,3',4'-pentachlorobiphenyl. *Toxicol Sci* **57**, 32-42.

Hadjiolov, N., and Bitsch, A. (1997). Early effects in chemical-induced rat liver carcinogenesis: an immunohistochemical study following exposure to 0.04% AAF. *Apoptosis* **2**, 91-100.

Hasegawa, R., and Ito, N. (1994). Hepatocarcinogenesis in the rat. In Carcinogenesis (M. P. Waalkes and J. M. Ward, eds.), pp. 39-65. Raven Press, Ltd., New York.

Hayes, R. B., Songnian, Y., Dosemeci, M., and Linet, M. (2001). Benzene and lymphohematopoietic malignancies in humans. *Am J Ind Med* **40**, 117-26.

Hethcote, H. W., and Knudson, A. G., Jr. (1978). Model for the incidence of embryonal cancers: application to retinoblastoma. *Proc Natl Acad Sci U S A* **75**, 2453-7.

Hetrick, D. M., Jarabek, A. M., and Travis, C. C. (1991). Sensitivity analysis for physiologically based pharmacokinetic models. *J Pharmacokinet Biopharm* **19**, 1-20.

Higashi, K., Hiai, H., Higashi, T., and Muramatsu, M. (2004). Regulatory mechanism of glutathione S-transferase P-form during chemical hepatocarcinogenesis: old wine in a new bottle. *Cancer Lett* **209**, 155-63.

Hill, A. B. (1965). The Environment and Disease: Association or Causation? *Proc R Soc Med* **58**, 295-300.

Howard, C. V., and Newby, J. A. (2004). Could the increase in cancer incidence be related to recent environmental changes? In Cancer as an environmental disease (P. Nicolopoulou-Stamati, L. Hens, C. V. Howard and N. van Larebeke, eds.), pp. 39-56. Kluwer Academic Publishers, Dordrecht.

Huff, J. E. (1994). Chemicals causally associated with cancers in humans and in laboratory animals: A perfect concordance. In Carcinogenesis (M. P. Waalkes and E. M. Ward, eds.), pp. 25-37. Raven Press, New York.

IARC (1999). The use of short- and medium-term tests for carcinogens and data on genetic effects in carcinogenic hazard evaluation (D.B. McGregor, J.M. Rice, S. Venitt, eds). In IARC Scientific Publications No. 146. International Agency for Research on Cancer, Lyon.

IARC (2003). World cancer report (B. W. Stewart and P. Kleihues, eds.), pp. 33-38. International Agency for Cancer Research, Lyon.

Ito, N., Imaida, K., de Camargo, J. L., Takahashi, S., Asamoto, M., and Tsuda, H. (1988). A new medium-term bioassay system for detection of environmental carcinogens using diethylnitrosamine-initiated rat liver followed by D-galactosamine treatment and partial hepatectomy. *Jpn J Cancer Res* **79**, 573-5.

Ito, N., Tamano, S., and Shirai, T. (2003). A medium-term rat liver bioassay for rapid in vivo detection of carcinogenic potential of chemicals. *Cancer Sci* **94**, 3-8.

Jacobs, A. (2005). Prediction of 2-year carcinogenicity study results for pharmaceutical products: how are we doing? *Toxicol Sci* **88**, 18-23.

Jacobs, J. B., Arai, M., Cohen, S. M., and Friedell, G. H. (1977). A long-term study of reversible and progressive urinary bladder cancer lesions in rats fed N-[4-(5-nitro-2-furyl)-2-thiazolyl]formamide. *Cancer Res* **37**, 2817-21.

Johnson, E. S. (1991). Human exposure to 2,3,7,8-TCDD and risk of cancer. *Crit Rev Toxicol* **21**, 451-63.

Jonsson, F. (2001). Physiologically based pharmacokinetic modeling in risk assessment: Development of Bayesian population methods. Ph.D. dissertation. Division of Pharmacokinetics and Drug Therapy, p. 52. Uppsala University, Stockholm.

Jonsson, F., and Johanson, G. (2001a). A Bayesian analysis of the influence of GSTT1 polymorphism on the cancer risk estimate for dichloromethane. *Toxicol Appl Pharmacol* **174**, 99-112.

Jonsson, F., and Johanson, G. (2001b). Bayesian estimation of variability in adipose tissue blood flow in man by physiologically based pharmacokinetic modeling of inhalation exposure to toluene. *Toxicology* **157**, 177-93.

Jonsson, F., and Johanson, G. (2003). The Bayesian population approach to physiological toxicokinetic-toxicodynamic models--an example using the MCSim software. *Toxicol Lett* **138**, 143-50.

Kim, A. H., Kohn, M. C., Portier, C. J., and Walker, N. J. (2002). Impact of physiologically based pharmacokinetic modeling on benchmark dose calculations for TCDD-induced biochemical responses. *Regul Toxicol Pharmacol* **36**, 287-96.

Kimbell, J. S., Gross, E. A., Richardson, R. B., Conolly, R. B., and Morgan, K. T. (1997). Correlation of regional formaldehyde flux predictions with the distribution of formaldehyde-induced squamous metaplasia in F344 rat nasal passages. *Mutat Res* **380**, 143-54.

Kimbell, J. S., Overton, J. H., Subramaniam, R. P., Schlosser, P. M., Morgan, K. T., Conolly, R. B., and Miller, F. J. (2001). Dosimetry modeling of inhaled formaldehyde: binning nasal flux predictions for quantitative risk assessment. *Toxicol Sci* **64**, 111-21.

King, F. G., Dedrick, R. L., Collins, J. M., Matthews, H. B., and Birnbaum, L. S. (1983). Physiological model for the pharmacokinetics of 2,3,7,8-tetrachlorodibenzofuran in several species. *Toxicol Appl Pharmacol* **67**, 390-400.

Kitagawa, T., and Sugano, H. (1978). Enhancing effect of phenobarbital on the development of enzyme-altered islands and hepatocellular carcinomas initiated by 3'-methyl-4-(dimethylamino) azobenzene or diethylnitrosamine. *Gann* **69**, 679-87.

Knudson, A. G., Jr., Hethcote, H. W., and Brown, B. W. (1975). Mutation and childhood cancer: a probabilistic model for the incidence of retinoblastoma. *Proc Natl Acad Sci U S A* **72**, 5116-20.

Knudson, A. G., Jr., and Strong, L. C. (1972). Mutation and cancer: a model for Wilms' tumor of the kidney. *J Natl Cancer Inst* **48**, 313-24.

Kohn, M. C. (1997). The importance of anatomical realism for validation of physiological models of disposition of inhaled toxicants. *Toxicol. Appl. Pharmacol.* **147**, 448-458.

Kohn, M. C., Lucier, G. W., Clark, G. C., Sewall, C., Tritscher, A. M., and Portier, C. J. (1993). A mechanistic model of effects of dioxin on gene expression in the rat liver. *Toxicol Appl Pharmacol* **120**, 138-54.

Kolonel, L. N., Altshuler, D., and Henderson, B. E. (2004). The multiethnic cohort study: exploring genes, lifestyle and cancer risk. *Nat Rev Cancer* **4**, 519-27.

Kopp-Schneider, A. (1997). Carcinogenesis models for risk assessment. *Stat Methods Med Res* **6**, 317-40.

Kopp-Schneider, A. (2003). Biostatistical evaluation of focal hepatic preneoplasia. *Toxicol Pathol* **31**, 121-5.

Kopp-Schneider, A., and Portier, C. J. (1991). Distinguishing between models of carcinogenesis: the role of clonal expansion. *Fundam Appl Toxicol* **17**, 601-13.

Kramers, P. G. (1975). The mutagenicity of saccharin. *Mutat Res* **32**, 81-92.

Krishnan, K., and Andersen, M. E. (1994). Physiologically based pharmacokinetic modeling in toxicology. In Principles and Methods of Toxicology (A.W. Hayes, ed), pp. 149-188. Raven Press Ltd., New York.

Krishnan, K., and Johanson, G. (2005). Physiologically-based pharmacokinetic and toxicokinetic models in cancer risk assessment. *J Environ Sci Health C Environ Carcinog Ecotoxicol Rev* **23**, 31-53.

Krutovskikh, V. (2002). Implication of direct host-tumor intercellular interactions in non-immune host resistance to neoplastic growth. *Semin Cancer Biol* **12**, 267-76.

Lai, D. Y., and Arcos, J. C. (1980). Minireview: dialkylnitrosamine bioactivation and carcinogenesis. *Life Sci* **27**, 2149-65.

Laib, R. J., Brockes, B., Schwaier, A., and Bolt, H. M. (1982). Strain and species differences in the induction of ATPase-deficient hepatic foci by diethylnitrosamine. *Cancer Lett* **15**, 145-8.

Lang, M., and Pelkonen, O. (1999). Metabolism of xenobiotics and chemical carcinogenesis. *IARC Sci Publ*, 13-22.

LeBoeuf, R. A., Kerckaert, K. A., Aardema, M. J., and Isfort, R. J. (1999). Use of Syrian hamster embryo and BALB/c 3T3 cell transformation for assessing the carcinogenic potential of chemicals. In The use of short- and medium-term tests for carcinogens and data on genetic effects in carcinogenic hazard evaluation. pp. 409-425. IARC Scientific Publications No. 146. International Agency for Research on Cancer, Lyon (D. B. McGregor, J. M. Rice and S. Venitt, eds.).

Leung, H. W., Ku, R. H., Paustenbach, D. J., and Andersen, M. E. (1988). A physiologically based pharmacokinetic model for 2,3,7,8-tetrachlorodibenzo-p-dioxin in C57BL/6J and DBA/2J mice. *Toxicol Lett* **42**, 15-28.

Leung, H. W., Paustenbach, D. J., and Andersen, M. E. (1989). A physiologically-based pharmacokinetic model for 2,3,7,8- tetrachlorodibenzo-para-dioxin. *Chemosphere* **18**, 659-664.

Leung, H. W., Paustenbach, D. J., Murray, F. J., and Andersen, M. E. (1990a). A physiological pharmacokinetic description of the tissue distribution and enzyme-inducing properties of 2,3,7,8-tetrachlorodibenzo-p-dioxin in the rat. *Toxicol Appl Pharmacol* **103**, 399-410.

Leung, H. W., Poland, A., Paustenbach, D. J., Murray, F. J., and Andersen, M. E. (1990b). Pharmacokinetics of [125I]-2-iodo-3,7,8-trichlorodibenzo-p-dioxin in mice: analysis with a physiological modeling approach. *Toxicol Appl Pharmacol* **103**, 411-9.

Liao, K. H., Gustafson, D. L., Fox, M. H., Chubb, L. S., Reardon, K. F., and Yang, R. S. H. (2001). A biologically based model of growth and senescence of Syrian hamster embryo (SHE) cells after exposure to arsenic. *Environ Health Perspect* **109**, 1207-13.

Littlefield, N. A., Farmer, J. H., Gaylor, D. W., and Sheldon, W. G. (1980). Effects of dose and time in a long-term, low-dose carcinogenic study. *J Environ Pathol Toxicol* **3**, 17-34.

Lu, Y. (2005). Dioxin and related compounds. In Physiologically Based Pharmacokinetic Modeling: Science and Applications (M. B. Reddy, R. S. H. Yang, M. E. Andersen and H. Clewell, 3rd, eds.), pp. 207-237. John Wiley & Sons, Hoboken.

Lu, Y., Lohitnavy, M., Reddy, M., Lohitnavy, O., Eickman, E., Ashley, A., Xu, Y., and Yang, R. S. H. (2006a). Promotion of liver GST-P foci by a chemical mixture of hexachlorobenzene (HCB) and 3, 3', 4, 4', 5-pentachlorobiphenyl (PCB126): Integration of computer modeling and biology of clonal growth [Abstract]. *Toxicologist* **90**, 435.

Lu, Y., Lohitnavy, M., Reddy, M. B., Lohitnavy, O., Ashley, A., and Yang, R. S. H. (2006b). An updated physiologically based pharmacokinetic model for

hexachlorobenzene: Incorporation of pathophysiological states following partial hepatectomy and hexachlorobenzene treatment. *Toxicol Sci* **91**, 29-41.

Luch, A. (2005). Nature and nurture - lessons from chemical carcinogenesis. *Nat Rev Cancer* **5**, 113-25.

Luebeck, E. G., Grasl-Kraupp, B., Timmermann-Trosiener, I., Bursch, W., Schulte-Hermann, R., and Moolgavkar, S. H. (1995). Growth kinetics of enzyme-altered liver foci in rats treated with phenobarbital or alpha-hexachlorocyclohexane. *Toxicol Appl Pharmacol* **130**, 304-15.

Luebeck, E. G., and Moolgavkar, S. H. (1991). Stochastic analysis of intermediate lesions in carcinogenesis experiments. *Risk Anal* **11**, 149-57.

Luebeck, E. G., and Moolgavkar, S. H. (1994). Simulating the process of malignant transformation. *Math Biosci* **123**, 127-46.

Luebeck, E. G., Moolgavkar, S. H., Buchmann, A., and Schwarz, M. (1991). Effects of polychlorinated biphenyls in rat liver: quantitative analysis of enzyme-altered foci. *Toxicol Appl Pharmacol* **111**, 469-84.

Luebeck, E. G., Watanabe, K., and Travis, C. (1999). Biologically based models of carcinogenesis. In Perspectives on biologically based cancer risk assessment (V. J. Cogliano, E. G. Luebeck and G. A. Zapponi, eds.), pp. 205-242. Kluwer Academic/Plenum Publishers, New York.

Lutz, R. J., Dedrick, R. L., Matthews, H. B., Eling, T. E., and Anderson, M. W. (1977). A preliminary pharmacokinetic model for several chlorinated biphenyls in the rat. *Drug Metabolism & Disposition* **5**, 386-96.

Lutz, W. K. (1998). Dose-response relationships in chemical carcinogenesis: superposition of different mechanisms of action, resulting in linear-nonlinear curves, practical thresholds, J-shapes. *Mutat Res* **405**, 117-24.

Lutz, W. K., and Schlatter, C. (1977). Saccharin does not bind to DNA of liver or bladder in the rat. *Chem Biol Interact* **19**, 253-7.

MacDonald, J. S. (2004). Human carcinogenic risk evaluation, part IV: assessment of human risk of cancer from chemical exposure using a global weight-of-evidence approach. *Toxicol Sci* **82**, 3-8.

Manton, K. G., and Stallard, E. (1980). A two-disease model of female breast cancer: mortality in 1969 among white females in the United States. *J Natl Cancer Inst* **64**, 9-16.

Marino, D. J., Clewell, H. J., 3rd, Gentry, P. R., Covington, T. R., Hack, C. E., David, R. M., and Morgott, D. A. (2006). Revised assessment of cancer risk to dichloromethane: Part I Bayesian PBPK and dose-response modeling in mice. *Regul Toxicol Pharmacol.*

Marsman, D. S., and Barrett, J. C. (1994). Apoptosis and chemical carcinogenesis. *Risk Anal* **14**, 321-6.

McGregor, D., and Anderson, D. (1999). DNA damage and repair in mammalian cells in vitro and in vivo as indicators of exposure to carcinogens. In The use of short- and medium-term tests for carcinogens and data on genetic effects in carcinogenic hazard evaluation. pp. 203-249. IARC Scientific Publications No. 146. International Agency for Research on Cancer, Lyon (D. B. McGregor, J. M. Rice and S. Venitt, eds.).

McLean, M., and Dutton, M. F. (1995). Cellular interactions and metabolism of aflatoxin: an update. *Pharmacol Ther* **65**, 163-92.

Moolgavkar, S. (1980). Multistage models for carcinogenesis. *J Natl Cancer Inst* **65**, 215-6.

Moolgavkar, S. H. (1978). The multistage theory of carcinogenesis and the age distribution of cancer in man. *J Natl Cancer Inst* **61**, 49-52.

Moolgavkar, S. H. (1983). Model for human carcinogenesis: action of environmental agents. *Environ Health Perspect* **50**, 285-91.

Moolgavkar, S. H. (1986). Carcinogenesis modeling: from molecular biology to epidemiology. *Annu Rev Public Health* **7**, 151-69.

Moolgavkar, S. H. (1988). Biologically motivated two-stage model for cancer risk assessment. *Toxicol Lett* **43**, 139-50.

Moolgavkar, S. H. (1991). Carcinogenesis models: an overview. *Basic Life Sci* **58**, 387-96; discussion 396-9.

Moolgavkar, S. H. (1993). Cell proliferation and carcinogenesis models: general principles with illustrations from the rodent liver system. *Environ Health Perspect* **101 Suppl 5**, 91-4.

Moolgavkar, S. H., Day, N. E., and Stevens, R. G. (1980). Two-stage model for carcinogenesis: Epidemiology of breast cancer in females. *J Natl Cancer Inst* **65**, 559-69.

Moolgavkar, S. H., Dewanji, A., and Venzon, D. J. (1988). A stochastic two-stage model for cancer risk assessment. I. The hazard function and the probability of tumor. *Risk Anal* **8**, 383-92.

Moolgavkar, S. H., and Knudson, A. G., Jr. (1981). Mutation and cancer: a model for human carcinogenesis. *J Natl Cancer Inst* **66**, 1037-52.

Moolgavkar, S. H., Luebeck, E. G., Buchmann, A., and Bock, K. W. (1996). Quantitative analysis of enzyme-altered liver foci in rats initiated with diethylnitrosamine and promoted with 2,3,7,8-tetrachlorodibenzo-p-dioxin or 1,2,3,4,6,7,8-heptachlorodibenzo-p-dioxin. *Toxicol Appl Pharmacol* **138**, 31-42.

Moolgavkar, S. H., Luebeck, E. G., de Gunst, M., Port, R. E., and Schwarz, M. (1990). Quantitative analysis of enzyme-altered foci in rat hepatocarcinogenesis experiments--I. Single agent regimen. *Carcinogenesis* **11**, 1271-8.

Moolgavkar, S. H., and Luebeck, G. (1990). Two-event model for carcinogenesis: biological, mathematical, and statistical considerations. *Risk Anal* **10**, 323-41.

Moolgavkar, S. H., and Venzon, D. J. (1979). Two-event models for carcinogenesis:Incidence curves for childhood and adult tumors. *Math Biosci* **47**, 55-77.

Moore, M. A., Nakamura, T., Shirai, T., Ichihara, A., and Ito, N. (1986). Immunohistochemical demonstration of increased glucose-6-phosphate dehydrogenase in preneoplastic and neoplastic lesions induced by propylnitrosamines in F344 rats and Syrian hamsters. *Jpn J Cancer Res* **77**, 131-8.

Nakanishi, K., Hagiwara, A., Shibata, M., Imaida, K., Tatematsu, M., and Ito, N. (1980). Dose response of saccharin in induction of urinary bladder hyperplasias in Fischer 344 rats pretreated with N-butyl-N-(4-hydroxybutyl)nitrosamine. *J Natl Cancer Inst* **65**, 1005-10.

Nestorov, I. A., Aarons, L. J., Arundel, P. A., and Rowland, M. (1998). Lumping of whole-body physiologically based pharmacokinetic models. *J Pharmacokinet Biopharm* **26**, 21-46.

Nestorov, I. A., Aarons, L. J., and Rowland, M. (1997). Physiologically based pharmacokinetic modeling of a homologous series of barbiturates in the rat: a sensitivity analysis. *J Pharmacokinet Biopharm* **25**, 413-47.

Nolan, R. J., Freshour, N. L., Rick, D. L., McCarty, L. P., and Saunders, J. H. (1984). Kinetics and metabolism of inhaled methyl chloroform (1,1,1-trichloroethane) in male volunteers. *Fundam Appl Toxicol* **4**, 654-62.

Novogradec, A., and Ali, S. H. (2004). Incorporating the environmental context in the study of cancer: issues and implications. In Cancer as an environmental disease (P. Nicolopoulou-Stamati, L. Hens, C. V. Howard and N. van Larebeke, eds.), pp. 11-38. Kluwer Academic Publishers, Dordrecht.

NTP (1986). Toxicology and carcinogenesis studies of dichloromethane (methylene chloride) (CAS No. 75-09-2) in F344/N rats and B6C3F1 mice (inhalation studies). National Toxicology Program. NTP-TRS-306.

NTP (2001). Ninth report on carcinogenesis: Hexachlorobenzene www.ehp.niehs.nih.gov/roc/toc9.html. National Toxicology Program.

NTP (2004). National Toxicology Program: Current Directions and Evolving Strategies. http://ntp-server.niehs.nih.gov/ntp/Main_Pages/PUBS/2004CurrentDirections.pdf.

NTP (2006). Descriptions of NTP study types: Toxicology/Carcinogenicity. http://ntp-server.niehs.nih.gov/ntpweb/index.cfm?objectid=72015DAF-BDB7-CEBA-F9A7F9CAA57DD7F5. Accessed 4/10/2006.

Ogiso, T., Tatematsu, M., Tamano, S., Hasegawa, R., and Ito, N. (1990). Correlation between medium-term liver bioassay system data and results of long-term testing in rats. *Carcinogenesis* **11**, 561-6.

Olin, S., Farland, W., Park, C., Rhomberg, L., Scheuplein, R., Starr, T., and Wilson, J. (1995). The use of biological data in cancer risk assessment. In Low-dose extrapolation of cancer risks: Issues and perspectives (S. Olin, W. Farland, C.

Park, L. Rhomberg, R. Scheuplein, T. Starr and J. Wilson, eds.), pp. 45-60. ISLI Press, Washington, D.C.

Omori, Y., Zaidan Dagli, M. L., Yamakage, K., and Yamasaki, H. (2001). Involvement of gap junctions in tumor suppression: analysis of genetically-manipulated mice. *Mutat Res* **477**, 191-6.

Ou, Y. C., Conolly, R. B., Thomas, R. S., Gustafson, D. L., Long, M. E., Dobrev, I. D., Chubb, L. S., Xu, Y., Lapidot, S. A., Andersen, M. E., and Yang, R. S. H. (2003). Stochastic simulation of hepatic preneoplastic foci development for four chlorobenzene congeners in a medium-term bioassay. *Toxicol Sci* **73**, 301-14.

Ou, Y. C., Conolly, R. B., Thomas, R. S., Xu, Y., Andersen, M. E., Chubb, L. S., Pitot, H. C., and Yang, R. S. H. (2001). A clonal growth model: time-course simulations of liver foci growth following penta- or hexachlorobenzene treatment in a medium-term bioassay. *Cancer Res.* **61**, 1879-1889.

Painter, J. T. (2005). Polychlorinated biphenyls and arsenic in hepatocarcinogenesis. Ph.D. dissertation. Department of Microbiology, Immunology and Pathology. Colorado State University, Fort Collins, CO.

Pitot, H. C. (1990). Altered hepatic foci: their role in murine hepatocarcinogenesis. *Annu Rev Pharmacol Toxicol* **30**, 465-500.

Pitot, H. C. (2001). Pathways of progression in hepatocarcinogenesis. *Lancet* **358**, 859-60.

Pitot, H. C., Barsness, L., Goldsworthy, T., and Kitagawa, T. (1978). Biochemical characterisation of stages of hepatocarcinogenesis after a single dose of diethylnitrosamine. *Nature* **271**, 456-8.

Pitot, H. C., and Dragan, Y. P. (1991). Facts and theories concerning the mechanisms of carcinogenesis. *Faseb J* **5**, 2280-6.

Pitot, H. C., and Dragan, Y. P. (2001a). Chemical carcinogenesis. In Casarett and Doull's Toxicology: The basic science of poisons (C. D. Klaassen, ed.), pp. 241-319. McGraw-Hill Companies, Inc., New York.

Pitot, H. C., and Dragan, Y. P. (2001b). Chemical carcinogenesis. In Casarett and Doull's Toxicology: The basic science of poisons (C.D. Klaassen, ed), pp. 241-319. McGraw-Hill Companies, Inc., New York.

Plante, I., Charbonneau, M., and Cyr, D. G. (2002). Decreased gap junctional intercellular communication in hexachlorobenzene-induced gender-specific hepatic tumor formation in the rat. *Carcinogenesis* **23**, 1243-9.

Portier, C., and el Masri, H. (1997). Statistical research needs in mechanistic modelling for carcinogenic risk assessment. *Stat Methods Med Res* **6**, 305-15.

Portier, C. J. (1987). Statistical properties of a two-stage model of carcinogenesis. *Environ Health Perspect* **76**, 125-31.

Portier, C. J. (1995). Quantitative models for cancer dose-response relationships: Parameter estimation. In Low-dose extrapolation of cancer risks:Issues and

perspectives (S. Olin, W. Farland, O. Park, L. Rhomberg, R. Scheuplein, T. Starr and J. Wilson, eds.), pp. 123-134. ILSI Press, Washington, D.C.

Portier, C. J., and Kaplan, N. L. (1989). Variability of safe dose estimates when using complicated models of the carcinogenic process. A case study: methylene chloride. *Fundam Appl Toxicol* **13**, 533-44.

Portier, C. J., Kohn, M., Sherman, C. D., and Lucier, G. (1994). Modeling the number and size of hepatic focal lesions following exposure to 2,3,7,8-TCDD. *Organohalogen Compd* **21**, 393-398.

Quillardet, P., and McGregor, D. (1999). Identification of carcinogenic substances by means of short-term tests in bacteria. In The use of short- and medium-term tests for carcinogens and data on genetic effects in carcinogenic hazard evaluation. pp. 487-497. IARC Scientific Publications No. 146. International Agency for Research on Cancer, Lyon (D. B. McGregor, J. M. Rice and S. Venitt, eds.).

Ramsey, J. C., and Andersen, M. E. (1984). A physiologically based description of the inhalation pharmacokinetics of styrene in rats and humans. *Toxicol Appl Pharmacol* **73**, 159-75.

Randi, A. S., Cocca, C., Carbone, V., Nunez, M., Croci, M., Gutierrez, A., Bergoc, R., and Kleiman de Pisarev, D. L. (2006). Hexachlorobenzene is a tumor co-carcinogen and induces alterations in insulin-growth factors signaling pathway in the rat mammary gland. *Toxicol Sci* **89**, 83-92.

Reddy, M. B., Dobrev, I. D., and Dennison, J. E. (2005a). Halogenated alkanes. In Physiologically Based Pharmacokinetic Modeling: Science and Applications (M. B. Reddy, R. S. H. Yang, M. E. Andersen and H. Clewell, 3rd, eds.), pp. 21-54. John Wiley & Sons, Hoboken.

Reddy, M. B., Yang, R. S. H., Andersen, M. E., and Clewell, H., 3rd, eds. (2005b). *Physiologically Based Pharmacokinetic Modeling: Science and Applications.* John Wiley & Sons, Hoboken.

Reitz, R. H., Gargas, M. L., Andersen, M. E., Provan, W. M., and Green, T. L. (1996). Predicting cancer risk from vinyl chloride exposure with a physiologically based pharmacokinetic model. *Toxicol Appl Pharmacol* **137**, 253-67.

Rinsky, R. A., Smith, A. B., Hornung, R., Filloon, T. G., Young, R. J., Okun, A. H., and Landrigan, P. J. (1987). Benzene and leukemia. An epidemiologic risk assessment. *N Engl J Med* **316**, 1044-50.

Sakai, H., Tsukamoto, T., Yamamoto, M., Kobayashi, K., Yuasa, H., Imai, T., Yanai, T., Masegi, T., and Tatematsu, M. (2002). Distinction of carcinogens from mutagens by induction of liver cell foci in a model for detection of initiation activity. *Cancer Lett* **188**, 33-8.

Saltelli, A., Tarantola, S., and Chan, K. P. S. (1999). A quantitative model-independent method for global sensitivity analysis of model output. *Technometrics* **41**, 39-56.

Sanderson, W. T., Ward, E. M., Steenland, K., and Petersen, M. R. (2001). Lung cancer case-control study of beryllium workers. *Am J Ind Med* **39**, 133-44.

Santella, R. M., Gammon, M., Terry, M., Senie, R., Shen, J., Kennedy, D., Agrawal, M., Faraglia, B., and Zhang, F. (2005). DNA adducts, DNA repair genotype/phenotype and cancer risk. *Mutat Res* **592**, 29-35.

Santostefano, M. J., Johnson, K. L., Whisnant, N. A., Richardson, V. M., DeVito, M. J., Diliberto, J. J., and Birnbaum, L. S. (1996). Subcellular localization of TCDD differs between the liver, lungs, and kidneys after acute and subchronic exposure: species/dose comparisons and possible mechanism. *Fundam Appl Toxicol* **34**, 265-75.

Satoh, K., and Hatayama, I. (2002). Anomalous elevation of glutathione S-transferase P-form (GST-P) in the elementary process of epigenetic initiation of chemical hepatocarcinogenesis in rats. *Carcinogenesis* **23**, 1193-8.

Schlosser, P. M. (1994). Experimental design for parameter estimation through sensitivity analysis. *J Toxicol Environ Health* **43**, 495-530.

Schoenig, G. P., Goldenthal, E. I., Geil, R. G., Frith, C. H., Richter, W. R., and Carlborg, F. W. (1985). Evaluation of the dose response and in utero exposure to saccharin in the rat. *Food Chem Toxicol* **23**, 475-90.

Schulte-Hermann, R., Timmermann-Trosiener, I., Barthel, G., and Bursch, W. (1990). DNA synthesis, apoptosis, and phenotypic expression as determinants of growth of altered foci in rat liver during phenobarbital promotion. *Cancer Res* **50**, 5127-35.

Schwarz, M., Pearson, D., Port, R., and Kunz, W. (1984). Promoting effect of 4-dimethylaminoazobenzene on enzyme altered foci induced in rat liver by N-nitrosodiethanolamine. *Carcinogenesis* **5**, 725-30.

Serota, D., Ulland, B., and Carlborg, F. W. (1984). Hazelton chronic oral study in mice. Food solvents workshop I: methylene chloride. March 8-9, Bethesda, MD.

Shirai, T., Hirose, M., and Ito, N. (1999). Medium-term bioassays in rats for rapid detection of the carcinogenic potential of chemicals. In The use of short- and medium-term tests for carcinogens and data on genetic effects in carcinogenic hazard evaluation. pp. 251-272. IARC Scientific Publications No. 146. International Agency for Research on Cancer, Lyon (D. B. McGregor, J. M. Rice and S. Venitt, eds.).

Sielken, R. L., Jr., Reitz, R. H., and Hays, S. M. (1996). Using PBPK modeling and comprehensive realism methodology for the quantitative cancer risk assessment of butadiene. *Toxicology* **113**, 231-7.

Simmons, J. E., Evans, M. V., and Boyes, W. K. (2005). Moving from external exposure concentration to internal dose: duration extrapolation based on physiologically based pharmacokinetic derived estimates of internal dose. *J Toxicol Environ Health A* **68**, 927-50.

Sinha, R., Kulldorff, M., Gunter, M. J., Strickland, P., and Rothman, N. (2005). Dietary benzo[a]pyrene intake and risk of colorectal adenoma. *Cancer Epidemiol Biomarkers Prev* **14**, 2030-4.

Squire, R. A., and Levitt, M. H. (1975). Report of a workshop on classification of specific hepatocellular lesions in rats. *Cancer Res* **35**, 3214-23.

Steenland, K., Deddens, J., and Piacitelli, L. (2001). Risk assessment for 2,3,7,8-tetrachlorodibenzo-p-dioxin (TCDD) based on an epidemiologic study. *Am J Epidemiol* **154**, 451-8.

Stucker, I., de Waziers, I., Cenee, S., Bignon, J., Depierre, A., Milleron, B., Beaune, P., and Hemon, D. (1999). GSTM1, smoking and lung cancer: a case-control study. *Int J Epidemiol* **28**, 829-35.

Sweeney, L. M., Gargas, M. L., Strother, D. E., and Kedderis, G. L. (2003). Physiologically based pharmacokinetic model parameter estimation and sensitivity and variability analyses for acrylonitrile disposition in humans. *Toxicol Sci* **71**, 27-40.

Sweeney, L. M., Kirman, C. R., Morgott, D. A., and Gargas, M. L. (2004). Estimation of interindividual variation in oxidative metabolism of dichloromethane in human volunteers. *Toxicol Lett* **154**, 201-16.

Swenberg, J. A., Dyroff, M. C., Bedell, M. A., Popp, J. A., Huh, N., Kirstein, U., and Rajewsky, M. F. (1984). O4-ethyldeoxythymidine, but not O6-ethyldeoxyguanosine, accumulates in hepatocyte DNA of rats exposed continuously to diethylnitrosamine. *Proc Natl Acad Sci U S A* **81**, 1692-5.

Tan, W. Y. (1991). *Stochastic models of carcinogenesis*. Marcel Dekker, New York.

Tatematsu, M., Mera, Y., Inoue, T., Satoh, K., Sato, K., and Ito, N. (1988). Stable phenotypic expression of glutathione S-transferase placental type and unstable phenotypic expression of gamma-glutamyltransferase in rat liver preneoplastic and neoplastic lesions. *Carcinogenesis* **9**, 215-20.

Tatematsu, M., Tsuda, H., Shirai, T., Masui, T., and Ito, N. (1987). Placental glutathione S-transferase (GST-P) as a new marker for hepatocarcinogenesis: in vivo short-term screening for hepatocarcinogens. *Toxicol Pathol* **15**, 60-8.

Teitelbaum, P. J. (1978). The hepatic uptake of 2,3,7,8-tetrachlorodibenzo-p-dioxin in the mouse. Ph.D. dissertation. University of Rochester, Rochester, NY.

Tennant, R. W., Spalding, J., Stasiewicz, S., and Ashby, J. (1990). Prediction of the outcome of rodent carcinogenicity bioassays currently being conducted on 44 chemicals by the National Toxicology Program. *Mutagenesis* **5**, 3-14.

Tennant, R. W., Stasiewicz, S., Mennear, J., French, J. E., and Spalding, J. W. (1999). Genetically altered mouse models for identifying carcinoges. In The use of short- and medium-term tests for carcinogens and data on genetic effects in carcinogenic hazard evaluation. pp. 123-150. IARC Scientific Publications No. 146. International Agency for Research on Cancer, Lyon (D. B. McGregor, J. M. Rice and S. Venitt, eds.).

Tharappel, J. C., Lee, E. Y., Robertson, L. W., Spear, B. T., and Glauert, H. P. (2002). Regulation of cell proliferation, apoptosis, and transcription factor activities

during the promotion of liver carcinogenesis by polychlorinated biphenyls. *Toxicol Appl Pharmacol* **179**, 172-84.

Thomas, R. S. (1998). The Use of Biologically-Based Models for Integrating Short-Term Cancer Bioassays, Mechanisms of Action, and Target Tissue Dosimetry: Application to Pentachlorobenzene. Ph.D. dissertation. Department of Environmental Health, Colorado State University, Fort Collins, CO.

Thomas, R. S., Conolly, R. B., Gustafson, D. L., Long, M. E., Benjamin, S. A., and Yang, R. S. H. (2000). A physiologically based pharmacodynamic analysis of hepatic foci within a medium-term liver bioassay using pentachlorobenzene as a promoter and diethylnitrosamine as an initiator. *Toxicol Appl Pharmacol* **166**, 128-37.

Thomas, R. S., Yang, R. S. H., Morgan, D. G., Moorman, M. P., Kermani, H. R., Sloane, R. A., O'Connor, R. W., Adkins, B., Jr., Gargas, M. L., and Andersen, M. E. (1996). PBPK modeling/Monte Carlo simulation of methylene chloride kinetic changes in mice in relation to age and acute, subchronic, and chronic inhalation exposure. *Environ Health Perspect* **104**, 858-65.

Thompson, K. L., Rosenzweig, B. A., Weaver, J. L., Zhang, J., Lin, K. K., and Sistare, F. D. (2003). Evaluation of the Tg.AC assay: specificity testing with three noncarcinogenic pharmaceuticals that induce selected stress gene promoters in vitro and the inhibitory effects of solvent components. *Toxicol Sci* **74**, 271-8.

Trosko, J. E., Chang, C. C., Upham, B. L., and Tai, M. H. (2005). The role of human adult stem cells and cell-cell communication in cancer chemoprevention and chemotherapy strategies. *Mutat Res* **591**, 187-97.

Tsuda, H., Fukushima, S., Wanibuchi, H., Morimura, K., Nakae, D., Imaida, K., Tatematsu, M., Hirose, M., Wakabayashi, K., and Moore, M. A. (2003). Value of GST-P positive preneoplastic hepatic foci in dose-response studies of hepatocarcinogenesis: evidence for practical thresholds with both genotoxic and nongenotoxic carcinogens. A review of recent work. *Toxicol Pathol* **31**, 80-6.

Tsuda, H., Park, C. B., and Moore, M. A. (1999). Short- and medium-term carcinogenicity tests: Simple initiation-promotion assay systems. In The use of short- and medium-term tests for carcinogens and data on genetic effects in carcinogenic hazard evaluation. pp. 203-249. IARC Scientific Publications No. 146. International Agency for Research on Cancer, Lyon (D. B. McGregor, J. M. Rice and S. Venitt, eds.).

Tuey, D. B., and Matthews, H. B. (1980a). Distribution and Excretion of 2,2',4,4',5,5'-Hexabromobiphenyl in Rats and Man - Pharmacokinetic Model Predictions. *Toxicol Appl Pharmacol* **53**, 420-431.

Tuey, D. B., and Matthews, H. B. (1980b). Use of a Physiological Compartmental Model for the Rat to Describe the Pharmacokinetics of Several Chlorinated Biphenyls in the Mouse. *Drug Metab Dispos* **8**, 397-403.

USEPA (1996). Proposed guidelines for carcinogen risk assessment. Report number: EPA/600/P-92/003C. U.S. Environmental Protection Agency, Washington, DC.

USEPA (1998). Health effects test guidelines OPPTS 870.5395 mammalian erythrocyte micronucleus test. EPA712-C-98-226. US Environmental Protection Agency.

USEPA (2005a). Approaches for the application of physiologically based pharmacokinetic (PBPK) models and supporting data in risk assessment. Report number: EPA/600/R-05/043A. U.S. Environmental Protection Agency, Washington, DC.

USEPA (2005b). Guidelines for carcinogen risk assessment. Report number: EPA/630/P-03/001F. U.S. Environmental Protection Agency, Washington, DC.

van Leeuwen, I. M., and Zonneveld, C. (2001). From exposure to effect: a comparison of modeling approaches to chemical carcinogenesis. *Mutat Res* **489**, 17-45.

van Zeeland, A. A., and Vrieling, H. (1999). Mutation in mammalian cells in vitro and in vivo as indicators of exposure to carcinogens. In The use of short- and medium-term tests for carcinogens and data on genetic effects in carcinogenic hazard evaluation. pp. 355-365. IARC Scientific Publications No. 146. International Agency for Research on Cancer, Lyon (D. B. McGregor, J. M. Rice and S. Venitt, eds.).

Vasquez, A., Atallah-Yunes, N., Smith, F. C., You, X., Chase, S. E., Silverstone, A. E., and Vikstrom, K. L. (2003). A role for the aryl hydrocarbon receptor in cardiac physiology and function as demonstrated by AhR knockout mice. *Cardiovasc Toxicol* **3**, 153-63.

Verna, L., Whysner, J., and Williams, G. M. (1996a). 2-Acetylaminofluorene mechanistic data and risk assessment: DNA reactivity, enhanced cell proliferation and tumor initiation. *Pharmacol Ther* **71**, 83-105.

Verna, L., Whysner, J., and Williams, G. M. (1996b). N-nitrosodiethylamine mechanistic data and risk assessment: bioactivation, DNA-adduct formation, mutagenicity, and tumor initiation. *Pharmacol Ther* **71**, 57-81.

Ward, J. M. (1981). Morphology of foci of altered hepatocytes and naturally-occurring hepatocellular tumors in F344 rats. *Virchows Arch A Pathol Anat Histol* **390**, 339-45.

Watanabe, K., and Williams, G. M. (1978). Enhancement of rat hepatocellular-altered foci by the liver tumor promoter phenobarbital: evidence that foci are precursors of neoplasms and that the promoter acts on carcinogen-induced lesions. *J Natl Cancer Inst* **61**, 1311-4.

Weisburger, J. H., and Williams, G. M. (1981). Carcinogen testing: current problems and new approaches. *Science* **214**, 401-7.

Weisburger, J. H., and Williams, G. M. (2000). The distinction between genotoxic and epigenetic carcinogens and implication for cancer risk. *Toxicol Sci* **57**, 4-5.

Williams, G. M. (2001). Mechanisms of chemical carcinogenesis and application to human cancer risk assessment. *Toxicology* **166**, 3-10.

Woodruff, T. J., and Bois, F. Y. (1993). Optimization issues in physiological toxicokinetic modeling - a case-study with benzene. *Toxicol Lett* **69**, 181-196.

Wosniok, W., Kitsos, C., and Watanabe, K. (1999). Statistical issues in the application of multistage and biologically based models. In Perspectives on biologically based cancer risk assessment (V. J. Cogliano, E. G. Luebeck and G. A. Zapponi, eds.), pp. 243-274. Kluwer Academic/Plenum Publishers, New York.

Wu, M. M., Kuo, T. L., Hwang, Y. H., and Chen, C. J. (1989). Dose-response relation between arsenic concentration in well water and mortality from cancers and vascular diseases. *Am J Epidemiol* **130**, 1123-32.

Xu, Y. H., Dragan, Y. P., Campbell, H. A., and Pitot, H. C. (1998). STEREO: a program on a PC-Windows 95 platform for recording and evaluating quantitative stereologic investigations of multistage hepatocarcinogenesis in rodents. *Comput Methods Programs Biomed* **56**, 49-63.

Xu, Y. H., and Pitot, H. C. (2003). An improved stereologic method for three-dimensional estimation of particle size distribution from observations in two dimensions and its application. *Comput Methods Programs Biomed* **72**, 1-20.

Yang, R. S. H. (1997). Toxicologic Interactions of Chemical Mixtures. In Comprehensive Toxicology. Vol. 1, General Principles, Toxicokinetics, and Mechanisms of Toxicity (J. Bond, ed), pp. 189-203. Elsevier Science Ltd., Oxford, England.

Yang, R. S. H., and Andersen, M. E. (1994). Pharmacokinetics. In Introduction to Biochemical Toxicology (E. Hodgson and P. E. Levi, eds.), pp. 49-73. Appleton&Lange, Norwalk.

Yang, R. S. H., Dennison, J. E., Andersen, M. E., Ou, Y. C., Liao, K. H., and Reisfeld, B. (2004). Physiologically based pharmacokinetic and pharmacodynamic modeling. In Mouse models of human cancer (E.C. Holland, ed). John Wiley & Sons, Inc., Hoboken, New Jersey.

Yang, R. S. H., and Lu, Y. (2006). The application of PBPK modeling to risk assessment. In Environmental Health Risk Assessment. In press (M. G. Robson and W. A. Toscana, eds.).

Yang, R. S. H., Thomas, R. S., Gustafson, D. L., Campain, J., Benjamin, S. A., Verhaar, H. J., and Mumtaz, M. M. (1998). Approaches to developing alternative and predictive toxicology based on PBPK/PD and QSAR modeling. *Environ Health Perspect* **106 Suppl 6**, 1385-1393.

Yusuf, A., Rao, P. M., Rajalakshmi, S., and Sarma, D. S. (1999). Development of resistance during the early stages of experimental liver carcinogenesis. *Carcinogenesis* **20**, 1641-4.

CHAPTER 2

An Updated PBPK Model for Hexachlorobenzene: Incorporation of Pathophysiological States Following Partial Hepatectomy and Hexachlorobenzene Treatment

Yasong Lu, Manupat Lohitnavy, Micaela B. Reddy, Ornrat Lohitnavy, Amanda Ashley, Raymond S.H. Yang

ABSTRACT

Physiologically based pharmacokinetic (PBPK) modeling is generally for describing xenobiotic disposition in animals and humans with normal physiological conditions. We describe here an updated PBPK model for hexachlorobenzene (HCB) in male F344 rats with the incorporation of pathophysiological conditions. Two more features contribute to the distinctness of this model from the earlier published versions. This model took erythrocyte binding into account, and a particular elimination process of HCB, the plasma-to-gastrointestinal (GI) lumen passive diffusion (*i.e.*, exsorption), was incorporated. Our PBPK model was developed using data mined from multiple pharmacokinetic studies in the literature, and then modified to simulate HCB disposition under the conditions of our integrated pharmacokinetics/liver foci bioassay. This model included plasma, erythrocytes, liver, fat, rapidly and slowly perfused compartments, and GI lumen. To account for the distinct characteristics of HCB absorption, the GI lumen was split into an upper and a lower part. HCB was eliminated through liver metabolism and the exsorption process. The pathophysiological changes after partial hepatectomy, such as alterations in the liver and body weights and fat volume, were incorporated in our

model. With adjustment of the transluminal diffusion-related parameters, the model adequately described the data from the literature and our bioassay. Our PBPK model simulation suggests that HCB absorption and exsorption processes depend on exposure conditions; different exposure conditions dictate different absorption and exsorption rates. This model forms a foundation for our further exploration of the quantitative relationship between HCB exposure and development of preneoplastic liver foci.

1. INTRODUCTION

Physiologically based pharmacokinetic (PBPK) modeling is generally used to describe and predict chemical pharmacokinetic profiles in animals or humans under normal physiological conditions. The performance of a PBPK model is usually based on *a priori* information, e.g., tissue/organ volumes, blood flow rates, partition coefficients, metabolism rates, etc. Such information is either available in the literature or obtainable through experimentation. Changes in some of those parameters are expected under pathophysiological and/or toxicological conditions and these changes should be incorporated into a PBPK model. PBPK modeling is an excellent tool for quantitatively analyzing chemical pharmacokinetics in pathophysiological and/or toxicological states (Roth *et al.* 1993b; Thomas 1998), although such applications are rare.

Hexachlorobenzene (HCB) is a persistent organic pollutant. Although its commercial production and use were banned, HCB still exists in the environment due to its chemical stability and high lipophilicity. HCB causes various toxic effects in laboratory animals and humans (Alvarez *et al.* 1999; Koss *et al.* 1978; Ralph *et al.* 2003; Schielen *et al.* 1995; Smith *et al.* 1987). Despite lack of genotoxicity (Siekel *et al.* 1991), HCB-induced

carcinogenicity was observed in laboratory animals with the liver being a main target organ (Erturk *et al.* 1986; Smith *et al.* 1985).

The pharmacokinetics of HCB have been intensively studied (Koss and Koransky 1975; Scheufler and Rozman 1984a, b; Yang *et al.* 1975; Yang *et al.* 1978). HCB primarily accumulates in the adipose tissue in the body. Some investigators (Gomez-Catalan *et al.* 1991; Scheufler and Rozman 1984a; Yang *et al.* 1975) reported that HCB binds to erythrocytes. Since this binding influences the disposition of HCB, it is important to take such a process into consideration in PBPK modeling. Furthermore, in addition to low level of metabolism in the liver, an important elimination pathway for HCB is passive diffusion from blood into the gastrointestinal (GI) lumen (Rozman *et al.* 1985), a process known as "exsorption" (Arimori and Nakano 1998; Israili and Dayton 1984). In updating PBPK modeling for HCB, therefore, this important exsorption process should also be incorporated.

There are three published PBPK models for HCB. Yesair *et al.* (1986) first developed a PBPK model for female rats and humans to describe HCB disposition after continuous dietary exposure. Freeman *et al.* (1989) constructed another PBPK model simulating HCB disposition following an intravenous (iv) dose in the rat. Roth *et al.* (1993a) reported a more complicated version for HCB, specially emphasizing the absorption and excretion processes. All these models were constructed for normal rats; no pathophysiological conditions were involved. Moreover, the erythrocyte binding and exsorption processes, important for HCB pharmacokinetics, were not incorporated in one or more of these models. Although exsorption was considered in the Freemen *et al.* (1989) model, their work was limited to iv dosing.

The medium-term liver foci bioassay by Ito *et al.* (2003) is a widely used alternative animal model for evaluating carcinogenicity. As shown in Fig. 2.1, the 8-week protocol involves administration of a potent initiator (diethylnitrosamine, DEN) followed by test chemical treatment and hepatocyte mitogenic stimulation (partial hepatectomy) in male F344 rats. The evaluation of carcinogenic potential is achieved by identification and analysis of hepatic glutathione S-transferase placental form (GST-P) preneoplastic foci at the end of the bioassay. In our laboratory, this protocol was modified by incorporating several sacrifice points to collect time-course data on test chemical pharmacokinetics and GST-P foci development (Ou *et al.* 2003; Ou *et al.* 2001; Thomas 1998; Yang *et al.* 1998).

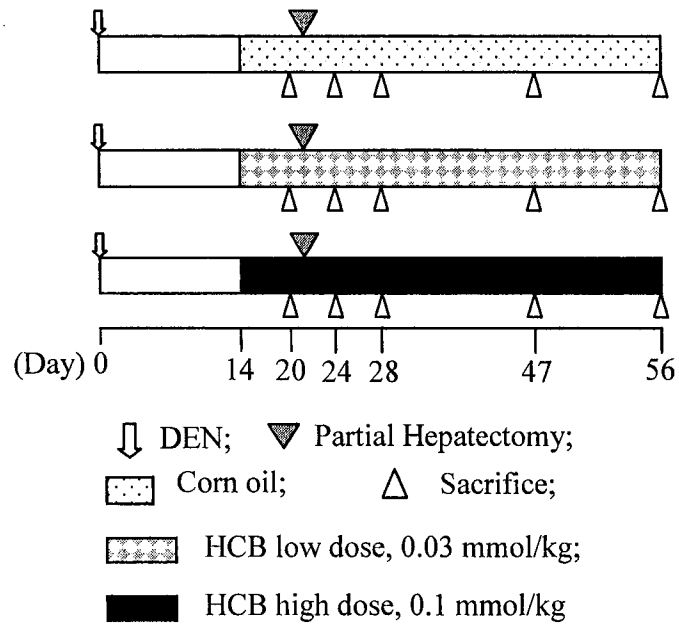

Fig. 2.1. Experimental design of the HCB pharmacokinetic study integrated in a time-course liver foci bioassay. A single ip injection of DEN was given on day 0. Daily oral gavage of corn oil (control) or HCB started from day 14. On day 21, a two-thirds partial hepatectomy was performed on the rats. On the surgery day and the following three days HCB was not administered to reduce the stress to the animals. Six rats from each treatment group were sacrificed on days 20, 24, 28, 47, and 56. The liver, kidney, blood, thigh muscle, and abdominal fat were collected for HCB analysis and PBPK modeling.

In the medium-term liver foci bioassay, repeated oral gavage of HCB in a corn oil vehicle significantly promoted GST-P foci development (Gustafson *et al.* 2000). The computational analyses (clonal growth modeling) in our laboratory successfully simulated the data of HCB-promoted foci development (Ou *et al.* 2003; Ou *et al.* 2001). We are interested in determining the relationship between oral exposure to HCB and liver GST-P foci development in the rat by coupling PBPK and clonal growth modeling. Given the limitations of the currently available PBPK models, an HCB PBPK model with the incorporation of pathophysiological conditions is needed.

The purposes of this study were twofold: (1) to modify the existing PBPK models of HCB by incorporating oral exposure route and, more importantly, the erythrocyte binding and exsorption processes, such that the model structure becomes more biologically realistic; and (2) to incorporate pathophysiological changes following partial hepatectomy and HCB treatment into the model to describe HCB pharmacokinetics in our medium-term liver foci bioassay. Thus, this study will form a foundation for our further exploration in the quantitative relationship between HCB exposure and GST-P foci development.

2. MATERIALS AND METHODS

This study consisted of two parts: (1) development of a PBPK model for HCB in the rat under normal physiological conditions with the incorporation of erythrocyte binding of HCB (Gomez-Catalan *et al.* 1991; Yang *et al.* 1975) and the exsorption process using pharmacokinetic data mined from the literature; and (2) experimental pharmacokinetic

study of HCB under the time-course medium-term liver foci bioassay protocol, and simulation of this data set by incorporation of the pathophysiological conditions.

2.1. Development of a PBPK model under normal physiological conditions with incorporation of erythrocyte binding and the exsorption process

2.1.1. Literature data sets

Three previously reported time-course data sets from independent studies with different dosing regimens were collected from the literature for model development.

Single iv dose study: Scheufler and Rozman (1984b) exposed male Sprague-Dawley rats, iv, to 1.5 mg ^{14}C-labeled HCB/kg body weight. HCB time-course tissue concentrations, converted from radioactivity in the tissues determined by liquid scintillation counting, were measured after exposure. The unit conversion was based on the observation that HCB was stored mainly unmetabolized in all tissues examined (Scheufler and Rozman 1984b). The concentration data were retrieved from the graphs in the paper (Scheufler and Rozman 1984b) using digiMatic® (Windows version 2.2c, FEB Software, Chesterfield, Virginia). In another study by the same group (Scheufler and Rozman 1984a), male Sprague-Dawley rats were exposed to the same regimen. Cumulative excretion of HCB and its metabolites, expressed as percentage of the dose, in feces and urine was quantified in a time-course manner up to 56 days. The related data were collected from Scheufler and Rozman (1984a) and two other papers (Freeman *et al.* 1989; Roth *et al.* 1993a). As the experimental conditions of the two studies were almost identical, the two data sets were pooled.

Single oral gavage study: Male Wistar rats were orally administrated with 0.2 mg HCB in 1 ml corn oil after an overnight fast (Yamaguchi *et al.* 1986). At various time

points after exposure, the HCB concentration was measured in adipose tissue, blood, and liver using gas chromatography.

Repeated oral gavage study: Koss *et al.* (1978) treated female Wistar rats orally with 50 mg/kg HCB in olive oil every other day up to 15 weeks. HCB concentrations in adipose tissue, liver, and blood were determined at weeks 3, 6, 9, 12, and 15. Time-course daily excretion of HCB in feces was recorded. The amounts of daily excreted main metabolites, *i.e.*, pentachlorophenol (PCP), tetrachlorohydroquinone (TCH), and pentachlorothiophenol (PCThP) in the urine, and PCP and PCThP in the feces, were also measured at the five time points. We calculated the daily sum of these metabolites in molar unit, which was an estimate of the amount of HCB metabolized per day; the metabolites retained in the tissues were neglected because they only accounted for a very small portion of the total metabolites.

2.1.2. Model development under normal physiological conditions

The model development under normal physiological conditions followed a 2-step process:

First, the development was based on the single iv dose data set (Scheufler and Rozman 1984a, b) because: (a) iv dosing studies, which bypassed the absorption phase, provided "cleaner" pharmacokinetic data, and (b) the data were from the most detailed studies, including both time-course tissue concentrations and excretion data;

Second, the model, once developed, was modified to describe the single oral exposure data (Yamaguchi *et al.* 1986) and the repeated oral exposure data (Koss *et al.* 1978) by incorporating the gastrointestinal absorption process.

This 2-step process was expected to progressively minimize the uncertainties in the model parameterization.

Model structure: The model structure included the liver, blood, fat, and rapidly and slowly perfused compartments, and GI lumen (Fig. 2.2). Blood was divided into two subcompartments: plasma and erythrocytes, based on the observations that in rats the HCB concentration in erythrocytes was 5.6-fold higher than in plasma *in vitro* (Yang *et al.* 1975) and about 10-fold higher *in vivo* (Gomez-Catalan *et al.* 1991; Scheufler and Rozman 1984a). Because the association and dissociation constants between HCB and erythrocytes are not available, a linear distribution of HCB between plasma and erythrocytes was assumed (see Appendix I for the equation). We feel that, in the absence of data, this is the simplest and least troublesome assumption to follow. HCB in plasma was available for tissue uptake, which was assumed flow-limited. To examine whether the incorporation of HCB binding with erythrocytes improves model simulation, we simulated the iv dosing data (Scheufler and Rozman 1984a, b) with and without the binding to erythrocytes (see Fig. 2.3D later).

Following an iv exposure, the amount was assumed to be immediately introduced into plasma at the start of simulation, from where it partitioned into erythrocytes and other compartments. Metabolism of HCB in the liver was very low and was assumed to be a first-order process. Once produced, the metabolites were rapidly excreted: 42% via urine and 58% via feces (Koss and Koransky 1975). As HCB is poorly metabolized, the metabolites in any tissue are negligible, which is experimentally supported (Koss and Koransky 1975). With this simplification, the tissue radioactivity, including in plasma, was considered the parent compound HCB. The excretion of the metabolites was traced

only during simulation of the single iv dose data. The induction of HCB metabolism was not considered due to lack of information.

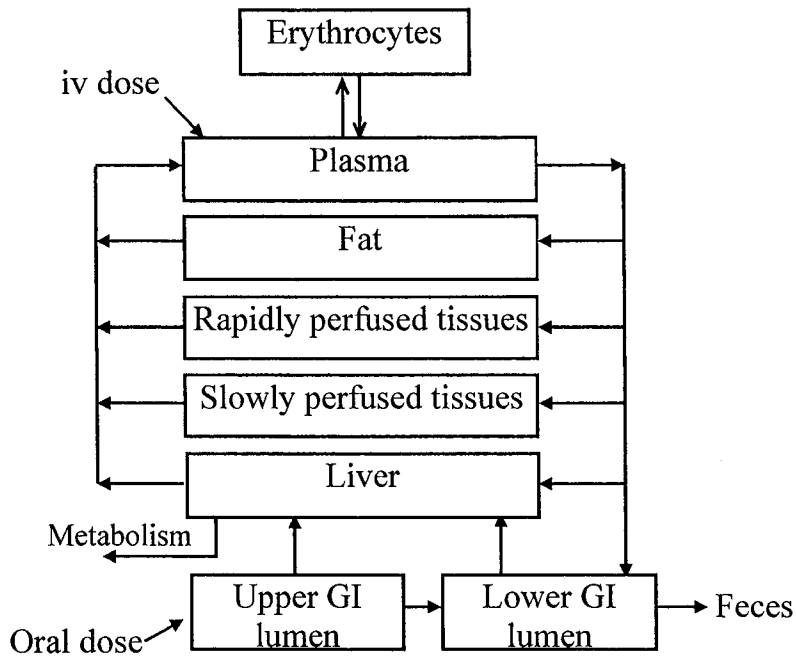

Fig. 2.2. Diagram of the PBPK model for HCB following iv or oral exposure. For an iv exposure, the upper GI lumen was turned off, and the excretion of metabolites was tracked. For oral exposures, the reverse was true.

Our initial attempt with a single-GI lumen structure could not simulate the shapes of the tissue concentration data following an oral dose (Yamaguchi *et al.* 1986). Since a two-GI lumen structure could adequately describe tissue concentrations following the oral exposure of some chemicals in corn oil (Staats *et al.* 1991) and HCB was administered in oily vehicles in the collected studies (Koss *et al.* 1978; Yamaguchi *et al.* 1986), the GI lumen was divided into an upper and a lower part (Fig. 2.2). For an oral administration, both parts played their respective roles, *i.e.*, HCB was absorbed from both

sites, meanwhile the chemical moved downwards through the whole lumen. The absorption and downward movement were described with first-order equations.

The blood-to-lumen exsorption process occurs in both small and large intestines (Richter and Schafer 1981), but only the large intestine determines the net excretion of HCB in the feces (Rozman *et al.* 1985). Thus, in our model, HCB was exsorbed only into the lower GI lumen, from where it may be reabsorbed into the liver or excreted via feces. HCB exsorption, (re)absorption, and excretion via feces were first-order processes. The absorption of orally dosed HCB and reabsorption of exsorbed HCB in the lower GI lumen may follow the same mechanism and thus were controlled by the same rate constant. The model equations are presented in Appendix I.

Parameterization: Since the rats in the reported studies were in a fast growth phase and the simulation durations were longer than 1 month, changes in the body weights and tissue/organ volumes were incorporated. The age-dependent body weights were obtained from the corresponding study (Koss *et al.* 1978) or other papers (Hida *et al.* 1999; Schoeffner *et al.* 1999). The growth curves were interpolated with a TABLE function (Advanced Continuous Simulation Language, ACSL, programming, AEgis Technologies Group, Huntsville, AL) in the model codes. The volume of each compartment was defined with body weight-dependent functions unless otherwise indicated. The cardiac output of blood (QBld) was proportional to (body weight)$^{0.75}$ (Brown *et al.* 1997). The cardiac output of plasma (QPl, L/h), *i.e.*, the flow rate of plasma through the heart, was then determined by

$$QPl = QBld \times (1.0 - HMTC) \quad \text{(Eq-1)}$$

where HMTC was rat hematocrit. The plasma flow rate to each compartment was governed by respective flow fraction of QPl. All physiological parameters used are summarized in Table 2.1.

Defined as the ratios of tissue concentrations over the plasma concentration, the partition coefficients (Table 2.2) of fat, liver, and rapidly perfused compartment were estimated from the repeated oral gavage data (Koss *et al.* 1978) where steady state was reached. As Freeman *et al.* (1989) had done in their study, we plotted the fat, liver, or kidney concentration as a function of the blood concentration at all five time points from Koss *et al.* (1978) data, and determined the slope (*i.e.*, $\Delta y/\Delta x$ or tissue concentration/blood concentration) using linear regression analysis with the function going through the origin. The slopes were then recognized as tissue partition coefficients (all correlation coefficients $r^2 > 0.96$). The partition coefficient of the rapidly perfused compartment was set the same as that of kidney. While it was not available in the repeated oral gavage study (Koss *et al.* 1978), the plasma concentration was estimated to be 4.8-fold lower than the blood concentration based on Gomez-Catalan *et al.* (1991). The partition coefficient of the slowly perfused compartment (represented by muscle) was from Freeman *et al.* (1989).

Other parameters with no information were optimized by model fitting to the data sets; they were considered as "adjustable parameters". For simulating the iv dose data (Scheufler and Rozman 1984a, b), there were four adjustable parameters: rate constants of metabolism, exsorption, reabsorption, and fecal excretion. Manual adjustment was initially used to get a sense of the effects of these parameters on the simulation results. Then with the best-visual-fit values as start values, ACSL MATH-based statistical

optimization was executed. This optimization process included: (1) Local optimization, *i.e.*, each individual parameter was adjusted to give the best fit to the piece of data to which this parameter had the most influence whereas the other adjustable parameters were held fixed. For example, the rate constants of exsorption and reabsorption were adjusted against the tissue concentrations, the metabolism rate constant against the amount of metabolites in urine, and the fecal excretion rate constant against the amount in feces; (2) Global optimization, *i.e.*, all the adjustable parameters were varied simultaneously against the whole data set. The locally optimized values were inputs for the global optimization, and they were constrained in narrow ranges to avoid statistically best but biologically implausible values. The optimization was performed using the Generalized Reduced Gradient method, with the heteroscedasticity value set to 2.

For simulating the single and repeated oral gavage data, there were six adjustable parameters: the rate constants of metabolism, exsorption, absorption from the upper GI lumen, absorption from the lower GI lumen, mass transfer from the upper to the lower GI lumen, and excretion in feces. According to the absorption and exsorption characteristics of HCB (see Discussion), we did not expect that a single set of the adjustable parameters would fit both oral data sets, which was supported by our initial trials. Hence, holding other adjustable parameters as constants in the two scenarios, we allowed the exsorption rate constant to vary with exposure conditions. Manual adjustment was made to achieve the best visual fit to these two data sets. All adjustable parameters are summarized in Table 2.2.

Table 2.1. Physiological Parameters for HCB PBPK Model

Parameters (abbreviation) (unit)	Single iv dose (Scheufler and Rozman 1984a, b)	Single oral gavage (Yamaguchi *et al.* 1986)	Repeated oral gavage (Koss *et al.* 1978)
Body weight (BW) at start of experiment (kg)	0.234[a]	0.125[b]	0.135[c]
Tissue volumes (or volume fractions)			
Fat volume fraction (VFC)	$0.199\times BW + 0.01664$[d,i]		0.05[d,e]
Liver volume (VL) (L)	$0.0321\times BW + 0.00197$[f,i]		N/A
Liver volume fraction (VLC)	N/A		0.037[g]
Blood volume (VB) (L)	$0.062\times BW + 0.0012$[h,i]		
Rapidly perfused (VR) (L)	$0.0333\times BW + 0.01203$[f,i]		
Slowly perfused (VS) (L)	$0.91\times BW\text{-}VF\text{-}VL\text{-}VB\text{-}VR$[i]		
Hematocrit (HMTC)	0.367[h]		
Cardiac output constant (QCC) ($L/h/kg^{0.75}$)	14.1[d]		
Tissue plasma flow fractions			
Fat (QFC)	0.07[d]		
Liver (QLC)	0.18[d]		
Rapidly perfused (QRC)	0.76-QLC		
Slowly perfused (QSC)	0.24-QFC		

a: age-dependent BW adopted from Schoeffner *et al.* (1999); *b*: age-dependent BW adopted from Hida *et al.* (1999); *c*: age-dependent BW recorded in (Koss *et al.* 1978); *d*: Brown *et al.* (1997); *e*: assumed to be constant because HCB inhibits fat accumulation in the body (Alvarez *et al.* 1999; Smith *et al.* 1987); *f*: Schoeffner *et al.* (1999); *g*: the value at the start of experiment was estimated from Brown *et al.* (1997) but the time-dependent values later in the experiment were from Koss *et al.* (1978); *h*: Lee and Blaufox (1985); *i*: BW was in kg in all equations.
N/A: not applicable

Table 2.2. Partition Coefficients and Rate Constants for HCB PBPK Model

	Single iv dose (Scheufler and Rozman 1984a, b)	**Single oral gavage (Yamaguchi *et al.* 1986)**	**Repeated oral gavage (Koss *et al.* 1978)**	**Medium-term bioassay (Low dose)[a]**	**Medium-term bioassay (High dose)[a]**
Partition coefficients					
Fat (PF)	315.0[b]	315.0[b]	315.0[b]	200.0[c]	200.0[c]
Liver (PL)	10.7[b]	10.7[b]	10.7[b]	10.7[b]	10.7[b]
Rapidly perfused (PR)	7.0[b]	7.0[b]	7.0[b]	7.0[b]	7.0[b]
Slowly perfused (PS)	3.2[d]	3.2[d]	3.2[d]	3.2[d]	3.2[d]
Rate constants (abbreviation) (unit)					
Metabolism (KMET) (L/h)	0.00195[e]	0.00195[f]	0.00195[f]	0.00195[f]	0.00195[f]
Exsorption (KBGI) (L/h)	0.03[e]	0.045[g]	0.02[g]	0.1[h]	0.1[h]
Upper GI absorption (KGILV1) (h^{-1})	N/A	0.082[g]	0.082[g]	0.012[h]	0.012[h]
Lower GI absorption (KGILV2) or Reabsorption (KGILV) (h^{-1})[j]	0.003[e]	0.007[g]	0.007[g]	0.0007[i]	0.0007[i]
Upper-to-lower transfer (KUpLow) (h^{-1})	N/A	0.004[g]	0.004[g]	0.004[i]	0.004[i]
Fecal excretion (KFEC) (h^{-1})	0.00065[e]	0.0014[g]	0.0014[g]	0.0014[i]	0.0014[i]

a: our pharmacokinetic study integrated in the liver foci bioassay; *b*: estimated from Koss *et al.* (1978); *c*: estimated from our bioassay data; *d*: from Freeman *et al.* (1989); *e*: ACSL MATH-based optimization against the iv dose data (Scheufler and Rozman 1984a, b); *f*: metabolism rate constant was assumed same in all exposure scenarios; *g*: visual fitting to two data sets (Koss *et al.* 1978; Yamaguchi *et al.* 1986); *h*: visual fitting to the low and high dose data from our bioassay; *i*: adopted from the single and repeated oral gavage studies; *j*: the lower GI absorption and reabsorption processes were controlled by the same rate constant.
N/A: not applicable

Model validation: A separate study, different from the data sets used to build the model, where female Wistar rats were given single oral dosing of ^{14}C-HCB at 20 or 180 mg/kg in olive oil (Koss and Koransky 1975) was used to validate the model. The tissue concentrations were determined by radioactivity. Koss and Koransky (1975) found that even at the level of 180 mg/kg the radioactivity in the liver and fat was nearly completely attributed to the parent compound; this result supports the appropriateness of using this data set for model validation.

Sensitivity analysis: Sensitivity analysis is a valuable method for identifying key parameters affecting a pharmacokinetic measurement. Clewell *et al.* (1994) defined log-normalized sensitivity parameters (LSPs) as

$$LSP = \frac{\partial \ln R}{\partial \ln x} \qquad \text{(Eq-2)}$$

where R is a model output and x is the parameter for which the sensitivity is being examined. This definition quantifies the percentage change in an output value due to the percentage change in a parameter. In this study, the liver concentration was an output of most concern. Thus, we determined the sensitivity of the liver concentration to the fat and liver volume fractions, tissue partition coefficients, and the adjustable parameters following a single oral gavage dose. The LSPs were calculated at multiple time points using the central difference method. The LSP greater than 1 indicates that error in a parameter results in amplified error in the related output (Clewell *et al.* 1994).

2.2. Simulation of the pharmacokinetic data from the time-course medium-term liver foci bioassay by incorporating the pathophysiological conditions

2.2.1. Pharmacokinetic study under the time-course liver foci bioassay protocol

HCB (99% purity) and 1,2,4,5-tetrabromobenzene (97% purity) were purchased from Aldrich Chemical (Milwaukee, WI). DEN was obtained from Sigma Chemical (St. Louis, MO). Toluene (99.9% purity) and sulfuric acid were supplied by VWR Scientific (Denver, CO). Anhydrous sodium sulfate was purchased from Fisher Scientific (Houston, TX). Florisil® was provided by Alltech Associates (Deerfield, IL).

Male F344 rats, 30 days of age, purchased from Harlan Sprague-Dawley (Indianapolis, IN), were housed in the Painter Center, Colorado State University. It is fully accredited by the American Association for Accreditation of Laboratory Animal Care (AAALAC). Animals were given food (Harlan Teklad NIH-07 diet, Madison, WI) and water *ad libitum* and lighting was set on a 12h light/dark cycle. The study was conducted in accordance with the National Institutes of Health (NIH) guidelines for the care and use of laboratory animals.

After four weeks of acclimation, the rats were randomized by weight, divided into three groups, and treated according to the time-course liver foci bioassay (Fig. 2.1). At week 0, the rats were given a single intraperitoneal (ip) injection of DEN (200 mg/kg) dissolved in 0.9% saline. Two weeks later, the rats began receiving daily oral gavage (5 ml/kg body weight) of corn oil (control), 8.55 mg/kg HCB (low dose), or 28.5 mg/kg HCB (high dose) in corn oil until sacrifice. According to the earlier work by our group (Ou *et al.* 2001), at 28.5 mg/kg, HCB significantly promoted GST-P foci formation in the medium-term liver foci bioassay. In this study we used a second dose, 8.55 mg/kg, in order to examine GST-P foci formation at this lower dose, although GST-P foci data were beyond the scope of this report. At week 3 (day 21), a two-thirds partial hepatectomy was performed on the rats. On the surgery day and the following three days,

HCB was not administered to reduce the stress to the animals while recovering from surgery. On days 20, 24, 28, 47, and 56, six rats from each group were sacrificed by aortic exsanguination under anesthesia. These time points cover pre- and post-partial hepatectomy periods. The body and liver weight of each rat were recorded at sacrifice. The liver, kidney, blood, thigh muscle, and abdominal fat were collected from each rat for HCB analysis and subsequent PBPK modeling. All tissue samples were frozen with liquid nitrogen and stored at -70°C until analysis.

Samples (0.5 ml blood, 0.1 g fat, and 0.2 g other tissues) of the HCB treated rats, spiked with 1,2,4,5-tetrabromobenzene as an internal standard, were digested with 3 ml of 60% sulfuric acid overnight, and then extracted with 5 ml of toluene 3 times. The resulting extracts were concentrated to about 2 ml and cleaned through a column containing 1 g anhydrous sodium sulfate and 1 g Florisil®. Each column was washed 5 times with 2 ml of pentane per time after the passage of the concentrated extract. The eluant was concentrated and then analyzed on an HP-5890 II Plus gas chromatograph (Hewlett Packard, Wilmington, DE) equipped with an electron capture detector. An EQUITY™-5 fused silica capillary column (Supelco, PA) was employed. Helium and nitrogen were used as the carrier and makeup gases with flow rates of 4 ml/min and 60 ml/min, respectively. The oven temperature was initially 150°C for 1 min, increased to 175°C at 10°C/min, where it remained for 10 min. The temperatures of the inlet and detector were 250°C and 300°C, respectively. The recoveries of HCB and the internal standard of this method were in the range of 70-100%.

Differences of the body weight, liver weight, and liver/body weight ratio among the control and treated groups were analyzed for significance with and without the factor of

time using ANOVA at $\alpha = 0.05$. All statistical analyses were performed using SAS (version 8.02; SAS Institute Inc., Cary, NC).

2.2.2 Simulation of the pharmacokinetic data by incorporating the pathophysiological conditions

The PBPK model, developed by us earlier, was employed to describe the data of HCB pharmacokinetic study integrated in the time-course liver foci bioassay. The DEN treatment and surgery on the liver distinguished the rats in this bioassay from those in other studies. As there was a two-week recovery interval after DEN injection, we assumed that DEN had negligible effect on HCB disposition after the beginning of HCB administration, and hence the DEN-related alterations were not considered in the model simulation. Following partial hepatectomy, drastic physiological responses occur in the liver and the whole body to signal and facilitate liver regeneration (Katagiri 1988; Michalopoulos and DeFrances 1997; Sabugal *et al.* 1996). Since it is impractical and unnecessary to capture every pathophysiological change mathematically in our model, simulation we chose to incorporate the changes in the body and liver weights and fat volume because of their major impacts on HCB disposition. HCB treatment may also contribute to those changes (Alvarez *et al.* 1999; Koss *et al.* 1978; Smith *et al.* 1987). After the partial hepatectomy, the liver weight immediately decreased by 70%; the body weight and fat volume also reduced (Katagiri 1988; Sabugal *et al.* 1996). The body and liver weights were recorded at several time points prior to and after the surgery, but the fat volume change was modeled based on the following rationale.

The fat volume fraction (VFC) prior to partial hepatectomy was calculated according to the equation derived from historical data by Brown *et al.* (1997):

$$VFC\ (\%\ BW) = 35 \times BW + 0.205 \quad \text{(Eq-3)}$$

where BW is in kg. After the surgery, to describe the fat mobilization and redeposit, we expressed the VFC with a two-term function as suggested by Thomas (1998):

$$VFC = a \times \exp[-b \times (t - 336)] + c \times (t - 336) \quad \text{(Eq-4)}$$

where t was the time (hours) following DEN injection; the number 336 referred to the time (hours) when HCB dosing began; a, b, and c were constants controlling the shape of the function. The constants a, b, and c were assigned with values 1.1, 0.017, and 6.0×10^{-5}, respectively, such that the VFC reduced to 2.38% from 7.6% (low dose group) or 7.4% (high dose group) in the first 7 days after PH and then gradually increased to approximately 6% at the end of simulation (1344 hours). This function was in line with our qualitative understanding in fat mobilization and redeposit after partial hepatectomy and it has helped us in the PBPK model simulation of pharmacokinetics of pentachlorobenzene in partially hepatectomized rats in our laboratory.

The partition coefficients of the liver and rapidly (set the same as kidney partition coefficient) and slowly perfused compartments (set the same as muscle partition coefficient) estimated from our data were similar to those from the repeated oral gavage data (Koss *et al.* 1978), hence the latter were used in the model simulation. The fat partition coefficient, however, was about 200.0, lower than that estimated from Koss *et al.* (1978). This discrepancy may result from the change in fat composition due to the mobilization of nonpolar lipids after partial hepatectomy (Katagiri 1988) in the bioassay. The value 200.0 was used and remained constant during the simulation.

Software The model was coded and the simulations and optimizations were performed using ACSL Tox 11.8.4 (AEgis Technologies Group, AL). The sensitivity

analysis was executed using acslXtreme 2.0.1.2. (Xcellon, West Austin, TX). The computer code of HCB PBPK model is attached in Appendix II.

3. RESULTS

3.1. Model performance under normal physiological conditions

3.1.1. Description of the iv dose study data

The model simulations of HCB concentrations in the liver, plasma, and muscle (slowly perfused compartments) (Fig. 2.3A) and in fat (Fig. 2.3B) were consistent with the experimental data reported by Scheufler and Rozman (1984a; 1984b). The percentages of the dose excreted in the urine and feces were also well described by the model simulation (Fig. 2.3C). According to the model simulation, HCB appeared in the lower GI lumen shortly after administration, which was observed by Scheufler and Rozman (1984b). The percentage of the dose in the GI lumen increased from 0 at the time of exposure to about 45.6% in 312 hours; thereafter the percentage gradually decreased to 24% at the end of simulation (1344 hours). Since biliary excretion is known to be a minor route of excretion (Ingebrigtsen *et al.* 1981), these results implied the importance of exsoprtion for HCB elimination.

The performance of the present model was compared with the model without considering HCB binding with erythrocytes as employed previously (Freeman *et al.* 1989; Roth *et al.* 1993a; Yesair *et al.* 1986). As shown in Fig. 2.3D, the simulations of the two PBPK models were different during the first ten hours: the present model traced the liver and plasma concentrations very well, whereas the model without HCB binding incorporated underpredicted the data.

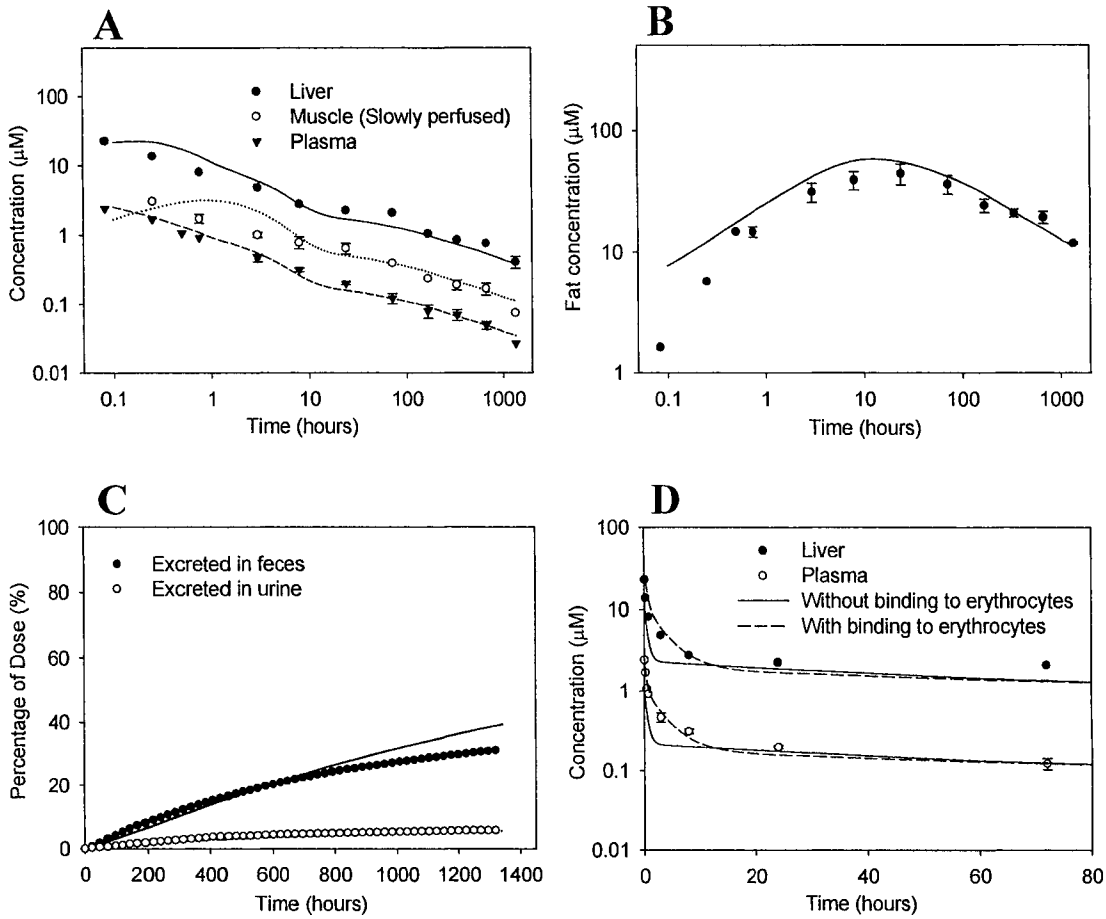

Fig. 2.3. For a single iv dose of 1.5 mg/kg in the rat, model simulations and data of (A) HCB concentrations in the liver, muscle (slowly perfused compartment), and plasma; (B) HCB concentration in the fat; (C) percentages of the dose excreted in the urine and feces; and (D) the liver and plasma concentrations in the first 80 h simulated with and without the incorporation of HCB binding to erythrocytes. The lines are simulations and the symbols are experimental data (Scheufler and Rozman 1984a, b).

3.1.2. Description of the single and repeated oral gavage study data

Comparisons between the model simulations and the single oral gavage data (Yamaguchi *et al.* 1986) are shown in Fig. 2.4 for the fat, liver, and blood HCB concentrations. The plot indicated that the model simulations were in good agreement with the data. The model also simulated the tissue HCB concentrations consistently with

the repeated oral gavage data (Koss *et al.* 1978) (Fig. 2.5A). The estimates of HCB excreted in the feces per day and metabolized per day at five time points were generally comparable to the experimental data (Fig. 2.5B, C). An approximately two-fold difference between the exsorption rate constants of the two exposure scenarios was necessary for a good description of both data sets (Table 2.2).

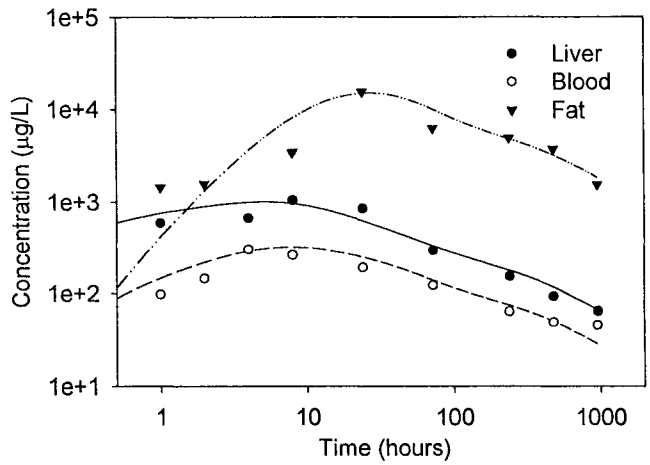

Fig. 2.4. For a single oral gavage of 0.2 mg HCB in the rat, model simulations and data of HCB concentrations in the fat, liver, and blood. The lines are simulations and the symbols are experimental data (Yamaguchi *et al.* 1986).

3.1.3. Model validation

Using Koss and Koransky (1975) time-course concentration data from rats, we validated our model under the condition of single oral gavage dosing. Since the value of one adjustable parameter, exsorption rate constant, had to be varied when fitting the single (Yamaguchi *et al.* 1986) and repeated (Koss *et al.* 1978) oral gavage data (0.045 vs 0.02 L/h, Table 2.2; see Discussion for the reasons), both values were tested during the validation. When the exsorption rate constant was set 0.02 L/h, the model predictions

agreed with the data (Fig. 2.6A and B) well. However, when the value was 0.045 L/h, the model notably underpredicted the second and third time points (data not shown).

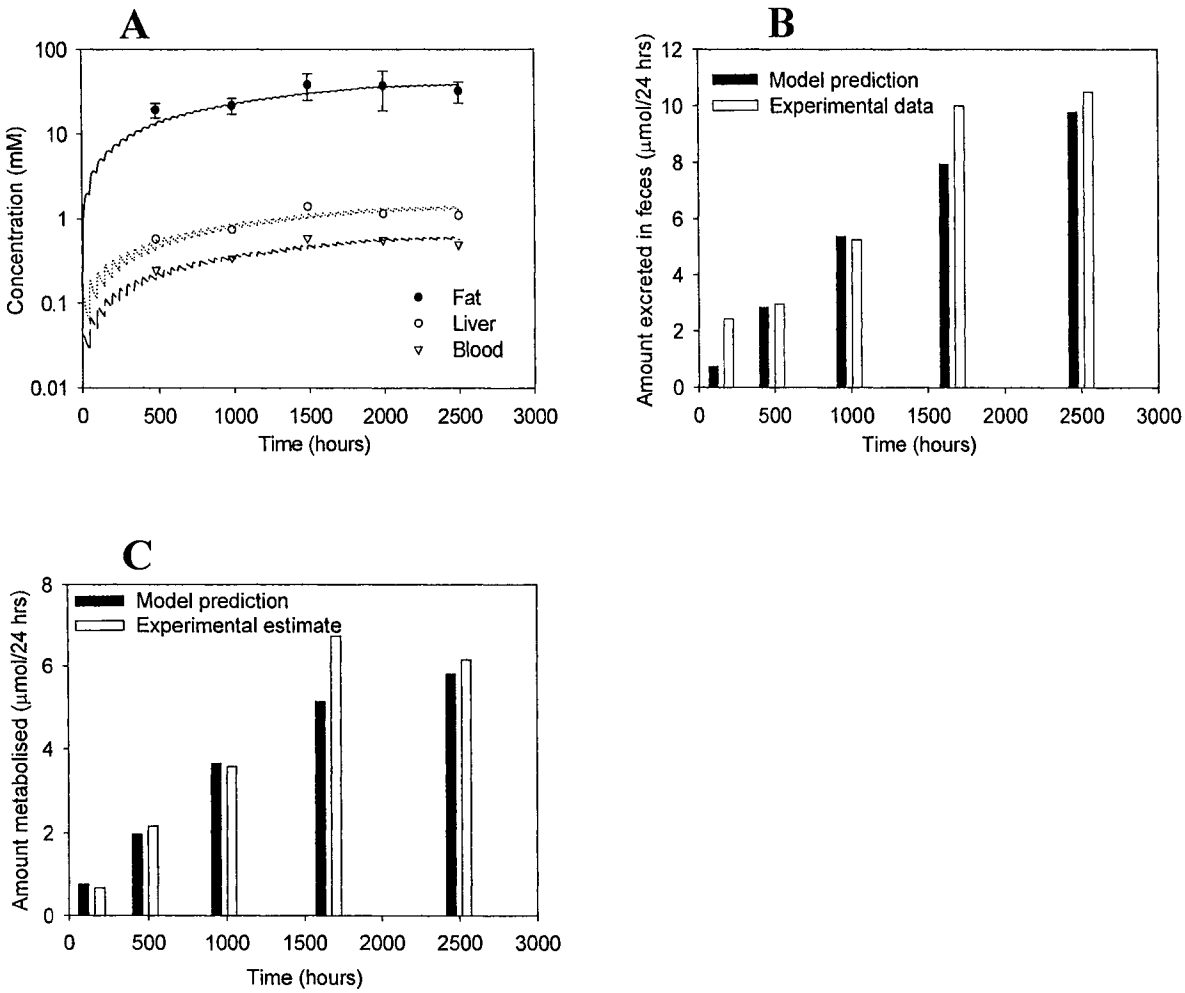

Fig. 2.5. For repeated oral gavage of 50 mg/kg HCB every other day in the rat, model simulations and data of HCB (A) concentrations in the fat, liver, and blood; (B) the amount excreted in feces per 24 h at five time points; and (C) the amount metabolized per 24 h at five time points. In (A) the lines are simulations and the symbols are experimental data (Koss *et al.* 1978).

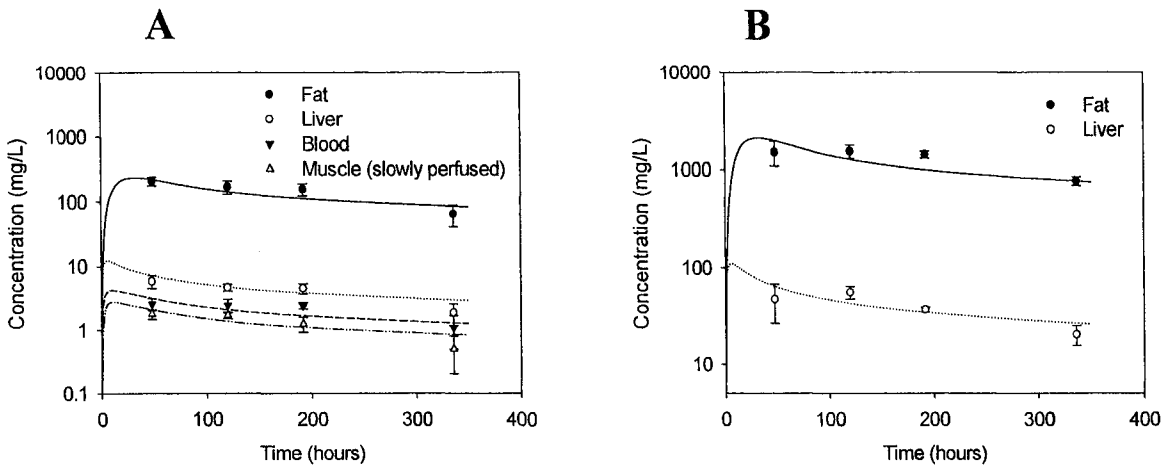

Fig. 2.6. For a single oral gavage dose of HCB in the rat, model simulations and data of HCB concentrations in the (A) fat, liver, blood, and muscle (slowly perfused compartment) at 20 mg/kg, and (B) fat and liver at 180 mg/kg.

Table 2.3. Log-normalized Sensitivity Parameter Values for HCB Liver Concentration

Parameters	Hours after a single oral dose			
	1	24	72	336
Volume fractions				
Liver	0	0	0	0
Fat	0.001	-0.4982	-0.338	-0.238
Partition coefficients				
Liver	1.5103	1.8236	1.8241	1.8176
Fat	-0.0037	-0.8275	-0.5628	-0.3540
Rapidly perfused	-0.1702	-0.0311	-0.0137	-0.0078
Slowly perfused	-0.0817	-0.0813	-0.0461	-0.0619
Rate constants				
Metabolism	0.0053	0.0042	0.004	0.004
Exsorption	-0.0918	0.1024	0.0966	0.0973
Upper GI absorption	0.1509	-0.0464	1.2297	-0.0373
Lower GI absorption	0.0008	0.0127	0.0137	0.0139
Upper-to-lower transfer	-0.0131	0.0089	0.0096	-0.0063
Fecal excretion	0	-0.0076	0.0031	0.0028

3.1.4. Sensitivity analysis

The sensitivity of the liver HCB concentration to the liver and fat volume fractions, tissue partition coefficients, and the adjustable parameters at multiple time points

following an oral dose was shown in Table 2.3. The liver partition coefficient had the largest effect on the liver concentration, the fat volume fraction and partition coefficient had moderate effects, and the other parameters had only mild to little effects.

3.2. Pharmacokinetic data from the time-course bioassay

3.2.1. Effects of HCB treatment on the liver and body weight of the rats

All the rats survived the study except one in the control group for an unknown reason. The body and liver weight of each rat were recorded at five sacrifice times (Table 2.4). The HCB treatment did not significantly change the body weight at any time point. The liver weight was significantly increased only on day 47 in the high dose group. The low dose HCB treatment increased the liver/body weight ratio on day 28, whereas the high dose increased this index significantly on days 20, 28, and 47. At the end of the experiment (day 56), the livers accounted for approximately 3.0% - 3.6% of the body weights.

3.2.2. HCB disposition in the tissues

Time-course HCB tissue concentrations are shown in Figs. 2.7A and B (low dose) and Figs. 2.8A and B (high dose). Similar disposition patterns were observed in both treated groups: the highest concentration in fat, followed by the liver, kidney, blood, and muscle. With a 3-fold difference in the exposure levels, there was approximately a 2- to 3-fold difference in the corresponding tissue concentrations of the two treated groups.

3.3. Simulation of the pharmacokinetic data in the time-course bioassay by incorporating pathophysiological conditions

Table 2.4. Body and Liver Weights and Liver/Body Weight Ratios of the Rats in the Liver Foci Bioassay

Days after DEN initiation	Body weight (g)			Liver weight (g)			Liver/body weight ratio (%)		
	Control	Low dose	High dose	Control	Low dose	High dose	Control	Low dose	High dose
20	204.6 ± 5.9	212.1 ± 13.0	205.0 ± 9.1	7.3 ± 0.2	7.5 ± 0.7	7.6 ± 0.4	3.56 ± 0.09	3.53 ± 0.13	3.71 ± 0.07*[!]
24	190.5 ± 9.0	191.6 ± 11.3	195.6 ± 13.4	5.3 ± 0.7	5.0 ± 0.4	5.3 ± 0.6	2.79 ± 0.33	2.63 ± 0.17	2.71 ± 0.17
28	204.9 ± 21.1	208.5 ± 14.9	207.4 ± 6.5	6.2 ± 0.6	7.0 ± 0.8	7.0 ± 0.6	3.04 ± 0.16	3.37 ± 0.24*	3.38 ± 0.21*
47	271.1 ± 15.4	262.7 ± 16.9	270.3 ± 20.5	8.4 ± 0.4	8.3 ± 0.6	9.3 ± 0.9*	3.08 ± 0.10	3.17 ± 0.07	3.45 ± 0.13*[!]
56	291.1 ± 25.1	284.9 ± 9.3	305.7 ± 21.1	9.5 ± 1.0	9.1 ± 0.8	10.5 ± 0.9[!]	3.28 ± 0.12	3.19 ± 0.24	3.44 ± 0.10

Note: The days 20, 24, 28, 47, and 56 after DEN initiation are equivalent to the days 6, 10, 14, 34, and 42 after the commencement of the oral administration with corn oil, 8.55, or 28.5 mg/kg HCB.
*: $p<0.05$, compared to the concurrent control group.
[!]: $p<0.05$, compared to the concurrent low dose group.

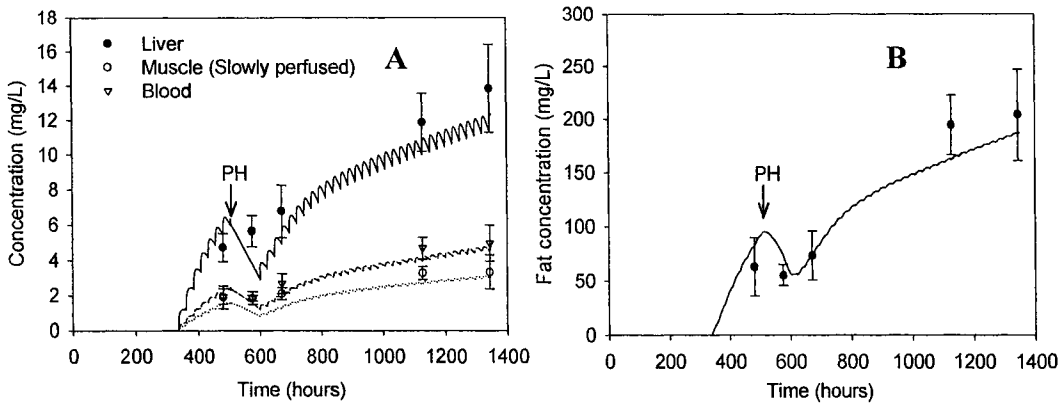

Fig. 2.7. Model simulations and experimental data of HCB concentrations in the (A) liver, muscle (slowly perfused compartment), and blood, and (B) fat in the rat in the pharmacokinetic study integrated in the liver foci bioassay where the dose of HCB was 8.55 mg/kg. The lines are simulations and the symbols are experimental data. The arrows indicate when the partial hepatectomy (PH) was performed.

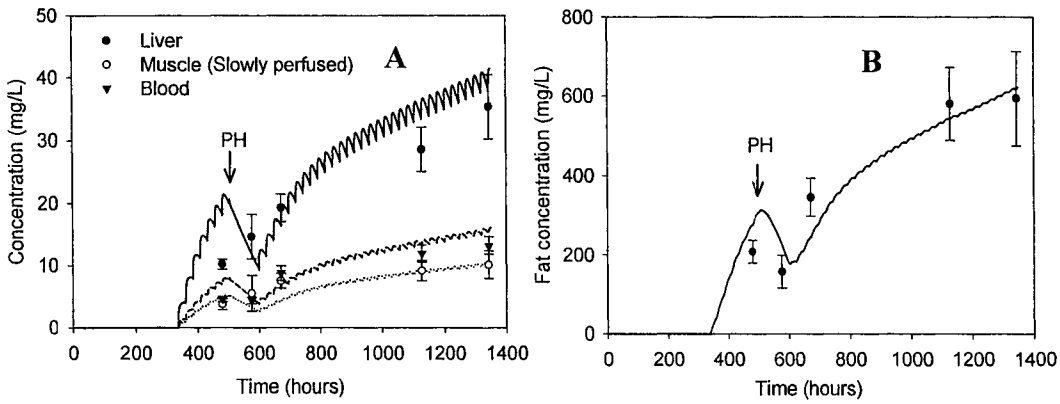

Fig. 2.8. Model simulations and experimental data of HCB concentrations in the (A) liver, muscle (slowly perfused compartment), and blood, and (B) fat in the rat in the pharmacokinetic study integrated in the liver foci bioassay where the dose of HCB was 28.5 mg/kg. The lines are simulations and the symbols are experimental data. The arrows indicate when the partial hepatectomy (PH) was performed.

The model simulations and experimental data are shown in Figs. 2.7A and B (low dose) and Figs. 2.8A and B (high dose). The concentrations in various tissues/organs started to increase immediately after 336 hour, when HCB administration began. Corresponding to the partial hepatectomy at 504 hour and, more importantly, the treatment suspension during 504 through 600 hour, there was concentration reduction in the interval. The model well predicted the late time points; yet the first time point was generally overpredicted.

4. DISCUSSION

This study reported an updated PBPK model for HCB in the rat with incorporation of erythrocyte binding, exsorption, and pathophysiological conditions following HCB treatment and partial hepatectomy. The model simulated well the pharmacokinetic data from a number of studies reported in the literature, as well as our own integrated pharmacokinetics/liver foci bioassay.

4.1. Necessity of building an updated PBPK model for HCB in the context of the medium-term liver foci bioassay

The conventional long-term carcinogenesis protocol is strikingly time and resource-intensive. With the large number of chemicals in commerce, it is virtually impossible to obtain carcinogenesis data on each chemical with the conventional method, let alone countless chemical mixtures to which humans are actually exposed. Therefore, alternative methods are in urgent need. Yang *et al.* (1998) proposed approaches integrating computational modeling with *in vitro* biological systems and *in vivo* bioassays. In this regard, the integration of biologically based computational modeling with a well-

recognized shorter-term bioassay for evaluating carcinogenesis would provide opportunity for the creation of predictive tools. In our laboratory, we have modified the Ito's medium-term liver foci bioassay into an integrated time-course pharmacokinetics/liver foci bioassay, and studied several chlorobenzenes (Ou *et al.* 2003; Thomas 1998). The GST-P foci development promoted by HCB, pentachlorobenzene, 1,2,4,5-tetrachlorobenzene, and 1,4-dichlorobenzene has been successfully simulated with clonal growth models (Ou *et al.* 2003; Ou *et al.* 2001; Thomas 1998). To build dose-response (foci development) relationships, chemical target doses (*i.e.*, liver concentrations of test chemicals in this case) should be achieved, which entails the application of PBPK modeling. It is possible that, by studying a series of congeners such as chlorobenzenes, quantitative structure-activity correlation can be established and coupled with PBPK and biologically based pharmacodynamic modeling (e.g., clonal growth modeling) for predictive purposes.

This reported study is a part of the larger ongoing project in our laboratory which aims at developing a predictive tool for carcinogenesis of chemical mixtures by integrating *in vitro* biological systems, medium-term pharmacokinetics/liver foci bioassays, and PBPK and clonal growth modeling. The PBPK model described here will be applied with a clonal growth model in the future to form a biologically based dose-response (BBDR) model for HCB that will shed light on the dose-response (GST-P foci formation) curve in the low-dose region and facilitate risk assessment.

Although there are three published PBPK models for HCB thus far (Freeman *et al.* 1989; Roth *et al.* 1993a; Yesair *et al.* 1986), we developed the present model because: (1) Simulating the liver concentration in the rat following HCB oral dosing and partial

hepatectomy was of our most concern, but the previous models do not fit our purpose well. The Freemen *et al.* intended to simulate and explain the distribution pattern of HCB in the body following an iv dose, and did not include an oral exposure route; the Yesair *et al.* focused on female rats and humans with inclusion of a breast compartment and pregnancy state; and the Roth *et al.* specifically emphasized gastrointestinal absorption and excretion processes. Furthermore, these models have structures, corresponding to their respective goals, that are unnecessarily complicated for our purpose; (2) We wanted to incorporate in the model the two features of HCB pharmacokinetics, exsoprtion (Rozman *et al.* 1985) and erythrocyte binding (Gomez-Catalan *et al.* 1991; Yang *et al.* 1975). The consideration of exsorption prevents assigning unreasonable high values to the parameters related to the minor elimination pathways (e.g., biliary excretion). The binding of HCB to erythrocytes hampers tissue uptake and reduces the declination of the concentrations in the plasma and tissues; incorporation of this binding process improved model simulation as illustrated in Fig. 2.3D; and (3) We needed to take into account pathophysiological state resulted from the experimental conditions of the liver foci bioassay. In order to build a dose-foci formation relationship, the prediction of liver concentration under the pathophysiological state is essential.

4.2. HCB pharmacokinetics

It is already clear that HCB distribution in the body is predominantly affected by the fat contents of tissues (Koss and Koransky 1975; Koss *et al.* 1978; Scheufler and Rozman 1984b) due to its high lipophilicity. Even in our liver foci bioassay, the fat still had the highest HCB concentration (Figs. 2.7 and 2.8) regardless of the unusual experimental conditions. Our model analysis indicated that the liver HCB concentration was

moderately sensitive to the fat volume and fat partition coefficient as shown in Table 2.3. In our time-course liver foci bioassay, partial hepatectomy was involved. Although the liver concentration was insensitive to the liver volume, the change in the liver volume (through partial hepatectomy) causes dramatic pathophysiological responses, including fat mobilization and redeposit. The sensitivity of liver concentration to fat volume warranted the inclusion of a change in the fat volume fraction (Eq-4) during simulation of the pharmacokinetic data from our bioassay.

There is pharmacokinetic difference for HCB in male and female rats (Kuiper-Goodman *et al.* 1977), which can largely be attributed to the different metabolism patterns in the two genders (Renner 1988). However, the fact that we were able to simulate all the data sets well without considering gender differences in the PBPK model suggests that the gender differences are not a sufficiently sensitive issue to affect our simulation outcomes. HCB can induce its own metabolism upon repeated dosing (Clark *et al.* 1981). However, HCB is relatively resistant to metabolism (Koss and Koransky 1975). Our sensitivity analysis suggested the liver concentration of HCB is insensitive to the metabolism rate constant. Therefore, during our model development, the assumptions that the pharmacokinetic difference between male and females rats was negligible and that the metabolism rate constant was not changed by repeated dosing were reasonable and did not affect the model simulations significantly.

4.3. Model parameter adjustment

Although the model structure in this study remained almost unchanged during the development and simulation processes, some transluminal diffusion (*i.e.*, absorption and exsorption) related parameters had to be varied to fit multiple data sets. Given the

specific absorption and excretion characteristics of HCB as described below, this adjustment is justifiable.

The absorption of HCB has been proposed as a passive diffusion process (Gobas *et al.* 1993). In the GI lumen, HCB is transported in micelles to the intestinal wall, where it separates from the lipid and bile salts to diffuse as a single molecule through the wall. At the other side of the intestinal wall, HCB is re-associated with lipids or lipoproteins for further transport. Essentially, the diffusion is governed by equilibrium partitioning between the blood and the lumen. However, the whole absorption process (from the GI lumen to blood) is also affected by the availability of bile salts, digestibility of lipids in the lumen, and the amount of lipids in the intestinal tissue. These lipid-related factors in the GI tract often vary with exposure conditions, such as the kind of oil vehicle, oral gavage volume, gavage frequency. If the animals are not fasted prior to treatment, the amount and the types of foods being given would also play a role in the absorption process.

It was reported that even if the lipid-based dietary HCB concentration was lower than the blood concentration, net absorption still occurred (Schlummer *et al.* 1998). To explain this observation, Schlummer *et al.* (1998) suggested a fat-flush hypothesis. In the small intestine, the absorbed dietary lipid elevates the lipid content in the intestinal tissue, diluting the local chemical concentration; meanwhile the lipid-based luminal concentration is increased due to the reduction in the lipid volume. These two changes, in combination, amplify the transluminal diffusion gradient and greatly facilitate absorption. This hypothesis illustrates the involvement of lipid in HCB absorption. It also points out

the complexity of absorption process in the GI tract and the inadequacy of relying on one absorption rate constant to simulate such a complicated phenomenon.

As a highly lipophilic and metabolically resistant chemical, HCB is predominantly excreted by blood-to-lumen passive diffusion (Rozman *et al.* 1985), *i.e.*, exsorption, which has been documented for hydrophobic drugs (Arimori and Nakano 1998; Israili and Dayton 1984). Although exsorption occurs at both small and large intestines (Richter and Schafer 1981), the latter is the major site for HCB net excretion (Rozman *et al.* 1985). The outward diffusion gradient, and thus the exsorption rely on the fat content in the large intestinal lumen, which comes from unabsorbed lipid, sloughed epithelial cells, or bacteria activity. Therefore, the exsorption rate constant is expected to vary in different situations. Indeed, in this study, adjustment of this parameter is necessary to fit all data sets.

The absorption and exsorption of HCB are two inverse processes, lumen-to-blood (absorption) vs. blood-to-lumen (exsorption) diffusion, which result in an enteroenteric recirculation (Israili and Dayton 1984). Due to the micro-environmental changes along the GI lumen, the absorption decreases and the exsorption increases gradually from the proximal to the distal end. The fate of the chemical relies on the relative magnitude of the two processes.

The absorption and exsorption processes of HCB, and probably other metabolically resistant and highly lipophilic chemicals as well, are very complicated. Given the above discussions, it is not surprising that a single set of parameters would not be adequate for simulation of multiple sets of experimental data. Variations in those processes across dose regimen are hitherto rarely studied. Wang *et al.* (2000) examined the dispositions of

2,3,7,8-tetrachlorodibenzo-*p*-dioxin (TCDD) across experimental conditions (oral gavage in female, iv injections in female and male Sprague-Dawley rats at comparable doses) using PBPK modeling. To fit the respective data sets, the rate constants of elimination from the kidney and liver had to vary among the studies. The Wang *et al.* (2000) study and the present study, on one hand, reveal the utility of PBPK modeling for studying the complex absorption and excretion kinetics of lipophilic chemicals through conducting *in silico* experimentations via computer simulation of different dosing scenarios. On the other hand, they form a challenge to the well-known capability of PBPK modeling in extrapolation across dosing scenarios and species. Although successful examples of dosimetry extrapolation for volatile chemicals using PBPK modeling have been published (Reitz *et al.* 1988), little has been reported for nonvolatile lipophilic chemicals, e.g., HCB, dioxins. Therefore, further study is warranted in the future to answer the following questions: What are the factors affecting the absorption and elimination processes of nonvolatile lipophilic chemicals? How do the factors vary across experimental condition? How do we describe these variations quantitatively?

4.4. Incorporation of pathophysiological conditions and uncertainties in the model simulation in the context of the liver foci bioassay

A notable treatment on the rats in our pharmacokinetic study integrated in the liver foci bioassay is partial hepatectomy. In addition to the desirable stimulated hepatocyte growth, many pathophysiological alterations ensue. The body and liver weights temporarily decrease, the latter more dramatically. The fat is mobilized to provide substrates and energy for liver regeneration, causing decrease in fat volume and increase in blood lipid level (Katagiri 1988). In the liver, lipoprotein lipase expression (Sabugal *et*

al. 1996) and lipid contents (Katagiri 1988) are elevated; various cell proliferation-related cytokines and hormones are imported or/and expressed (Michalopoulos and DeFrances 1997). Some, if not all, of these alterations will influence HCB kinetics.

From the modeling perspective, the incorporation of any pathophysiological condition is exercised by adjustment of parameters according to the underline mechanism(s) related to the condition. In our study, the two-thirds partial hepatectomy resulted in the loss of body weight and mobilization of fat due to the trauma and the needed energy for growing back the liver mass. Thus, the pathophysiological conditions were reflected by the changes in the body and liver weight and fat volume and were incorporated into our modeling. Theoretically, other pathophysiological changes, such as those in the liver partition coefficient (probably increased due to fat accumulation in the liver) and in other partition coefficients (plasma concentration would be increased due to hyperlipidemia after partial hepatectomy), can also occur and they should be included into the modeling. However, we currently do not have sufficient experimental information on these potential changes and these aspects are beyond the scope of the present paper.

There are uncertainties in simulating our HCB pharmacokinetic data in the bioassay using the established PBPK model: (1) Fat mobilization and redeposit following partial hepatectomy are qualitatively known; but to our knowledge, no accurate time-course fat volume data under such conditions are available. (2) In both normal and partially hepatectomized rats, HCB is likely to have same absorption and exsorption mechanisms. However, the rate constants could be altered due to partial hepatectomy, dose level, dose duration, or continuous application of corn oil. In this study, the rate constants were fixed

throughout the simulation durations. The first time point of the HCB concentration in this bioassay was generally overpredicted, which implied that lower absorption rate constants might be valid prior to partial hepatectomy.

In summary, an updated PBPK model for HCB was developed based on our current knowledge on HCB, the data sets from the literature, as well as from our experiment. The model development followed a sequential process from simulating the single iv dose study data to the single and repeated oral gavage study data. The model successfully described the data sets. The established PBPK model was then employed to simulate HCB disposition by incorporating the conditions as well as pathophysiological changes in the medium-term liver foci bioassay. With necessary adjustment of the rate constants of absorption and exsorption, the simulations were consistent with our data. The necessity of variation of the absorption and exsorption parameters for different exposure scenarios reflected the complex kinetics of HCB in the GI tract.

ACKNOWLEDGEMENTS

This study is supported by the NIOSH/CDC grant 1 RO1 OH07556, NIEHS Training Grant 1 T32 ES 07321, and scholarships from U.S. Fulbright Foundation and Naresuan University, Thailand. The authors thank Ms. Laura Chubb, Ms. Tracy Nichols, Drs. Todd Painter and Charles Dean, and other colleagues in the Quantitative and Computational Toxicology Group for their excellent technical assistance. The valuable suggestions from Dr. Melvin Andersen on model development are greatly appreciated. The authors also thank Mr. Xiaohui Xu for supporting statistical analysis of experimental data.

REFERENCES

Alvarez, L., Randi, A., Alvarez, P., Kolliker Frers, R., and Kleiman de Pisarev, D. L. (1999). Effect of hexachlorobenzene on NADPH-generating lipogenic enzymes and L-glycerol-3-phosphate dehydrogenase in brown adipose tissue. *J Endocrinol Investig* **22**, 436-445.

Arimori, K., and Nakano, M. (1998). Drug exsorption from blood into the gastrointestinal tract. *Pharmacol Res* **15**, 371-376.

Brown, R. P., Delp, M. D., Lindstedt, S. L., Rhomberg, L. R., and Beliles, R. P. (1997). Physiological parameter values for physiologically based pharmacokinetic models. *Toxicol Ind Health* **13**, 407-484.

Clark, D. E., Ivie, G. W., and €amp, B. J. (1981). Effects of dietary hexachlorobenzene on in vivo biotransformation, residue deposition, and elimination of certain xenobiotics by rats. *J Agric Food Chem* **29**, 600-608.

Clewell, H. J., 3rd, Lee, T. S., and Carpenter, R. L. (1994). Sensitivity of physiologically based pharmacokinetic models to variation in model parameters: methylene chloride. *Risk Anal* **14**, 521-31.

Erturk, E., Lambrecht, R. W., Peters, H. A., Cripps, D. J., Gocmen, A., Morris, C. R., and Bryan, G. T. (1986). Oncogenicity of hexachlorobenzene. *IARC Sci Publ* 77, 417-423.

Freeman, R. A., Rozman, K. K., and Wilson, A. G. E. (1989). Physiological pharmacokinetic model of hexachlorobenzene in the rat. *Health Phys* **57(Suppl 1)**, 139-147.

Gobas, F. A., McCorquodale, J. R., and Haffner, G. G. (1993). Intestinal absorption and biomagnification of organochlorines. *Environ Toxicol Chem* **12**, 567-576.

Gomez-Catalan, J., To-Figueras, J., Rodamilans, M., and Corbella, J. (1991). Transport of organo-chlorine residues in rat and human blood. *Arch Environ Contam Toxicol* **20**, 61-66.

Gustafson, D. L., Long, M. E., Thomas, R. S., Benjamin, S. A., and Yang, R. S. H. (2000). Comparative hepatocarcinogenicity of hexachlorobenzene, pentachlorobenzene, 1,2,4,5-tetrachlorobenzene, and 1,4-dichlorobenzene: application of a medium-term liver focus bioassay and molecular and cellular indices. *Toxicol Sci* **53**, 245-52.

Hida, Y., Matsui, N., Kawada, T., and Fushiki, T. (1999). Ultrasonography evaluation of abdominal fat in live rats. *J Nutr Sci Vitamintol* **45**, 609-619.

Ingebrigtsen, K., Skaare, J. U., Nafstad, I., and Forde, M. (1981). Studies on the biliary excretion and metabolism of hexachlorobenzene in the rat. *Xenobiotica* **11**, 795-800.

Israili, Z. H., and Dayton, P. G. (1984). Enhancement of xenobiotic elimination: Role of intestinal excretion. *Drug Metab Rev* **15**, 1123-1159.

Ito, N., Tamano, S., and Shirai, T. (2003). A medium-term rat liver bioassay for rapid in vivo detection of carcinogenic potential of chemicals. *Cancer Sci* **94**, 3-8.

Katagiri, S. (1988). [Experimental study on lipid metabolism after partial hepatectomy--with reference to mitochondrial function of the regenerating liver]. *Nippon Geka Gakkai Zasshi* **89**, 694-702.

Koss, G., and Koransky, W. (1975). Studies on the toxicology of hexachlorobenzene I.Pharmacokinetics. *Arch Toxicol* **34**, 203-212.

Koss, G., Seubert, S., Seubert, A., Koransky, W., and Ippen, H. (1978). Studies on the toxicology of hexachlorobenzene. III. Observations in a long-term experiment. *Arch Toxicol* **40**, 285-294.

Kuiper-Goodman, T., Grant, D. L., Moodie, C. A., Korsrud, G. O., and Munro, I. C. (1977). Subacute toxicity of hexachlorobenzene in the rat. *Toxicol Appl Pharmacol* **40**, 529-79.

Lee, H. B., and Blaufox, M. D. (1985). Blood volume in the rat. *J Nucl Med* **25**, 72-76.

Michalopoulos, G. K., and DeFrances, M. C. (1997). Liver regeneration. *Science* **276**, 60-66.

Ou, Y. C., Conolly, R. B., Thomas, R., Gustafson, D. L., Long, M. E., Dovrev, I. D., Chubb, L. S., Xu, Y., Lapidot, S., Andersen, M. E., and Yang, R. S. H. (2003). Stochastic simulation of hepatic preneoplasic foci development for four chlorobenzene congeners in a medium-term bioassay. *Toxicol Sci* **73**, 301-314.

Ou, Y. C., Conolly, R. B., Thomas, R. S., Xu, Y., Andersen, M. E., Chubb, L. S., Pitot, H. C., and Yang, R. S. H. (2001). A clonal growth model: time-course simulations of liver foci growth following penta- or hexachlorobenzene treatment in a medium-term bioassay. *Cancer Res* **61**, 1879-1889.

Ralph, J. L., Orgebin-Crist, M. C., Lareyre, J. J., and Nelson, C. C. (2003). Disruption of androgen regulation in the prostate by the environmental contaminant hexachlorobenzene. *Environ Health Perspect* **111**, 461-466.

Reitz, R. H., McDougal, J. N., Himmelstein, M. W., Nolan, R. J., and Schumann, A. M. (1988). Physiologically based pharmacokinetic modeling with methylchloroform: implications for interspecies, high dose/low dose, and dose route extrapolations. *Toxicol Appl Pharmacol* **95**, 185-99.

Renner, G. (1988). Hexachlorobenzene and its metabolism. *Toxicol Environ Chem* **18**, 51-78.

Richter, E., and Schafer, S. G. (1981). Intestinal excretion of hexachlorobenzene. *Arch Toxicol* **47**, 233-9.

Roth, W. L., Freeman, R. A., and Wilson, A. G. E. (1993a). A physiologically based model for gastrointestinal absorption and excretion of chemicals carried by lipids. *Risk Anal* **13**, 531-543.

Roth, W. L., Weber, L. W. D., Stahl, B. U., and Rozman, K. (1993b). A phmarcodynamic model of triglyceride transport and deposition during feed deprivation or

following treatment with 2,3,7,8-tetrachlorodibenzo-p-dioxin (TCDD) in the rat. *Toxicol Appl Pharmacol* **120**, 126-137.

Rozman, T., Scheufler, E., and Rozman, K. (1985). Effect of partial jejunectomy and colectomy on the disposition of hexachlorobenzene in rats treated or not treated with hexadecane. *Toxicol Appl Pharmacol* **78**, 421-427.

Sabugal, R., Robert, M. Q., Julve, J., Auwerx, J., Llobera, M., and Peinado-Onsurbe, J. (1996). Hepatic regeneration induces changes in lipoprotein lipase activity in several tissues and its re-expression in the liver. *Biochem J* **318(Pt 2)**, 597-602.

Scheufler, E., and Rozman, K. (1984a). Comparative decontamination of hexachlorobenzene-exposed rats and rabbits by hexadecane. *J Toxicol Environ Health* **14**, 353-362.

Scheufler, E., and Rozman, K. (1984b). Effect of hexadecane on the pharmacokinetics of hexachlorobenzene. *Toxicol Appl Pharmacol* **75**, 190-197.

Schielen, P., Den Besten, C., Vos, J. G., Van Bladeren, P. J., Seinen, W., and Bloksma, N. (1995). Immune effects of hexachlorobenzene in the rat: role of metabolism in a 13-week feeding study. *Toxicol Appl Pharmacol* **131**, 37-43.

Schlummer, M., Andreas Moser, G., and McLachlan, M. S. (1998). Digestive tract absorption of PCDD/Fs,PCBs,and HCB in humans:Mass balances and mechanistic considerations. *Toxicol Appl Pharmacol* **152**, 128-137.

Schoeffner, D. J., Warren, D. A., Muralidara, S., Bruckner, J. V., and Simmons, J. E. (1999). Organ weights and fat volume in rats as a function of strain and age. *J Toxicol Environ Health A* **56**, 449-462.

Siekel, P., Chalupa, I., Beno, J., Blasko, M., Novotny, J., and Burian, J. (1991). A genotoxicological study of hexachlorobenzene and pentachloroanisole. *Teratog Carcinog Mutagen* **11**, 55-60.

Smith, A. G., Dinsdale, D., Cabral, J. R., and Wright, A. L. (1987). Goitre and wasting induced in hamsters by hexachlorobenzene. *Arch Toxicol* **60**, 343-349.

Smith, A. G., Francis, J. E., Dinsdale, D., Manson, M. M., and Cabral, J. R. (1985). Hepatocarcinogenicity of hexachlorobenzene in rats and the sex difference in hepatic iron status and development of porphyria. *Carcinogenesis* **6**, 631-636.

Staats, D. A., Fisher, J. W., and Connolly, R. B. (1991). Gastrointestinal absorption of xenobiotics in physiologically based pharmacokinetic models. A two-compartment description. *Drug Metab Dispos* **19**, 144-148.

Thomas, R. S. (1998). The Use of Biologically-Based Models for Integrating Short-Term Cancer Bioassays, Mechanisms of Action, and Target Tissue Dosimetry: Application to Pentachlorobenzene. Ph.D. dissertation. Department of Environmental Health, Colorado State University, Fort Collins, CO.

Wang, X., Santostefano, M. J., DeVito, M. J., and Birnbaum, L. S. (2000). Extrapolation of a PBPK model for dioxins across dosage regimen, gender, strain, and species. *Toxicol Sci* **56**, 49-60.

Yamaguchi, Y., Kawano, M., and Tatsukawa, R. (1986). Tissue distribution and excretion of hexabromobenzene and hexachlorobenzene administered to rats. *Chemosphere* **15**, 453-459.

Yang, R. S. H., Coulston, F., and Golberg, L. (1975). Binding of hexachlorobenzene to erythrocytes:Species variation. *Life Sci* **17**, 545-550.

Yang, R. S. H., Pittman, K. A., Rourke, D. R., and Stein, V. B. (1978). Pharmacokinetics and metabolism of hexachlorobenzene in the rat and Rhesus monkey. *J Agric Food Chem* **26**, 1076-83.

Yang, R. S. H., Thomas, R. S., Gustafson, D. L., Campain, J., Benjamin, S. A., Verhaar, H. J., and Mumtaz, M. M. (1998). Approaches to developing alternative and predictive toxicology based on PBPK/PD and QSAR modeling. *Environ Health Perspect* **106(Suppl 6)**, 1385-1393.

Yesair, D. W., Feder, P. I., Chin, A. E., Naber, S. J., Kuiper-Goodman, T., Scott, C. S., and Robinson, P. E. (1986). Development, evaluation and use of a pharmacokinetic model for hexachlorobenzene. *IARC Sci Publ* **77**, 297-318.

CHAPTER 3

Remarkable Changes in Hexachlorobenzene Disposition by PCB 126 Coexposure in a Time-course Medium-term Liver Foci Bioassay

Yasong Lu, Manupat Lohitnavy, Ornrat Lohitnavy, Elizabeth Eickman, Raymond S.H. Yang

ABSTRACT

Hexachlorobenzene (HCB) is a persistent organic pollutant and probable human carcinogen. Despite the prohibition of its production and use, HCB still exists in the environment due to its persistence and continuous emissions from combustion and industrial processes. Human exposure to HCB is often accompanied by 3,3',4,4',5-pentachlorobiphenyl (PCB 126), a dioxin-like compound and the most potent congener of polychlorinated biphenyls (PCBs). Earlier, PCB 126 was observed to alter the kinetics of some chemicals, e.g., 2,2',4,4',5,5'-hexachlorobipheneyl (PCB 153), by disturbing fat metabolism. Here, we report the remarkable changes in HCB pharmacokinetics by PCB 126 coexposure. Our study included two separate kinetic experiments (HCB alone and HCB+PCB 126 mixture) integrated into the time-course medium-term liver foci bioassays. Both bioassays were performed at two dose levels. Time-course HCB concentrations were determined in blood, liver, kidney, fat, and muscle. In both bioassays, the fat had the highest concentrations, followed by the liver and other tissues. PCB 126 coexposure changed the accumulation of HCB in the body and the partitioning of HCB into tissues. The underlying mechanisms were proposed to be the results of interruption

of HCB absorption and/or exsorption (*i.e.*, the reverse diffusion from the blood to the gastrointestinal lumen) by PCB 126 and the more severe disturbance of fat metabolism under the mixture treatment.

1. INTRODUCTION

Hexachlorobenzene (HCB) is a persistent organic pollutant. Although its commercial production and use have been banned, HCB still exists in the environment due to its chemical and thermal stability and high lipophilicity. Moreover, global emissions of new HCB as much as 14,000-73,000 kg/year are expected from sources such as combustion and chemical-industrial processes (Bailey 2001). HCB remains detectable in the environment (Marvin *et al.* 2004; Meijer *et al.* 2003), ecosystem (Weber and Goerke 2003), food (Schecter *et al.* 2003), and human tissues (Covaci *et al.* 2002; Dewailly *et al.* 1999).

As a highly lipophilic chemical, HCB primarily accumulates in the adipose tissue in the body. It is slowly metabolized in the liver and the metabolites are excreted in both urine and feces (Koss and Koransky 1975). The more important elimination pathway for HCB is passive diffusion from the blood into the gut lumen (Rozman 1985; Rozman *et al.* 1985). HCB elicits various toxic effects in laboratory animals and humans such as hepatic cytochrome P450 induction (Gustafson *et al.* 2000), liver enlargement (Kuiper-Goodman *et al.* 1977), endocrine disruption (Foster *et al.* 1993; Ralph *et al.* 2003), fat metabolism disturbance (Alvarez *et al.* 1999; Smith *et al.* 1987), immunotoxicity (Vos 1986), and porphyria (Gocmen *et al.* 1986). Despite the lack of genotoxicity (Siekel *et al.* 1991), HCB-induced carcinogenicity was observed in the laboratory animals with the liver being

one of the main target organs (Erturk *et al.* 1986; Smith *et al.* 1985). HCB has been classified as "reasonably anticipated to be a human carcinogen" (NTP 2001).

3,3',4,4',5-Pentachlorobiphenyl (PCB 126) is a dioxin-like compound and the most toxic congener of the family of polychlorinated biphenyls (PCBs) (Safe 1994). It has been detected in the environment (Finley *et al.* 1997), foodstuffs (Focant *et al.* 2003; Jordan and Feeley 1999), and human tissues (Bates *et al.* 2004; Shadel *et al.* 2001). In many cases, PCB 126 is one of the most important contributors to the total toxic equivalency of PCBs and dioxins. PCB 126 was reported to significantly increase tumor incidence in multiple sites (e.g., the liver, lung, and oral mucosa) in the female Sprague-Dawley rats in a two-year oral gavage study (NTP 2004).

Although toxicological studies often focus on individual chemicals, humans are actually exposed to many chemicals coexistent in the environment and food chain. For example, PCB 126 and HCB were both found present in a surrounding area of a waste incinerator (Blais *et al.* 2003) and in human tissues (Liljegren *et al.* 1998). Possible interactions among chemicals, occurring at the levels of pharmacokinetics and pharmacodynamics, may modulate the toxicity of each individual chemical. Consequently, it is difficult to accurately predict effects of a chemical mixture solely based on the information of each component. Research on chemical mixtures should be encouraged (de Rosa *et al.* 2004; Yang 1998).

Coexposure to PCB 126 caused an increase in 2,2',4,4',5,5'-hexachlorobipheneyl (PCB 153) concentration in the liver and a decrease in the fat in the rats (Dean *et al.* 2002) and mice (Lee *et al.* 2002). These alterations were suggested to be a result of PCB 126-induced disruption of fat metabolism: lipid accumulation in the liver and inhibition of the

buildup of the adipose tissues (Lee *et al.* 2002). Based on this explanation, it is reasonable to hypothesize that the effect of PCB 126 on PCB 153 disposition could apply to most, if not all, lipophilic chemicals, including HCB.

Our laboratory has been developing an approach for predicting carcinogenic potential of chemical mixtures by integrating a medium-term liver foci bioassay with computational modeling (Lu *et al.* 2006a; Lu *et al.* 2006b; Ou *et al.* 2003; Ou *et al.* 2001; Thomas 1998; Thomas *et al.* 2000; Yang *et al.* 1998). The medium-term liver foci bioassay we use is a modified version of the well recognized Ito's protocol (Ito *et al.* 1988; Ito *et al.* 2003) and has been reported earlier (Lu *et al.* 2006b; Thomas 1998). In this study, we conducted experiments on the pharmacokinetics in parallel with pharmacodynamics (preneoplastic liver foci development) of HCB alone and the mixture of HCB and PCB 126 in the context of our time-course medium-term liver foci bioassay (Fig. 3.1). While the pharmacodynamic data will be reported elsewhere, this paper was focused on the pharmacokinetics of HCB and the effect of PCB 126 coexposure on HCB disposition.

2. MATERIALS AND METHODS

This study included two time-course liver foci bioassays (Fig. 3.1) on HCB alone and HCB+PCB 126, respectively. Each bioassay had one control group and chemical-treated groups at two doses (Table 3.1). The bioassays were conducted separately because each bioassay utilized a total of approximately 100 rats and approached the maximal surgical and experimental capacity of a team of four scientists in our laboratory. Except

the chemical treatments (HCB vs. HCB+PCB 126), the other conditions were kept identical to the extent possible between the two bioassays.

2.1. Chemicals

HCB (99% purity) and 1,2,4,5-tetrabromobenzene (97% purity) were purchased from Aldrich Chemical (Milwaukee, WI). PCB 126 was obtained from AccuStandard (New Haven, CT). Diethylnitrosamine (DEN) was from Sigma Chemical (St. Louis, MO). Toluene (99.9% purity) and sulfuric acid solution were supplied by VWR Scientific (Denver, CO). Anhydrous sodium sulfate was from Fisher Scientific (Houston, TX). Florisil® was bought from Alltech Associates (Deerfield, IL).

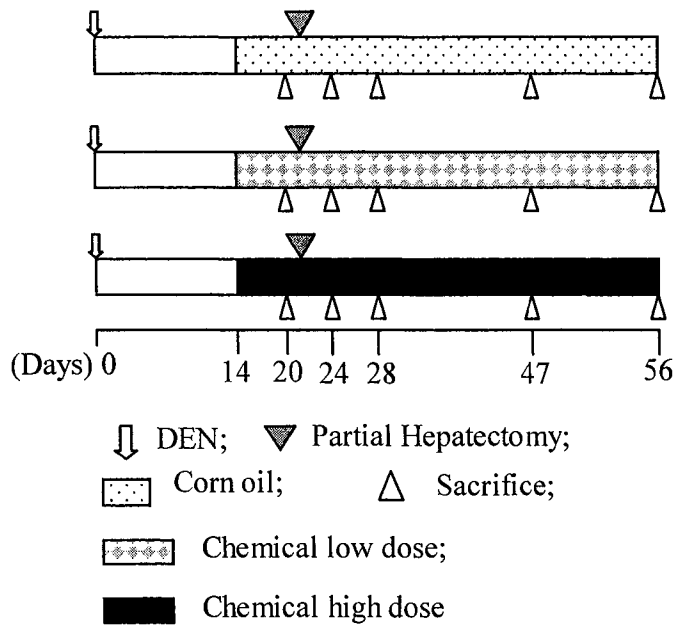

Fig. 3.1. Experimental design of the time-course medium-term liver foci bioassay. A single intraperitoneal injection of DEN was given on day 0. Daily oral gavage of corn oil (control), low dose, and high dose of HCB or HCB+PCB 126 mixture in corn oil started from day 14. On day 21, a two-thirds partial hepatectomy was performed on the rats. On the surgery day and the following three days, the gavage was suspended to reduce the stress to the animals while recovering from surgery. Six rats from each treatment group were sacrificed on days 20, 24, 28, 47, and 56. The liver, kidney, blood, thigh muscle, and abdominal fat were collected from each rat for HCB analysis.

2.2 Animals and treatments

In each bioassay, male F344 rats, 30 days of age, purchased from Harlan Sprague-Dawley (Indianapolis, IN), were housed in the Painter Center, Colorado State University. It is fully accredited by the American Association for Accreditation of Laboratory Animal Care (AAALAC). Animals were given food (Harlan Teklad NIH-07 diet, Madison, WI) and water *ad libitum* and lighting was set on a 12h light/dark cycle.

Table 3.1. Chemical Treatment in the HCB alone and HCB+PCB 126 Bioassays

Bioassay	Treatment	HCB (mg/kg)	PCB 126 (μg/kg)
HCB	Control	-	-
	Low	8.55	-
	High	28.5	-
HCB+PCB 126	Control	-	-
	Low	8.55	3.3
	High	28.5	9.8

After four weeks of acclimation, the rats were randomized by weight, divided into three groups, and treated following the time-course medium-term liver foci bioassay (Fig. 3.1). At week 0, the rats were given a single intraperitoneal (i.p.) injection of diethylnitrosamine (DEN) (200 mg/kg) dissolved in 0.9% saline. Two weeks later, they began receiving daily oral gavage of corn oil (control), low, and high dose of HCB or the mixture (Table 3.1) in corn oil until sacrifice. At week 3 (day 21), a two-thirds partial hepatectomy was performed on the rats. On the surgery day and the following three days, the gavage was suspended to reduce the stress to the animals while recovering from surgery. Six rats from each group were sacrificed by aortic exsanguination under anesthesia at five time points, days 20, 24, 28, 47, and 56 after DEN injection. The body and liver weight of each rat were recorded at sacrifice. The liver, kidney, blood, thigh

muscle, and abdominal fat were collected from each rat. All samples except blood were frozen with liquid nitrogen and stored at -70°C until analysis. The study was conducted in accordance with the National Institutes of Health (NIH) guidelines for the care and use of laboratory animals.

2.3. HCB analysis

Samples (0.5 ml blood, 0.1 g fat, and 0.2 g other tissues) of the HCB treated rats, spiked with 1,2,4,5-tetrabromobenzene as an internal standard, were digested with 3 ml of 60% sulfuric acid overnight, and then extracted with 5 ml of toluene 3 times. The resulting extracts were concentrated to about 2 ml and cleaned through a column containing 1 g anhydrous sodium sulfate and 1 g Florisil®. Each column was washed 5 times with 2 ml of pentane per time after the passage of the concentrated extract. The eluant was concentrated and then analyzed on an HP-5890 II Plus gas chromatograph (Hewlett Packard, Wilmington, DE) equipped with an electron capture detector. An EQUITY™-5 fused silica capillary column (Supelco, PA) was employed. Helium and nitrogen were used as the carrier and makeup gases with flow rates of 4 ml/min and 60 ml/min, respectively. The oven temperature was initially 150°C for 1 min, increased to 175°C at 10°C/min, where it remained for 10 min. The temperatures of the inlet and detector were 250°C and 300°C, respectively. The recoveries of HCB and the internal standard of this method were in the range of 70-100%. The existence of PCB 126 in some samples did not interfere with HCB identification and quantification.

2.4. Statistical analysis

ANOVA at $\alpha = 0.05$ was applied to analyze statistical differences of body and organ weights between the chemical-treated groups and the concurrent control and of the

corresponding tissue concentrations following HCB alone and the mixture treatment at each time point. All statistical analyses were performed with Minitab (Windows version 11.21).

3. RESULTS

3.1. Effects of HCB on the body weight and the organ weights

These results have been reported earlier (Chapter 2)(Lu *et al.* 2006c) and are presented here for the reader's convenience. The HCB treatment did not significantly change the body weight at any time point. The liver weight was significantly increased only on day 47 in the high dose group. The low dose HCB treatment increased the liver/body weight ratio on day 28, whereas the high dose increased this index significantly on days 20, 28, and 47. HCB did not significantly change the kidney weight and the kidney/body weight ratio.

3.2. Effects of the mixture on the body weight and the organ weights

No rats died of the mixture treatment. We observed remarkable changes in the body weight and the liver weight of the rats due to the mixture treatment. The body weight (Fig. 3.2.) significantly reduced in a dose-dependent manner on days 47 and 56; on day 28 the decrease was significant only in the high dose group. As shown in Table 3.2, the liver weight was significantly increased at the later three time points, and the kidney weight was slightly yet significantly increased at the last two time points. Dose-dependent increases in the liver/body weight and kidney/body weight ratios were observed at the later three time points. Note that the liver/body weight ratio since day 28 was approximately doubled by the mixture treatment.

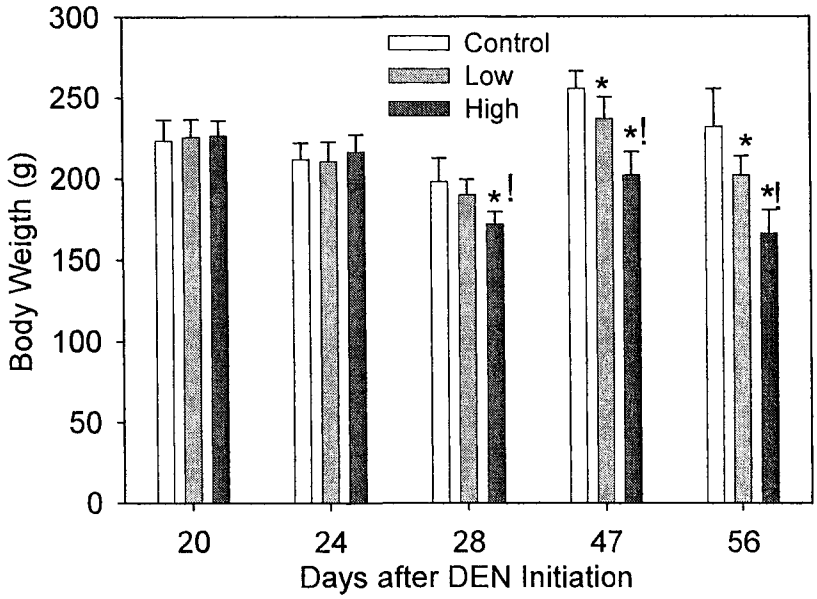

Fig 3.2. The body weight of the rats following corn oil (control), low, and high dose of HCB+PCB 126 treatment in the mixture bioassay.
*: significantly different ($p<0.05$) from the corresponding control group;
!: significantly different ($p<0.05$) from the corresponding low dose group.

Table 3.2. Organ Weights and Organ/Body Weight Ratios of Rats in HCB+PCB 126 Mixture Bioassay

	Treatment	Days after DEN initiation				
		20	24	28	47	56
Liver weight (g)	Control	7.39 ± 0.60	4.92 ± 0.41	5.03 ± 0.43	6.81 ± 0.40	7.70 ± 1.74
	Low dose	7.52 ± 0.43	4.94 ± 0.24	7.43 ± 0.66*	13.13 ± 1.03*	12.73 ± 0.56*
	High dose	7.60 ± 0.31	5.36 ± 0.41	7.84 ± 0.63*	12.17 ± 1.74*	11.93 ± 1.26*
Liver/body weight ratio (%)	Control	3.31 ± 0.09	2.32 ± 0.12	2.54 ± 0.06	2.67 ± 0.12	3.36 ± 0.95
	Low dose	3.34 ± 0.08	2.35 ± 0.13	3.91 ± 0.20*	5.54 ± 0.20*	6.31 ± 0.24*
	High dose	3.36 ± 0.10	2.48 ± 0.11	4.56 ± 0.25*!	6.00 ± 0.46*!	7.21 ± 0.67*!
Kidney weight (g)	Control	1.50 ± 0.12	1.53 ± 0.15	1.31 ± 0.08	1.62 ± 0.09	1.31 ± 0.08
	Low dose	1.46 ± 0.11	1.51 ± 0.09	1.37 ± 0.10	1.83 ± 0.11*	1.37 ± 0.10
	High dose	1.48 ± 0.09	1.62 ± 0.09!	1.38 ± 0.08	1.69 ± 0.14	1.41 ± 0.05*
Kidney/body weight ratio (%)	Control	0.67 ± 0.03	0.72 ± 0.04	0.66 ± 0.01	0.63 ± 0.02	0.57 ± 0.06
	Low dose	0.65 ± 0.04	0.72 ± 0.02	0.72 ± 0.03*	0.77 ± 0.02*	0.68 ± 0.07*
	High dose	0.65 ± 0.03	0.75 ± 0.01	0.80 ± 0.02*!	0.84 ± 0.02*!	0.85 ± 0.05*!

*: $p<0.05$, compared to the concurrent control group.
!: $p<0.05$, compared to the concurrent low dose group.

3.3. HCB disposition following the HCB alone treatment

The result was presented in plots in Chapter 2 and Lu *et al.* (2006c) and is again repeated here in Table 3.3 and Fig. 3.3 for the ease of comparison with the HCB concentration data from the HCB+PCB 126 mixture bioassay. At both doses, the highest concentration was observed in the fat, followed by the liver, kidney, blood, and muscle. With a 3-fold difference in the exposure levels, there was approximately a 2- to 3-fold difference in the corresponding tissue concentrations of the two treated groups.

3.4. HCB disposition following the HCB+PCB 126 mixture treatment

Time-course tissue concentrations of HCB following the HCB+PCB 126 mixture treatment are shown in Table 3.4. Surprisingly, HCB was not detectable in all the tissues at the first time point at both dose levels. Although no chemical was given from day 21 through day 24, HCB was detected in the tissues on day 24. Remarkable increases in the tissue concentrations were observed between days 24 and 28. The concentrations on day 47 were comparable to those on day 28. From day 47 to day 56, another notable increase in the tissue concentrations was observed. Although the ratio of the HCB doses was about 3 in the two mixture-treated groups, the ratios of the HCB tissue concentrations in the two groups were in a range of 1.7-6.3, dependent on the tissue and time.

3.5. Comparisons between HCB disposition patterns following HCB alone and the mixture treatment

HCB disposition following the mixture treatment was dramatically different from that following HCB alone treatment; that is, PCB 126 coexposure altered HCB disposition. The disposition patterns following both treatments are juxtaposed in Fig. 3.3. The comparisons were performed quantitatively from two perspectives:

Table 3.3. HCB Tissue Concentrations (Mean ± Standard Deviation) in HCB Bioassay

Treatment (HCB)	Tissue	Time-point (Days after DEN initiation)				
		20	**24**	**28**	**47**	**56**
8.55 mg/kg	Blood (μg/ml)	1.91 ± 0.43	1.83 ± 0.17	2.65 ± 0.56	4.67 ± 0.61	4.95 ± 1.01
	Liver (μg/g)	4.71 ± 0.79	5.63 ± 0.89	6.77 ± 1.49	11.87 ± 1.68	13.84 ± 2.56
	Kidney (μg/g)	3.80 ± 0.75	3.73 ± 0.63	4.97 ± 0.93	6.92 ± 1.08	8.43 ± 2.70
	Fat (μg/g)	63.14 ± 26.87	55.27 ± 9.82	73.58 ± 22.45	194.32 ± 27.94	204.13 ± 42.96
	Muscle (μg/g)	1.86 ± 0.64	1.83 ± 0.37	2.07 ± 0.34	3.26 ± 0.37	3.32 ± 0.97
28.5 mg/kg	Blood (μg/ml)	4.57 ± 0.39	4.37 ± 0.50	8.75 ± 1.21	11.94 ± 1.38	13.20 ± 1.42
	Liver (μg/g)	10.19 ± 0.80	14.67 ± 3.62	19.31 ± 2.22	28.61 ± 3.50	35.39 ± 5.10
	Kidney (μg/g)	9.41 ± 2.34	6.48 ± 0.59	11.34 ± 2.75	20.55 ± 3.49	24.02 ± 6.42
	Fat (μg/g)	207.71 ± 28.87	156.91 ± 41.94	345.99 ± 47.52	580.49 ± 91.43	593.89 ± 118.52
	Muscle (μg/g)	3.74 ± 0.91	5.46 ± 2.88	7.50 ± 1.19	9.19 ± 1.64	10.09 ± 2.26

Table 3.4. HCB Tissue Concentrations (Mean ± Standard Deviation) in HCB+PCB 126 Mixture Bioassay

Treatment (HCB+PCB 126)	Tissue	Time-point (Days after DEN initiation)				
		20	**24**	**28**	**47**	**56**
8.55 mg/kg + 3.3 µg/kg	Blood (µg/ml)	ND*	0.86 ± 0.29	13.30 ± 1.41	14.93 ± 2.75	25.45 ± 9.86
	Liver (µg/g)	ND	4.80 ± 2.04	127.94 ± 19.94	132.57 ± 18.50	182.44 ± 27.84
	Kidney (µg/g)	ND	2.35 ± 0.18	16.89 ± 2.47	21.53 ± 3.48	45.39 ± 14.85
	Fat (µg/g)	ND	49.97 ± 10.42	848.84 ± 128.68	1236.93 ± 278.37	2184.46 ± 679.47
	Muscle (µg/g)	ND	1.14 ± 0.05	6.65 ± 0.87	11.57 ± 5.74	13.78 ± 4.74
28.5 mg/kg + 9.9 µg/kg	Blood (µg/ml)	ND	3.04 ± 0.82	67.32 ± 48.83	60.28 ± 9.92	159.94 ± 61.19
	Liver (µg/g)	ND	16.13 ± 3.26	351.60 ± 186.41	274.12 ± 50.21	642.14 ± 182.55
	Kidney (µg/g)	ND	4.04 ± 0.46	71.11 ± 27.79	91.84 ± 27.62	232.52 ± 70.78
	Fat (µg/g)	ND	137.38 ± 43.29	3025.36 ± 1232.00	4139.51 ± 622.79	9934.45 ± 2129.61
	Muscle (µg/g)	ND	1.93 ± 0.33	23.40 ± 5.96	39.27 ± 19.95	55.30 ± 14.74

* ND: not detectable.

3.5.1.Comparison of the tissue concentrations following both treatments

Because of the remarkable increases, in the later time points, of tissue HCB concentrations in the HCB+PCB 126 mixture bioassay, for each tissue, we calculated the ratio of HCB concentration in the mixture bioassay over the HCB concentration in the HCB bioassay (Table 3.5). On days 20 and 24, the ratios for all tissues were generally less than 1.0; at the later three time points, however, the ratios were much higher and as high as 18.9. These results suggested that the amount of HCB accumulated in the body was decreased at the first two time points and increased at the later three time points because of PCB 126 coexposure.

Table 3.5. Ratios of Tissue Concentrations ($[HCB_{mixture\ bioassay}]/[HCB_{single\ chemical\ bioassay}]$) Following Mixture or HCB treatment*

		Time-point (Days after DEN initiation)				
Tissue	**Treatment**	**20**	**24**	**28**	**47**	**56**
Blood	Low	N/A	0.5	5.0	3.2	5.1
	High	N/A	0.7	7.7	5.0	12.1
Liver	Low	N/A	0.9	18.9	11.2	13.2
	High	N/A	1.1	18.2	9.6	18.1
Kidney	Low	N/A	0.6	3.4	3.1	5.4
	High	N/A	0.6	6.3	4.5	9.7
Fat	Low	N/A	0.9	11.5	6.4	10.7
	High	N/A	0.9	8.7	7.1	16.7
Muscle	Low	N/A	0.6	3.2	3.5	4.1
	High	N/A	0.4	3.1	4.3	5.5

N/A: not available because HCB was not detectable on day 20 in the mixture bioassay.
*: Whether or not the difference between the concentrations in the HCB bioassay and the mixture bioassay is statistically significant is shown in Fig. 3.3.

3.5.2. Comparison of the relative tissue concentrations following both treatments

The relative tissue concentration was defined as the ratio of tissue concentration over the corresponding blood concentration, which reflects the partitioning of HCB into a

tissue. The relative tissue concentrations following HCB and the mixture treatments are presented in Table 3.6. The partitioning of HCB into the liver and fat was significantly increased and into muscle was generally significantly decreased under PCB 126 coexposure. These results implied that PCB 126 coexposure changed the partitioning of HCB into the tissues.

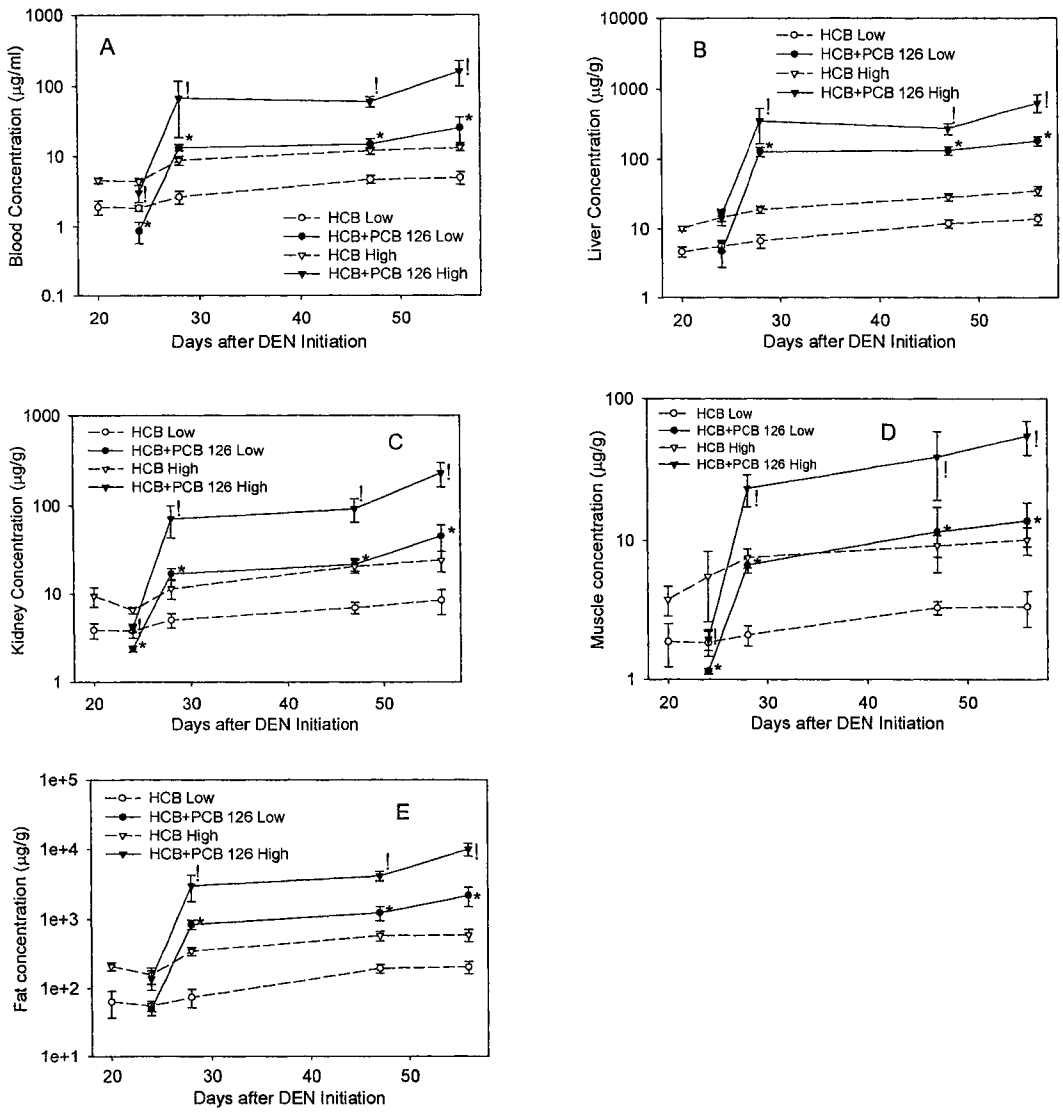

Fig. 3.3. HCB concentrations following HCB alone and HCB+PCB 126 mixture treatment in the (A) blood, (B) liver, (C) kidney, (D) muscle, and (E) fat in the bioassays.
*: significantly different ($p<0.05$) from the low dose group in the HCB bioassay;
!: significantly different ($p<0.05$) from the high dose group in the HCB bioassay.

4. DISCUSSION

We studied the dispositions of HCB following the dosing of HCB alone and the mixture of HCB+PCB 126 in the context of a time-course medium-term liver foci bioassay. Our results showed that HCB disposition was altered by PCB 126 coexposure in two aspects: (1) The partitioning of HCB into the liver and fat was increased and that into muscle generally was decreased; and (2) The tissue concentrations were decreased at the first two time points and increased at the later three.

Table 3.6. Relative Tissue HCB Concentrations (Mean ± Standard Deviation) Following Mixture or HCB treatment

		Time-point (Days after DEN initiation)				
Tissue	**Treatment**	**20**	**24**	**28**	**47**	**56**
Liver	HCB-low	2.5±0.2	3.1±0.4	2.6±0.1	2.6±0.2	2.9±0.5
	Mixture-low	N/A*	5.5±0.8*	9.6±1.1*	9.0±1.2*	7.8±2.4*
	HCB-high	2.2±0.1	3.3±0.6	2.2±0.4	2.4±0.3	2.7±0.3
	Mixture-high	N/A*	5.6±1.7*	5.8±1.9*	4.6±0.9*	4.2±1.0*
Kidney	HCB-low	2.0±0.3	2.0±0.2	1.9±0.4	1.5±0.3	1.7±0.4
	Mixture-low	N/A*	2.9±0.7*	1.3±0.1*	1.5±0.2	1.9±0.6
	HCB-high	2.1±0.6	1.5±0.1	1.3±0.2	1.7±0.4	1.8±0.3
	Mixture-high	N/A*	1.4±0.2	1.2±0.3	1.5±0.3	1.6±0.6
Fat	HCB-low	31.8±9.0	30.1±3.9	27.4±3.2	41.5±1.1	41.2±2.1
	Mixture-low	N/A*	60.2±7.7*	63.7±6.2*	83.1±14.3*	89.1±19.5*
	HCB-high	45.3±2.4	35.3±9.2	39.7±3.5	48.6±4.0	44.7±5.5
	Mixture-high	N/A*	45.2±4.4*	51.3±12.7	69.5±11.9*	66.6±15.4*
Muscle	HCB-low	1.0±0.2	1.0±0.2	0.8±0.2	0.7±0.1	0.7±0.1
	Mixture-low	N/A*	1.4±0.4*	0.5±0.1*	0.8±0.5	0.6±0.1
	HCB-high	0.8±0.3	1.2±0.6	0.9±0.2	0.8±0.1	0.8±0.1
	Mixture-high	N/A*	0.6±0.1*	0.5±0.3*	0.7±0.3	0.4±0.1*

N/A: not available because HCB was not detectable on day 20 in the mixture bioassay.
*: Significantly different ($p<0.05$) from the corresponding value in the HCB bioassay.

The first aspect can be explained with the disturbance of fat metabolism in the body. HCB was reported to be able to inhibit body weight gain following a long-term exposure

(Kuiper-Goodman *et al.* 1977) and to stimulate lipid accumulation in the liver (Billi de Catabbi *et al.* 1997) in the rats. PCB 126 has the same effects with higher potency (Chu *et al.* 1994; Van Birgelen *et al.* 1994). Nevertheless, we have observed only trivial effects on those indices following PCB 126 (Lohitnavy *et al.*, unpublished data) or HCB alone treatment (Lu *et al.* 2006c); the lack of effects may be attributed to the relatively low doses and short treatment durations. Interestingly, under the same conditions, HCB+PCB 126 mixture treatment amplified those effects to a much greater magnitude. In addition, in our mixture bioassay, we found a decrease in the volume of abdominal fat depots and a remarkable augmentation of lipid droplets in the liver slides (see Fig. 3.4). The occurrence of the amplified effects indicated kinetic and/or dynamic interactions between HCB and PCB 126.

The mechanisms of fat metabolism disturbance by HCB and 2,3,7,8-tetrachlorodibenzo-*p*-dioxin (TCDD) were intensively studied. Because of the similarity between TCDD and PCB 126, the mechanisms of TCDD may apply to PCB 126. These mechanisms include: (1) *De novo* fatty acid synthesis is stimulated in the liver and inhibited in the adipose tissues by modulation of the lipogenic enzymes (Alvarez *et al.* 1999; Gorski *et al.* 1988); (2) The activity of lipoprotein lipase, a regulator for fatty acids uptake in adipose tissues, is inhibited (Brewster and Matsumura 1988; Olsen *et al.* 1998); and (3) The metabolism of glucose is impaired (Mazzetti *et al.* 2004; Weber *et al.* 1991), resulting in fat mobilization to meet the normal energy demand. The consequences of the disturbance of fat metabolism are fat volume reduction, hepatic lipid accumulation, and hyperlipidemia.

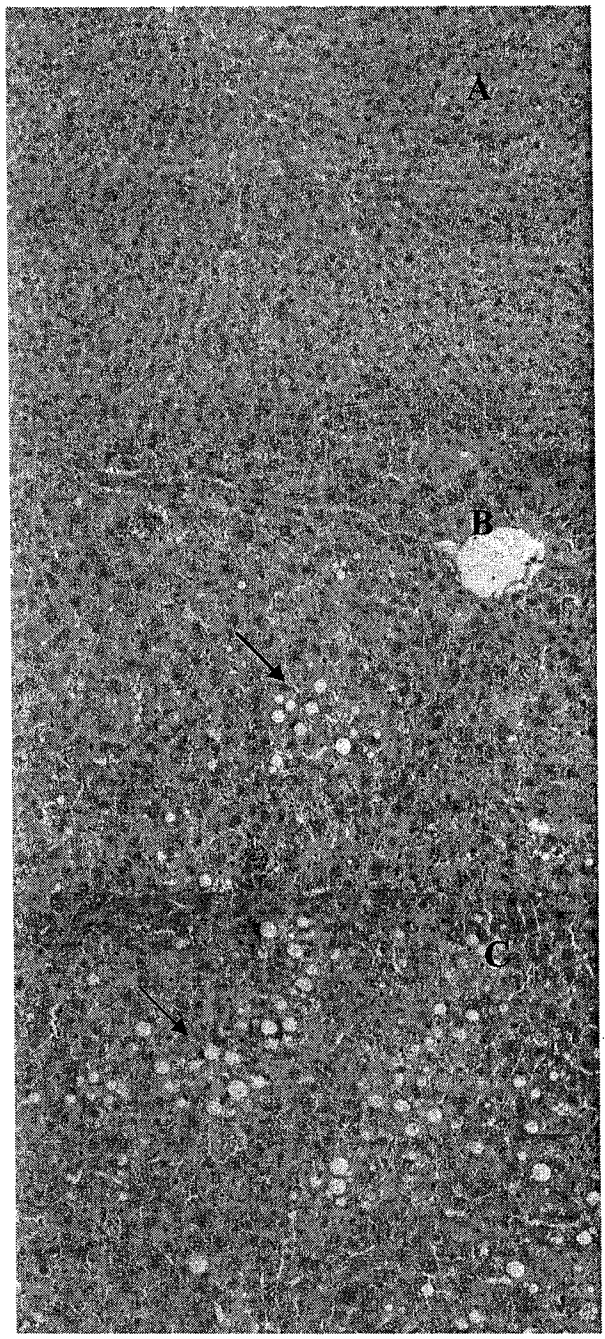

Fig. 3.4. Comparison of lipid accumulation in the livers (H&E stained slides) of the rats in the control (A), low (B), and high dose (C) groups in the HCB+PCB 126 mixture bioassay. The round vacant areas, marked by the arrows, are lipid vacuoles inside hepatocytes, indicating the presence of lipid droplets before the preparation for microscopy. The pictures were taken at 40X magnification.

Since tissue partition of HCB is governed by lipid content, HCB disposition should be inevitably affected by altered fat metabolism. In our mixture bioassay, the relative fat concentration of HCB was elevated probably because the fat volume was reduced. The liver with abnormal lipid accumulation attracted more HCB and thus had higher relative concentration. The hyperlipidemia hampered the partitioning of HCB into the muscle, leading to a reduced relative concentration in the muscle.

As for the second aspect of the alteration of HCB disposition (*i.e.*, tissue concentration decrease at the first two time points and increase at the later three), fat metabolism disturbance appears not to be a reasonable explanation. Rather, it seemed that HCB accumulation in the body was changed by PCB 126. The absorption and excretion processes of HCB are the possible targets of PCB 126.

The intestinal absorption of HCB is a passive diffusion process. Gobas *et al.* (1993) proposed that orally administered HCB is transported in micelles to the intestinal wall, where it separates from the lipid and bile salts to diffuse as a single molecule through the wall. On the other side of the intestinal wall, HCB is reassociated with lipid or lipoproteins for further transport. Essentially, the diffusion is governed by equilibrium partitioning between the blood and the intestinal lumen. However, the whole absorption process (from the intestinal lumen to blood) is also affected by the availability of bile salts, digestibility of lipids in the lumen, and the amount of lipids in the intestinal tissue. The importance of lipid in HCB absorption was also illustrated by Schlummer *et al.* (1998). As a highly lipophilic and metabolically resistant chemical, HCB is predominantly excreted by an outward, *i.e.*, blood-to-lumen, passive diffusion (Rozman 1985). This excretion pathway, known as exsorption, has been documented for

hydrophobic drugs (Arimori and Nakano 1998; Israili and Dayton 1984). HCB exsorption occurs at both small and large intestines (Richter and Schafer 1981) and the latter is more vital for the net excretion (Rozman *et al.* 1985). Mass accumulation in the body is determined by the difference between the absorption and exsorption processes.

In the mixture bioassay, HCB was not detectable in the tissues at the first time point, indicating no net HCB absorption. Thus we speculated that the PCB 126 coexposure inhibited HCB absorption in the early stage. After the second time point, HCB concentrations became much higher than the counterparts in the HCB bioassay, leading to an assumption that PCB 126 stimulates HCB absorption and/or inhibits exsorption at this stage. However, the underlying mechanism of these bidirectional effects is unknown. Recently, P-glycoproteins, encoded by multiple drug resistance (mdr) genes, have stirred great interest. With high expression in the intestine (Brady *et al.* 2002), one group of P-glycoproteins is associated with chemotherapeutic drug resistance and reduced drug absorption by an outward-oriented active transport. Drug kinetic interactions involving modulation of intestinal P-glycoprotein expression have been reviewed (Sun *et al.* 2004). The study on these proteins in toxicology has also been active. For example, Liu *et al.* (2002) reported that mdr1 gene knockout mice were more sensitive than the wild type to arsenic because more arsenic was accumulated in the tissues of the mutant mice. Brady *et al.* (2002) found *in vivo* treatment of PCB 126 induced intestinal expression of mdr1 mRNA in the rats. Whether or not P-glycoproteins play a significant role in the impact of PCB 126 on HCB disposition needs further investigation.

Using physiologically based pharmacokinetic (PBPK) modeling, we examined the reasonableness of the two assumptions proposed above regarding the alteration of HCB

disposition: fat metabolism disturbance and interruption of HCB absorption and/or exsorption. A PBPK model for HCB was published earlier (Lu *et al.* 2006b) and was adopted for this hypothesis-testing purpose. The fat volume fraction and the partition coefficients of the fat, liver, and slowly perfused tissue (muscle) were adjusted to reflect the disturbance of fat metabolism, and the rate constants of absorption and exsoprtion were varied to incorporate the interruption of HCB absorption and exsorption processes. The HCB tissue concentrations following the mixture treatment were well simulated (Fig. 3.5.)(Lu *et al.* 2005), which lent support to our assumptions.

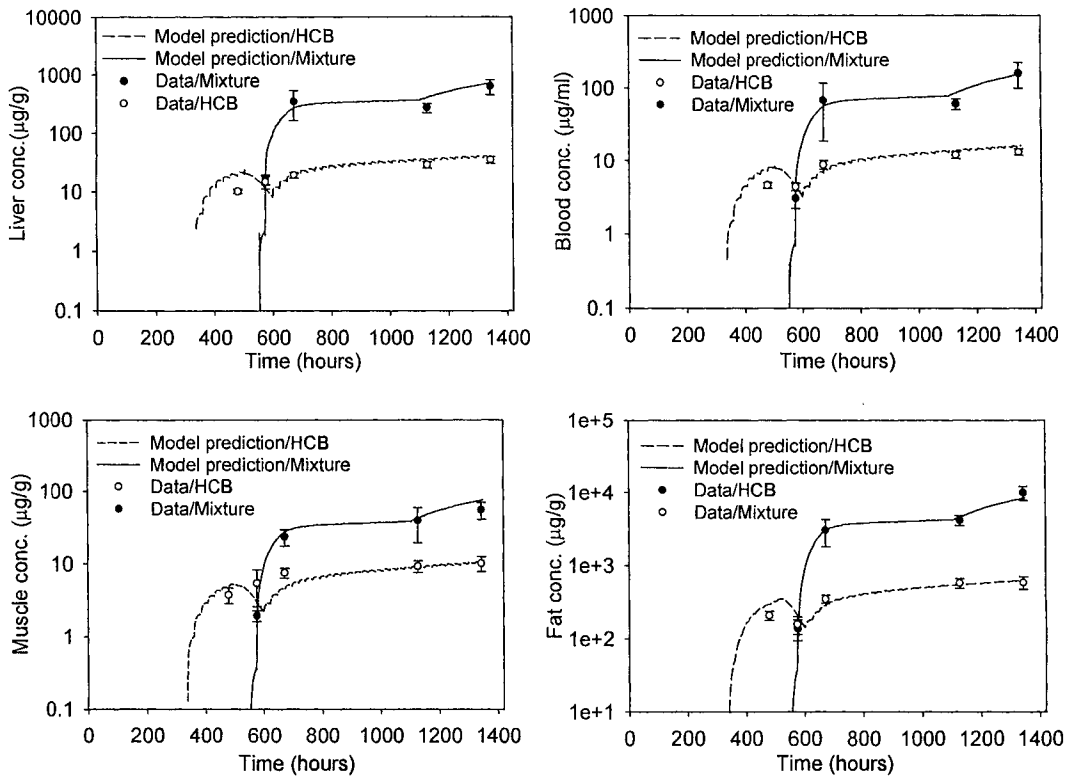

Fig. 3.5. Experimental data (symbols) and PBPK modeling simulations (curves) of HCB concentrations in the liver, blood, muscle, and fat in the HCB alone (28.5 mg/kg) and the HCB (28.5 mg/kg) + PCB 126 (9.8 µg/kg) mixture bioassays. The simulations (broken curves) for the HCB alone bioassay were from Lu *et al.* (2006c). Some parameters of the Lu *et al.* (2006c) PBPK model were adjusted according to the assumptions of fat metabolism disturbance and interruption of HCB absorption and/or exsorption processes (Lu *et al.* 2005), which resulted in the simulations (solid curves) for the mixture bioassay.

One striking feature of the rats in this study was that they were subjected to partial hepatectomy. This surgery causes drastic physiological changes to facilitate liver regeneration (Katagiri 1988; Michalopoulos and DeFrances 1997; Sabugal *et al.* 1996); among them are fat mobilization and hyperlipidemia. These changes are somewhat reversible. However, the mixture treatment may magnify them and interfere with the recovery. Thus the partial hepatectomy is likely to contribute to the alteration in HCB disposition.

The kidney is one of the target organs of HCB and PCB 126. The long-term treatments with these chemicals increased the relative kidney weight (Koss *et al.* 1978; Kuiper-Goodman *et al.* 1977). In our studies, the mixture treatment had greater effect on the kidney than HCB alone. In HCB-induced nephrotoxicity, a low molecular weight protein, $\alpha_{2\mu}$ globulin, is involved in male rats (Bouthillier *et al.* 1991). Once bound to HCB, this protein becomes less digestible and hence accumulates in the lysosomes in the renal proximal tubules (Borghoff *et al.* 1990). The protein accumulation causes cell injury and death and compensatory cell regeneration (Borghoff *et al.* 1990). The mechanism of PCB 126-induced nephrotoxicity has not yet been addressed. The relative kidney concentrations of HCB were similar in our HCB alone and HCB+PCB 126 mixture bioassays (Table 3.5), which suggests the partitioning into the kidney is not changed by PCB 126 coexposure regardless of the kidney enlargement.

The kinetic interaction between HCB and PCB 126 is of toxicological significance. The alteration in HCB kinetics likely leads to modulations in the spectrum and magnitude of the toxicity of this chemical. Further study is needed to explore how the toxicity of HCB is affected by kinetic interactions.

In this study, we did not measure PCB 126 concentrations in the tissues. This was because the PCB 126 levels were three orders of magnitude lower than the HCB levels, and the tiny peak of PCB 126 in the gas chromatograph was severely interfered by the huge peak of HCB; consequently, the quantification of PCB 126 was not possible.

In summary, we studied the impacts of PCB 126 coexposure on HCB disposition in a medium-term liver foci bioassay. The pharmacokinetic studies paralleled liver GST-P foci bioassays after treatment with HCB alone or HCB+PCB 126 mixture, both being performed at two dose levels. PCB 126 coexposure decreased the body accumulation of HCB at the early stage and increased the accumulation at the late stage. The coexposure also changed the partitioning of HCB into the liver, fat, and muscle. We proposed that the altered body accumulation of HCB was due to the interruption of HCB absorption and/or excretion processes and that the changes in the tissue partitioning were a result of fat metabolism disturbance. Further studies are necessary to verify these hypotheses and to clarify the toxicological significance of these pharmacokinetic interactions.

ACKNOWLEDGEMENTS

This study is supported by the NIOSH/CDC grant 1 RO1 OH07556, NIEHS Training Grant 1 T32 ES 07321, and scholarships from U.S. Fulbright Foundation and Naresuan University, Thailand. The authors thank Ms. Laura Chubb, Ms. Amanda Ashley, Ms. Tracy Nichols, Drs. Todd Painter, Charles Dean, and Ying Zhang, and other colleagues in the Quantitative and Computational Toxicology Group for their excellent technical assistance.

REFERENCES

Alvarez, L., Randi, A., Alvarez, P., Kolliker Frers, R., and Kleiman de Pisarev, D. L. (1999). Effect of hexachlorobenzene on NADPH-generating lipogenic enzymes and L-glycerol-3-phosphate dehydrogenase in brown adipose tissue. *J Endocrinol Invest* **22**, 436-445.

Arimori, K., and Nakano, M. (1998). Drug exsorption from blood into the gastrointestinal tract. *Pharm Res* **15**, 371-376.

Bailey, R. E. (2001). Global hexachlorobenzene emissions. *Chemosphere* **43**, 167-182.

Bates, M. N., Buckland, S. J., Garrett, N., Ellis, H., Needham, L. L., Patterson, D. G., Jr., Turner, W. E., and Russell, D. G. (2004). Persistent organochlorines in the serum of the non-occupationally exposed New Zealand population. *Chemosphere* **54**, 1431-43.

Billi de Catabbi, S., Sterin-Speziale, N., Fernandez, M. C., Minutolo, C., Aldonatti, C., and San Martin de Viale, L. (1997). Time course of hexachlorobenzene-induced alterations of lipid metabolism and their relation to porphyria. *Int J Biochem Cell Biol* **29**, 335-44.

Blais, J. M., Froese, K. L., Kimpe, L. E., Muir, D. C., Backus, S., Comba, M., and Schindler, D. W. (2003). Assessment and characterization of polychlorinated biphenyls near a hazardous waste incinerator: analysis of vegetation, snow, and sediments. *Environ Toxicol Chem* **22**, 126-33.

Borghoff, S. J., Short, B. G., and Swenberg, J. A. (1990). Biochemical mechanisms and pathobiology of alpha 2u-globulin nephropathy. *Annu Rev Pharmacol Toxicol* **30**, 349-67.

Bouthillier, L., Greselin, E., Brodeur, J., Viau, C., and Charbonneau, M. (1991). Male rat specific nephrotoxicity resulting from subchronic administration of hexachlorobenzene. *Toxicol Appl Pharmacol* **110**, 315-26.

Brady, J. M., Cherrington, N. J., Hartley, D. P., Buist, S. C., Li, N., and Klaassen, C. D. (2002). Tissue distribution and chemical induction of multiple drug resistance genes in rats. *Drug Metab Dispos* **30**, 838-44.

Brewster, D. W., and Matsumura, F. (1988). Reduction of adipose tissue lipoprotein lipase activity as a result of in vivo administration of 2,3,7,8-tetrachlorodibenzo-p-dioxin to the guinea pig. *Biochem Pharmacol* **37**, 2247-53.

Chu, I., Villeneuve, D. C., Yagminas, A., LeCavalier, P., Poon, R., Feeley, M., Kennedy, S. W., Seegal, R. F., Hakansson, H., Ahlborg, U. G., and et al. (1994). Subchronic toxicity of 3,3',4,4',5-pentachlorobiphenyl in the rat. I. Clinical, biochemical, hematological, and histopathological changes. *Fundam Appl Toxicol* **22**, 457-68.

Covaci, A., Jorens, P., Jacquemyn, Y., and Schepens, P. (2002). Distribution of PCBs and organochlorine pesticides in umbilical cord and maternal serum. *Sci Total Environ* **298**, 45-53.

de Rosa, C. T., El-Masri, H. A., Pohl, H., Cibulas, W., and Mumtaz, M. M. (2004). Implications of chemical mixtures in public health practice. *J Toxicol Environ Health B Crit Rev* **7**, 339-50.

Dean, C. E., Jr., Benjamin, S. A., Chubb, L. S., Tessari, J. D., and Keefe, T. J. (2002). Nonadditive hepatic tumor promoting effects by a mixture of two structurally different polychlorinated biphenyls in female rat livers. *Toxicol Sci* **66**, 54-61.

Dewailly, E., Mulvad, G., Pedersen, H. S., Ayotte, P., Demers, A., Weber, J. P., and Hansen, J. C. (1999). Concentration of organochlorines in human brain, liver, and adipose tissue autopsy samples from Greenland. *Environ Health Perspect* **107**, 823-828.

Erturk, E., Lambrecht, R. W., Peters, H. A., Cripps, D. J., Gocmen, A., Morris, C. R., and Bryan, G. T. (1986). Oncogenicity of hexachlorobenzene. *IARC Sci Publ*, 417-423.

Finley, B. L., Trowbridge, K. R., Burton, S., Proctor, D. M., Panko, J. M., and Paustenbach, D. J. (1997). Preliminary assessment of PCB risks to human and ecological health in the lower Passaic River. *J Toxicol Environ Health* **52**, 95-118.

Focant, J. F., Pirard, C., Massart, A. C., and De Pauw, E. (2003). Survey of commercial pasteurised cows' milk in Wallonia (Belgium) for the occurrence of polychlorinated dibenzo-p-dioxins, dibenzofurans and coplanar polychlorinated biphenyls. *Chemosphere* **52**, 725-33.

Foster, W. G., Pentick, J. A., McMahon, A., and Lecavalier, P. R. (1993). Body distribution and endocrine toxicity of hexachlorobenzene (HCB) in the female rat. *J Appl Toxicol* **13**, 79-83.

Gobas, F. A., McCorquodale, J. R., and Haffner, G. G. (1993). Intestinal absorption and biomagnification of organochlorines. *Environ Toxicol Chem* **12**, 567-576.

Gocmen, A., Peters, H. A., Cripps, D. J., Morris, C. R., and Dogramaci, I. (1986). Porphyria turcica: hexachlorobenzene-induced porphyria. *IARC Sci Publ*, 567-573.

Gorski, J. R., Weber, L. W., and Rozman, K. (1988). Tissue-specific alterations of de novo fatty acid synthesis in 2,3,7,8-tetrachlorodibenzo-p-dioxin (TCDD)-treated rats. *Arch Toxicol* **62**, 146-51.

Gustafson, D. L., Long, M. E., and Thomas, R. (2000). Comparative hepatocarcinogenicity of hexachlorobenzene,pentachlorobenzene,1,2,4,5-tetrachlorobenzene,and 1,4-dichlorobenzene:Application of a medium-term liver focus bioassay and molecular and cellular indices. *Toxicol Sci* **53**, 245-252.

Israili, Z. H., and Dayton, P. G. (1984). Enhancement of xenobiotic elimination: Role of intestinal excretion. *Drug Metab Rev* **15**, 1123-1159.

Ito, N., Imaida, K., de Camargo, J. L., Takahashi, S., Asamoto, M., and Tsuda, H. (1988). A new medium-term bioassay system for detection of environmental carcinogens using diethylnitrosamine-initiated rat liver followed by D-galactosamine treatment and partial hepatectomy. *Jpn J Cancer Res* **79**, 573-5.

Ito, N., Tamano, S., and Shirai, T. (2003). A medium-term rat liver bioassay for rapid in vivo detection of carcinogenic potential of chemicals. *Cancer Sci* **94**, 3-8.

Jordan, S. A., and Feeley, M. M. (1999). PCB congener patterns in rats consuming diets containing Great Lakes salmon: analysis of fish, diets, and adipose tissue. *Environ Res* **80**, S207-S212.

Katagiri, S. (1988). [Experimental study on lipid metabolism after partial hepatectomy--with reference to mitochondrial function of the regenerating liver]. *Nippon Geka Gakkai Zasshi* **89**, 694-702.

Koss, G., and Koransky, W. (1975). Studies on the toxicology of hexachlorobenzene I.Pharmacokinetics. *Arch Toxicol* **34**, 203-212.

Koss, G., Seubert, S., Seubert, A., Koransky, W., and Ippen, H. (1978). Studies on the toxicology of hexachlorobenzene. III. Observations in a long-term experiment. *Arch Toxicol* **40**, 285-294.

Kuiper-Goodman, T., Grant, D. L., Moodie, A., and al., e. (1977). Subacute toxicity of hexachlorobenzene in the rat. *Toxicol Appl Pharmacol* **40**, 529-79.

Lee, S. K., Ou, Y. C., and Yang, R. S. H. (2002). Comparison of pharmacokinetic interactions and physiologically based pharmacokinetic modeling of PCB 153 and PCB 126 in nonpregnant mice, lactating mice, and suckling pups. *Toxicol Sci* **65**, 26-34.

Liljegren, G., Hardell, L., Lindstrom, G., Dahl, P., and Magnuson, A. (1998). Case-control study on breast cancer and adipose tissue concentrations of congener specific polychlorinated biphenyls, DDE and hexachlorobenzene. *Eur J Cancer Prev* **7**, 135-40.

Liu, J., Liu, Y., Powell, D. A., Waalkes, M. P., and Klaassen, C. D. (2002). Multidrug-resistance mdr1a/1b double knockout mice are more sensitive than wild type mice to acute arsenic toxicity, with higher arsenic accumulation in tissues. *Toxicology* **170**, 55-62.

Lu, Y., Lohitnavy, M., Lohitnavy, O., Eickman, E., and Yang, R. S. H. (2005). Alteration of hexachlorobenzene (HCB) kinetics by PCB126 coexposure and application of PBPK modeling in a medium-term liver foci bioassay [Abstract]. *Toxicologist.*

Lu, Y., Lohitnavy, M., Reddy, M., Lohitnavy, O., Eickman, E., Ashley, A., Xu, Y., and Yang, R. S. H. (2006a). Promotion of liver GST-P foci by a chemical mixture of hexachlorobenzene (HCB) and 3, 3', 4, 4', 5-pentachlorobiphenyl (PCB126): Integration of computer modeling and biology of clonal growth [Abstract]. *Toxicologist* **90**, 435.

Lu, Y., Lohitnavy, M., Reddy, M. B., Lohitnavy, O., Ashley, A., and Yang, R. S. H. (2006b). An updated physiologically based pharmacokinetic model for hexachlorobenzene: Incorporation of pathophysiological states following partial hepatectomy and hexachlorobenzene treatment. *Toxicol Sci* **91**, 29-41.

Lu, Y., Lohitnavy, M., Reddy, M. B., Lohitnavy, O., Ashley, A., and Yang, R. S. H. (2006c). An updated physiologically based pharmacokinetic model for hexachlorobenzene: Incorporation of pathophysiological states following partial hepatectomy and hexachlorobenzene treatment. *Toxicol Sci* **91**, 29-41.

Marvin, C. H., Painter, S., Charlton, M. N., Fox, M. E., and Lina Thiessen, P. A. (2004). Trends in spatial and temporal levels of persistent organic pollutants in Lake Erie sediments. *Chemosphere* **54**, 33-40.

Mazzetti, M. B., Taira, M. C., Lelli, S. M., Dascal, E., Basabe, J. C., and De Viale, L. C. (2004). Hexachlorobenzene impairs glucose metabolism in a rat model of porphyria cutanea tarda: a mechanistic approach. *Arch Toxicol* **78**, 25-33.

Meijer, S. N., Ockenden, W. A., Steinnes, E., Corrigan, B. P., and Jones, K. C. (2003). Spatial and temporal trends of POPs in Norwegian and UK background air: implications for global cycling. *Environ Sci Technol* **37**, 454-61.

Michalopoulos, G. K., and DeFrances, M. C. (1997). Liver regeneration. *Science* **276**, 60-66.

NTP (2001). Ninth report on carcinogenesis: Hexachlorobenzene. National Toxicology Program.

NTP (2004). Toxicology and carcinogenesis studies of 3,3',4,4',5-pentachlorobiphenyl (PCB 126) (CAS No. 57465-28-8) in female Harlan Sprague-Dawley rats (gavage studies). National Toxicology Program, Research Triangle Park, NC.

Olsen, H., Enan, E., and Matsumura, F. (1998). 2,3,7,8-Tetrachlorodibenzo-p-dioxin mechanism of action to reduce lipoprotein lipase activity in the 3T3-L1 preadipocyte cell line. *J Biochem Mol Toxicol* **12**, 29-39.

Ou, Y. C., Conolly, R. B., Thomas, R., Gustafson, D. L., Long, M. E., Dovrev, I. D., Chubb, L. S., Xu, Y., Lapidot, S., Andersen, M. E., and Yang, R. S. H. (2003). Stochastic simulation of hepatic preneoplasic foci development for four chlorobenzene congeners in a medium-term bioassay. *Toxicol Sci* **73**, 301-314.

Ou, Y. C., Conolly, R. B., Thomas, R. S., Xu, Y., Andersen, M. E., Chubb, L. S., Pitot, H. C., and Yang, R. S. H. (2001). A clonal growth model: time-course simulations of liver foci growth following penta- or hexachlorobenzene treatment in a medium-term bioassay. *Cancer Res* **61**, 1879-1889.

Ralph, J. L., Orgebin-Crist, M. C., Lareyre, J. J., and Nelson, C. C. (2003). Disruption of androgen regulation in the prostate by the environmental contaminant hexachlorobenzene. *Environ Health Perspect* **111**, 461-466.

Richter, E., and Schafer, S. G. (1981). Intestinal excretion of hexachlorobenzene. *Arch Toxicol* **47**, 233-9.

Rozman, K. (1985). Intestinal excretion of toxic substances. *Arch Toxicol* **Suppl 8**, 87-93.

Rozman, T., Scheufler, E., and Rozman, K. (1985). Effect of partial jejunectomy and colectomy on the disposition of hexachlorobenzene in rats treated or not treated with hexadecane. *Toxicol Appl Pharmacol* **78**, 421-427.

Sabugal, R., Robert, M. Q., Julve, J., Auwerx, J., Llobera, M., and Peinado-Onsurbe, J. (1996). Hepatic regeneration induces changes in lipoprotein lipase activity in several tissues and its re-expression in the liver. *Biochem J* **318(Pt 2)**, 597-602.

Safe, S. H. (1994). Polychlorinated biphenyls (PCBs): environmental impact, biochemical and toxic responses, and implications for risk assessment. *Crit Rev Toxicol* **24**, 87-149.

Schecter, A., Quynh, H. T., Pavuk, M., Papke, O., Malisch, R., and Constable, J. D. (2003). Food as a source of dioxin exposure in the residents of Bien Hoa City, Vietnam. *J Occup Environ Med* **45**, 781-788.

Schlummer, M., Andreas Moser, G., and McLachlan, M. S. (1998). Digestive tract absorption of PCDD/Fs,PCBs,and HCB in humans:Mass balances and mechanistic considerations. *Toxicol Appl Pharmacol* **152**, 128-137.

Shadel, B. N., Evans, R. G., Roberts, D., Clardy, S., Jordan-Izaguirre, D., Patterson, D. G., Jr., and Needham, L. L. (2001). Background levels of non-ortho-substituted (coplanar) polychlorinated biphenyls in human serum of Missouri residents. *Chemosphere* **43**, 967-76.

Siekel, P., Chalupa, I., Beno, J., Blasko, M., Novotny, J., and Burian, J. (1991). A genotoxicological study of hexachlorobenzene and pentachloroanisole. *Teratog Carcinog Mutagen* **11**, 55-60.

Smith, A. G., Dinsdale, D., Cabral, J. R., and Wright, A. L. (1987). Goitre and wasting induced in hamsters by hexachlorobenzene. *Arch Toxicol* **60**, 343-349.

Smith, A. G., Francis, J. E., Dinsdale, D., Manson, M. M., and Cabral, J. R. (1985). Hepatocarcinogenicity of hexachlorobenzene in rats and the sex difference in hepatic iron status and development of porphyria. *Carcinogenesis* **6**, 631-636.

Sun, J., He, Z. G., Cheng, G., Wang, S. J., Hao, X. H., and Zou, M. J. (2004). Multidrug resistance P-glycoprotein: crucial significance in drug disposition and interaction. *Med Sci Monit* **10**, RA5-14.

Thomas, R. S. (1998). The Use of Biologically-Based Models for Integrating Short-Term Cancer Bioassays, Mechanisms of Action, and Target Tissue Dosimetry: Application to Pentachlorobenzene. Ph.D. dissertation. Department of Environmental Health, Colorado State University, Fort Collins, CO.

Thomas, R. S., Conolly, R. B., Gustafson, D. L., Long, M. E., Benjamin, S. A., and Yang, R. S. H. (2000). A physiologically based pharmacodynamic analysis of hepatic foci within a medium-term liver bioassay using pentachlorobenzene as a promoter and diethylnitrosamine as an initiator. *Toxicol Appl Pharmacol* **166**, 128-37.

Van Birgelen, A. P., Van der Kolk, J., Fase, K. M., Bol, I., Poiger, H., Brouwer, A., and Van den Berg, M. (1994). Toxic potency of 3,3',4,4',5-pentachlorobiphenyl relative to and in combination with 2,3,7,8-tetrachlorodibenzo-p-dioxin in a subchronic feeding study in the rat. *Toxicol Appl Pharmacol* **127**, 209-21.

Vos, J. G. (1986). Immunotoxicity of hexachlorobenzene. *IARC Sci Publ*, 347-56.

Weber, K., and Goerke, H. (2003). Persistent organic pollutants (POPs) in antarctic fish: levels, patterns, changes. *Chemosphere* **53**, 667-678.

Weber, L. W., Lebofsky, M., Stahl, B. U., Gorski, J. R., Muzi, G., and Rozman, K. (1991). Reduced activities of key enzymes of gluconeogenesis as possible cause

of acute toxicity of 2,3,7,8-tetrachlorodibenzo-p-dioxin (TCDD) in rats. *Toxicology* **66**, 133-44.

Yang, R. S. H. (1998). Some critical issues and concerns related to research advances on toxicology of chemical mixtures. *Environ Health Perspect* **106 Suppl 4**, 1059-63.

Yang, R. S. H., Thomas, R. S., Gustafson, D. L., Campain, J., Benjamin, S. A., Verhaar, H. J., and Mumtaz, M. M. (1998). Approaches to developing alternative and predictive toxicology based on PBPK/PD and QSAR modeling. *Environ Health Perspect* **106(Suppl 6)**, 1385-1393.

CHAPTER 4

Promotion of Liver GST-P Foci by a Chemical Mixture of Hexachlorobenzene and PCB 126: Integration of Computer Modeling and Biology of Clonal Growth

Yasong Lu, Manupat Lohitnavy, Micaela Reddy, Ornrat Lohitnavy, Elizabeth Eickman, Amanda Ashley, Lisa Gerjevic, Yihua Xu, Rory B. Conolly, Raymond S. H. Yang

ABSTRACT

The objectives of this study were two-fold: (1) evaluating the carcinogenic potential of a mixture of two persistent environmental pollutants, hexachlorobenzene (HCB) and 3,3',4,4',5-pentachlorobiphenyl (PCB 126), in an initiation/promotion bioassay involving the development of glutathione S-transferase placental form (GST-P) liver foci; and (2) integrating computer modeling with the biology of GST-P foci growth in the bioassay. The 8-week bioassay involved a single injection of an initiator, a two-thirds partial hepatectomy, and daily oral gavage of the HCB+PCB 126 mixture in F344 rats. The animals were serially sacrificed for time-course data. The mixture treatment significantly increased GST-P foci size and number in the liver, indicating the carcinogenic potential of this mixture. Our biologically based computer model (*i.e.*, clonal growth model) was developed to simulate the appearance and development of initiated GST-P cells in the liver over time. The model outputs of relative foci volume, foci number/cm^3 liver, and size distribution were consistent with the experimentally derived data. Our modeling exercises further supported the negative selection and two-cell hypotheses on foci development proposed earlier. Furthermore, our model illustrated the size-dependency of

foci growth kinetics and the impact of the chemical mixture on this characteristic. This study exemplified how mechanism based computer modeling can improve our understanding in the carcinogenic process with or without chemical treatment. This study continues our development of a predictive tool for carcinogenic potential of chemical mixtures by integrating computer modeling with biology of foci development.

1. INTRODUCTION

Although toxicological studies often focus on individual chemicals, human exposure is rarely, if ever, limited to one single chemical (Yang 1994; Yang 1997; Yang *et al.* 1995; Yang *et al.* 1998). Potential interactions among chemicals, at the levels of pharmacokinetics and pharmacodynamics, may modulate the toxicity of each individual chemical. Consequently, it is difficult to accurately predict effects of a chemical mixture solely based on the information of each component. Thus, research on toxicology of chemical mixtures should be encouraged.

Among the numerous chemicals humans are exposed to are two persistent organic pollutants, hexachlorobenzene (HCB) and 3,3',4,4',5-pentachlorobiphenyl (PCB 126). They were both present in the environment (Blais *et al.* 2003) and in human tissues (Liljegren *et al.* 1998). Their respective carcinogenicities, along with other toxicities, have been intensively studied. HCB-induced carcinogenicity was observed in the laboratory animals with the liver being a main target organ (Erturk *et al.* 1986; Smith *et al.* 1985). HCB has been classified as "reasonably anticipated to be a human carcinogen" by the US National Toxicology Program (NTP 2001). PCB 126 was reported to significantly increase tumor incidence in multiple sites, e.g., the liver, lung, and oral

mucosa, in the female Sprague-Dawley rats in a two-year oral gavage study (NTP 2004b). The carcinogenic potential of some mixtures, e.g., PCB 126 and PCB 153 (Dean *et al.* 2002; Yoshizawa *et al.* 2005), PCB 126 and PCB 118 (Yoshizawa *et al.* 2005), PCB 105 and PCB 153 (Haag-Gronlund *et al.* 1998), has been experimentally examined. However, no study has addressed the carcinogenicity of the mixture of PCB 126 and HCB.

There are more than 80,000 chemicals registered in the U.S., and each year, an additional 2,000 new chemicals are introduced for use in such everyday items as foods, personal care products, drugs, household cleaners, and lawn care products (NTP 2004a). It is already "mission impossible" to characterize toxicities, particularly carcinogenicity, of these chemicals individually, let alone the astronomical number of mixtures derived from these chemicals (Yang 1997; Yang *et al.* 2004; Yang *et al.* 1998). Thus, scientifically sound predictive tools must be developed to evaluate carcinogenic potentials, among other toxicities, for chemicals and chemical mixtures.

For evaluating chemical carcinogenicity, in addition to the "gold standard" two-year animal bioassay, several short- and medium-term liver foci bioassays have emerged in the past two decades. One well recognized approach was proposed by Ito *et al.* (Ito *et al.* 1998; Ito *et al.* 2003; Ito *et al.* 1989). As shown in Fig. 4.1, the Ito's 8-week protocol involves administration of diethylnitrosamine (DEN) at a relatively high dose (200 mg/kg, intraperitoneal, i.p., injection) as an initiator, followed by test chemical (promoter) treatment and hepatocyte mitogenic stimulation (partial hepatectomy) in young male F344 rats. After sacrifice of all animals at 8 weeks, the evaluation of carcinogenic potential is achieved by identification and analysis of hepatic glutathione S-transferase placental form (GST-P) preneoplastic foci as the end-point marker. The GST-P foci

formation promoted by a chemical is well correlated with the carcinogenicity of that chemical (Ito *et al.* 2003). In our laboratory, this protocol was modified by incorporating a series of sacrifice time points to collect time-course data on test chemical pharmacokinetics and GST-P foci formation (Lu *et al.* 2006; Ou *et al.* 2003; Ou *et al.* 2001; Thomas 1998; Thomas *et al.* 2000a; Thomas *et al.* 2000b; Yang *et al.* 1998).

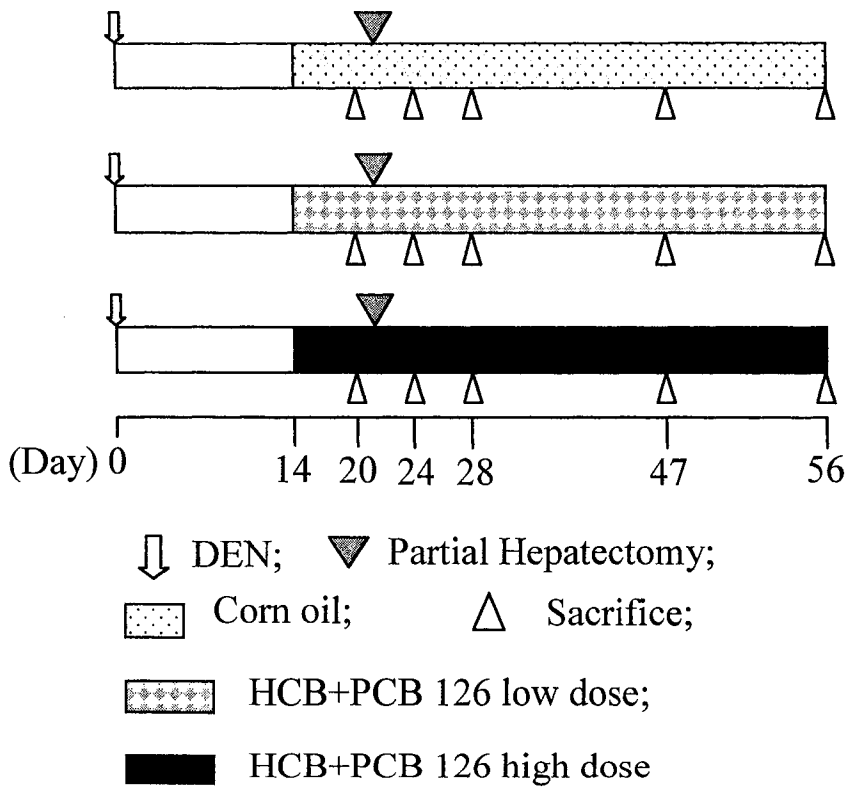

Fig. 4.1. Experimental design of the time-course medium-term liver foci bioassay. A single i.p. injection of 200 mg/kg DEN was given on day 0. Daily oral gavage of corn oil or HCB+PCB 126 mixture (low or high dose) started from day 14 through sacrifice. On day 21, a two-thirds partial hepatectomy was performed on the rats. On the day of surgery and the following three days the gavage was suspended to reduce the stress to the animals. Six rats from each treatment group were sacrificed on days 20, 24, 28, 47, and 56. The liver was sectioned and saved appropriately for GST-P foci measurement and other analyses.

To quantitatively describe and predict tumor incidence in human populations and chemically treated laboratory animals, Moolgavkar and co-workers (Moolgavkar *et al.* 1988; Moolgavkar and Knudson 1981; Moolgavkar and Venzon 1979) developed a biologically based mathematical model based on the initiation-promotion two-stage theory on carcinogenesis. The model, known as two-stage MVK model, was advantageous over other existing models because of its incorporation of cell kinetics. As a great body of data on liver foci formation has been attained after the increasing application of the liver foci bioassays, the first stage of the MVK model, *i.e.*, appearance and growth of the initiated cells, was applied to describe those data (Conolly and Andersen 1997; Conolly and Kimbell 1994; Luebeck *et al.* 2000; Moolgavkar *et al.* 1996; Ou *et al.* 2003; Ou *et al.* 2001; Portier *et al.* 1996; Thomas *et al.* 2000b). As preneoplastic liver foci are the consequence of clonal expansion of individual initiated cells, the model describing foci formation is designated as clonal growth model (Conolly and Kimbell 1994).

By comparing model simulations with experimental data, clonal growth modeling provides insight into growth kinetics of preneoplasic foci and modes of action of carcinogens. For example, the cells initiated by DEN in the rats were initially assumed to be a single population. However, inspired by Jirtle *et al.* (1991), Conolly and Andersen (1997), in their biologically based computer modeling, suggested that the initiated cell pool could consist of two subpopulations (A and B cells) with different growth kinetics. This two-cell hypothesis was supported by further modeling work (Haag-Gronlund *et al.* 2000; Ou *et al.* 2003; Ou *et al.* 2001; Thomas *et al.* 2000b). These results lent support to the "negative selection" mechanism for hepatic tumor promotion (Andersen *et al.* 1995;

Jirtle *et al.* 1991). The growth of GST-P cells in a focus was implied to depend on the focal size by Moolgavkar and co-workers (Grasl-Kraupp *et al.* 2000; Luebeck *et al.* 1995; Moolgavkar *et al.* 1996), nevertheless the size-dependency needs further quantitative exploration.

A long-term goal of our laboratory is to develop a tool for predicting chemical mixture carcinogenicity by integrating medium-term animal bioassays with computational modeling. As a step towards that goal, this study included: (1) Evaluating the joint carcinogenic potential of the mixture of HCB and PCB 126 using a medium-term liver foci bioassay where pharmacokinetics and pharmacodynamics were studied in parallel; and (2) Analyzing the collected data quantitatively using a clonal growth model with an emphasis on the size-dependency of the growth kinetics of initiated cells. While the pharmacokinetic results will be published elsewhere, this paper focuses on the pharmacodynamics (*i.e.*, GST-P foci formation) and clonal growth modeling.

2. MATERIALS AND METHODS

2.1. Medium-term Liver Foci Bioassay and Data Collection

2.1.1. Chemicals

HCB (99% purity) was purchased from Aldrich Chemical (Milwaukee, WI). PCB 126 was obtained from AccuStandard (New Haven, CT). DEN was from Sigma Chemical (St. Louis, MO).

2.1.2. Animals and Treatment

Male F344 rats, 30 days of age, purchased from Harlan Sprague-Dawley (Indianapolis, IN), were housed in the Painter Center, Colorado State University. It is

fully accredited by the American Association for Accreditation of Laboratory Animal Care (AAALAC). Animals were given food (Harlan Teklad NIH-07 diet, Madison, WI) and water *ad libitum* and lighting was set on a 12h light/dark cycle.

After four weeks of acclimation, the rats were randomized by weight, divided into three groups, and treated according to the time-course medium-term liver foci bioassay (Fig. 4.1). At week 0, the rats were given a single i.p. injection of DEN (200 mg/kg) in 0.9% saline. Two weeks later, the rats began receiving daily oral gavage of corn oil (control), low dose (8.55 mg/kg + 3.3 μg/kg), and high dose (28.5 mg/kg + 9.8 μg/kg) of HCB+PCB 126 mixture in corn oil until sacrifice. The dose levels were determined on the basis of the previous work in our laboratory (Dean *et al.* 2002; Ou *et al.* 2001). At week 3 (day 21), a two-thirds partial hepatectomy was performed on the rats. On the day of surgery and the following three days, the gavage was suspended to reduce the stress to the animals while recovering from surgery. On days 20, 24, 28, 47, and 56, six rats from each treatment group were sacrificed by aortic exsanguination under anesthesia. The body and liver weight of each rat were recorded at sacrifice. A slice of liver was taken along the longest axis of each lobe, fixed in 10% neutral-buffered formalin, embedded in paraffin, and then serially sectioned at thickness of 5 μm. The study was conducted in accordance with the National Institutes of Health (NIH) guidelines for the care and use of laboratory animals.

The experimental protocol described above utilized a total of approximately 100 rats including sentinels. This approached the maximal surgical and experimental capacity of a team of four scientists in our laboratory. Therefore, we studied the single chemicals

separately with their respective controls. Comparisons of the HCB+PCB 126 mixture and the respective single chemicals are presented in Chapter 5.

2.1.3. GST-P Foci Measurement

GST-P foci identification and quantification followed the methods previously described (Ou *et al.* 2001; Thomas 1998). Liver slides were deparaffinized in xylene and rehydrated by passage through an alcohol series. Endogenous peroxidase was quenched in 3% hydrogen peroxide for 10 min. The slides were then rinsed with deionized water and placed in PBS (pH 7.4; 2.7 mM KCl, 0.14 M NaCl, 1.5 mM KH_2PO_4, and 8.1 mM Na_2PO_4). A standard avidin-biotin complex method protocol (Vector Labs, Burlingame, CA) was followed, and foci were identified with GST-P primary antibody (Binding Site, San Diego, CA). GST-P foci were measured using an Olympus BX51 light microscope (Olympus Optical Co., Tokyo, Japan) coupled with a BioQuant NOVA image analysis system (B&M Biometrics, Nashville, TN). Foci having two or more cells were recorded.

2.1.4. Hepatocyte Proliferation Determination

Osmotic minipumps (Alzet model 2ML1, 10 µl/hr; Durect Corporation, Cupertino, CA), filled with 5-bromo-2'-deoxyuridine (BrdU) (20 mg/ml), were implanted subcutaneously over the dorsal midscapular region 3 days prior to sacrifice. Detection of BrdU labeled cells was conducted on the liver slides using standard avidin-biotin complex method and immunoperoxidase kits (Vector Labs, Burlingame, CA) with primary BrdU antibody (Biogenex Labs, San Ramon, CA) and 3-amino-9-ethylcarbozole (Biomeda, Foster City, CA). At least 1000 cells/rat and four rats/group were counted. The labeling index (LI), defined as the number of labeled cells divided by the total number of counted cells, was obtained using CHRIS (version 1.1L; Sverdrup Technology, Fort

Walton Beach, FL). The hepatocyte division rate constant (α, 1/day) was calculated using an equation previously proposed (Moolgavkar and Luebeck 1992):

$$\alpha = \frac{1}{2t} \times \ln\left(\frac{1}{1-LI}\right) \qquad \text{(Eq-1)}$$

where t is the number of days of exposure to BrdU (t = 3 in our study). This result was seen as the division rate constant of the normal hepatocytes; in this study no effort was made to determine the division rate constant of the cells within foci.

2.1.5. Hepatocyte Numerical Density Quantification

The numerical density (cell number/cm^3) of hepatocyte was represented by the numerical density of hepatocyte nuclei that was evaluated on liver H&E slides. Ten random fields per rat were analyzed. The calculation of numerical density followed the formula reported by Weibel *et al.* (1969):

$$N_V = \frac{K}{\lambda} \times \frac{N_A^{3/2}}{V_V^{1/2}} \qquad \text{(Eq-2)}$$

where N_V is hepatocyte numerical density, λ is nuclear shape coefficient, K is nuclear size distribution coefficient, N_A is number of nuclei per cm^2 test area, and V_V is nuclear volume density. In our study, λ = 1.38 according to Weibel and Gomez (1962); K = 1.02 for all groups at day 20, and 1.1 for all groups at other time points accounting for the large variations in nuclear size (Weibel *et al.* 1969). The unbiased estimate of V_V is the nuclear area density, *i.e.*, total area of nuclei per cm^2 test area. The derived numerical density was assumed applicable to both normal and initiated cells.

2.1.6. Stereologic Methods

The foci data obtained from liver slides were 2-dimensional (2D) and must be converted to 3-dimensional (3D) expressions for comparison with model outputs. A

program developed by Xu and Pitot (2003) at the McArdle Laboratory for Cancer Research, University of Wisconsin, was used for the conversion. This program uses data containing tissue information (e.g., liver weight and slide area) and individual focal areas as the input to provide quantitative stereology results on a 3D basis. The outputs include relative foci volume (% liver volume occupied by foci), number of foci/cm^3, and foci size distribution. The theories of the program were detailed in Xu and Pitot (2003). The relative foci volume was computed by the method of Delesse. Foci number/cm^3 liver was calculated using a modified Saltykov method, in which 25 size classes were defined. The diameter ratio of two neighboring classes was $10^{-0.1}$. In our study allocation of foci into classes was based on focal volume rather than cell number. At the hepatocyte density of $1.2\times10^8/cm^3$, the classes 1-13 were corresponding to cell numbers of 8-16, 17-32, 33-64, 65-127, 128-253, 254-505, 506-1007, 1008-2009, 2010-4009, 4010-8000, 8001-15962, 15963-31847, and 31848-63543, respectively. The classes 14-25 were omitted here because there were no foci therein. Note that these classes were employed only for interpreting the size distribution pattern of foci in each group.

The focal diameter truncation value (*i.e.*, all foci smaller than that diameter were considered not reliably detectable and thus ignored) for our calculation was set as 63.1 μm for the mixture-treated groups on days 28, 47, and 56, and 50.12 μm for the control group and the earlier time points (days 20 and 24) of the mixture groups. The differentiation of the truncation value in different groups and time points was necessary due to hepatocyte enlargement (hypertrophy) after mixture treatment.

2.1.7. Statistical Analysis

ANOVA at $\alpha = 0.05$ was applied to analyze the statistical differences of the body weight, relative liver weight, hepatocyte numerical density, foci number, and foci area among the control and mixture groups with and without the factor of time. All statistical analyses were performed using SAS (version 8.02; SAS Institute Inc., Cary, NC).

2.2. Clonal Growth Modeling

Based on the work previously reported (Conolly and Andersen 1997; Conolly and Kimbell 1994; Ou *et al.* 2003; Ou *et al.* 2001; Thomas *et al.* 2000b), our clonal growth model had these assumptions: (1) The liver is composed of hepatocytes whose cellular kinetics are deterministic; (2) All hepatocytes are susceptible cells; (3) The occurrence of initiated cells follows a nonhomogeneous (*i.e.*, the occurrence rate varies over time) Poisson process; (4) The initiated cells are uniformly distributed in the liver; (5) The initiated cells consist of two different subpopulations; and (6) The growth kinetics of a focus is dependent on its size. Like any models, these assumptions represent a simplification of biological reality in our modeling simulation. The model algorithm described the growth kinetics of normal hepatocytes, occurrence of initiated cells induced by DEN, and growth kinetics of the initiated cells. Further mutations in the initiated cells were not considered because it was beyond the present scope of our model. A structure of the model has been presented earlier by our group (Ou *et al.* 2001; Thomas *et al.* 2000b).

2.2.1 Basics of the Clonal Growth Model

(a) *Growth kinetics of normal hepatocytes.* The growth of normal hepatocytes was described deterministically by a function of division (α, 1/day) and death (β, 1/day) rate constants:

$$\frac{dN}{dt} = N(\alpha - \beta) \qquad \text{(Eq-3)}$$

where N is the number of normal hepatocytes/cm^3 (*i.e.*, hepatocyte numerical density), and β includes different kinds of cell death including apoptosis and necrosis.

(b) *Occurrence of initiated cells.* Upon DEN treatment, some hepatocytes may express GST-P that is absent under normal conditions (Kato *et al.* 1993a; Satoh *et al.* 1989). These cells have been recognized as initiated cells and precursors of preneoplastic foci (Ito *et al.* 2003; Satoh *et al.* 1989). The occurrence of initiated cells, termed "mutation" in this study, was assumed to be a stochastic process following a Poisson distribution. The expected number of initiated cells in a small time step was defined by a function of mutation probability and division rate constant:

$$N_m = N\alpha\mu\Delta t \qquad \text{(Eq-4)}$$

where N_m is the expected number of initiated cells during a time step Δt, N is normal hepatocyte number/cm^3, and μ is mutation probability per division. As proposed by Conolly and Kimbell (1994), a random deviate about N_m denoting the number of initiated cells during Δt was drawn from a Poisson distribution using the function POIDEV[1] (Press *et al.* 1989). The inputs to POIDEV were the expected number and a pseudorandom number between 0 and 1 generated by the algorithm UNIFL[2] (Bratley *et al.* 1987). Since experiments (Imai *et al.* 1997; Yusuf *et al.* 1999) and modeling exercises (Conolly and Andersen 1997; Haag-Gronlund *et al.* 2000; Ou *et al.* 2001; Thomas *et al.* 2000b) suggested heterogeneity of the pool of initiated cells, we assumed that there were two subpopulations (*i.e.*, A and B cells) in the pool. The proportion of B cells was small upon

---

[1] A function designed to generate random deviates drawn from Poisson distributions in computer-aided scientific calculations.

[2] A function designed to generate pseudorandom numbers in computer-aided scientific calculations.

occurrence and gradually increased because of the growth advantage of B cells over A cells. We denoted the mutation probability leading to each subpopulation μ_a and μ_b.

(c) *Growth kinetics of initiated cells.* Once produced, an initiated cell could undergo one of the three random events, *i.e.*, division, death, or no change within a given time step. Growth of initiated cells gave rise to GST-P foci. Death of initiated cells included apoptosis, necrosis, and loss of GST-P phenotype. When a focus was larger than 1000 cells, its growth was assumed to be deterministic. Otherwise (*i.e.*, a focus $\leq$ 1000 cells), the growth kinetics of each cell in the clone were treated stochastically according to Conolly and Kimbell (1994). The probabilities of division and death were calculated from the rate constants of division (α_a, α_b, 1/day) and death (β_a, β_b, 1/day), respectively (Conolly and Kimbell 1994). The simulation program tracked the behavior of each initiated cell and calculated focal size (cells/focus) and number (foci/cm^3) over time. Divided by hepatocyte numerical density, the total foci size was converted to relative foci volume. The model outputs were 3-dimensional and compared to the 3D data converted from the experimental 2D results by the stereologic methods discussed above.

2.2.2. Modeling Strategies

(a) Time intervals of piecewise constants. The animals in this study were sequentially subjected to three kinds of treatments: DEN (day 0), HCB+PCB 126 mixture dosing (day 14-56), and partial hepatectomy (day 21). These treatments were expected to alter various parameters. Hence, it was necessary to divide the whole simulation duration (56 days) into intervals related to the effects of the treatments. With a modification of the strategy by Ou *et al.* (2001), we divided the duration into 6 intervals: days 0-7, 7-14, 14-21.5 [using 21.5 instead of 21 to reflect the lag of 0.5 days between the partial hepatectomy

and the onset of regenerative proliferation (Fukuhara *et al.* 2003)], 21.5-24.5, 24.5-28.5, and 28.5-56. The reasons for designating the first three intervals were discussed in Ou *et al.* (2001). The split of the duration of days 21.5-28.5 into two intervals was expected to better characterize foci development after the partial hepatectomy. The parameters related to the growth of initiated cells were fixed within each interval and varied among different intervals.

(b) Detection limit of foci. In the 2D analysis, all foci having 2 or more cells were counted. During the 2D to 3D conversion, the influence of hepatocyte density was incorporated as the mixture treatment enlarged hepatocytes. Our calculation using the information of hepatocyte density and diameters of 2-cell foci in a 2D setting suggested that the 3D detection limit was approximately 8 cells throughout the experimental duration. Therefore, any focus smaller than 8 cells in the 3D setting was treated undetectable; otherwise it was detectable and contributed to the final simulation outputs.

(c) Size-dependent growth kinetics. Experimental results (Buchmann *et al.* 1994; Grasl-Kraupp *et al.* 2000) and modeling exercises (Luebeck *et al.* 1995; Moolgavkar *et al.* 1996) have suggested that the growth of foci is likely to be size-dependent. In the present study, our preliminary modeling analyses showed that the distribution of sizes of foci could not be described well without considering the impact of size on cell kinetics. Based on these findings, we hypothesized that the growth kinetics of GST-P foci promoted by HCB+PCB 126 mixture were dependent on focal size. Thus we divided the foci in both A and B subpopulations into several categories in terms of size and each category had specific growth kinetic characteristics. In general, the larger the foci, the higher the rate constants of division and death. This result was an improvement over the earlier

publications (Conolly and Andersen 1997; Haag-Gronlund *et al.* 2000; Ou *et al.* 2001; Thomas *et al.* 2000b) where the growth kinetics of initiated cells were assumed independent of focal size.

2.2.3. Parameterization

(a) Division and death rate constants of normal hepatocytes. The division rate constant of normal hepatocytes was obtained from experiments. Prior to the regenerative proliferation due to partial hepatectomy (day 21.5), the time-course division rate constant was calculated using Eq-1 with the BrdU labeling index data from Kato *et al.* (1993a) as well as the results from our bioassay (day 20 data). The results were formulated into empirical functions to describe the division rate constant over time until day 21.5. On day 21.5, the division rate constant was set at 0.40/day to account for the proliferation surge due to partial hepatectomy (Ou *et al.* 2003; Ou *et al.* 2001). Thereafter, the constant during the segments of days 21.5-24, 24-28, 28-47, and 47-56 was derived from our BrdU labeling index experimental data that were obtained on days 24, 28, 47, and 56.

The death rate constant, not experimentally achievable, was related to the total hepatocyte number and division rate constant as shown in Eq-3. The total hepatocyte number was inferred by liver weight and hepatocyte density. Prior to day 6, the death rate constant was described by a function fitting to the time course liver weight after an i.p. injection of 150 mg/kg DEN reported by Kato *et al.* (1993a). Thereafter, the death rate constant was equal to a background value, which was set the same as the lowest division rate constant, 8.6×10^{-4}/day, determined in the control group in our bioassay. The rationale for this choice was that the death rate constant was presumably stable six days after DEN treatment and that the rate constants of death and division were similar when the liver

weight was not changing significantly with time. For the high dose group following day 28, the death rate constant was set 2-fold higher than the background, accounting for the cytotoxicity of the mixture treatment.

(b) Mutation probability. In this study, the mutation probability was comprised of two portions: the background level and, more importantly, the increased level due to DEN treatment. The background mutation probability was set at 1.7×10^{-6}/division for both A and B cells (Ou *et al.* 2001). The strategy of determining the increase over the background was different from the earlier approach, in which the increase was calibrated with experimental foci number (Conolly and Andersen 1997; Conolly and Kimbell 1994; Ou *et al.* 2001). Since not all initiated cells give rise to detectable foci (Grasl-Kraupp *et al.* 2000; Kato *et al.* 1993b), the earlier approach might give an underestimated mutation probability. To alleviate this drawback, we set the increased fold at a level that produced approximately 10^4 initiated cells per cm^3 of liver (Haag-Gronlund *et al.* 2000; Luebeck *et al.* 2000; Satoh *et al.* 1989). Since only a small percentage (5-23%) of the foci generated by DEN was resistant to selective mitoinhibitory pressures (Yusuf *et al.* 1999), in our modeling, the ratio of the mutation probabilities generating A and B cells was assumed to be 10:1 (μ_a:μ_b[3] = 10:1) (Table 4.3). After partial hepatectomy, a 5-fold increase in both μ_a and μ_b from the background levels was employed for insufficient monitoring and repairing of genetic or epigenetic alterations.

---

[3] Note that μ_a and μ_b refer to the probabilities of mutations occurring in normal hepatoctyes that generate A and B cells, and they should not be mistaken for the probabilities of further mutations in A and B cells.

(c) Categorization and division and death rate constants of foci. To relate cellular kinetics to focal size, the A and B foci were both categorized according to their sizes. Note that here the categories were different from the size classes introduced earlier. The categorization dividers were selected on the basis of two criteria: (i) to account for the present understanding in the growth kinetics of initiated cells (Grasl-Kraupp *et al.* 2000), and (ii) to replicate the size distribution patterns through computer simulations. Each category had distinct growth kinetics. To reduce the number of unknown parameters, we assigned A and B cells with the same division rate constant in each category within each time interval. The death rate constant of A cells was generally assumed to be higher than that of B cells, reflecting the higher sensitivity of A cells to the selective mitoinhibitory pressure (Conolly and Andersen 1997; Yusuf *et al.* 1999). We adjusted the category dividers and the cellular division and death rate constants to simulate three pieces of data simultaneously: relative foci volume, foci number/cm^3, and size distribution.

More technical details of the model implementation were introduced earlier (Conolly and Andersen 1997; Conolly and Kimbell 1994; Ou *et al.* 2003; Ou *et al.* 2001; Thomas *et al.* 2000b). The model presented here is parameter-rich; however, all parameters were from the literature, our bioassay, or calibrated to our foci data as discussed above. Because of the stochasticity of the growth of initiated cells, the model was run for 20 times; the averages of the 20 runs were compared to our data for calibration.

2.2.4. Software

The clonal growth model was coded and the simulations were performed using ACSL Tox 11.8.4 (AEgis Technologies Group, Huntsville, AL). The computer code of this model is presented in Appendix III.

3. RESULTS

3.1. Experimental Data Collection

3.1.1. Effect of the mixture treatment on the body and liver weight and liver section area

Part of these results has been reported in Chapter 3 and is not repeated here. Significant increase in the liver weight of the two mixture groups over the control group was observed on days 28, 47, and 56, but there was no difference between the two mixture groups (Fig. 4.2). In agreement with the increase in the liver weight, the area of the liver section was also increased on days 28, 47, and 56 with no difference between the two mixture groups (Table 4.1).

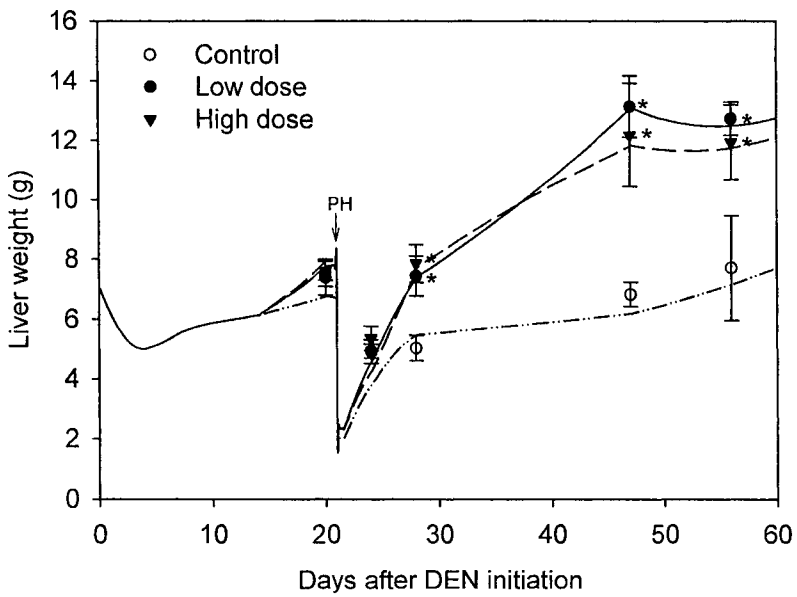

Fig. 4.2. Time-course liver weight recorded in the experiment and simulated by the clonal growth model. The symbols are experimental data and the curves are model simulations. The arrow indicates when the partial hepatectomy (PH) was performed.
*: significantly different ($p<0.05$) from the concurrent control group.

3.1.2. Hepatocyte division rate constant

The hepatocyte division rate constant (Table 4.1) was calculated from the experimentally derived labeling index. On day 24, the constant was around 0.12/day for all groups; this division rate was about 50-fold higher than that on day 20. This remarkable elevation was due to the regenerative cell proliferation following the partial hepatectomy on day 21. After day 24, a great reduction was observed. On day 28, the division rate constant in the high dose group was 0.028/day, two- and four-fold higher than that in the low and control group, respectively. The constants in all groups were further reduced on day 47, but somewhat increased again at the last time point, day 56. At the late three time points, days 28, 47, and 56, the constant was remarkably increased in the high dose group.

Table 4.1. Time-course Liver Section Area, Hepatocyte Division Rate Constant, and Hepatocyte Numerical Density in HCB+PCB 126 Medium-term Bioassay

Treatment	Day 20	Day 24	Day 28	Day 47	Day 56
	Liver section area$^{\#}$ (cm^2)				
Control	2.89±0.48	3.69±0.11	3.65±0.38	4.43±0.25	4.22±0.62
Low dose	2.39±0.40	3.92±0.51	4.61±0.54*	7.12±0.82*	6.92±0.32*
High dose	2.58±0.49	4.00±0.35	4.81±0.57*	6.28±0.85*	6.07±0.63*
	Hepatocyte division rate constant (α, $\times 10^{-3}$/day)				
Control	2.3±0.8	113.4±23.4	7.3±5.1	0.9±0.5	1.1±0.4
Low dose	2.4±1.3	130.0±59.7	14.9±9.0	0.8±0.8	3.7±3.5
High dose	2.5±1.7	126.4±43.2	27.7±10.0!	3.5±2.9!	14.2±6.9!
	Hepatocyte density ($\times 10^8/cm^3$)				
Control	1.10±0.17	1.20±0.08	1.10±0.11	1.20±0.01	1.00±0.01
Low dose	0.99±0.16	0.99±0.06	0.83±0.01*	0.57±0.02*	0.64±0.02*
High dose	0.97±0.18	1.10±0.12	0.81±0.08*	0.60±0.16*	0.64±0.06*

Note: The results were expressed as mean ± SD. *: Significantly different from the concurrent control group, $p<0.05$; !: Significantly different from the concurrent other groups, $p<0.05$; $^{\#}$: Each slice of liver was taken consistently along the longest axis of each lobe. Thus, the increase in the liver section area indicated the enlargement of liver.

3.1.3. Hepatocyte numerical density

The hepatocyte numerical density of a naive adult F344 rat determined using our method was $1.2\times10^8/cm^3$, which was close to the values reported in the literature (Moolgavkar *et al.* 1990; Weibel *et al.* 1969). The mixture treatment caused hepatocyte enlargement with concomitant numerical density reduction as shown in Table 4.1. The reduction on days 28, 47, and 56 of both mixture groups was significant relative to the control group, yet the difference between the mixture groups was not significant. The change in hepatocyte numerical density was incorporated in our model.

3.1.4. 2D GST-P foci data

The foci formation was measured by total foci area and foci number identified from the GST-P stained liver slides. We analyzed these measurements with and without the standardization by the liver area, in order to examine the impact of liver enlargement (25-65% larger than the control) on the results.

Without the standardization, the total foci areas in all groups, shown in Fig. 4.3A, increased with time. At the first time point, there was no difference among all groups. On day 24, the foci area in the high dose group was significantly increased compared to the other two groups. Thereafter, the foci areas of the two mixture groups, not different from one another, were significantly higher (2-3 fold) than that of the control. As shown in Fig. 4.3B, the foci number in the control group remained around 50-60/liver at all time points. In the first week after the partial hepatectomy, there was a sharp increase (roughly 3-fold) in the foci number in both mixture groups. Thereafter, it was relatively stable until day 56.

When the foci area and foci number were standardized by the liver area, the difference between the control and the mixture groups remained statistically significant

($p<0.05$) with one exception; on day 56, the relative foci area in the low dose group was not significantly different from the control. The magnitude of the difference among the groups was somewhat diminished.

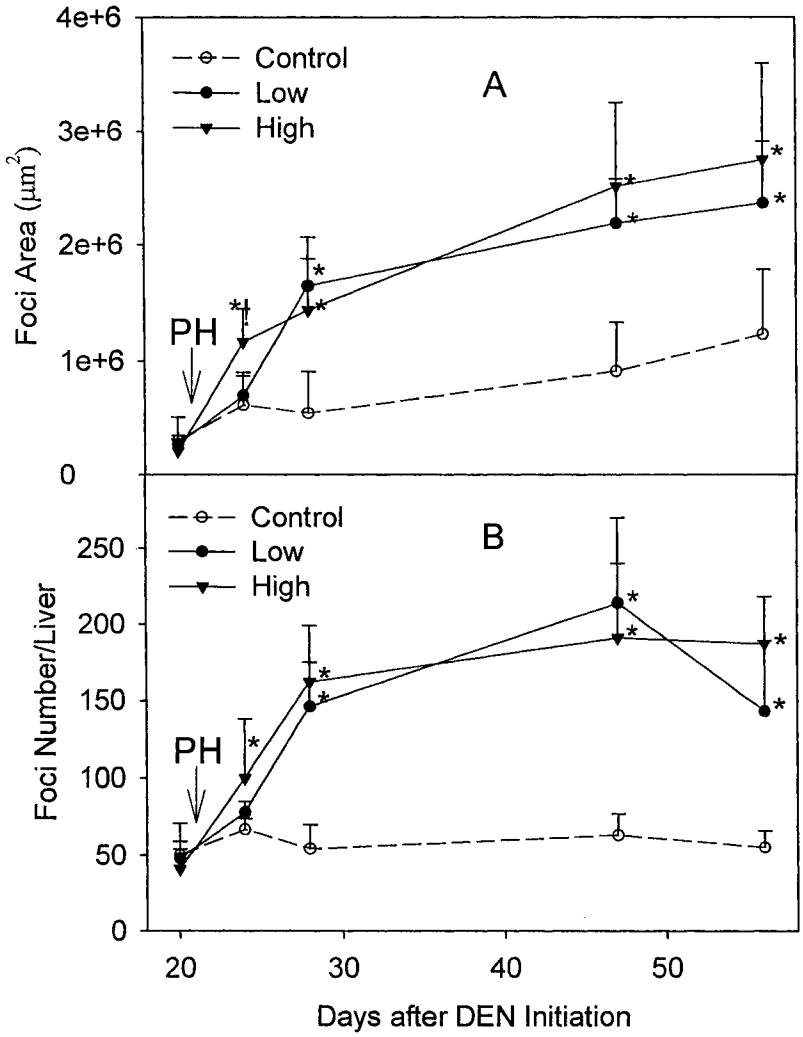

Fig. 4.3. Time-course foci area (A) and foci number (B) measured from the liver slides of the rats treated with corn oil or HCB+PCB 126 mixture. The arrows indicate when the partial hepatectomy (PH) was performed.
*: significantly different ($p<0.05$) from the concurrent control group;
!: significantly different ($p<0.05$) from the concurrent low dose group.

3.1.5. 3D GST-P foci data

The slide-derived 2D measurements were converted to 3D expressions for calibrating the clonal growth model. The conversions provided the data of relative foci volume (Fig. 4.4A, C, E), foci number/cm^3 liver (Fig. 4.4B, D, F), and size distribution (Table 4.2). The foci in the mixture groups were shifted to larger classes (*i.e.*, larger foci) compared to those in the control group, suggesting the promotion effect of the mixture treatment. Between the two mixture groups the distribution patterns were similar.

It is interesting to note that the development of GST-P foci, in terms of area, number, and size distribution, was similar between the two mixture groups even though there was a three-fold difference between the dose levels (HCB 8.55 mg/kg + PCB 126 3.3 μg/kg vs HCB 28.5 mg/kg + PCB 126 9.8 μg/kg).

3.2. Clonal Growth Model Simulations

3.2.1. Calibration of hepatocyte death rate constant

The hepatocyte death rate constant was calibrated using the time-course liver weight. As shown in Fig. 4.2, the liver weight was simulated well with the experimentally derived division rate constant and the calibrated death rate constant. At the beginning of the simulation, the death rate constant was at a background level (8.6×10^{-4}/day). After 0.1 days, the lag between DEN exposure and the onset of cytotoxicity, the death rate constant peaked to 0.15/day, and linearly declined until day 6.1 to the background. Thereafter the death rate constant was held at the background level, with the exception that it was doubled after day 28 in the high dose group to account for the cytotoxicity of the mixture treatment.

3.2.2. Simulation of the foci data

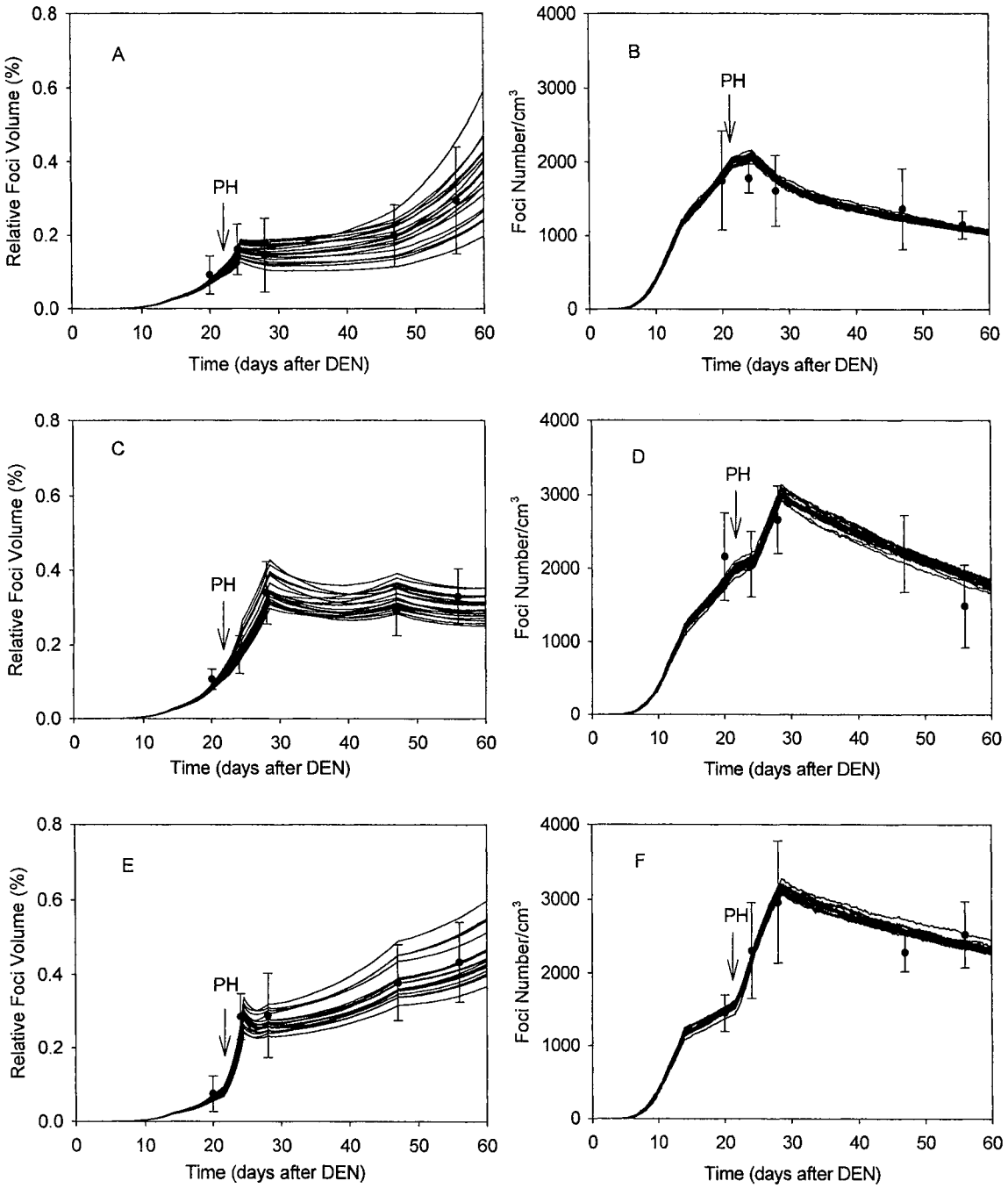

Fig. 4.4. Experimental and simulated time-course foci relative volume and foci number/cm^3 in the control (A, B), low dose (C, D), and high dose (E, F) groups. The symbols are data converted from the experimental 2D results and the curves are model simulations of 20 runs. The arrows indicate when the partial hepatectomy (PH) was performed.

Table 4.2. Experimental and Simulated* 3-Dimensional Foci Size Distribution (Number of Foci/Class)

Treat-ment	Size class	Time points									
		Day 20		Day 24		Day 28		Day 47		Day 56	
		Data	*Model*	Data	*Model*	Data	*Model*	Data	*Model*	Data	*Model*
Control	1	764	*602*	626	*569*	483	*455*	361	*203*	208	*148*
	2	458	*442*	412	*448*	548	*419*	339	*362*	276	*315*
	3	310	*391*	234	*415*	316	*407*	267	*334*	291	*314*
	4	167	*247*	253	*352*	155	*296*	133	*208*	136	*200*
	5	24	*103*	149	*194*	46	*146*	113	*72*	126	*73*
	6	67	*24*	51	*61*	38	*18*	57	*20*	35	*28*
	7	26	*3*	30	*11*	17	*13*	26	*15*	31	*18*
	8	0	*1*	23	*8*	17	*10*	24	*9*	20	*16*
	9	0	*0*	0	*4*	3	*6*	18	*9*	14	*7*
	10	0	*0*	1	*1*	3	*3*	3	*4*	7	*6*
	11	0	*0*	0	*0*	1	*1*	0	*2*	7	*4*
	12	0	*0*	0	*0*	0	*0*	0	*1*	0	*2*
	13	0	*0*	0	*0*	0	*0*	0	*0*	0	*0*
Low	1	893	*692*	739	*689*	-#	-	-	-	-	-
	2	474	*430*	477	*393*	903	*828*	803	*607*	523	*519*
	3	397	*382*	369	*438*	748	*444*	548	*523*	355	*432*
	4	197	*289*	221	*382*	450	*423*	410	*461*	244	*348*
	5	72	*122*	104	*242*	306	*357*	229	*311*	150	*243*
	6	50	*38*	64	*96*	128	*215*	146	*158*	114	*96*
	7	23	*5*	32	*12*	71	*82*	47	*90*	63	*115*
	8	0	*2*	20	*10*	43	*11*	28	*44*	36	*42*
	9	0	*1*	2	*5*	4	*9*	7	*3*	6	*2*
	10	0	*0*	2	*3*	1	*5*	2	*3*	7	*3*
	11	0	*0*	0	*1*	1	*2*	0	*1*	1	*1*
	12	0	*0*	0	*0*	0	*1*	0	*1*	1	*1*
	13	0	*0*	0	*0*	0	*0*	0	*0*	0	*0*
High	1	635	*626*	670	*668*	-	-	-	-	-	-
	2	396	*282*	552	*356*	1207	*1137*	866	*928*	759	*759*
	3	232	*341*	421	*304*	739	*324*	580	*490*	776	*429*
	4	130	*242*	378	*294*	540	*294*	323	*402*	458	*338*
	5	74	*93*	133	*325*	230	*328*	257	*425*	240	*344*
	6	11	*26*	84	*181*	148	*258*	100	*225*	176	*253*
	7	11	*2*	45	*67*	33	*32*	96	*46*	86	*70*
	8	0	*1*	38	*15*	20	*18*	24	*32*	30	*45*
	9	3	*0*	18	*3*	0	*7*	14	*18*	21	*19*
	10	0	*0*	2	*1*	0	*2*	3	*7*	2	*9*
	11	0	*0*	0	*1*	0	*0*	1	*1*	0	*2*
	12	0	*0*	0	*0*	1	*0*	1	*0*	2	*0*
	13	0	*0*	0	*0*	0	*0*	0	*0*	0	*0*

*: The simulations (*Model*) were averages of 20 runs of the clonal growth model.
#: In the low and high dose groups on days 28, 47, and 56, due to cell hypertrophy, the class 1 was equivalent to the class 2 at the other time points in terms of focal volume and hence was placed in the line of class 2, and likewise for the larger classes.

Table 4.3. Division and Death Rate Constants of Initiated Cells and Normal Cell Mutation Probabilities in the Clonal Growth Model

Parameter	Foci category	Treatment	Simulation interval (days)					
			0-7	7-14	14-21.5	21.5-24.5	24.5-28.5	28.5-56
α_a, α_b (1/day)	Single cell	Control	0.03	0.012	0.02	0.004	0.001	0.001
		Low	0.03	0.012	0.02	0.004	0.001	0.001
		High	0.03	0.012	0.02	0.004	0.001	0.001
	Minifoci	Control	0.3	0.22	0.11	0.09	0.08	0.1
		Low	0.3	0.22	0.11	0.099	0.192	0.175
		High	0.3	0.22	0.055	0.27	0.24	0.17
	Medium-foci	Control	0.41	0.35	0.2	0.17	0.17	0.1
		Low	0.41	0.35	0.2	0.17	0.315	0.138
		High	0.41	0.35	0.2	0.476	0.187	0.12
	Large-foci	Control	0.42	0.42	0.42	0.4	0.25	0.1
		Low	0.42	0.42	0.42	0.4	0.25	0.095
		High	0.42	0.42	0.42	0.472	0.25	0.07
β_a (1/day)	Single cell	Control	0.0008	0.0008	0.0008	0.002	0.0005	0.0001
		Low	0.0008	0.0008	0.0008	0.002	0.0005	0.0001
		High	0.0008	0.0008	0.0008	0.002	0.0005	0.0001
	Minifoci	Control	0.0008	0.0008	0.0015	0.07	0.18	0.18
		Low	0.0008	0.0008	0.0015	0.07	0.045	0.216
		High	0.0008	0.0008	0.0033	0.07	0.126	0.18
	Medium-foci	Control	0.0008	0.05	0.04	0.06	0.28	0.12
		Low	0.0008	0.05	0.04	0.06	0.224	0.184
		High	0.0008	0.05	0.072	0.06	0.28	0.144
	Large-foci	Control	0.0008	0.01	0.01	0.01	0.2	0.09
		Low	0.0008	0.01	0.01	0.01	0.22	0.198
		High	0.0008	0.01	0.01	0.01	0.64	0.27
β_b (1/day)	Single cell	Control	0.00008	0.00008	0.00008	0.001	0.0005	0.0001
		Low	0.00008	0.00008	0.00008	0.001	0.0005	0.0001
		High	0.00008	0.00008	0.00008	0.001	0.0005	0.0001
	Minifoci	Control	0.00008	0.00008	0.00008	0.02	0.13	0.15
		Low	0.00008	0.00008	0.00008	0.02	0.013	0.09
		High	0.00008	0.00008	0.00008	0.02	0.026	0.075
	Medium-foci	Control	0.00008	0.0008	0.0008	0.02	0.23	0.06
		Low	0.00008	0.0008	0.0008	0.02	0.138	0.057
		High	0.00008	0.0008	0.0008	0.02	0.23	0.024
	Large-foci	Control	0.00008	0.0008	0.0008	0.01	0.16	0.04
		Low	0.00008	0.0008	0.0008	0.01	0.16	0.082
		High	0.00008	0.0008	0.0008	0.01	0.16	0.046
μ_a ($\times 1.7\times10^{-6}$)			350	20	1	5	2	1
μ_b ($\times 1.7\times10^{-6}$)			35	2	1	5	2	1

As a tradeoff between model parsimony and adequate simulation of data (especially size distribution), the foci were placed into 4 categories: single cell, minifoci (2-11 cells), medium-foci (12-399 cells), and large-foci (>399 cells). Note that the categories were introduced for characterizing the growth kinetics of initiated cells, and should be distinguished from the size classes (see Table 4.2 for size classes). A direct comparison of the categories and size classes is as follows: The single cells were too small to be in any size class, the minifoci category covered the lower portion of class 1, the medium-foci category covered the upper portion of class 1 through the lower portion of class 6, and the large-foci category covered the other classes.

Our model simulations of the relative foci volume and foci number/cm^3 were consistent with the experimental data (Fig. 4.4). Furthermore, the size distribution patterns of all groups were also well simulated as shown in Table 4.2. In the control group, the foci numbers in the smaller classes gradually decreased, and the distribution of all foci shifted towards the larger classes in the later time points. In the mixture groups, the foci also became larger with time; moreover, the numbers in the smaller classes were remarkably increased from day 28 compared to the concurrent control.

3.2.3. Parameters related to initiated cells and foci development

The mutation probabilities (μ_a, μ_b) and rate constants for division (α_a, α_b) and death (β_a, β_b) of initiated cells calibrated with the data are listed in Table 4.3. While the division rate constants (α_a's, α_b's) of mini-, medium-, and large-foci were determined by simulating the experimental data, those for single cells were assigned with theoretical values because of the lack of reliable data on single cells. Thus, the division rate constants for single cells were assumed to be independent of the mixture treatment and

the values assigned were lower than those for normal cells. The latter is supported by the earlier finding (Grasl-Kraupp *et al.* 2000) that the labeling index of the GST-P single cells was lower than that of normal hepatocytes after injection of [^{3}H]-thymidine in the rat. In general, the α_a and α_b in our study, being set equal, had trends of gradual decrease over time and increase with focal size. After the partial hepatectomy, the mixture treatment, especially the high dose, remarkably stimulated the division of cells in minifoci (α's increased), which contributed to the significant increase in the foci number in the smaller classes. The higher division rate constants of medium-foci in the mixture groups led to the increase in the relative foci volume and size distribution shift. The division of large foci, however, was less affected by the mixture treatment. The β_a was higher than β_b, and the mixture treatment further elevated β_a and reduced β_b. The (α_b-β_b) was generally higher than (α_a-β_a), especially after day 24.5, reflecting the enhancement of the growth advantage of B cells from the mixture treatment.

The effects of the mixture dose on α's, β's, and (α-β)'s were not always consistent and they were dependent on focal size and time. In the first week following partial hepatectomy (days 21.5-28.5), the division rate constants and the net growth rate (α_b-β_b) of minifoci and medium-foci were notably different between the low and high dose groups (Table 4.3).

4. DISCUSSION

4.1. HCB+PCB 126 promotion of GST-P foci

In our time-course medium-term bioassay, the HCB+PCB 126 mixture treatment significantly elevated the foci number/liver and foci area starting from day 28 compared

to the concurrent control. The foci number was tripled and the foci area was doubled. Both HCB (Cabral *et al.* 1996; Ou *et al.* 2001) and PCB 126 (Bager *et al.* 1995; Dean *et al.* 2002) alone were reported to promote the growth of altered hepatic foci in rats, hence it is not surprising to observe the promotional effect of the mixture of these two chemicals.

There was a three-fold difference between the low (HCB 8.55 mg/kg + PCB 126 3.3 μg/kg) and high (HCB 28.5 mg/kg + PCB 126 9.8 μg/kg) dose levels. Interestingly, the development of GST-P foci, in terms of area, number, and size distribution, was not significantly different between the two mixture groups. In our previous study with the same protocol, PCB 126 at the level of 9.8 μg/kg significantly promoted the development of GST-P foci, but at the level of 3.3 μg/kg the effect was not significant (Lohitnavy *et al.*, unpublished data; see Chapter 5 for the data). HCB only significantly increased the foci number on day 56 at 28.5 mg/kg; at 8.55 mg/kg the effect was insignificant (Lu *et al.* unpublished data; see Chapter 5 for the data). These results imply the possibility of a greater-than-additivity interaction between HCB and PCB 126 at the low dose in this study. Further studies are needed (1) to explore the mechanism(s) of the interaction between these two chemicals, and (2) to examine the promotion potency of the mixture at even lower doses.

Although the low and high dose treatments yielded similar observations, the kinetic parameters of the initiated cells and foci, according to our modeling analyses, were dose dependent, especially in the intervals following the partial hepatectomy. This result suggests that the development of GST-P foci may be dose-dependent, even though the

dependency was not observable at the level of foci areas or numbers. It also illustrates one of the powerful utilities of the clonal growth modeling—hypothesis generating.

4.2. Support for the hypothesis of "negative selection mechanism"

Jirtle *et al.* (1991) first proposed a negative selection mechanism for hepatic tumor promotion by phenobarbital. Later Andersen *et al.* (1995) suggested that this mechanism may be applicable to a diverse group of mitogenic tumor promoters. According to the hypothesis, exposure to tumor promoters leads to mitogenesis of normal and initiated hepatocytes, which activates homeostatic mitoinhibition via tumor growth factor (TGF) β1. Escape from TGFβ1 mitoinhibitory effect due to genetic or epigenetic alterations renders the initiated cells growth advantages over normal hepatocytes. Consequently, the initiated cells outgrow normal cells and expand. In the two-cell setting as presented in this study, the negative selection hypothesis can be extended to the point that the resistant foci (consisting of type B cells) outgrow the non-resistant foci (consisting of type A cells) and normal cells. Under our specific experimental conditions, the B foci had higher net growth rate than the A foci and normal hepatocytes.

4.3. Support for the two-cell hypothesis

In the earlier clonal growth models (Conolly and Kimbell 1994; Moolgavkar *et al.* 1990; Portier *et al.* 1996), the foci were assumed to rise from a single type of initiated cells which were induced by DEN. Later, Conolly and Andersen (1997) incorporated a two-cell concept into their model on the foci formation following DEN, partial hepatectomy, and TCDD treatment. This concept has been substantiated in our computer modeling of the clonal expansion of the liver GST-P foci (Ou *et al.* 2003; Ou *et al.* 2001; Thomas *et al.* 2000b). According to this concept, there are two types of initiated cells

(named A and B) induced by DEN with different division and/or death rates. A cells predominate the initiated cell pool at the early stage and are gradually replaced by B cells due to the sensitivity of A cells to homeostatic control such as apoptosis. In our study, the divergent trends in the foci number/cm^3 (decreased after day 28) and relative foci volume (increased after day 28) were also observed and well described in the two-cell framework.

So far the genetic and phenotypic difference between A and B cells remains unclear. Three kinds of DNA adducts with different persistence (O^6-alkylguanine adduct with a short half life, O^2- and O^4-ethylthimidine adduct with longer half lives) are known to be formed after DEN administration (Dragan *et al.* 1994; Swenberg *et al.* 1984). However, it is uncertain, at this point, to equate the cells with O^6-alkylguanine adduct to A cells and those with the other adducts to B cells. The possibility that GST-P expression might not be a result of genetic damage (Higashi *et al.* 2004; Satoh and Hatayama 2002) further complicates this issue.

4.4. Size-dependent growth kinetics of GST-P foci

The most notable finding in this current study was that the growth kinetics of GST-P foci depended on focal size. To describe the data of foci size distribution successfully, the influence of focal size on the division and death rate constants had to be taken into account. We grouped the foci into 4 categories according to the focal sizes. In our model, the net growth rates of both A and B types of foci were generally increased with focal size.

The phenomenon of differential growth of foci has been experimentally observed by other investigators as well. Grasl-Kraupp *et al.* (2000) reported that GST-P single cells induced by N-nitrosomorpholine had lower replication than the cells in multicellular foci.

Buchmann *et al.* (1994) found that BrdU incorporation in focal nuclei, in both control and TCDD-treated rats, was dependent on focal size. In addition, the growth rate within a focus is also heterogeneous: the highest growth presents at the surface of foci (Buchmann *et al.* 1994).

The expansion of foci is a result of continuous competition between the growth capability of initiated cells and the homeostatic control mechanisms. One of such mechanisms is gap junctional intercellular communication (GJIC) (Omori *et al.* 2001), which exists among initiated and surrounding normal cells (heterologous GJIC) and among initiated cells (homologous GJIC) (Krutovskikh 2002). GJIC organizes cells in a society and places each cell under the monitoring of all the neighboring cells. When an initiated hepatocyte appears, it is effectively monitored by its neighbors and its proliferation is checked by receiving growth-controlling signals through gap junctions (Krutovskikh 2002). This is one of the reasons why the division rate constant of single cells in our model was set very low compared to that of other categories. GJIC is likely to be inhibited by chemicals, e.g., HCB (Plante *et al.* 2002), PCB 126 (Bager *et al.* 1997), and thus the single cells are somewhat released from proliferation check. This effect was not embodied in our study due to lack of necessary data.

As single cells become foci with multiple cells, the proliferation check via heterologous GJIC from normal cells is lessened because on average each initiated cell is surrounded by fewer normal cells. Chemical treatments such as HCB (Plante *et al.* 2002) and PCB 126 (Bager *et al.* 1997) may further reduce the proliferation check. Meanwhile, the initiated cells may share factors via the homologous GJIC counterbalancing growth-controlling signals. These two aspects, in combination, stimulate replication of initiated

cells in foci. With the increase in focal size, the growth control is further abolished and focal expansion becomes more autonomous, reflected by the higher net growth rates in larger foci observed in our study. Krutovskikh (2002) proposed a dynamic process of focal expansion and GJIC inhibition. Given GJIC is a basic homeostatic mechanism, it is likely that the focal size-dependent promotion by HCB+PCB 126 mixture is also applicable to other tumor promoters.

4.5. Model configuration and parameterization

Our clonal growth model had a structure with two compartments, normal hepatocytes and initiated cells. The change of each compartment and the transition from normal hepatocytes to initiated cells were described by dynamic functions. The functions, along with the pertinent parameters, were assigned on the basis of estimation and experimental data. Since our current knowledge was too limited to determine how accurately the functions and parameters captured the reality, the model should be recognized as a semi-quantitative rather than a fully quantitative model. As such, in this study, we focused on the question of "what can we learn from the model?" rather than "what predictions can we make using the model?"

The parameterization in a carcinogenesis model using tumor incidence data has suffered from several statistical difficulties (Portier and el Masri 1997; Portier 1987; Portier 1995; Wosniok *et al.* 1999), including parameter nonidentifiability and nonestimability and model nondifferentiability. In a clonal growth model, however, some of the difficulties may be alleviated to certain degree because of the much more information contained in a foci dataset. The foci size constrains the value of the difference between the division and death rate constant, and the foci number constrains

the values of the individual constants (Dewanji *et al.* 1989). During our parameterization, all division and death rate constants were constrained by the foci size, number, and size distribution simultaneously, and thus we believe that our parameter set is likely to be unique. Indeed, we could not find another set fitting the three pieces of data equally well at the same time.

In summary, in the current study, HCB+PCB 126 mixture significantly promoted GST-P foci formation in the context of a medium-term liver foci bioassay. We constructed a clonal growth model incorporating negative selection and two-cell hypotheses to describe the experimental foci data and explore the growth kinetics of foci with the presence of the mixture. The data were simulated satisfactorily with the consideration of the size-dependent foci growth kinetics. In addition to lending support to the negative selection and two-cell hypotheses, this study explicitly and quantitatively revealed that the growth kinetics of foci was size-dependent, and that HCB+PCB 126 mixture particularly stimulated the growth of minifoci and medium-foci. It exemplified how a mechanism based computer modeling can improve our understanding in the carcinogenic process with or without chemical treatment. This study marks our continuous effort on the development of a predictive tool for carcinogenic potential of chemical mixtures based on the integration of computer modeling and biological information related to preneoplastic liver foci formation.

ACKNOWLEDGEMENTS

This study is supported by the NIOSH/CDC grant 1 RO1 OH07556, NIEHS Training Grant 1 T32 ES 07321, and scholarships from U.S. Fulbright Foundation and Naresuan

University, Thailand. The authors thank Dr. Ying C. Ou for her help with the computer code and thank Ms. Tracy Nichols, Drs. Todd Painter and Charles Dean, and other colleagues in the Quantitative and Computational Toxicology Group for their excellent technical assistance. The support on statistical analysis of the experimental data from Mr. Xiaohui Xu is greatly appreciated.

REFERENCES

Andersen, M. E., Mills, J. J., Jirtle, R. L., and Greenlee, W. F. (1995). Negative selection in hepatic tumor promotion in relation to cancer risk assessment. *Toxicology* **102**, 223-37.

Bager, Y., Hemming, H., Flodstrom, S., Ahlborg, U. G., and Warngard, L. (1995). Interaction of 3,4,5,3',4'-pentachlorobiphenyl and 2,4,5,2',4',5'-hexachlorobiphenyl in promotion of altered hepatic foci in rats. *Pharmacol Toxicol* **77**, 149-54.

Bager, Y., Kato, Y., Kenne, K., and Warngard, L. (1997). The ability to alter the gap junction protein expression outside GST-P positive foci in liver of rats was associated to the tumour promotion potency of different polychlorinated biphenyls. *Chem Biol Interact* **103**, 199-212.

Blais, J. M., Froese, K. L., Kimpe, L. E., Muir, D. C., Backus, S., Comba, M., and Schindler, D. W. (2003). Assessment and characterization of polychlorinated biphenyls near a hazardous waste incinerator: analysis of vegetation, snow, and sediments. *Environ Toxicol Chem* **22**, 126-33.

Bratley, P., Fox, B. L., and Schrage, L. E. (1987). *A Guide to Simulation*. Springer-Verlag, New York.

Buchmann, A., Stinchcombe, S., Korner, W., Hagenmaier, H., and Bock, K. W. (1994). Effects of 2,3,7,8-tetrachloro- and 1,2,3,4,6,7,8-heptachlorodibenzo-p-dioxin on the proliferation of preneoplastic liver cells in the rat. *Carcinogenesis* **15**, 1143-50.

Cabral, R., Hoshiya, T., Hakoi, K., Hasegawa, R., and Ito, N. (1996). Medium-term bioassay for the hepatocarcinogenicity of hexachlorobenzene. *Cancer Lett* **100**, 223-226.

Conolly, R. B., and Andersen, M. E. (1997). Hepatic foci in rats after diethylnitrosamine initiation and 2,3,7,8-tetrachlorodibenzo-p-dioxin promotion: evaluation of a quantitative two-cell model and of CYP 1A1/1A2 as a dosimeter. *Toxicol Appl Pharmacol* **146**, 281-93.

Conolly, R. B., and Kimbell, J. S. (1994). Computer simulation of cell growth governed by stochastic processes: application to clonal growth cancer models. *Toxicol Appl Pharmacol* **124**, 284-95.

Dean, C. E., Jr., Benjamin, S. A., Chubb, L. S., Tessari, J. D., and Keefe, T. J. (2002). Nonadditive hepatic tumor promoting effects by a mixture of two structurally different polychlorinated biphenyls in female rat livers. *Toxicol Sci* **66**, 54-61.

Dewanji, A., Venzon, D. J., and Moolgavkar, S. H. (1989). A stochastic two-stage model for cancer risk assessment. II. The number and size of premalignant clones. *Risk Anal* **9**, 179-87.

Dragan, Y. P., Hully, J. R., Nakamura, J., Mass, M. J., Swenberg, J. A., and Pitot, H. C. (1994). Biochemical events during initiation of rat hepatocarcinogenesis. *Carcinogenesis* **15**, 1451-8.

Erturk, E., Lambrecht, R. W., Peters, H. A., Cripps, D. J., Gocmen, A., Morris, C. R., and Bryan, G. T. (1986). Oncogenicity of hexachlorobenzene. *IARC Sci Publ*, 417-423.

Fukuhara, Y., Hirasawa, A., Li, X. K., Kawasaki, M., Fujino, M., Funeshima, N., Katsuma, S., Shiojima, S., Yamada, M., Okuyama, T., Suzuki, S., and Tsujimoto, G. (2003). Gene expression profile in the regenerating rat liver after partial hepatectomy. *J Hepatol* **38**, 784-92.

Grasl-Kraupp, B., Luebeck, G., Wagner, A., Low-Baselli, A., de Gunst, M., Waldhor, T., Moolgavkar, S., and Schulte-Hermann, R. (2000). Quantitative analysis of tumor initiation in rat liver: role of cell replication and cell death (apoptosis). *Carcinogenesis* **21**, 1411-21.

Haag-Gronlund, M., Conolly, R., Scheu, G., Warngard, L., and Fransson-Steen, R. (2000). Analysis of rat liver foci growth with a quantitative two-cell model after treatment with 2,4,5,3',4'-pentachlorobiphenyl. *Toxicol Sci* **57**, 32-42.

Haag-Gronlund, M., Johansson, N., Fransson-Steen, R., Hakansson, H., Scheu, G., and Warngard, L. (1998). Interactive effects of three structurally different polychlorinated biphenyls in a rat liver tumor promotion bioassay. *Toxicol Appl Pharmacol* **152**, 153-65.

Higashi, K., Hiai, H., Higashi, T., and Muramatsu, M. (2004). Regulatory mechanism of glutathione S-transferase P-form during chemical hepatocarcinogenesis: old wine in a new bottle. *Cancer Lett* **209**, 155-63.

Imai, T., Masui, T., Ichinose, M., Nakanishi, H., Yanai, T., Masegi, T., Muramatsu, M., and Tatematsu, M. (1997). Reduction of glutathione S-transferase P-form mRNA expression in remodeling nodules in rat liver revealed by in situ hybridization. *Carcinogenesis* **18**, 545-51.

Ito, N., Imaida, K., Hirose, M., and Shirai, T. (1998). Medium-term bioassays for carcinogenicity of chemical mixtures. *Environ Health Perspect* **106 Suppl 6**, 1331-6.

Ito, N., Tamano, S., and Shirai, T. (2003). A medium-term rat liver bioassay for rapid in vivo detection of carcinogenic potential of chemicals. *Cancer Sci* **94**, 3-8.

Ito, N., Tatematsu, M., Hasegawa, R., and Tsuda, H. (1989). Medium-term bioassay system for detection of carcinogens and modifiers of hepatocarcinogenesis utilizing the GST-P positive liver cell focus as an endpoint marker. *Toxicol Pathol* **17**, 630-41.

Jirtle, R. L., Meyer, S. A., and Brockenbrough, J. S. (1991). Liver tumor promoter phenobarbital: a biphasic modulator of hepatocyte proliferation. *Prog Clin Biol Res* **369**, 209-16.

Kato, M., Popp, J. A., Conolly, R. B., and Cattley, R. C. (1993a). Relationship between hepatocyte necrosis, proliferation, and initiation induced by diethylnitrosamine in the male F344 rat. *Fundam Appl Toxicol* **20**, 155-62.

Kato, T., Imaida, K., Ogawa, K., Hesegawa, R., Shirai, T., and Tatematsu, M. (1993b). Three-dimensional analysis of glutathione S-transferase placental form-positive lesion development in early stages of rat hepatocarcinogenesis. *Jpn J Cancer Res* **84**, 1252-7.

Krutovskikh, V. (2002). Implication of direct host-tumor intercellular interactions in non-immune host resistance to neoplastic growth. *Semin Cancer Biol* **12**, 267-76.

Liljegren, G., Hardell, L., Lindstrom, G., Dahl, P., and Magnuson, A. (1998). Case-control study on breast cancer and adipose tissue concentrations of congener specific polychlorinated biphenyls, DDE and hexachlorobenzene. *Eur J Cancer Prev* **7**, 135-40.

Lu, Y., Lohitnavy, M., Reddy, M. B., Lohitnavy, O., Ashley, A., and Yang, R. S. H. (2006). An updated physiologically based pharmacokinetic model for hexachlorobenzene: Incorporation of pathophysiological states following partial hepatectomy and hexachlorobenzene treatment. *Toxicol Sci* **91**, 29-41.

Luebeck, E. G., Buchmann, A., Stinchcombe, S., Moolgavkar, S. H., and Schwarz, M. (2000). Effects of 2,3,7,8-tetrachlorodibenzo-p-dioxin on initiation and promotion of GST-P-positive foci in rat liver: A quantitative analysis of experimental data using a stochastic model. *Toxicol Appl Pharmacol* **167**, 63-73.

Luebeck, E. G., Grasl-Kraupp, B., Timmermann-Trosiener, I., Bursch, W., Schulte-Hermann, R., and Moolgavkar, S. H. (1995). Growth kinetics of enzyme-altered liver foci in rats treated with phenobarbital or alpha-hexachlorocyclohexane. *Toxicol Appl Pharmacol* **130**, 304-15.

Moolgavkar, S. H., Dewanji, A., and Venzon, D. J. (1988). A stochastic two-stage model for cancer risk assessment. I. The hazard function and the probability of tumor. *Risk Anal* **8**, 383-92.

Moolgavkar, S. H., and Knudson, A. G., Jr. (1981). Mutation and cancer: a model for human carcinogenesis. *J Natl Cancer Inst* **66**, 1037-52.

Moolgavkar, S. H., and Luebeck, E. G. (1992). Interpretation of labeling indices in the presence of cell death. *Carcinogenesis* **13**, 1007-10.

Moolgavkar, S. H., Luebeck, E. G., Buchmann, A., and Bock, K. W. (1996). Quantitative analysis of enzyme-altered liver foci in rats initiated with diethylnitrosamine and promoted with 2,3,7,8-tetrachlorodibenzo-p-dioxin or 1,2,3,4,6,7,8-heptachlorodibenzo-p-dioxin. *Toxicol Appl Pharmacol* **138**, 31-42.

Moolgavkar, S. H., Luebeck, E. G., de Gunst, M., Port, R. E., and Schwarz, M. (1990). Quantitative analysis of enzyme-altered foci in rat hepatocarcinogenesis experiments--I. Single agent regimen. *Carcinogenesis* **11**, 1271-8.

Moolgavkar, S. H., and Venzon, D. J. (1979). Two-event models for carcinogenesis: Incidence curves for childhood and adult tumors. *Math Biosci* **47**, 55-77.

NTP (2001). Ninth report on carcinogenesis:Hexachlorobenzene www.ehp.niehs.nih.gov/roc/toc9.html. National Toxicology Program.

NTP (2004a). National Toxicology Program: Current Directions and Evolving Strategies. http://ntp-server.niehs.nih.gov/ntp/Main_Pages/PUBS/2004CurrentDirections.pdf.

NTP (2004b). Toxicology and carcinogenesis studies of 3,3',4,4',5-pentachlorobiphenyl (PCB 126) (CAS No. 57465-28-8) in female Harlan Sprague-Dawley rats (gavage studies). National Toxicology Program, Research Triangle Park, NC.

Omori, Y., Zaidan Dagli, M. L., Yamakage, K., and Yamasaki, H. (2001). Involvement of gap junctions in tumor suppression: analysis of genetically-manipulated mice. *Mutat Res* **477**, 191-6.

Ou, Y. C., Conolly, R. B., Thomas, R., Gustafson, D. L., Long, M. E., Dovrev, I. D., Chubb, L. S., Xu, Y., Lapidot, S., Andersen, M. E., and Yang, R. S. H. (2003). Stochastic simulation of hepatic preneoplasic foci development for four chlorobenzene congeners in a medium-term bioassay. *Toxicol Sci* **73**, 301-314.

Ou, Y. C., Conolly, R. B., Thomas, R. S., Xu, Y., Andersen, M. E., Chubb, L. S., Pitot, H. C., and Yang, R. S. H. (2001). A clonal growth model: time-course simulations of liver foci growth following penta- or hexachlorobenzene treatment in a medium-term bioassay. *Cancer Res* **61**, 1879-1889.

Plante, I., Charbonneau, M., and Cyr, D. G. (2002). Decreased gap junctional intercellular communication in hexachlorobenzene-induced gender-specific hepatic tumor formation in the rat. *Carcinogenesis* **23**, 1243-9.

Portier, C., and el Masri, H. (1997). Statistical research needs in mechanistic modelling for carcinogenic risk assessment. *Stat Methods Med Res* **6**, 305-15.

Portier, C. J. (1987). Statistical properties of a two-stage model of carcinogenesis. *Environ Health Perspect* **76**, 125-31.

Portier, C. J. (1995). Quantitative models for cancer dose-response relationships: Parameter estimation. In Low-dose extrapolation of cancer risks:Issues and perspectives (S. Olin, W. Farland, O. Park, L. Rhomberg, R. Scheuplein, T. Starr and J. Wilson, eds.), pp. 123-134. ILSI Press, Washington, D.C.

Portier, C. J., Sherman, C. D., Kohn, M., Edler, L., Kopp-Schneider, A., Maronpot, R. M., and Lucier, G. (1996). Modeling the number and size of hepatic focal lesions following exposure to 2,3,7,8-TCDD. *Toxicol Appl Pharmacol* **138**, 20-30.

Press, W. H., Flannery, B. P., Teukolsky, S. A., and Vetterling, W. T. (1989). *Numerical Recipes (Fortran)*. Cambridge University Press, Cambridge, England.

Satoh, K., and Hatayama, I. (2002). Anomalous elevation of glutathione S-transferase P-form (GST-P) in the elementary process of epigenetic initiation of chemical hepatocarcinogenesis in rats. *Carcinogenesis* **23**, 1193-8.

Satoh, K., Hatayama, I., Tateoka, N., Tamai, K., Shimizu, T., Tatematsu, M., Ito, N., and Sato, K. (1989). Transient induction of single GST-P positive hepatocytes by DEN. *Carcinogenesis* **10**, 2107-11.

Smith, A. G., Francis, J. E., Dinsdale, D., Manson, M. M., and Cabral, J. R. (1985). Hepatocarcinogenicity of hexachlorobenzene in rats and the sex difference in hepatic iron status and development of porphyria. *Carcinogenesis* **6**, 631-636.

Swenberg, J. A., Dyroff, M. C., Bedell, M. A., Popp, J. A., Huh, N., Kirstein, U., and Rajewsky, M. F. (1984). O4-ethyldeoxythymidine, but not O6-ethyldeoxyguanosine, accumulates in hepatocyte DNA of rats exposed continuously to diethylnitrosamine. *Proc Natl Acad Sci U S A* **81**, 1692-5.

Thomas, R. S. (1998). The Use of Biologically-Based Models for Integrating Short-Term Cancer Bioassays, Mechanisms of Action, and Target Tissue Dosimetry: Application to Pentachlorobenzene. Ph.D. dissertation. Department of Environmental Health, Colorado State University, Fort Collins, CO.

Thomas, R. S., Conolly, R. B., Gustafson, D. L., Long, M. E., Benjamin, S. A., and Yang, R. S. (2000a). A physiologically based pharmacodynamic analysis of hepatic foci within a medium-term liver bioassay using pentachlorobenzene as a promoter and diethylnitrosamine as an initiator. *Toxicol Appl Pharmacol* **166**, 128-37.

Thomas, R. S., Conolly, R. B., Gustafson, D. L., Long, M. E., Benjamin, S. A., and Yang, R. S. H. (2000b). A physiologically based pharmacodynamic analysis of hepatic foci within a medium-term liver bioassay using pentachlorobenzene as a promoter and diethylnitrosamine as an initiator. *Toxicol Appl Pharmacol* **166**, 128-37.

Weibel, E. R., and Gomez, D. M. (1962). A principle for counting tissue structures on random sections. *J Appl Physiol* **17**, 343-348.

Weibel, E. R., Staubli, W., Gnagi, H. R., and Hess, F. A. (1969). Correlated morphometric and biochemical studies on the liver cell. I. Morphometric model, stereologic methods, and normal morphometric data for rat liver. *J Cell Biol* **42**, 68-91.

Wosniok, W., Kitsos, C., and Watanabe, K. (1999). Statistical issues in the application of multistage and biologically based models. In Perspectives on biologically based cancer risk assessment (V. J. Cogliano, E. G. Luebeck and G. A. Zapponi, eds.), pp. 243-274. Kluwer Academic/Plenum Publishers, New York.

Xu, Y. H., and Pitot, H. C. (2003). An improved stereologic method for three-dimensional estimation of particle size distribution from observations in two dimensions and its application. *Comput Methods Programs Biomed* **72**, 1-20.

Yang, R. S. H. (1994). Introduction to the Toxicology of Chemical Mixtures. In Toxicology of Chemical Mixtures: Case Studies, Mechanisms, and Novel Approaches (R. S. H. Yang, ed.), pp. 1-10. Academic Press, San Diego, CA.

Yang, R. S. H. (1997). Toxicologic Interactions of Chemical Mixtures. In Comprehensive Toxicology. Vol. 1, General Principles, Toxicokinetics, and Mechanisms of Toxicity (J. Bond, ed.), pp. 189-203. Elsevier Science Ltd., Oxford, England.

Yang, R. S. H., Dennison, J. E., Andersen, M. E., Ou, Y. C., Liao, K. H., and Reisfeld, B. (2004). Physiologically based pharmacokinetic and pharmacodynamic modeling. In Mouse models of human cancer (E. C. Holland, ed.) John Wiley & Sons, Inc., Hoboken, New Jersey.

Yang, R. S. H., el-Masri, H. A., Thomas, R. S., and Constan, A. A. (1995). The use of physiologically-based pharmacokinetic/pharmacodynamic dosimetry models for chemical mixtures. *Toxicol Lett* **82-83**, 497-504.

Yang, R. S. H., Thomas, R. S., Gustafson, D. L., Campain, J., Benjamin, S. A., Verhaar, H. J., and Mumtaz, M. M. (1998). Approaches to developing alternative and predictive toxicology based on PBPK/PD and QSAR modeling. *Environ Health Perspect* **106(Suppl 6)**, 1385-1393.

Yoshizawa, K., Walker, N. J., Jokinen, M. P., Brix, A. E., Sells, D. M., Marsh, T., Wyde, M. E., Orzech, D., Haseman, J. K., and Nyska, A. (2005). Gingival carcinogenicity in female Harlan Sprague-Dawley rats following two-year oral treatment with 2,3,7,8-tetrachlorodibenzo-p-dioxin and dioxin-like compounds. *Toxicol Sci* **83**, 64-77.

Yusuf, A., Rao, P. M., Rajalakshmi, S., and Sarma, D. S. (1999). Development of resistance during the early stages of experimental liver carcinogenesis. *Carcinogenesis* **20**, 1641-4.

CHAPTER 5

Cross Utilization of the Clonal Growth Model for a Chemical Mixture for Its Component Chemicals Hexachlorobenzene and PCB 126

Yasong Lu, Manupat Lohitnavy, Micaela Reddy, Ornrat Lohitnavy, Elizabeth Eickman, Amanda Ashley, Lisa Gerjevic, Yihua Xu, Rory B. Conolly, Raymond S. H. Yang

ABSTRACT

To continue the earlier work on clonal growth modeling, in this study, we attempted to cross-utilize the clonal growth model built for the mixture of hexachlorobenzene (HCB) and 3,3',4,4',5-pentachlorobiphenyl (PCB 126) for its single component chemicals. Experimentally, the time-course medium-term liver foci bioassay protocol was similarly employed except that the single chemicals of the mixture, HCB or PCB 126, each at two doses, were used. Briefly, the 8-week bioassay involved a series of treatments, including a single injection of an initiator, a two-thirds partial hepatectomy, and daily oral gavage of HCB or PCB 126 solution in F344 rats. Time-course data of glutathione S-transferase placental form (GST-P) liver foci were collected. The foci data suggested that there appeared to be an interaction between HCB and PCB 126, greater than additivity at the low doses and less than additivity at the high doses. Modeling wise, we did not alter the structure of the clonal growth model constructed for the parent mixture. However, certain parameter adjustments were necessary because these parameters were expected to be different under different test chemical treatments. The foci data of the component chemicals were simulated well by the model. The model derived kinetic parameters for

initiated cells suggested a greater-than-additivity interaction in stimulating the proliferation of mini- and medium-foci at low doses and a less-than-additivity interaction in stimulating the proliferation of large-foci at high doses between HCB and PCB 126. This study illustrated the utility of clonal growth modeling in chemical mixture toxicology and carcinogenesis research.

1. INTRODUCTION

For a model to be useful, it should ideally possess a broad applicability. The two-stage carcinogenesis model by Moolgavkar and co-workers (Moolgavkar *et al.* 1988; Moolgavkar and Knudson 1981; Moolgavkar and Venzon 1979) is an excellent example. In this model (known as MVK model), a tumor was recognized as a result of two consecutive and irreversible genetic mutations. The first mutation transforms a normal cell into an initiated cell, and the second transforms an initiated cell into a malignant cell. The growth kinetics of the normal and initiated cells were incorporated in the model. With reasonable parameter adjustments, the MVK model was able to simulate multiple epidemiologic data sets of lung cancer (Moolgavkar and Knudson 1981) and female breast cancer (Moolgavkar *et al.* 1980; Moolgavkar and Knudson 1981). Within the framework of this model, Moolgavkar and co-workers (Moolgavkar 1986; Moolgavkar and Knudson 1981) provided biologically plausible explanations to the modifying effects of smoking and smoking abstinence on lung cancer and of menarche, menopause, and pregnancy on female breast cancer incidences.

Another model that has been reported to be broadly applicable is the clonal growth model, which describes the first stage (*i.e.*, transformation from normal to initiated cells

and the growth of the normal and initiated cells) of the MVK model. Using the clonal growth model, Dewanji *et al.* (1989) first derived the theoretical variables characterizing the development of preneoplastic foci, resulting from clonal expansion of initiated cells, using analytical solutions. Moolgavkar *et al.* (1990) then applied this model to simulate the results of hepatic ATPase-deficient foci in the rats following continuous exposure to N-nitrosomorpholine at various doses via drinking water. Thereafter, this model was cross-utilized to simulate multiple data sets of liver foci promoted by 3-methylcholanthrene, 4-monochlorobiphenyl, 2,2',4,5'-tetrachlorobiphenyl, 3,3',4,4'-tetrachlorobiphenyl (Luebeck *et al.* 1991), phenobarbital, α-hexachlorocyclohexane (Luebeck *et al.* 1995), 2,3,7,8-tetrachlorodibenzo-*p*-dioxin, and 1,2,3,4,6,7,8-heptachlorodibenzo-*p*-dioxin (Moolgavkar *et al.* 1996).

Conolly and Kimbell (1994) proposed a strategy of using computer simulation to replace analytical solutions in the clonal growth modeling. This strategy can cope with time-dependent parameters effectively. It has been adopted by our laboratory (Lu *et al.* 2006a; Ou *et al.* 2003; Ou *et al.* 2001; Thomas 1998; Thomas *et al.* 2000). Ou *et al.* (2001) developed a clonal growth model for hexachlorobenzene (HCB) by incorporating the negative selection mechanism (Andersen *et al.* 1995; Jirtle *et al.* 1991) and the two-cell hypothesis (Conolly and Andersen 1997; Thomas 1998; Thomas *et al.* 2000). Their model was cross-utilized for other congeners, *i.e.*, 1,4-dichlorobenzene, 1,2,4,5-tetrachlorobenzene, and pentachlorobenzene, in the chlorobenzene family.

Inspired by the earlier observations (Buchmann *et al.* 1994; Grasl-Kraupp *et al.* 2000; Luebeck *et al.* 1995; Moolgavkar *et al.* 1996; Schulte-Hermann *et al.* 1990) that the expansion of a preneoplastic focus is less than exponential and depends on focal size, we

felt that the size-dependency of foci growth should be incorporated in a clonal growth model for satisfactory simulation of foci size distribution. Therefore, we included this concept in our clonal growth model, based on the Ou *et al.* model (Ou *et al.* 2003; Ou *et al.* 2001), for the chemical mixture of HCB and 3,3',4,4',5-pentachlorobiphenyl (PCB 126) (Chapter 4)(Lu *et al.* 2006a). The modeling results simulated the number, volume, and size distribution data of hepatic foci well. This practice can be recognized as an improvement over the earlier models developed in our laboratory (Ou *et al.* 2003; Ou *et al.* 2001; Thomas 1998; Thomas *et al.* 2000). We expect that our model for the HCB+PCB 126 mixture would be applicable to the two component chemicals.

The interactions among components of a chemical mixture may fall into four groups: synergism, antagonism, potentiation, and additivity. These terms have been explained and discussed earlier (Cassee *et al.* 1998; Eaton and Klaassen 2001; Hertzberg and MacDonell 2002). Identification of interaction types and the underlying mechanisms is valuable for mixture risk assessment. The approaches currently employed for assessing chemical interactions and joint toxicity of mixtures include, but are not limited to, experimental testing using wild type or genetically engineered animals (Benjamin *et al.* 1999; Bucher and Lucier 1998), *in vitro* testing (Bae *et al.* 2001; Bae *et al.* 2002; Mumtaz *et al.* 2002), statistical and mathematical modeling (Gennings *et al.* 2005; Groten *et al.* 2001; Olmstead and Leblanc 2005; Rider and LeBlanc 2005; Wilkinson *et al.* 2000), (quantitative) structure-activity relationship modeling (Lin *et al.* 2003; Mwense *et al.* 2006; Yu *et al.* 2001), and mechanistic modeling (*i.e.*, physiologically based pharmacokinetic/dynamic modeling) (Dennison *et al.* 2004; Dobrev *et al.* 2001; el-Masri *et al.* 1995; Haddad *et al.* 2001; Krishnan *et al.* 2002; Liao *et al.* 2002). The integration of

experimentation and computer modeling is instrumental for study of chemical mixture toxicology, including data collection and interpretation and exploration of the type and underlying mechanism(s) of an interaction.

In this study, we (1) tested the applicability of our earlier clonal growth model for the HCB+PCB 126 mixture for the two component chemicals; and (2) examined the interactions between the two chemicals at the levels of experimental foci data and the model-derived parameters related to foci growth.

2. MATERIALS AND METHODS

This study was composed of (1) two medium-term liver foci bioassays in the rats for the two individual chemicals, HCB and PCB 126[1], and (2) the analyses of the bioassay results by cross-utilization of the clonal growth model developed earlier for the HCB+PCB 126 mixture. The two animal bioassays generated glutathione S-transferase placental form (GST-P) foci data as well as other measurements. We conducted the bioassays separately because each bioassay used a total of approximately 100 rats and approached the maximal surgical and experimental capacity of a team of four scientists in our laboratory. The clonal growth models simulated the two sets of foci data and suggested the growth kinetics of the initiated cells under each chemical treatment.

The experimental design and the clonal growth modeling in this study were very similar to those in the mixture study reported earlier in Chapter 4. They are repeated here for the reader's convenience.

---

[1]The PCB 126 bioassay was in the charge of Mr. Manupat Lohitnavy. Mr. Lohitnavy kindly provided the data for the analysis presented in this paper.

2.1. Medium-term Liver Foci Bioassay and Data Collection

2.1.1. Chemicals

HCB (99% purity) was from Aldrich Chemical (Milwaukee, WI), PCB 126 was purchased from AccuStandard (New Haven, CT), and diethylnitrosamine (DEN) was from Sigma Chemical (St. Louis, MO).

2.1.2. Animals and Treatment

In each bioassay, male F344 rats, 30 days of age, purchased from Harlan Sprague-Dawley (Indianapolis, IN), were housed in the Painter Center, Colorado State University. It is fully accredited by the American Association for Accreditation of Laboratory Animal Care (AAALAC). Animals were given food (Harlan Teklad NIH-07 diet, Madison, WI) and water *ad libitum*. The lighting was set on a 12h light/dark cycle.

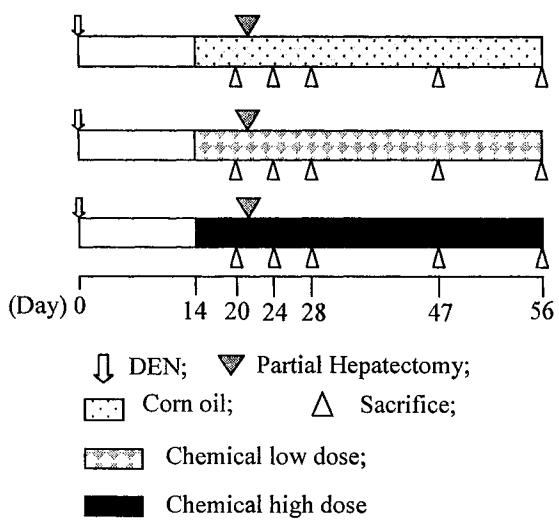

Fig. 5.1. Experimental design of the time-course medium-term liver foci bioassay. A single intraperitoneal injection of 200 mg/kg DEN was given on day 0. Daily oral gavage of corn oil or chemical (HCB or PCB 126) solution started from day 14 until sacrifice. On day 21, a two-thirds partial hepatectomy was performed on the rats. On the day of surgery and the following three days the gavage was suspended to reduce the stress to the animals. Six rats from each treatment group were sacrificed on days 20, 24, 28, 47, and 56. The liver was sectioned and saved appropriately for GST-P foci measurement and other analyses.

After four weeks of acclimation, the rats were randomized by weight, divided into three groups, and treated according to the time-course medium-term liver foci bioassay (Fig. 5.1). At week 0, the rats were given a single intraperitoneal injection of DEN (200 mg/kg) in 0.9% saline. Two weeks later, the rats began receiving daily oral gavage of corn oil (control), low, and high dose of chemical in corn oil until sacrifice. The dose levels (Table 5.1) were selected on the basis of the previous work in our laboratory (Dean *et al.* 2002; Ou *et al.* 2001). At week 3 (day 21), a two-thirds partial hepatectomy was performed on the rats. On the day of surgery and the following three days, the gavage was suspended to reduce the stress to the animals while recovering from surgery. On days 20, 24, 28, 47, and 56, six rats from each treatment group were sacrificed by aortic exsanguination under anesthesia. The body and liver weight of each rat were recorded at sacrifice. A slice of liver was taken along the longest axis of each lobe, fixed in 10% neutral-buffered formalin, embedded in paraffin, and then serially sectioned at thickness of 5 μm. The study was conducted in accordance with the National Institutes of Health (NIH) guidelines for the care and use of laboratory animals.

Table 5.1. Chemical Doses in the Liver Foci Bioassays

Study	Treatment	HCB (mg/kg)	PCB 126 (μg/kg)
HCB	Control	-	-
	Low	8.55	-
	High	28.5	-
PCB 126	Control	-	-
	Low	-	3.3
	High	-	9.8
HCB + PCB 126*	Control	-	-
	Low	8.55	3.3
	High	28.5	9.8

*: The doses of the mixture bioassay are included here for the ease of comparison with those in the individual chemical bioassays.

2.1.3. GST-P Foci Measurement

The GST-P focus is the end-point marker for evaluating carcinogenic potential of a tested chemical (Ito *et al.* 2003; Ito *et al.* 1989). GST-P foci identification and quantification followed the methods previously described (Ou *et al.* 2001; Thomas 1998). Liver slides were deparaffinized in xylene and rehydrated by passage through an alcohol series. Endogenous peroxidase was quenched in 3% hydrogen peroxide for 10 min. The slides were then rinsed with deionized water and placed in PBS (pH 7.4; 2.7 mM KCl, 0.14 M NaCl, 1.5 mM KH_2PO_4, and 8.1 mM Na_2PO_4). A standard avidin-biotin complex method protocol (Vector Labs, Burlingame, CA) was followed, and foci were identified with GST-P primary antibody (Binding Site, San Diego, CA). GST-P foci were measured using an Olympus BX51 light microscope (Olympus Optical Co., Tokyo, Japan) coupled with a BioQuant NOVA image analysis system (B&M Biometrics, Nashville, TN). Foci having two or more cells were recorded.

2.1.4. Hepatocyte Proliferation Determination

Osmotic minipumps (Alzet model 2ML1, 10 μl/hr; Durect Corporation, Cupertino, CA), filled with 5-bromo-2'-deoxyuridine (BrdU) (20 mg/ml), were implanted subcutaneously over the dorsal midscapular region 3 days prior to sacrifice. Detection of BrdU labeled cells was conducted on the liver slides using standard avidin-biotin complex method and immunoperoxidase kits (Vector Labs, Burlingame, CA) with primary BrdU antibody (Biogenex Labs, San Ramon, CA) and 3-amino-9-ethylcarbozole (Biomeda, Foster City, CA). At least 1000 cells/rat and four rats/group were counted. The labeling index (LI), defined as the number of labeled cells divided by the total number of counted cells, was obtained using CHRIS (version 1.1L; Sverdrup Technology, Fort

Walton Beach, FL). The hepatocyte division rate constant (α, 1/day) was calculated using an equation previously proposed (Moolgavkar and Luebeck 1992):

$$\alpha = \frac{1}{2t} \times \ln\left(\frac{1}{1-LI}\right) \qquad \text{(Eq-1)}$$

where t is the number of days of exposure to BrdU (t = 3 in this study). This result represented the division rate constant of the normal hepatocytes; in this study no effort was made to determine the division rate constant of the cells within foci.

2.1.5. Hepatocyte Numerical Density Quantification

The numerical density (cell number/cm^3) of hepatocyte was represented by the numerical density of hepatocyte nuclei that was evaluated on liver H&E slides. Ten random fields per rat were analyzed. The calculation of numerical density followed the formula reported by Weibel *et al.* (1969):

$$N_V = \frac{K}{\lambda} \times \frac{N_A^{3/2}}{V_V^{1/2}} \qquad \text{(Eq-2)}$$

where N_V is hepatocyte numerical density, λ is nuclear shape coefficient, K is nuclear size distribution coefficient, N_A is number of nuclei per cm^2 test area, and V_V is nuclear volume density. In this study, λ = 1.38 according to Weibel and Gomez (1962). K = 1.02 for all groups at any time point in the two bioassays (Weibel *et al.* 1969). The unbiased estimate of V_V is the nuclear area density, *i.e.*, total area of nuclei per cm^2 test area. The derived numerical density was assumed applicable to both normal and initiated cells.

2.1.6. Stereologic Methods

The foci data obtained from liver slides were 2-dimensional (2D) and must be converted to 3-dimensional (3D) expressions for comparison with the outputs of the clonal growth model. A program developed by Xu and Pitot (2003) at the McArdle

Laboratory for Cancer Research, University of Wisconsin, was used for the conversion. This program uses data containing tissue information (e.g., liver weight and slide area) and individual focal areas as the input to provide 3D stereology results. The outputs include relative foci volume (% liver volume occupied by foci), number of foci/cm^3, and foci size distribution. The theories of the program were discussed in Xu and Pitot (2003). The relative foci volume was computed by the method of Delesse, and the foci number/cm^3 liver was calculated using a modified Saltykov method, in which 25 size classes were defined. The diameter ratio of two neighboring classes was $10^{-0.1}$. The allocation of foci into classes was based on focal volume instead of cell number. At the hepatocyte density of $1.2\times10^8/cm^3$, the classes 1-13 were corresponding to cell numbers of 8-16, 17-32, 33-64, 65-127, 128-253, 254-505, 506-1007, 1008-2009, 2010-4009, 4010-8000, 8001-15962, 15963-31847, and 31848-63543, respectively. The classes 14-25 were omitted here because there were no foci therein. Note that these classes were employed only for interpreting the size distribution pattern of foci in each group.

The focal diameter truncation value (*i.e.*, all foci smaller than that diameter were considered not reliably detectable and thus ignored) for the conversion was set at 50.12 μm, which corresponded to the size of two hepatocytes.

2.1.7. Statistical Analysis

ANOVA at $\alpha = 0.05$ was applied to analyze the statistical differences of the body weight, liver weight, hepatocyte numerical density, foci number, and foci area among the chemical treated groups and the concurrent controls. All statistical analyses were performed using SAS (version 8.02; SAS Institute Inc., Cary, NC).

2.2. Clonal Growth Modeling

The clonal growth model algorithm described the growth kinetics of normal hepatocytes, occurrence of initiated cells, and growth kinetics of the initiated cells. The structure, basic assumptions and simplifications, and technical details of the clonal growth modeling have been reported (see Chapter 4)(Conolly and Andersen 1997; Conolly and Kimbell 1994; Ou *et al.* 2003; Ou *et al.* 2001; Thomas 1998; Thomas *et al.* 2000). In this paper, we followed the same modeling framework as that for the HCB+PCB 126 mixture earlier (see Chapter 4)(Lu *et al.* 2006a). The essence of the modeling is presented below.

2.2.1. Basics of the Clonal Growth Model

(a) *Growth kinetics of normal hepatocytes.* The growth of normal hepatocytes was described deterministically by a function of division (α, 1/day) and death (β, 1/day) rate constants:

$$\frac{dN}{dt} = N(\alpha - \beta) \qquad \text{(Eq-3)}$$

where N is the number of normal hepatocytes/cm^3 (*i.e.*, hepatocyte numerical density), and β represents different kinds of cell death including apoptosis and necrosis.

(b) *Occurrence of initiated cells.* Upon DEN treatment, some hepatocytes may express GST-P that is absent under normal conditions (Kato *et al.* 1993; Satoh *et al.* 1989), a process named "mutation" in this study. These cells have been recognized as initiated cells and precursors of preneoplastic foci (Ito *et al.* 2003; Satoh *et al.* 1989). The occurrence of initiated cells was assumed to be a stochastic process following a Poisson distribution. The expected number of initiated cells in a small time step was defined by a function of mutation probability and division rate constant:

$$N_m = N\alpha\mu\Delta t \qquad \text{(Eq-4)}$$

where N_m is the expected number of initiated cells during a time step Δt, N is normal hepatocyte number/cm^3, and μ is mutation probability per division. As proposed by Conolly and Kimbell (1994), a random deviate about N_m denoting the number of initiated cells during Δt was drawn from a Poisson distribution using the function POIDEV (Press *et al.* 1989). The inputs to POIDEV were the expected number and a pseudorandom number between 0 and 1 generated by the algorithm UNIFL (Bratley *et al.* 1987). Since experiments (Imai *et al.* 1997; Yusuf *et al.* 1999) and modeling exercises (Conolly and Andersen 1997; Haag-Gronlund *et al.* 2000; Lu *et al.* 2006a; Ou *et al.* 2001; Thomas *et al.* 2000) suggested kinetic heterogeneity of the pool of initiated cells, we assumed that there were two subpopulations (*i.e.*, A and B cells) in the pool. The proportion of B cells was small upon occurrence and gradually increased due to the growth advantage of B over A cells. We denoted the mutation probability leading to each subpopulation μ_a and μ_b.

(c) *Growth kinetics of initiated cells.* Once produced, an initiated cell could undergo one of the three random events, *i.e.*, division, death, or no change within a given time step. Growth of initiated cells gave rise to GST-P foci. Death of initiated cells included apoptosis, necrosis, and loss of GST-P phenotype. When a focus was larger than 1000 cells, its growth was assumed to be deterministic. Otherwise (*i.e.*, a focus $\leq$ 1000 cells), the growth kinetics of each cell in the clone were treated stochastically according to Conolly and Kimbell (1994). The probabilities of division and death were calculated from the rate constants of division (α_a, α_b, 1/day) and death (β_a, β_b, 1/day), respectively (Conolly and Kimbell 1994). The simulation program tracked the behavior of each initiated cell and calculated focal size (cells/focus) and number (foci/cm^3) over time. Divided by hepatocyte numerical density, the total foci size was converted to relative foci

volume. The model outputs were 3-dimensional and compared to the 3D data converted from the experimental 2D results by the stereologic methods discussed above.

2.2.2 Modeling Strategies

(a) Time intervals of piecewise constants. The animals in this study were sequentially subjected to three kinds of treatments: DEN (day 0), partial hepatectomy (day 21), and chemical (HCB or PCB 126) dosing (day 14-56). These treatments were expected to alter various parameters. Hence, it was necessary to divide the whole simulation duration (56 days) into intervals related to the effects of the treatments. With our earlier strategy (see Chapter 4), we divided the duration into 6 intervals: days 0-7, 7-14, 14-21.5, 21.5-24.5, 24.5-28.5, and 28.5-56. The parameters related to the growth of initiated cells were fixed within each interval and varied among different intervals.

(b) Detection limit of foci. In the 2D analysis, all foci having 2 or more cells were counted. During the 2D to 3D conversion, our calculation using the information of hepatocyte density and diameters of 2-cell foci in a 2D setting suggested that the 3D detection limit was approximately 8 cells at all time. Therefore, any focus smaller than 8 cells in the 3D setting was treated undetectable; otherwise it was detectable and contributed to the final simulation outputs.

(c) Size-dependent growth kinetics. Experimental results (Buchmann *et al.* 1994; Grasl-Kraupp *et al.* 2000) and modeling exercises (Luebeck *et al.* 1995; Moolgavkar *et al.* 1996) have suggested that the growth of foci is likely to be size-dependent. Our earlier modeling on the HCB+PCB 126 mixture (see Chapter 4) quantitatively explored the size-dependent kinetics by grouping all foci into four categories according to their sizes. Each category had distinct growth kinetics. The same strategy was employed in this study.

2.2.3. Parameterization

(a) Division and death rate constants of normal hepatocytes. The division rate constant of normal hepatocytes was obtained from experiments. Prior to the regenerative proliferation due to partial hepatectomy (day 21.5), the time-course division rate constant was calculated using Equation (1) with the BrdU labeling index data from Kato *et al.* (1993) as well as the results from our bioassays (day 20 data). The results were formulated into empirical functions to describe the division rate constant over time until day 21.5. On day 21.5, the division rate constant was set at 0.40/day to account for the proliferation surge due to partial hepatectomy (Ou *et al.* 2003; Ou *et al.* 2001). Thereafter, the constant during the segments of days 21.5-24, 24-28, 28-47, and 47-56 was derived from our BrdU labeling index experimental data that were obtained on days 24, 28, 47, and 56.

The death rate constant, not experimentally achievable, was related to the total hepatocyte number and division rate constant as shown in Eq-3. The total hepatocyte number was inferred by liver weight and hepatocyte density. Prior to day 6, the death rate constant was described by a function fitting to the time course liver weight after an intraperitoneal injection of 150 mg/kg DEN reported by Kato *et al.* (1993). Thereafter, the death rate constant was equal to a background value of 8.6×10^{-4}/day (see Chapter 4).

(b) Mutation probability. The mutation probability in this study comprised of two portions: the background level and, much more importantly, the increased level due to DEN treatment. The latter was expected to be time-dependent (see Chapter 4)(Ou *et al.* 2003; Ou *et al.* 2001). Since the dose of DEN in this study was identical to that in the HCB+PCB 126 mixture study, we assumed that the time-course mutation probability

calibrated in the mixture study could be applied to the two component chemicals in this study. The background mutation probability was set at 1.7×10^{-6}/division for both A and B cells (Ou *et al.* 2001). The strategy of determining the increase over the background was described earlier (see Chapter 4). The ratio of the mutation probabilities generating A and B cells was set at 10:1 (μ_a:μ_b = 10:1) (see Chapter 4); it was because only a small percentage (5-23%) of the foci generated by DEN was resistant to selective mitoinhibitory pressures (Yusuf *et al.* 1999).

(c) Categorization and division and death rate constants of foci. To relate cellular kinetics to focal size, the A and B foci were both categorized according to their sizes. The categorization dividers were selected on the basis of two criteria: (i) to account for the present understanding in the growth kinetics of initiated cells (Grasl-Kraupp *et al.* 2000), and (ii) to replicate the size distribution patterns through computer simulations. In our earlier modeling for HCB+PCB 126, the categories included single cells, mini- (2-11 cells), medium- (12-399 cells), and large-foci (>399 cells) (see Chapter 4). Here we adopted these categories. Each category had distinct growth kinetics. To reduce the number of unknown parameters, we assigned A and B cells with the same division rate constant in each category within each time interval. The death rate constant of A cells was generally assumed to be higher than that of B cells, reflecting the higher sensitivity of A cells to the selective mitoinhibitory pressure (Conolly and Andersen 1997; Yusuf *et al.* 1999). We adjusted the cellular division and death rate constants under each chemical treatment to simulate three pieces of data simultaneously: relative foci volume, foci number/cm^3, and size distribution. Because of the stochasticity of the growth of initiated

cells, the model was run for 20 times; the averages of the 20 runs were compared to our data for calibration.

2.2.4. Software

The clonal growth model was coded and the simulations were performed using ACSL Tox 11.8.4 (AEgis Technologies Group, Huntsville, AL).

3. RESULTS

Although this paper was primarily focused on the two individual chemicals, HCB and PCB 126, some results in the HCB+PCB 126 mixture study are repeated here for the comparisons between the mixture and its component chemicals.

3.1. Experimental data collections

3.1.1. Effects of chemical treatments on the body and liver weight and liver section area

The individual chemicals of HCB (see Chapter 2)(Lu *et al.* 2006b) and PCB 126 had only slight effects on the body weight, liver weight, liver/body weight ratio, and the liver section area even though the effects were statistically significant at some time points. In contrast, HCB+PCB 126 affected the following endpoints in a remarkable manner: reduced the body weight and increased the other indices on days 28, 47, and 56 (Table 5.2).

3.1.2. Hepatocyte numerical density

The numerical density measures the average size of hepatocytes. The HCB or PCB 126 treatment did not significantly change the numerical density. In these two bioassays, the density was in the range of $1\text{-}2\times10^{8}$ cells/cm^{3} liver in all groups. In the mixture

bioassay, however, a significant decrease in the density due to HCB+PCB 126 treatment was observed on days 28, 47, and 56 (Table 5.2).

Table 5.2. Time-course Liver Section Area, Hepatocyte Division Rate Constant, and Hepatocyte Numerical Density in HCB+PCB 126 Medium-term Bioassay

Treatment	Day 20	Day 24	Day 28	Day 47	Day 56
	Body weight (g)				
Control	223.2 ± 13.1	211.6 ± 10.2	198.0 ± 14.4	255.4 ± 10.6	231.8 ± 23.5
Low dose	225.5 ± 11.1	210.4 ± 12.1	189.7 ± 9.7	236.9 ± 13.5*	202.0 ± 11.6*
High dose	226.5 ± 9.2	216.3 ± 10.6	171.6 ± 7.8*!	202.0 ± 14.3*!	165.8 ± 14.8*!
	Liver weight (g)				
Control	7.39 ± 0.60	4.92 ± 0.41	5.03 ± 0.43	6.81 ± 0.40	7.70 ± 1.74
Low dose	7.52 ± 0.43	4.94 ± 0.24	7.43 ± 0.66*	13.13 ± 1.03*	12.73 ± 0.56*
High dose	7.60 ± 0.31	5.36 ± 0.41	7.84 ± 0.63*	12.17 ± 1.74*	11.93 ± 1.26*
	Liver/body weight ratio (%)				
Control	3.31 ± 0.09	2.32 ± 0.12	2.54 ± 0.06	2.67 ± 0.12	3.36 ± 0.95
Low dose	3.34 ± 0.08	2.35 ± 0.13	3.91 ± 0.20*	5.54 ± 0.20*	6.31 ± 0.24*
High dose	3.36 ± 0.10	2.48 ± 0.11	4.56 ± 0.25*!	6.00 ± 0.46*!	7.21 ± 0.67*!
	Liver section area[#] (cm^2)				
Control	2.89±0.48	3.69±0.11	3.65±0.38	4.43±0.25	4.22±0.62
Low dose	2.39±0.40	3.92±0.51	4.61±0.54*	7.12±0.82*	6.92±0.32*
High dose	2.58±0.49	4.00±0.35	4.81±0.57*	6.28±0.85*	6.07±0.63*
	Hepatocyte density ($\times 10^8/cm^3$)				
Control	1.10±0.17	1.20±0.08	1.10±0.11	1.20±0.01	1.00±0.01
Low dose	0.99±0.16	0.99±0.06	0.83±0.01*	0.57±0.02*	0.64±0.02*
High dose	0.97±0.18	1.10±0.12	0.81±0.08*	0.60±0.16*	0.64±0.06*

Note: The results were expressed as mean ± SD.
*: Significantly different from the concurrent control group, $p<0.05$;
!: Significantly different from the concurrent other groups, $p<0.05$;
[#]: Each slice of liver was taken consistently along the longest axis of each lobe. Thus, the increase in the liver section area indicated the enlargement of liver.

3.1.3. Hepatocyte division rate constant

The hepatocyte division rate constant was calculated from experimentally derived BrdU-labeling index and is shown in Fig. 5.2. In all groups, the division rate constant

surged remarkably on day 24 due to the mitogenic effect of the partial hepatectomy on day 21. HCB dosing had no impact on the division rate constant. The same was generally true for PCB 126 treatment with one exception; on day 20 the PCB 126-treated groups had lower division rate constants than that in the concurrent control. The high dose of mixture treatment significantly increased the division rate constant on days 28, 47, and 56.

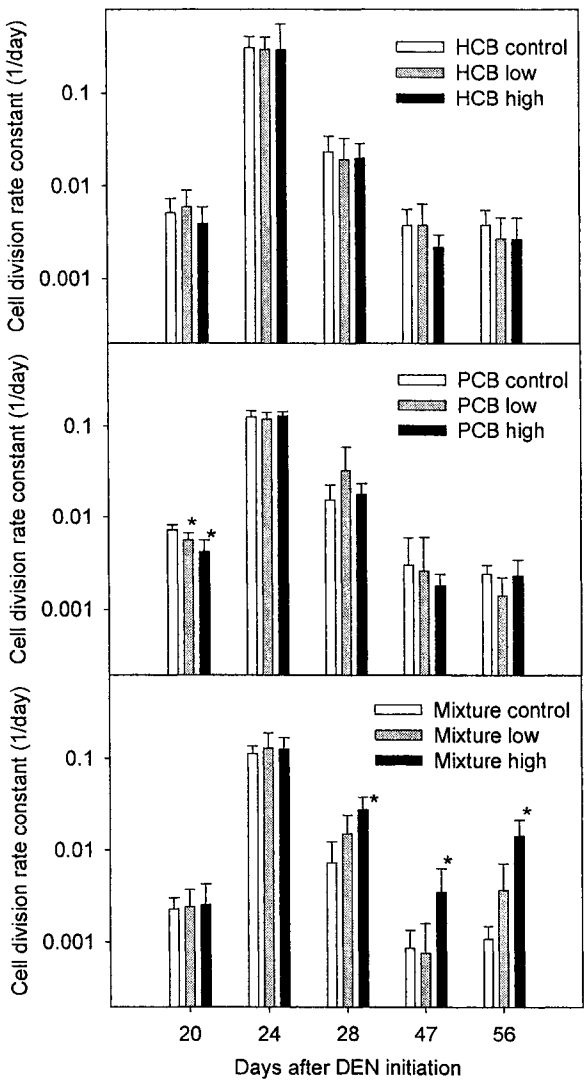

Fig. 5.2. Time-course hepatocyte division rate constants for HCB or PCB 126. The data for mixture bioassays are included here for comparison. Note that the plots are in semilog scales. *: significantly different ($p<0.05$) from the concurrent control group.

3.1.4. 2D GST-P foci data

In a 2D setting, the GST-P foci development is measured by the relative foci area (% of liver area occupied by GST-P foci) and foci number/cm^2. The results of these two indices in our bioassays are illustrated in Fig. 5.3 (left: relative foci area; right: foci number/cm^2). The high dose of HCB treatment slightly yet significantly increased the foci number/cm^2 on day 56. At the other time points, both low and high dose of HCB failed to elevate the relative foci area or foci number/cm^2. In the PCB 126 bioassay, the high dose significantly increased the relative foci area at the later three time points and the foci number/cm^2 at the later four time points. The low dose, however, had no effect on the two indices. In the mixture bioassay, the effects of the low and high dose treatment were generally comparable. The increases in the relative foci area and foci number/cm^2 at both doses were observed at most time points. These results suggested the carcinogenic potential of HCB, PCB 126, and their mixture.

3.1.5. Comparison of the foci development under HCB, PCB 126, and HCB+PCB 126 treatment

We compared the net effects of HCB and PCB 126 with those of the mixture at the last time point (day 56). The net effect of a chemical treatment was defined as the difference between the measurements in a chemical-treated group and a concurrent control. Figure 5.4 shows the net relative foci area and net foci number/cm^2 attributable to HCB, PCB, or the mixture. The predicted values of the two indices based on additivity are also shown in Fig. 5.4. At the low doses (HCB 8.55 mg/kg, PCB 126 3.3 μg/kg), the additivity predictions were apparently lower than the experimental results from the HCB+PCB 126 bioassay. At the high doses (HCB 28.5 mg/kg, PCB 126 9.8 μg/kg),

however, the reverse was true (*i.e.*, the additivity predictions appeared to be higher than the results from the HCB+PCB 126 bioassay).

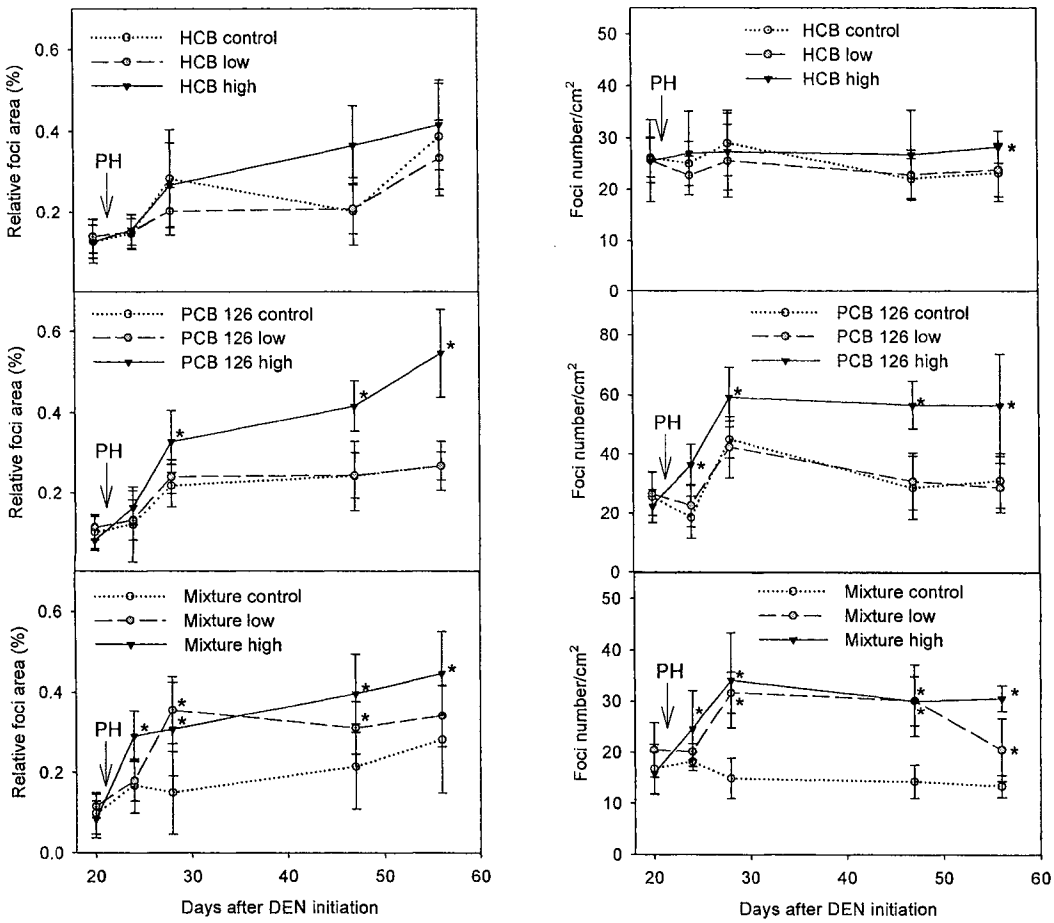

Fig. 5.3. Relative foci area (left) and foci number/cm^2 (right) derived from the liver slides of the rats treated with corn oil, HCB or PCB 126. The data for HCB+PCB 126 mixture are included for comparison. The arrows indicate when the partial hepatectomy (PH) was performed.
*: significantly different ($p<0.05$) from the concurrent control group.

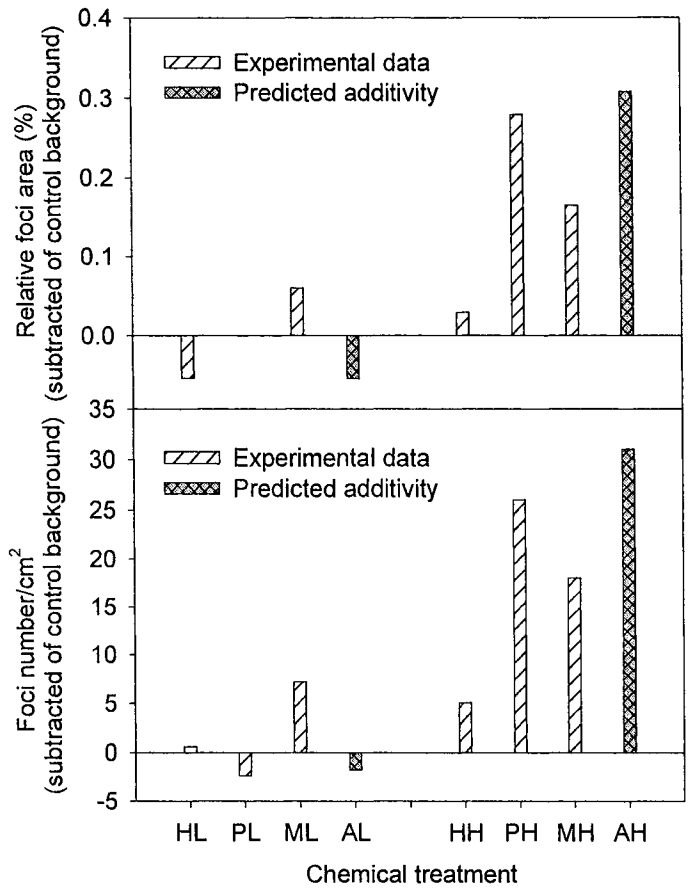

Fig. 5.4. Relative foci area (top) and foci number/cm^2 (bottom), subtracted of the corresponding control values, in the HCB, PCB 126, and mixture groups on day 56. The sums (predicted additivity) of the adjusted relative foci area as well as foci number/cm^2 from the HCB and PCB 126 groups were included for determination of the interaction between these two chemicals. HL: HCB low dose, PL: PCB 126 low dose, ML: mixture low dose, AL: predicted additivity at low dose, HH: HCB high dose, PH: PCB 126 high dose, MH: mixture high dose, AH: predicted additivity at high dose.

3.2. Clonal growth model simulations

3.2.1. Simulation of the foci data

Our earlier clonal growth model for the HCB+PCB 126 mixture (see Chapter 4)(Lu *et al.* 2006a) was applied to simulate the GST-P foci data from the HCB or PCB 126 bioassays with appropriate adjustments in some parameters (e.g., the liver weight, hepatocyte numerical density, hepatocyte division rate constant, and the division and

death rate constants of the initiated cells). The adjustments were necessary because these parameters were different following the different chemical treatments in the bioassays. The model simulations were in good agreement with the data of foci volume (Figs. 5.5 and 5.6), number (Figs. 5.5 and 5.6), and size distribution (Tables 5.3 and 5.4) in the HCB or PCB 126 bioassays. The distribution of the foci shifted to the larger classes over time. The treatment of HCB or PCB 126 increased the foci number in the smaller classes (e.g., classes 1 and 2). PCB 126 also promoted the enlargement of foci. The same pattern of change in size distribution upon PCB 126 treatment was observed for HCB+PCB 126 earlier (see Chapter 4)(Lu *et al.* 2006a).

3.2.2. Initiated cell growth kinetic parameters

The division and death rate constants of the initiated cells (Tables 5.5 and 5.6) were calibrated with foci volume, number, and size distribution data. The constants in the HCB or PCB 126 groups were generally lower than those in the mixture groups (see Chapter 4 for the parameters in the HCB+PCB 126 model). The effects of chemical treatments on the kinetic parameters manifested after the partial hepatectomy on day 21 and were notable at the high doses (*i.e.*, HCB 28.5 mg/kg and PCB 126 9.8 μg/kg). Since A cells were assumed to be sensitive to selective pressures, their net growth rate was reduced by the chemicals. As for B cells, HCB inhibited their death and had minimal effect on their division. PCB 126 and the mixture, however, not only inhibited the death, but also stimulated the division of B cells.

3.2.3. Comparison of the kinetic parameters in the HCB, PCB 126, and HCB+PCB 126 groups

CHAPTER 6

Overall Summary and Future Directions

Yasong Lu

1. DISSERTATION SUMMARY

Our Quantitative and Computational Toxicology Group has been developing an approach for predicting carcinogenic potential of chemicals and chemical mixtures by integrating experimental methods, including a medium-term liver foci bioassay, *in vitro* hepatocyte culture, and genomic techniques, and computer modeling, including PBPK, clonal growth, and quantitative structure-activity relationship modeling. The earlier work towards this goal in our laboratory has been reported in multiple publications (Dean 2003; el-Masri *et al.* 1997; Gustafson *et al.* 1998; Gustafson *et al.* 2000; Lee *et al.* 2002; Liao *et al.* 2001; Lu *et al.* 2006a; Lu *et al.* 2006b; Ou *et al.* 2003; Ou *et al.* 2001; Painter 2005; Thomas 1998; Thomas *et al.* 2000; Thomas *et al.* 1998; Yang *et al.* 1995; Yang *et al.* 1998). More recently, efforts have been continued in a project, Physiologically-based Pharmacokinetic and Clonal Growth Modeling: Predicting Cancer Potential of Chemical Mixtures. This project involves collecting pharmacokinetic and GST-P foci data for HCB, PCB 126, arsenic, and their binary and ternary mixtures in an established medium-term liver foci bioassay, developing PBPK and clonal growth modeling based on the data generated, and making predictions of carcinogenic potential of higher level mixtures based on the acquired understanding in the individual chemical and lower level mixtures.

As a part of the project, the dissertation research presented above concentrated on HCB, PCB 126, and their mixture (HCB+PCB 126). The results obtained are summarized as follows:

HCB pharmacokinetics and impacts of PCB 126 coexposure. HCB pharmacokinetics were examined in a time-course medium-term liver foci bioassay. In accordance with its high lipophilicity, HCB was mainly distributed in the fat, followed by the liver, kidney, blood, and muscle. The particular treatment in the rats in the bioassay, two-thirds partial hepatectomy, did not cause notable change in the disposition pattern of HCB. When HCB was co-administrated with PCB 126, its disposition was remarkably affected in two aspects: (1) The amount of HCB accumulated in the body was reduced before the partial hepatectomy and dramatically increased afterwards. We proposed that this change can be attributed to the modifications in HCB absorption and exsorption processes by PCB 126; and (2) The partitioning of HCB into the fat and liver was augmented by PCB 126, which can be resulted from the severe fat mobilization under the conditions of partial hepatectomy and the treatment of HCB+PCB 126.

HCB PBPK modeling. We developed a PBPK model for HCB under normal physiological conditions using several data sets mined from the literature. In contrast to the previous versions (Freeman *et al.* 1989; Yesair *et al.* 1986), our model included two new features: division of the blood compartment into plasma and erythrocytes due to the binding of HCB to erythrocytes, and the exsorption process (*i.e.*, the passive diffusion from plasma to the gastrointestinal lumen). The PBPK model was modified to simulate our pharmacokinetic data from the HCB bioassay with appropriate adjustments in some

parameters such as the body weight, liver volume fraction, fat volume fraction, and the rate constants of absorption and exsorption.

Carcinogenic potential of HCB, PCB 126, and their mixture. The carcinogenic potential of HCB, PCB 126, and their mixture was examined in the time-course medium-term liver foci bioassays with GST-P foci formation as the endpoint. The size, number, and size distribution of foci were determined at two doses for each chemical treatment. HCB significantly increased the foci number at 28.5 mg/kg but not 8.55 mg/kg, PCB 126 increased both the size and the number of foci at 9.8 μg/kg but not 3.3 μg/kg, and the mixture increased both indices at two doses (HCB 8.55 mg/kg + PCB 126 3.3 μg/kg and HCB 28.5 mg/kg + PCB 126 9.8 μg/kg). The treatment with HCB increased the foci number in the smaller size classes. However, PCB 126 and the mixture (HCB+PCB 126) not only increased the foci number in the smaller classes, but also stimulated the shift of foci to the higher classes (*i.e.*, foci enlargement).

We compared the foci data from the HCB, PCB 126, and the mixture bioassays. At the last time point (day 56), there appeared to be a greater-than-additivity interaction at the low doses and less-than-additivity interaction at the high doses between HCB and PCB 126 in terms of foci size and number.

Clonal growth modeling. In this research, a clonal growth model was developed. It was a semi-quantitative model that was used primarily for testing and generating hypotheses, but not for making predictions. The clonal growth model was developed first for simulating the foci data from the HCB+PCB 126 bioassay. This model was an extension of the earlier versions by Conolly *et al.* (Conolly and Andersen 1997; Conolly and Kimbell 1994; Haag-Gronlund *et al.* 2000) and Yang *et al.* (Ou *et al.* 2003; Ou *et al.*

2001; Thomas *et al.* 2000). The concept of negative selection and two-cell (types A and B; the latter with growth advantage) hypothesis were incorporated in the model. Furthermore, we explored the size-dependent growth kinetics of the initiated cells by grouping the foci into four categories by size. Each category was assumed to have distinct growth kinetics. The model was parameterized with the information from the literature and our own study. Its simulations were in good agreement with three pieces of data: relative foci volume, foci number/cm^3, and size distribution. The mixture treatment particularly stimulated the expansion of the B type mini- (2-12 cells) and medium-foci (13-400 cells). The clonal growth model was then cross-utilized to simulate the foci data in the HCB and PCB 126 bioassays with reasonable adjustments in some parameters.

The interaction between HCB and PCB 126 was also examined by comparing the growth kinetic parameters of type B initiated cells/foci under HCB, PCB 126, and the mixture treatment. At the low doses, the adjusted net growth rates (*i.e.*, the net growth rate under chemical treatment subtracted of the corresponding control) of the mini- and medium-foci under the mixture treatment were remarkably higher than the sum of the corresponding adjusted rates under the individual chemical treatments. It suggested that a greater-than-additivity interaction between HCB and PCB 126 occurred in the mini- and medium-foci categories. At the high doses, the adjusted net growth rate of the large foci under the mixture treatment appeared to be lower than the sum of the corresponding adjusted rates under the individual chemical treatments, implying that a less-than-additivity interaction between the two chemical took place in the large-foci (>400 cells) category.

This research improved our understanding in the pharmacokinetics and the pharmacodynamics regarding carcinogenic potential of HCB, PCB 126, and their mixture in the context of a medium-term liver foci bioassay. Continuing the earlier contribution in PBPK and clonal growth modeling from our laboratory, the present work added the unique perspectives of considering the pharmacokinetics and pharmacodynamics of a chemical mixture, as well as the refinement of clonal growth modeling by categorizing liver GST-P foci into different classes. Once again, we were able to illustrate how the biologically based computational modeling facilitated our study on chemical carcinogenesis.

2. FUTURE DIRECTIONS

Some issues were not addressed in this dissertation research yet deserve future study:

2.1. Effect of HCB on the pharmacokinetics of PCB 126

In the HCB+PCB 126 mixture bioassay, the tissues concentrations of PCB 126 were not determined. In this bioassay, the doses of HCB (8.55 and 28.5 mg/kg) were roughly three orders of magnitude higher than those of PCB 126 (3.3 and 9.8 μg/kg). Thus, the tissue concentrations of HCB were much higher than PCB 126. In the gas chromatograph, the tiny peak of PCB 126 was severely interfered with by the huge peak of HCB and consequently the quantification of PCB 126 was not possible. Overcoming this difficulty would be valuable for determining the pharmacokinetics of PCB 126 under the condition of HCB coexposure, hence yielding a better picture of the pharmacokinetic interaction between the two chemicals.

2.2. Characterization of A and B cells

The hypothesis that DEN-induced GST-P cells may be composed of two subpopulations, A and B, was formed from experimental observations (Dragan *et al.* 1994; Jirtle *et al.* 1991; Swenberg *et al.* 1984), and have been supported by more experimental (Yusuf *et al.* 1999) and theoretical (Conolly and Andersen 1997; Haag-Gronlund *et al.* 2000; Lu *et al.* 2006a; Ou *et al.* 2003; Ou *et al.* 2001; Thomas *et al.* 2000) evidence. However, thus far, little progress has been made in studying the two types of cells directly using proteomic and genomic approaches. It is due to two major technical difficulties: capturing GST-P cells from the liver and separating A and B cells. The former has recently been overcome by the advent of laser microdissection technique (Ogawa *et al.* 2005; Suzuki *et al.* 2004). The latter remains to be a problem and needs to be investigated. Once the A and B cells are harvested separately, their proteomic and genomic characteristics could be identified. The information would be helpful for understanding the mechanisms of preneoplastic foci development and how carcinogens affect the process.

2.3. Connection of the PBPK and clonal growth models

A PBPK model provides a dosimetry of a chemical of interest, and a clonal growth model generates a time course of development of preneoplastic foci. If the two models are coupled, a biologically based quantitative relationship between chemical exposure and liver preneoplastic foci formation can be formulated. Conceptually, the connection between the two kinds of models can be achieved by linking the dose metrics with the division and death related parameters for the initiated cells. More effort is needed to fulfill this goal.

REFERENCES

Conolly, R. B., and Andersen, M. E. (1997). Hepatic foci in rats after diethylnitrosamine initiation and 2,3,7,8-tetrachlorodibenzo-p-dioxin promotion: evaluation of a quantitative two-cell model and of CYP 1A1/1A2 as a dosimeter. *Toxicol Appl Pharmacol* **146**, 281-93.

Conolly, R. B., and Kimbell, J. S. (1994). Computer simulation of cell growth governed by stochastic processes: application to clonal growth cancer models. *Toxicol Appl Pharmacol* **124**, 284-95.

Dean, C. E., Jr. (2003). Mechanisms of hepatic tumor promotion by polychlorinated biphenyl mixtures. Ph.D. dissertation. Department of Microbiology, Immunology and Pathology. Colorado State University, Fort Collins.

Dragan, Y. P., Hully, J. R., Nakamura, J., Mass, M. J., Swenberg, J. A., and Pitot, H. C. (1994). Biochemical events during initiation of rat hepatocarcinogenesis. *Carcinogenesis* **15**, 1451-8.

el-Masri, H. A., Reardon, K. F., and Yang, R. S. H. (1997). Integrated approaches for the analysis of toxicologic interactions of chemical mixtures. *Crit Rev Toxicol* **27**, 175-97.

Freeman, R. A., Rozman, K. K., and Wilson, A. G. E. (1989). Physiological pharmacokinetic model of hexachlorobenzene in the rat. *Health Phys* **57(Suppl 1)**, 139-147.

Gustafson, D. L., Coulson, A. L., Feng, L., Pott, W. A., Thomas, R. S., Chubb, L. S., Saghir, S. A., Benjamin, S. A., and Yang, R. S. H. (1998). Use of a medium-term liver focus bioassay to assess the hepatocarcinogenicity of 1,2,4,5-tetrachlorobenzene and 1,4-dichlorobenzene. *Cancer Lett* **129**, 39-44.

Gustafson, D. L., Long, M. E., Thomas, R. S., Benjamin, S. A., and Yang, R. S. H. (2000). Comparative hepatocarcinogenicity of hexachlorobenzene, pentachlorobenzene, 1,2,4,5-tetrachlorobenzene, and 1,4-dichlorobenzene: application of a medium-term liver focus bioassay and molecular and cellular indices. *Toxicol Sci* **53**, 245-52.

Haag-Gronlund, M., Conolly, R., Scheu, G., Warngard, L., and Fransson-Steen, R. (2000). Analysis of rat liver foci growth with a quantitative two-cell model after treatment with 2,4,5,3',4'-pentachlorobiphenyl. *Toxicol Sci* **57**, 32-42.

Jirtle, R. L., Meyer, S. A., and Brockenbrough, J. S. (1991). Liver tumor promoter phenobarbital: a biphasic modulator of hepatocyte proliferation. *Prog Clin Biol Res* **369**, 209-16.

Lee, S. K., Ou, Y. C., and Yang, R. S. H. (2002). Comparison of pharmacokinetic interactions and physiologically based pharmacokinetic modeling of PCB 153 and PCB 126 in nonpregnant mice, lactating mice, and suckling pups. *Toxicol Sci* **65**, 26-34.

Liao, K. H., Gustafson, D. L., Fox, M. H., Chubb, L. S., Reardon, K. F., and Yang, R. S. H. (2001). A biologically based model of growth and senescence of Syrian hamster embryo (SHE) cells after exposure to arsenic. *Environ Health Perspect* **109**, 1207-13.

Lu, Y., Lohitnavy, M., Reddy, M., Lohitnavy, O., Eickman, E., Ashley, A., Xu, Y., and Yang, R. S. H. (2006a). Promotion of liver GST-P foci by a chemical mixture of hexachlorobenzene (HCB) and 3, 3', 4, 4', 5-pentachlorobiphenyl (PCB126): Integration of computer modeling and biology of clonal growth [Abstract]. *Toxicologist* **90**, 435.

Lu, Y., Lohitnavy, M., Reddy, M. B., Lohitnavy, O., Ashley, A., and Yang, R. S. H. (2006b). An updated physiologically based pharmacokinetic model for hexachlorobenzene: incorporation of pathophysiological states following partial hepatectomy and hexachlorobenzene treatment. *Toxicol Sci* **91**, 29-41.

Ogawa, K., Asamoto, M., Suzuki, S., Tsujimura, K., and Shirai, T. (2005). Downregulation of apoptosis revealed by laser microdissection and cDNA microarray analysis of related genes in rat liver preneoplastic lesions. *Med Mol Morphol* **38**, 23-9.

Ou, Y. C., Conolly, R. B., Thomas, R. S., Gustafson, D. L., Long, M. E., Dobrev, I. D., Chubb, L. S., Xu, Y., Lapidot, S. A., Andersen, M. E., and Yang, R. S. H. (2003). Stochastic simulation of hepatic preneoplastic foci development for four chlorobenzene congeners in a medium-term bioassay. *Toxicol Sci* **73**, 301-14.

Ou, Y. C., Conolly, R. B., Thomas, R. S., Xu, Y., Andersen, M. E., Chubb, L. S., Pitot, H. C., and Yang, R. S. H. (2001). A clonal growth model: time-course simulations of liver foci growth following penta- or hexachlorobenzene treatment in a medium-term bioassay. *Cancer Res* **61**, 1879-89.

Painter, J. T. (2005). Polychlorinated biphenyls and arsenic in hepatocarcinogenesis. Ph.D. dissertation. Department of Microbiology, Immunology and Pathology. Colorado State University, Fort Collins.

Suzuki, S., Asamoto, M., Tsujimura, K., and Shirai, T. (2004). Specific differences in gene expression profile revealed by cDNA microarray analysis of glutathione S-transferase placental form (GST-P) immunohistochemically positive rat liver foci and surrounding tissue. *Carcinogenesis* **25**, 439-43.

Swenberg, J. A., Dyroff, M. C., Bedell, M. A., Popp, J. A., Huh, N., Kirstein, U., and Rajewsky, M. F. (1984). O4-ethyldeoxythymidine, but not O6-ethyldeoxyguanosine, accumulates in hepatocyte DNA of rats exposed continuously to diethylnitrosamine. *Proc Natl Acad Sci U S A* **81**, 1692-5.

Thomas, R. S. (1998). The Use of Biologically-Based Models for Integrating Short-Term Cancer Bioassays, Mechanisms of Action, and Target Tissue Dosimetry: Application to Pentachlorobenzene. Ph.D. dissertation. Department of Environmental Health, Colorado State University, Fort Collins, CO.

Thomas, R. S., Conolly, R. B., Gustafson, D. L., Long, M. E., Benjamin, S. A., and Yang, R. S. H. (2000). A physiologically based pharmacodynamic analysis of hepatic

foci within a medium-term liver bioassay using pentachlorobenzene as a promoter and diethylnitrosamine as an initiator. *Toxicol Appl Pharmacol* **166**, 128-37.

Thomas, R. S., Gustafson, D. L., Ramsdell, H. S., el-Masri, H. A., Benjamin, S. A., and Yang, R. S. H. (1998). Enhanced regional expression of glutathione S-transferase P1-1 with colocalized AP-1 and CYP 1A2 induction in chlorobenzene-induced porphyria. *Toxicol Appl Pharmacol* **150**, 22-31.

Yang, R. S. H., el-Masri, H. A., Thomas, R. S., Constan, A. A., and Tessari, J. D. (1995). The application of physiologically based pharmacokinetic/pharmacodynamic (PBPK/PD) modeling for exploring risk assessment approaches of chemical mixtures. *Toxicol Lett* **79**, 193-200.

Yang, R. S. H., Thomas, R. S., Gustafson, D. L., Campain, J., Benjamin, S. A., Verhaar, H. J., and Mumtaz, M. M. (1998). Approaches to developing alternative and predictive toxicology based on PBPK/PD and QSAR modeling. *Environ Health Perspect* **106 Suppl 6**, 1385-93.

Yesair, D. W., Feder, P. I., Chin, A. E., Naber, S. J., Kuiper-Goodman, T., Scott, C. S., and Robinson, P. E. (1986). Development, evaluation and use of a pharmacokinetic model for hexachlorobenzene. *IARC Sci Publ* **77**, 297-318.

Yusuf, A., Rao, P. M., Rajalakshmi, S., and Sarma, D. S. (1999). Development of resistance during the early stages of experimental liver carcinogenesis. *Carcinogenesis* **20**, 1641-4.

APPENDICES

APPENDIX I: Equations of the PBPK Model for Hexachlorobenzene

In the fat (F) and rapidly (R) and slowly (S) perfused compartments, the mass balance for the concentrations, CX, is

$$VX \times \frac{dCX}{dt} = QX \times (CA - CVX) \quad \text{(AI-1)}$$

where X stands for F, R, and S, t is time, VX is the volume of each compartment, QX is the plasma flow rate to each compartment, CA is the concentration in plasma, and CVX is the plasma concentration leaving each compartment.

In the liver (L), the mass balance for the concentration, CL, is

$$VL \times \frac{dCL}{dt} = QL \times (CA - CVL) - KMET \times CVL + KGILV1 \times AGIUp + KGILV2 \times AGILow \quad \text{(AI-2)}$$

where KMET is the metabolism rate constant in the liver, KGILV1 and KGILV2 are the absorption rate constants from the upper and the lower GI lumen compartments, and the AGIUp and AGILow are the amounts of HCB in the two GI lumen compartments.

In the blood, the change of HCB amount is same as the change in plasma due to tissue uptake and exsorption. The mass balance for the concentration, CBld, is

$$VBld \times \frac{dCBld}{dt} = (\sum QZ \times CVZ) - QC \times CA - KBGI \times CA \quad \text{(AI-3)}$$

where Bld represents blood, Z stands for F, R, S, and L, QC is the cardiac output of plasma, and KBGI is the rate constant of exsorption. The concentration in plasma, CA, assumed linearly related to CBld, is

$$CA = \frac{CBld}{RBldPlsm} \quad \text{(AI-4)}$$

where RBldPlsm is the ratio of blood concentration over plasma concentration which can be experimentally determined at equilibrium.

The mass balance in the upper GI lumen is

$$\frac{dAGIUp}{dt} = -KGILV1 \times AGIUp - KGIUpLow \times AGIUp \quad \text{(AI-5)}$$

where KGIUpLow is the rate constant of mass transfer from the upper to the lower GI lumen compartment. For iv dosing, AGIUp is 0. In the lower GI lumen compartment, the mass balance is

$$\frac{dAGILow}{dt} = KGIUpLow \times AGIUp - KGILV2 \times AGILow + KBGI \times CA - KFEC \times AGILow \quad \text{(AI-6)}$$

where KFEC is the fecal excretion rate constant.

Appendix II: Computer Code of the PBPK Model for Hexachlorobenzene

```
PROGRAM HighDoseBioassay.csl

!Finalized by Y.Lu 2/8/2005.
!MulOral.csl is modified to simulate QCT HCB data (Y.LU et al.) from a medium-
!term liver foci bioassay.
!Time 0 is the time of DEN initiation (day 0); fist gavage(day 14).
!The codes for HCB under the conditions of single iv dose, single oral, and multiple oral
!dosing were written separately. Here only the code for the high dose of liver foci
!bioassay is presented.
!---------!---------!---------!---------!---------!---------!---------!--------

INITIAL

!Physiological parameters
Table BWt,1,8/0., 336., 480., 504., 576., 672., 1128., 1344.,&
    0.1695, 0.1932, 0.205, 0.205, 0.1956, 0.2074, 0.2703, 0.3057/
        !High dose group body weight; QCT data, Y.Lu et al.
Table VLt,1,7/0., 503., 504., 576., 672., 1128., 1344.,&
          0.0059, 0.0076, 0.0023, 0.0053, 0.007, 0.0093, 0.0105/
        !Liver volume,L. Time 0 value is an estimate (3.5% BW is liver); Hour
        !504 value is also an estimate (30% liver of day 20), Y.Lu et al data
 BW=BWt(t)
 VL=VLt(t)
constant VBC=0.062D0        !Blood volume fraction; (D0,explicit double precision)
        !Lee,H.B., Blaufox,M.D. Blood volume in the rat. J Nucl Med,1985, 25:72-76
constant HMTC=0.367D0       !Corrected hematocrit; Lee and Blaufox,1985
constant QCC=14.1D0         !Cardiac output constant,L/hr/kg**0.75; Brown et al.1997
constant QFC=0.07D0         !Fat blood flow fraction; Brown et al.1997
constant QLC=0.18D0         !Liver blood flow fraction; Brown et al.1997
constant QRC=0.58D0         !Rapidly blood flow fraction; 0.76-QLC
 QSC=1.0-QFC-QLC-QRC
 VFC=(35*BW+0.205)/100      !Fat volume fraction at initial condition
constant a=1.1d0 !0.694d0   !Fit to my hypothesized pattern of the change in fat
constant b=0.017d0          !Volume fraction to describe fat mobilization and
constant c=6.0d-5           !Rebuildup.

!Scaled parameters
 VF=BW*VFC                  !Fat volume,L
 VB=BW*VBC+0.0012           !Blood volume,L; Lee and Blaufox,1985
```

```
VRBC=HMTC*VB                !Red Blood Cells volume, L
VPlsm=(1.0-HMTC)*VB         !Plasma volume, L
VR=(33.3*BW+12.03)/1000.0   !Rapidly=total organ-liver,L; Schoeffner et al. 1999
VS=0.91*BW-VF-VL-VB-VR      !Slowly perfused, L
QBld=QCC*BW**0.75           !Blood cardiac output, L/hr; Brown et al.1997
QC=(1.0-HMTC)*QBld          !Plasma cardiac output, L/hr
QF=QC*QFC                   !Fat blood flow rate, L/hr
QL=QC*QLC                   !Liver blood flow rate, L/hr
QR=QC*QRC                   !Rapidly blood flow rate, L/hr
QS=QC*QSC                   !Slowly blood flow rate, L/hr

!Chemical-specific paramters
!Partition coefficients
constant PF=200D0
  !Estimate from our data ([Fat]/[Blood]*4.87),disagreeing with estimate from
  !Koss data (315.0).
  !Possible reasons:1.disposition of HCB in fat has not reached steady state.
  !2.Higher blood free fatty acid concentration in PHed than in normal rats.
  !3.Alteration in fat composition. The 3rd one is very likely.
constant PL=10.7D0  !Liver:plasma; estimated from Koss et al. Arch Toxicol 1978
constant PR=7.0D0   !Rapidly:plasma; estimated from Koss et al. Arch Toxicol 1978
constant PS=3.2D0   !Slowly:plasma; adopted from Freeman et al. Health Phys 1989

!Partition into RBC
constant FPlsm=0.13D0       !Fraction of HCB mass in plasma
 !Gomez-Catalan,J. Transport of organo-chlorine residues in rat and human blood.
 !1991, Arch Environ Contamin Toxicol, 20:61-66
RRbcPl=((1.0-FPlsm)/HMTC)/(FPlsm/(1.0-HMTC))      ![RBC]/[plasma]=11.54
RBldPlsm=(1/1)/(FPlsm/(1.0-HMTC))                 ![Blood]/[Plasma]=4.87

!Elimination parameters
constant KBGI=0.095D0       !L/hr, from blood to lower GI lumen, visual fit
constant KGILV1=0.012D0     !/hr, from upper GI lumen to liver, visual fit
constant KGILV2=7D-4        !/hr, lower GI to liver, visual fit
constant KUpLow=0.004D0     !from upper to lower GI lumen; from HCBiv model
constant KFEC=0.0014D0      !/hr, excretion in feces; from SinOral model
constant KMET=0.00195D0     !metabolism, L/hr; adopted fom HCBiv model

!Simulation parameters
constant TSTOP=1350         !hr.
cinterval CINT=0.1          !Communication interval, hr

!Initial total dose
 TotalDose=0.0
constant DoseRate0=28.5d0   !mg/kg
```

```
!Dosetime and frequency
 DoseFrq=24.0                !hrs, daily dosing
 k=0                         !counter of doses

END                          !of initial
!---------!---------!---------!---------!---------!---------!---------!--------
DYNAMIC

ALGORITHM IALG=2

!Amount removed with 2/3 liver
IF (T.eq.503.9) THEN
  AL=AL*0.3
  ARemove=AL*0.7
 ELSE
  AL=AL
ENDIF                        !These lines should be in this part; otherwise it is wrong.

DERIVATIVE
!These parameters are updated at each round of calculation.
 BW=BWt(t)
 VL=VLt(t)
 VFC=(35*BW+0.205)/100
 VF=BW*VFC                   !Fat volume,L
 VB=BW*VBC+0.0012            !Blood volume,L;Lee and Blaufox,1985
 VRBC=HMTC*VB                !Red Blood Cells volume,L
 VPlsm=(1.0-HMTC)*VB         !Plasma volume,L
 VR=(33.3*BW+12.03)/1000.0   !Rapidly=total organ-liver,L; Schoeffner et al. 1999
 VS=0.91*BW-VF-VL-VB-VR      !Slowly perfused, L
 QBld=QCC*BW**0.75           !Blood cardiac output, L/hr; Brown et al.1997
 QC=(1.0-HMTC)*QBld          !Plasma cardiac output, L/hr
 QF=QC*QFC                   !Fat blood flow rate, L/hr
 QL=QC*QLC                   !Liver blood flow rate, L/hr
 QR=QC*QRC                   !Rapidly blood flow rate, L/hr
 QS=QC*QSC                   !Slowly blood flow rate, L/hr

!Dose rate and dose
IF (t.lt.336.0) THEN
  Doserate=0.0D0             !mg/kg
  Dose=0.0
 ELSE IF (t.gt.480.0.and.t.lt.600) THEN
  Doserate=0.0
  Dose=0.0
 ELSE
  Doserate=Doserate0         !mg/kg
```

```
  Dose=BW*Doserate
ENDIF

IF (T.lt.504) THEN
  VFC=(35*BW+0.205)/100
 ELSE
  VFC=a*exp(-b*(T-336.))+c*(T-336.)        !Fat mobilization and re-buildup
ENDIF                                      !Thomas R. PhD thesis
!---------!---------!---------!---------!---------!---------!---------!--------
!Mass balance in fat
 RAF=QF*(CA-CVF)
 AF=INTEG(RAF,0.0)
 CF=AF/VF
 CVF=CF/PF

!Mass balance in liver
 RAL=QL*(CA-CVL)-KMET*CVL+KGILV1*AGIUp+KGILV2*AGILow
 AL=INTEG(RAL,0.0)
 CL=AL/VL
 CVL=CL/PL

  RAbsorb=KGILV1*AGIUp+KGILV2*AGILow
  Absorb=integ(RAbsorb,0.)

!Amount metabolized
 RAM=KMET*CVL
 AM=INTEG(RAM,0.0)

!Mass balance in rapidly perfused tissues
 RAR=QR*(CA-CVR)
 AR=INTEG(RAR,0.0)
 CR=AR/VR
 CVR=CR/PR

!Mass balance in slowly perfused tissues
 RAS=QS*(CA-CVS)
 AS=INTEG(RAS,0.0)
 CS=AS/VS
 CVS=CS/PS

!Mass balance in blood
 RAB=QF*CVF+QL*CVL+QR*CVR+QS*CVS-QC*CA-KBGI*CA
 AB=INTEG(RAB,0.0)
 CB=AB/VB                          !Blood concentration
 CA=CB/RBldPlsm                    !Plasma concentration
```

```
!Upper GI lumen
 RAGIUp=-KGILV1*AGIUp-KUpLow*AGIUp
 AGIUp=INTEG(RAGIUp,0.0)+totaldose

!Lower GI lumen
 RAGILow=KUpLow*AGIUp-KGILV2*AGILow+KBGI*CA-KFEC*AGILow
 AGILow=INTEG(RAGILow,0.0)
 AGI=AGIUp+AGILow

!Exsorption to GI
 RAEXS=KBGI*CA
 AEXS=INTEG(RAEXS,0.)
 PERAEXS=AEXS/(TOTALDOSE+1D-30)*100

!Excretion in feces
 RAFEC=KFEC*AGILow
 AFEC=INTEG(RAFEC,0.0)

!------------Total dose---------------------------------------
!Total mass
! TMASS=AF+AL+AM+AR+AS+AB+AGIup+AGIlow+AFEC
! MB=(TotalDose-TMASS)*100.0/(TotalDose+1d-30)
!Don't know how to write the equation for TMASS in which the portion
!of HCB removed with the 2/3 liver is included.

PROCEDURAL
dosetime=k*DoseFrq
IF (t.ge.dosetime) THEN
  TotalDose=TotalDose+Dose
  k=k+1
ENDIF
END

TERMT (T.GE.TSTOP)
END             !OF DERIVATIVE
END             !OF DYNAMIC
END             !OF PROGRAM
```

```
!File HighDoseBioassay.cmd. Command file.
!high dose group, 28.5mg/kg

SET GRDCPL=.F.              !no grid on line plots
SET TITLE = 'HCB model-Liver foci bioassay, high dose'
PREPARE /ALL

PROCEDURE CHECK
START
PLOT TMASS, TOTALDOSE, MB
PRINT T,TMASS,TOTALDOSE, MB
END

PROCEDURE BW
plot /DATA=BodyWt bw /char=3 /xtag='hr' /tag='Body weight (kg)'
plot /DATA=LiverWt vl /char=3 /xtag='hr' /tag='Liver volume percent'
plot Vf /char=3 /xtag='hr' /tag='Fat volume (L)'
End

DATA BodyWt (T,BW)              !kg
0       0.1695
336     0.1932
480     0.2050
504     0.2050
576     0.1956
672     0.2074
1128    0.2703
1344    0.3057
END

DATA LiverWt (T,vl)             !L
0.0     0.0059
503.9   0.0076
504.    0.0023
576.    0.0053
672.    0.0070
1128.   0.0093
1344.   0.0105
END

PROCED plots
START
PLOT /DATA=QCT CF /lo=0 /char=2 /xtag='hr' /tag='Fat mg/L'
PLOT /DATA=QCT CL /lo=0 /char=1 /xtag='hr' /tag='Liver mg/L'
PLOT /DATA=QCT CR /lo=0 /char=5 /xtag='hr' /tag='Rapidly mg/L'
PLOT /DATA=QCT CS /lo=0 /char=5 /xtag='hr' /tag='Slowly mg/L'
```

```
PLOT /DATA=QCT CB /lo=0 /char=3 /xtag='hr' /tag='Blood mg/L'
END

DATA QCT(T,CB,CL,CS,CF,CR)                    !mg/L
480    4.57   10.19  3.74   207.71 9.41
576    4.37   14.67  5.46   156.91 6.48
672    8.75   19.31  7.5    345.99 11.34
1128   11.94  28.61  9.19   580.49 20.55
1344   13.2   35.39  10.09  593.89 24.02
END
```

Appendix III: Computer Code of the Clonal Growth Model for the Mixture of Hexachlorobenzene and PCB 126

```
PROGRAM BinaryMixtureLu.CSL

!Yasong Lu,starting on 9/1/04; preliminarily done on 11/17/04; scrutinized on 11/17/04.

!This code is to simulate the GST-P foci formation following DEN/Binary Mixture (HCB+PCB 126)
!treatment in male F344 rats. The study was run by Y.Lu and M.Lohitnavy et al. in 2003.
!This code is based on YC Ou's code for HCB (Cancer Res 2001).
!ACSL tox 11.8. Size 10 perfect for printing.

!Initially, the growth kinetics of foci was seen not related to focal size. It was not hard to fit the volume
!fraction and number simultaneously. However, it was not possible to also fit the size distribution data.
!Thus, the clones were categorized into four kinds: single cell, minifoci (2-12 cells), multicell foci (13-400
!cells), and big foci in terms of growth kinetics. This strategy greatly improves the description of the size
!distribution data. When a focus is very big, the average growth rate in terms of the whole cell population
!in the foci is likely to be low. That kind of size, however, may not be reached in our studies.

!This code cannot be migrated to acslXtreme directly. Modifications of syntaxes ('write' not supported) and
!structures (switching out (goto) an 'if-then-else' structure) are necessary.

!1/19/05.
!Initially the cutoff for 2D to 3D conversion was set constant (50.12um), accordingly the cutoffcellno of
!detectable clones varied with hepatocyte density. The variation of cutoffcellno caused spiking on the
!predicted curve of foci number of the low and high dose groups.
!My second thought is that setting the cutoffcellno constant (2 cells in 2D,conversion needed) is more
!reasonable as all the clones having 2 or more than 2 cells were counted in the immunohistochemically
!stained slides. Now the problem is how to convert a 2D 2-cell cutoff to a 3D cutoffcellno.

!8/1/05.
!Revisit this code because in my manuscript I would like to have the model simulations (volume and
!number) of multiple runs rather than a single run.
!I don't know how to deal with this situation in this code; but AEgis suggested the use of m file in ACSL
!Math. The correspondence and all m files are attached in Notebook Binary II.
!Similar averages were obtained from 20, 25, 50, and 100 runs. I will set 20 runs for all dose groups.

!This code should be run at double precision; at single precision, Array A overflows and the program aborts.

!8/28/05. Comments on initiated cell growth added.

!9/2/05. Modified successfully to calculate the average size distribution of multiple runs. Still don't know
!how to get the average time-course voldetect and cnumdetect. Can use the averages of the five time points
!to do parameterization.

!6/21/06. Modified to include calculations of standard deviations of the volumes and numbers simulated by
!multiple runs of the model, and to include the variables of size distribution necessary for optimization.

INITIAL
```

```
!MISCELLANEOUS
integer i,j(3),k,w,seed1,seed2,repeat,count
integer losta,lostb,invisa,invisb,invis
integer cnumdetecta,cnumdetectb,cnumt,cnumta,cnumtb
integer cmax,cmaxx,numsum,repeatsizesum
integer n0a,n0b
parameter (cmax=50000, cmaxx=100000)
dimension clonesa(cmax,2),clonesb(cmax,2)
  !only 3-dimensional (3D) data; 2D not considered.
  !cmax rows and 2 columns, column 1 for clonal cell number and column 2 for clonal volume converted
  !from cell number. The column 2 will be used for size distribution.
dimension bin3d(25,101),clones(cmaxx,2),repeatsize(25,50)
dimension repeatsizeday7(25,50),repeatsizeday14(25,50)
dimension repeatsizeday20(25,50),repeatsizeday24(25,50)
dimension repeatsizeday28(25,50),repeatsizeday47(25,50)
dimension repeatsizeday56(25,50)
dimension sizedist20(15),sizedist24(15),sizedist28(15)
dimension sizedist47(15),sizedist56(15)
  !Bin3d(25,101) stores clone numbers of all 25 size classes;
  !clones stores all A and B foci.
  !RepeatsizedayXX(25,50) stores clone numbers and the averages of repeated runs of all 25 classes on
  !dayXX; here 50 implies the max repeat number is 49. The last column is for the averages. For more runs
  !"50" should be replaced with a larger number.
  !SizedistXX(15) stores the first 15 classes of foci of the final result; those after 15 are expected to be 0
  !and thus ignored. It is defined for display the size distribution at each time point.
logical dist
constant dist = .false.
logical messa,messb
messa = .false.
messb = .false.
character buffer*80   !for writing to the screen in ACSL for Windows
constant buffer = ' '
constant jmod2=2000437866
constant jmod3=1999976575

!SEEDS FOR RANDOM NUMBER GENERATOR
j(2)=jmod2
j(3)=jmod3
seed1=j(2)
seed2=j(3)

!Define arrays for storing results of multiple runs.
!Store sums of voltotdetect and cnumdetect of the 5 time points (20,24, 28,47,and 56) from multiple runs.
!Cannot store all points in this way.
!For that purpose, ACSL Math is used to define arrays for the results having the same sizes as 'days'
!(Suggestion from AEgis).
dimension multisumclonedata(5,2)
do rew2 i = 1,5
  do tre2  k = 1,2
    multisumclonedata(i,k) = 0
  tre2: continue
rew2: continue

!Store averages of multiple runs
dimension meanclonedata(5,2)
do rew3 i = 1,5
```

```
  do tre3  k = 1,2
    meanclonedata(i,k) = 0
  tre3: continue
rew3: continue

!For calculating standard deviations of results
dimension sumsqclonedata(5,2)
do rew40 i = 1,5
  do tre40  k = 1,2
    sumsqclonedata(i,k) = 0
  tre40: continue
rew40: continue

dimension sdterm1_clonedata(5,2)
do rew41 i = 1,5
  do tre41  k = 1,2
    sdterm1_clonedata(i,k) = 0
  tre41: continue
rew41: continue

dimension sdclonedata(5,2)
do rew42 i = 1,5
  do tre42  k = 1,2
    sdclonedata(i,k) = 0
  tre42: continue
rew42: continue

!Initialize the repeatsize dimension
do rew4 i = 1,25
  do tre4  k = 1,50
    repeatsizeday7(i,k) = 0
    repeatsizeday14(i,k) = 0
    repeatsizeday20(i,k) = 0
    repeatsizeday24(i,k) = 0
    repeatsizeday28(i,k) = 0
    repeatsizeday47(i,k) = 0
    repeatsizeday56(i,k) = 0
    repeatsize(i,k) = 0
  tre4: continue
rew4: continue

!Initialize the sizedist dimensions
do rew5 i = 1,15
    sizedist20(i)=0
    sizedist24(i)=0
    sizedist28(i)=0
    sizedist47(i)=0
    sizedist56(i)=0
rew5: continue

!Initialize the sum of all repeatsize in the same class
  repeatsizesum = 0

constant repeat=1          !multiple runs if repeat > 1; results of each run stored
count=0                    !initialize counter for multiple runs
!**************
```

```
!RESTART FOR MULTIPLE RUNS TO SEE STOCHASTIC BEHAVIOR
begin: continue              !restart here
count=count+1                !run number
if (repeat.gt.1) then
  write(buffer,25) count,repeat
  call disstr(buffer)
  25: format(' Starting run number ',i3,'   of ',i3)
endif

!DIFFERENT PROMOTER DOSE LEVEL/DIFFERENT CELL GROWTH KINETICS
constant promodose = -1   !promoter dose
      !test birth and death rate, only DEN, promoter dose = -1;
      !DEN control group, promoter dose = 0;
      !Mixture low, promoter dose = 1;
      !Mixture high, promoter dose = 2;
      !Dose-specific parameters are defined separately rather than being bound in TABLE functions for
      !readability.

!TIMING COMMANDS
variable days              !name of independent variable
days = 0.                  !initialize
weeks = 0.                 !initialize, use weeks for plotting
months = 0.                !initialize, use for plotting
constant pmax = 0.05       !max. prob. used for stochastic calculations
constant tstop = 60.       !duration of simulated experiment
cinterval cint = 0.1       !interval for saving simulated data

!LIVER
!hepatocyte volume and cutoffcellnumber value adjusted w/ time following DEN and corn oil treatment
!hespdt following HCB+PCB 126 mixture set in CMD file separately
table hepsdtdays,1,7/0., 14., 20., 24., 28., 47., 56., &
    1.20e8, 1.20e8, 1.14e8, 1.20e8, 1.10e8, 1.16e8, 1.01e8/
!Experimentally derived at CETT by Y. Lu, Aug., 2004
constant hepsdt0 = 1.20e8
hepsdt = hepsdtdays(days)

constant cutoffcellno=7.9          !clones detectable if bigger than 7.9 cells.
!When hepatocytes are not enlarged (in the early stage and in the control group) the cutoff of 3D
!conversion is 50.12 um, which is corresponding to 65922.16 um^3 = 6.59222e-8 cm^3 and density of
!1.2e8/cm^3. Here the cutoff of cell number in a clone is the product of hepsdt0 and 6.59222e-8 cm^3.
!Same value is obtained when hepsdt and cutoff of conversion are 6e7 and 63.1 um. The underlying
!mathematic calculation is same as the one in Conolly & Andersen 1997 TAP.
!The cutoffcellno is set constant as the same value is obtained for different senarios of hepsdt and cutoff for
!conversion.
!The cutoff for conversion is adjusted to account for the variation of hepsdt.
!Day          0     14      20      24      28      47      56
!Control
!Hepsdt       1.2e8 1.2e8   1.14e8  1.2e8   1.1e8   1.16e8  1e8
!Cutoff for
!conversion(um) 50.12 50.12  50.12   50.12   50.12   50.12   50.12
!Low
!Hepsdt       1.2e8 1.2e8   9.9e7   9.9e7   8.3e7   5.69e7  6.43e7
!Cutoff for
!conversion(um) 50.12 50.12  50.12   50.12   63.1    63.1    63.1
!High
!Hepsdt       1.2e8 1.2e8   9.7e7   1e8     8.12e7  6e7     6.4e7
```

```
!Cutoff for
!conversion(um)  50.12    50.12    50.12    50.12    63.1     63.1     63.1
!Hepsdt 0.9-1.2e8 <---> 50.12 um
!Hepsdt 5.0-9.0e7 <---> 63.1  um

constant cutoffvolum0 = 6.59222e-8      !cm^3,~ 50.12 um diameter,hepsdt 0.9-1.2e8
constant cutoffvolum1 = 1.31549e-7      !cm^3,~ 63.10 um diameter,hepsdt 5.0-9.0e7
   cutoffvolum = 0.                     !Adjusted by treatment and days (actually hespdt)
constant lw = 7.0                       !liver weight at start of experiment (g)
                                        !3.5% of the body weight of 200g
lwc = lw                                !lw determined by division and death rates
an0 = lw*hepsdt0                        !number of hepatocytes at start of experiment
an0c = an0                              !number of hepatocytes in lwc
constant pmutac = 1.7e-6                !basal prob. of mutation to "a".Source?
constant pmutbc = 1.7e-6                !basal prob. of mutation to "b".Source?
pmuta = pmutac
pmutb = pmutbc
constant slimit = 1000.                 !deterministic growth if > slimit (# of cells)

!MALE F-344 RAT CONTROL LIVER NORMAL CELL GROWTH RATES
constant rbn0c = 2.27519e-3             !division rate (1/days) at day 0.Kato 1993.
rbn0=rbn0c
constant rdn0c = 8.6e-4                 !death rate (1/days),=lowest birth rate
                                        !Liver weight insensitive to this parameter.
rdn0 =rdn0c

!PARTIAL HEPATECTOMY
constant phtime = 21.0                  !day of partial hepatectomy
constant phremove = 0.7                 !fraction of liver removed by PH
constant rcpdel = 0.5                   !delay until regen. cell prolif. (days)
remvwt = 0.                             !liver weight removed
remvcell = 0.                           !liver cells removed

!TIME FOR START OF MIXTURE EXPOSURE
constant mixtime = 14.                  !(days)

!Growth of "A" CELLS
rbn1a = 0.0                             !initialization;stepwise adjusted
rdn1a = 0.0                             !initialization;stepwise adjusted
deltaa= 0.0                             !=rbn1a-rdn1a
constant cycletime = 1.4125             !(Rotstein, Cancer Res.46:2377,1986)
constant apoptime = 0.1667              !length of apoptosis [4 hr] (day)
constant famax = 1.0                    !birth/death parameter boundary
constant minitomulti=12                 !divider between mini- and multicell-foci;
                                        !sensitive
constant multitobig=400                 !divider between multicell- and big foci
                                        !predictions are not sensitive to multitobig0; in the range of
                                        !200-4000 predictions are not significantly affected.
faincycle=0.
fasingleincycle=0.
faminiincycle=0.
famultiincycle=0.
fabigincycle=0.

!Growthof "B" CELLS
rbn1b = 0.0                             !initialization;stepwise adjusted
```

```
rdn1b = 0.0                          !initialization;stepwise adjusted
deltab= 0.0                          !=rbn1b-rdn1b
constant fbmax = 1.0                 !birth/death parameter bounding
fbincycle=0.
fbsingleincycle=0.
fbminiincycle=0.
fbmultiincycle=0.
fbbigincycle=0.

!INITIALIZATIONS AT START OF RUN
do 11 i = 1,cmax
  clonesa(i,1) = -1
  clonesa(i,2) = -1
  clonesb(i,1) = -1
  clonesb(i,2) = -1
11: continue

!SIZE DISTRIBUTION
if (.not.dist) goto outdis
do 19 i = 1,25
  do 18 w = 1,101
    bin3d(i,w) = 0!
  18: continue
19: continue
  !25 size classes in Xu's improved conversion method.
  !Maximum diameter of the smallest class is 63.1 um and increased by 10^0.1 until 15848.93 um in the
  !largest class. Actually the foci in our study will only occupy the first 10-15 classes.
  !The cell number is sucessively doubled along the classes, given the cell density is constant.
outdis..continue

!Deterministic calculation
ica = 0.        !initial number deterministic intermediate cells
icb = 0.        !initial number deterministic intermediate cells
numad = 0.      !all deterministic clone A number
numbd = 0.      !all deterministic clone B number
numtotd = 0.    !deterministic clone number
n0n1a = 0.      !expected number of muts. per cm**3 during time step
n0n1b = 0.      !expected number of muts. per cm**3 during time step
voltotd = 0.    !all foci volume percentage

!Stochastic calculation
xma = 0.        !expected number of muts. per cm**3 during time step
xmb = 0.        !expected number of muts. per cm**3 during time step
n0a = 0.        !real number of muts. per cm**3 during time step
n0b = 0.        !real number of muts. per cm**3 during time step
mutota = 0      !total number of mutations per cm**3
mutotb = 0      !total number of mutations per cm**3
losta = 0       !number of extinct clones per cm**3
lostb = 0       !number of extinct clones per cm**3
singlea = 0     !number of sinlge cell A per cm**3
singleb = 0     !number of sinlge cell B per cm**3
single = 0      !number of sinlge cell per cm**3
allcellnoa = 0. !all cells in all clones per cm**3
allcellnob = 0. !all cells in all clones per cm**3
detectcellnoa = 0.      !all cells in detectable clones/cm**3
detectcellnob = 0.      !all cells in detectable clones/cm**3
```

```
cnumdetecta = 0.          !number of clones detectable per cm**3
cnumdetectb = 0.          !number of clones detectable per cm**3
cnumdetect=0.             !total number of detectable clones A+B
cnumta = 0.               !number of clones per cm**3
cnumtb = 0.               !number of clones per cm**3
cnumt = 0.                !number of clones per cm**3
vola = 0.                 !volume percentage of A clones
volb = 0.                 !volume percentage of B clones
voltot = 0.               !volume percentage of all clones
voladetect = 0.           !volume percentage of detectable clones
volbdetect = 0.           !volume percentage of detectable clones
voltotdetect = 0.         !total volume percentage of detectable clones A+B
avga = 0.                 !average cell number per clone (detectable)
avgb = 0.                 !average cell number per clone (detectable)
fatboya = 0.              !size (cell number) of biggest clone
fatboyb = 0.              !size (cell number) of biggest clone
invisa = 0.               !number of undetectable clones
invisb = 0.               !number of undetectable clones
invis = 0.                !number of undetectable clones

!Initiated cell growth
rbn1asingle=0.
rbn1amini=0.
rbn1amulti=0.
rbn1abig=0.
rdn1asingle=0.
rdn1amini=0.
rdn1amulti=0.
rdn1abig=0.
rbn1bsingle=0.
rbn1bmini=0.
rbn1bmulti=0.
rbn1bbig=0.
rdn1bsingle=0.
rdn1bmini=0.
rdn1bmulti=0.
rdn1bbig=0.
deltaasingle=0.
deltaamini=0.
deltaamulti=0.
deltaabig=0.
deltabsingle=0.
deltabmini=0.
deltabmulti=0.
deltabbig=0.

!Size classes,with conversion cutoff of 50.12 um.
!Allocation in to classes based on volume rather than cell number
constant volclass1 = 1.31549e-7    !cm**3,max diameter 63.1   um
constant volclass2 = 2.62393e-7    !cm**3,max diameter 79.43  um
constant volclass3 = 5.23598e-7    !cm**3,max diameter 100    um
constant volclass4 = 1.04465e-6    !cm**3,max diameter 125.89 um
constant volclass5 = 2.08451e-6    !cm**3,max diameter 158.49 um
constant volclass6 = 4.15933e-6    !cm**3,max diameter 199.53 um
constant volclass7 = 8.29861e-6    !cm**3,max diameter 251.19 um
constant volclass8 = 1.6558e-5     !cm**3,max diameter 316.23 um
```

```
constant volclass9 = 3.30375e-5     !cm**3,max diameter 398.11  um
constant volclass10= 6.59182e-5     !cm**3,max diameter 501.19  um
constant volclass11= 1.315236e-4    !cm**3,max diameter 630.96  um
constant volclass12= 2.624225e-4    !cm**3,max diameter 794.33  um
constant volclass13= 5.235983e-4    !cm**3,max diameter 1000    um
constant volclass14= 1.044727e-3    !cm**3,max diameter 1258.93 um
constant volclass15= 2.084470e-3    !cm**3,max diameter 1584.89 um
constant volclass16= 4.159075e-3    !cm**3,max diameter 1995.26 um
constant volclass17= 8.29851e-3     !cm**3,max diameter 2511.89 um
constant volclass18= 1.655767e-2    !cm**3,max diameter 3162.28 um
constant volclass19= 3.303678e-2    !cm**3,max diameter 3981.07 um
constant volclass20= 6.591703e-2    !cm**3,max diameter 5011.87 um
constant volclass21= 0.13152174     !cm**3,max diameter 6309.57 um
constant volclass22= 0.26242057     !cm**3,max diameter 7943.28 um
constant volclass23= 0.52359833     !cm**3,max diameter 10000   um
constant volclass24= 1.044715       !cm**3,max diameter 12589.25 um
constant volclass25= 2.08448175     !cm**3,max diameter 15848.93 um
  !At density 1.2e8/cm^3,cell number = 8*2^(N-1), N is class number
  !At density 0.6e8/cm^3,cell number = 8*2^(N-2), N class number,>=2
  !When hepatocyte is enlarged,orinigal class N is shifted to N+1.

!Initial number in each class;they, as variables like voltotdetect, are
!necessary for optimization
        sizeclass1=0
        sizeclass2=0
        sizeclass3=0
        sizeclass4=0
        sizeclass5=0
        sizeclass6=0
        sizeclass7=0
        sizeclass8=0
        sizeclass9=0
        sizeclass10=0
        sizeclass11=0
        sizeclass12=0
        sizeclass13=0
        sizeclass14=0
        sizeclass15=0

logical DEN
constant DEN=.true.             !always given DEN in our experimental condition
constant dentime=0.
constant deneffdelay=0.04       !DEN effects appear 1hr post-dosing.Assumption.
constant turnoff1=7.            !reduce DEN effects
constant turnoff2=14.           !reduce DEN effects

logical PH
constant PH=.true.              !always PH in our experimental condition
constant phon=21.               !PH time
constant phoff=24.              !reduce PH effects
constant phoff2=28.             !reduce PH effects,adjust cell growth kinetics

schedule Maincore .at. 0.

if (DEN) then
schedule DENON .at. dentime+deneffdelay
```

```
schedule DENOFF1 .at. turnoff1
schedule DENOFF2 .at. turnoff2
end if

if (PH) then
schedule PHepON .at. phon+rcpdel
schedule PHepOff1 .at. phoff+rcpdel
schedule PHepOff2 .at. phoff2+rcpdel
end if

c1 = 0.1

dimension clonedata(5,2)            !Store voltotdetect and cnumdetect at 5 time points
do rew i = 1,5
  do tre  k = 1,2
    clonedata(i,k) = -1
  tre: continue
rew: continue

END                                 !of INITIAL section
!--------1---------2---------3---------4---------5---------6---------7---------8
DYNAMIC

DISCRETE Maincore
!Approach is to set parameter values at the end of time step, jump across, then calculate growth of normal
!cells and cells in foci for the time step just crossed.

termt(days.ge.tstop)        !run is over
weeks = days/7.             !use for plotting
months = days/30.           !use for plotting

if(days.eq.0.) goto 170     !to set parameters

hepsdt = hepsdtdays(days)

if (promodose.eq.1.and.days.ge.28) then
  cutoffvolum = cutoffvolum1
 else if (promodose.eq.2.and.days.ge.28) then
  cutoffvolum = cutoffvolum1
 else
  cutoffvolum = cutoffvolum0
end if

!DETERMINISTIC GROWTH OF LIVER
divs = an0c*(exp(c1*rbn0)-1.)/lwc          !divisions per cm**3 per time step
n0n1a = divs*pmuta                         !mutations per cm**3 per time step
n0n1b = divs*pmutb                         !mutations per cm**3 per time step
an0c = an0c*exp(c1*(rbn0-rdn0))            !normal cells at end of time step
lwc = an0c/hepsdt                          !liver wt.(gm) at end of time step

!^^^^^^^^^^^^^^^^^^^^^^^^^^^^^^^^^^^^^^^^^^^^^^^^^^^^^^^^^^^^^^^^^^^^^^^^^^^^^^^^^^^^^^
!DETERMINISTIC INTERMEDIATE CELLS PER CM**3 LIVER
!This calculation is based on deterministic rather than stochastic process. The deterministic result is
!presumably same as the mean of the stochastic results. Initially it is for comparison of the results.
!Here this part is not well written because rbn1a and rdn1a are not set to vary according to the size of ica
!even if they should. So the value for comparison is lost. IT IS DELETEABLE.
```

```
!ica = n0n1a + ica*exp(c1*(rbn1a-rdn1a))
!volad = ica/hepsdt
!numad = numad+n0n1a
!icb = n0n1b + icb*exp(c1*(rbn1b-rdn1b))  !Not adjusted by hepsdt(days)
!volbd = icb/hepsdt                        !because the experiment data
!numbd = numbd+n0n1b                       !are not adjusted accordingly.
!voltotd = 100*(volad+volbd)               !deterministic volume percent
!numtotd = numad + numbd                   !clone number per cm**3
!^^^^^^^^^^^^^^^^^^^^^^^^^^^^^^^^^^^^^^^^^^^^^^^^^^^^^^^^^^^^^^^^^^^^^^^^^^^^^

!STOCHASTIC MUTATION OF NORMAL HEPATOCYTES
if(pmuta.gt.0.) then              !don't sample POIDEV when pmut = 0
  xma = divs*pmuta                !mean of Poisson distribution
  n0a = poidev(xma,j)             !real mutation times
  mutota = mutota + n0a
else
  n0a = 0                         !no mutation when pmut = 0
endif

if(pmutb.gt.0.) then              !don't sample POIDEV when pmut = 0
  xmb = divs*pmutb                !mean of Poisson distribution
  n0b = poidev(xmb,j)
  mutotb = mutotb + n0b
else
  n0b = 0                         !no mutation when pmut = 0
endif

!In Conolly and Kimbell 1994 (Tox Appl Pharmacol,124:284-295), mutation is processed deterministically.

!ALLOCATION OF THE INITIATED CELLS IN DIMENSION ELEMENTS
!The value of an element:
!-1: empty and never occupied
!0:  once occupied but the occupant disappeared
!1:  1 cell in there; integer > 1: clone growing
! "A" CELLS
k = 0
if (n0a.ge.1) then
  do 50 i = 1,n0a                 !for every new A cell
    35: continue
    k = k+1
    if (k.gt.cmax-1) then         !Array overflow
      write(buffer,*) ' Stopped:  Array for "A" clones is full.'
      call disstr(buffer)
      count = repeat + 1
      termt(count.gt.repeat)
      goto 500
    endif
    if(clonesa(k,1).lt.1) then    !search all arrays to find available
      clonesa(k,1) = 1            !element and store a cell in there.
    else
      goto 35
    endif
  50: continue
endif

! "B" CELLS
```

```
k = 0
if (n0b.ge.1) then
  do 60 i = 1,n0b                    !for every new B cell
    65: continue
    k = k+1
    if (k.gt.cmax-1) then            !Array overflow
      write(buffer,*) ' Stopped:  Array for "B" clones is full.'
      call disstr(buffer)
      count = repeat + 1
      termt(count.gt.repeat)
      goto 500
    endif
    if(clonesb(k,1).lt.1) then
      clonesb(k,1) = 1
    else
      goto 65
    endif
  60: continue
endif

!ADJUST DIVISION RATE BY CLONE SIZE
!Growth of "A" CLONES
do 100 i = 1,cmax                    !for every clone
  if(clonesa(i,1).eq.-1) goto 105
  if(clonesa(i,1).eq.0)  goto 100
  if(clonesa(i,1).eq.1) then         !single-cell foci
    rbn1a=rbn1asingle
    rdn1a=rdn1asingle
    deltaasingle=rbn1a-rdn1a
    fasingleincycle = cycletime*rbn1a + apoptime*rdn1a
  else if(clonesa(i,1).ge.2.and.clonesa(i,1).lt.minitomulti) then
    rbn1a=rbn1amini                  !minifoci
    rdn1a=rdn1amini
    deltaamini=rbn1a-rdn1a
    faminiincycle = cycletime*rbn1a + apoptime*rdn1a
  else if(clonesa(i,1).ge.minitomulti.and.clonesa(i,1).lt.multitobig) then
    rbn1a=rbn1amulti                 !multicell foci
    rdn1a=rdn1amulti
    deltaamulti=rbn1a-rdn1a
    famultiincycle = cycletime*rbn1a + apoptime*rdn1a
  else if(clonesa(i,1).ge.multitobig) then
    rbn1a=rbn1abig                   !big foci
    rdn1a=rdn1abig
    deltaabig=rbn1a-rdn1a
    fabigincycle = cycletime*rbn1a + apoptime*rdn1a
  end if
  deltaa=rbn1a-rdn1a
  faincycle = cycletime*rbn1a + apoptime*rdn1a
  if(faincycle.gt.famax) then
    messa = .true.
    goto 105
  end if
  pbn1 = rbn1a*c1                    !probability of division during c1
                                     !probability = rate * time given time is small; Conolly 1994 TAP
  pdn1 = rdn1a*c1                    !probability of death during c1
  pbd = pbn1+pdn1                    !p(division) + p(death) during c1
```

```
                                        !probability of something happening
  if(clonesa(i,1).gt.slimit) then
    clonesa(i,1) = clonesa(i,1)*exp(c1*deltaa)
    goto 100
  endif
  call bd(j,losta,pbn1,pdn1,pbd,clonesa(i,1))
100: continue
105: continue

!Growth of "B" CLONES
do 160 i = 1,cmax                       !for every clone
  if(clonesb(i,1).eq.-1.) goto 170
  if(clonesb(i,1).eq.0.)  goto 160
  if(clonesb(i,1).eq.1.) then           !single-cell foci
    rbn1b=rbn1bsingle
    rdn1b=rdn1bsingle
    deltabsingle=rbn1b-rdn1b
    fbsingleincycle = cycletime*rbn1b + apoptime*rdn1b
  else if(clonesb(i,1).ge.2.and.clonesb(i,1).lt.minitomulti) then
    rbn1b=rbn1bmini                     !minifoci
    rdn1b=rdn1bmini
    deltabmini=rbn1b-rdn1b
    fbminiincycle = cycletime*rbn1b + apoptime*rdn1b
  else if(clonesb(i,1).ge.minitomulti.and.clonesb(i,1).lt.multitobig) then
    rbn1b=rbn1bmulti
    rdn1b=rdn1bmulti
    deltabmulti=rbn1b-rdn1b
    fbmultiincycle = cycletime*rbn1b + apoptime*rdn1b
  else if(clonesb(i,1).ge.multitobig) then
    rbn1b=rbn1bbig
    rdn1b=rdn1bbig
    deltabbig=rbn1b-rdn1b
    fbbigincycle = cycletime*rbn1b + apoptime*rdn1b
  end if
  deltab=rbn1b-rdn1b
  fbincycle = cycletime*rbn1b + apoptime*rdn1b
  if(fbincycle.gt.fbmax) then
    messb = .true.
    goto 170
  end if
  pbn1 = rbn1b*c1                       !probability of division during c1
  pdn1 = rdn1b*c1                       !probability of death during c1
  pbd = pbn1+pdn1                       !p(division) + p(death) during c1
  if(clonesb(i,1).gt.slimit) then
    clonesb(i,1) = clonesb(i,1)*exp(c1*deltab)
    goto 160
  endif
  call bd(j,lostb,pbn1,pdn1,pbd,clonesb(i,1))
160: continue
170: continue

!--------1---------2---------3---------4---------5---------6---------7---------8
!*****SET PARAMETER VALUES FOR NEXT TIME STEP*****

!ADJUST LIVER SIZE FOR PARTIAL HEPATECTOMY
if (days.eq.phtime) then                !time of partial hepatectomy
```

```
  remvwt = phremove*lwc          !gm liver removed by partial hep.
  lwc = lwc - remvwt
  remvcell = remvwt*hepsdt       !# hepatocytes removed by partial hep.
  an0c = an0c - remvcell
  call logd(.true.)              !data logging, not indispensable.
endif

!Growth kinetics of NORMAL hepatocytes
PROCEDURAL
!NORMAL CELL BIRTH RATE CONSTANT AFTER DEN
!To fit Kato 1993 data:
if (days.gt.dentime+deneffdelay.and.days.le.4.) then
 rbn0=0.0022*exp(0.881*days)
end if
if (days.gt.4.and.days.lt.10.1) rbn0=0.2321*exp(-0.2837*days)
if (days.ge.10.1.and.days.lt.phtime+rcpdel) then
 rbn0=0.01151-0.0004*(days-10.)
end if

!REGENERATIVE PROLIFERATION AFTER PARTIAL HEPATECTOMY
!Empirical functions to fit our experimental liver weight
!Birth rate constants during day 20 and 24 of three treatment groups similar
if (days.eq.phtime+rcpdel) then
  rbn0=0.40
end if

if (days.gt.phtime+rcpdel.and.days.le.24.) then
  rbn0=0.40-0.1085*(days-(phtime+rcpdel))
end if

!Linear interpolation, fit to our data of liver weight
if (days.gt.24..and.days.lt.28.) then
  if (promodose.le.0) then
    rbn0=0.1288-0.0303*(days-24.)
   else if (promodose.eq.1) then
    rbn0=0.1288-0.0285*(days-24.)
   else if (promodose.eq.2) then
    rbn0=0.1288-0.0252*(days-24.)
  end if
end if

!During day 28 and 56, modification of the division rate constant must be made to fit the liver weight
!(i.e., assigned values not close to the experimental derivatives).
if (days.ge.28..and.days.le.47.) then
  if (promodose.le.0) then
     rbn0=0.01                   !arbitrarily elevated to fit liver weight
   else if (promodose.eq.1) then
     rbn0=0.018-0.0007*(days-28.)
   else if (promodose.eq.2) then
     rbn0=max(0.02-0.001286*(days-28.),rdn0c)
  end if
end if

if (days.gt.47.) then
  if (promodose.le.0) then
     rbn0=0.002
```

```
    else if (promodose.eq.1) then
      rbn0=0.0025+0.0015*(days-47.)
    else if (promodose.eq.2) then
      rbn0=0.0032+0.001194*(days-47.)
   end if
end if

!NORMAL CELL DEATH RATE CONSTANT AFTER DEN
!Early time points,0-14 days, fit the Kato data.
!The decreased hepatocyte density causes abnormal increase in "lwc". This abnormality is partially
!corrected with elevated death rate constant.
if (days.ge.dentime+deneffdelay.and.days.le.6) then
  rdn0=0.1545-0.0256*days
else if (days.ge.28.and.promodose.eq.2.) then
  rdn0=2.0*rdn0c    !cytotoxicity, lwc insensitive to it.
else
  rdn0=rdn0c
end if
if (rdn0.le.rdn0c) then
  rdn0=rdn0c
end if

END ! of PROCEDURAL

!STORE THE FIVE TIME POINTS SIMULATED RESULTS
if (days.eq.20.) then
  clonedata(1,1) = voltotdetect
  clonedata(1,2) = cnumdetect
endif
if (days.eq.24.) then
  clonedata(2,1) = voltotdetect
  clonedata(2,2) = cnumdetect
endif
if (days.eq.28.) then
  clonedata(3,1) = voltotdetect
  clonedata(3,2) = cnumdetect
endif
if (days.eq.47.) then
  clonedata(4,1) = voltotdetect
  clonedata(4,2) = cnumdetect
endif
if (days.eq.56.) then
  clonedata(5,1) = voltotdetect
  clonedata(5,2) = cnumdetect
endif

!CALCULATE THE TIME STEP C1;
!upper bound on C1 is calculated from rbn1* or rdn1* of initiated cells

procedural                    !setting c1
if (rbn1a.gt.0..and.rdn1a.gt.0.) then
  c1a = min(pmax/rbn1a,pmax/rdn1a)
else
  c1a = 0.
endif
```

```
if (rbn1b.gt.0..and.rdn1b.gt.0.) then
  c1b = min(pmax/rbn1b,pmax/rdn1b)
else
  c1b = 0.
endif

c1 = 1.e6
if (c1.ge.c1a.and.c1a.gt.0.) c1 = c1a
if (c1.ge.c1b.and.c1b.gt.0.) c1 = c1b

!REDUCE C1 IF NEEDED TO KEEP NUMBER OF MUTATIONS PER TIME STEP SMALL
if (pmuta.eq.0..and.pmutb.eq.0.) goto outc1  !no mutations
if (c1.le.0.1) goto outc1                    !<0.1 is small enough
if (pmuta.gt.0.) then
  c1a = log(lwc/(pmuta*an0c)+1.)/rbn0        !time step expected for 1 mut.
else
  c1a = 0.
endif
if (pmutb.gt.0.) then
  c1b = log(lwc/(pmutb*an0c)+1.)/rbn0        !time step expected for 1 mut.
else
  c1b = 0.
endif
if (c1a.gt.0..and.c1b.gt.0.) c1x = min(c1a,c1b)
if (c1a.gt.0..and.c1b.eq.0.) c1x = c1a
if (c1a.eq.0..and.c1b.gt.0.) c1x = c1b
if (c1x.ge.c1) goto outc1                    !don't change c1
if (c1x.lt.c1) c1 = c1x                      !reduce c1 to c1x
if (c1.lt.0.1) c1 = 0.1                      !increase c1 to 0.1 if needed
outc1: continue

!REDUCE C1 IF NEEDED TO HIT TIME FOR DEN EFFECTS
if (days.lt.dentime+deneffdelay.and.days+c1.gt.dentime+deneffdelay) then
   c1 = dentime + deneffdelay - days
endif

!REDUCE C1 IF NEEDED TO HIT TIME FOR PARTIAL HEPATECTOMY
if (days.lt.phtime.and.days+c1.gt.phtime) c1 = phtime - days

!REDUCE C1 IF NEEDED TO HIT TIME FOR REGENERATIVE CELLULAR PROLIFERATION
if (days.lt.phtime+rcpdel.and.days+c1.gt.phtime+rcpdel) then
   c1 = phtime + rcpdel - days
endif

!REDUCE C1 IF NEEDED TO HIT TIME FOR START OF MIXTURE DOSING
if (days.lt.mixtime.and.days+c1.gt.mixtime) c1 = mixtime-days

!REDUCE C1 IF NEEDED TO HIT TIME FOR TURN OFF DEN EFFECTS
if (days.lt.turnoff1.and.days+c1.gt.turnoff1) c1 = turnoff1-days
if (days.lt.turnoff2.and.days+c1.gt.turnoff2) c1 = turnoff2-days

if (days.lt.7.and.days+c1.gt.7)  c1 = 7  - days
    !for checking predictions of day 7
if (days.lt.14.and.days+c1.gt.14) c1 = 14 - days
    !for checking predictions of day 14
if (days.lt.20.and.days+c1.gt.20) c1 = 20 - days
```

```
if (days.lt.24.and.days+c1.gt.24) c1 = 24 - days
if (days.lt.28.and.days+c1.gt.28) c1 = 28 - days
if (days.lt.47.and.days+c1.gt.47) c1 = 47 - days
if (days.lt.56.and.days+c1.gt.56) c1 = 56 - days

!REDUCE C1 IF NEEDED TO HIT TIME FOR END OF SIMULATION
if (days.lt.tstop.and.days+c1.gt.tstop) c1 = tstop-days
if (days.eq.tstop) call logd(.true.)

500: continue
if (c1.gt.0.1) c1 = 0.1
end !of procedural

schedule Maincore .at. days + c1
END !of Maincore

!--------1---------2---------3---------4---------5---------6---------7---------8
DISCRETE DENON
!Adjusts mutation probability,birth and death rate constants at start of DEN dosing.

!Literature 1:
!Yusuf, A, et al. Carcinogenesis,1999,20(8):1641-1644. Development of resistance during the early stages
!of experimental liver carcinogenesis. Male F344 rats, single 200mg/kg DEN, no other treatment and killed
!8 weeks later. Only 23% of DEN-induced foci were resistant to the mitoinhibitory effect of 2-AAF and 5%
!to the effect of orotic acid. This implies that the initiated cells are heterogeneous and the majority are not
!resistant to mitoinhibition. With treatment of promoters (2-AAF and CCl4), the proportion of resistant foci
!is higher than 50%.
!Assumption 1: Two cell populations: A not resistant, B is; the ratio of emergence of A and B is 10:1.
!Assumption 2: Due to lack of data, the growth related parameters of A and B are set same at some time
!points.

!Literature 2:
!Grasl-Kraupp B. et al., Quantitative analysis of tumor initiation in rat liver: role of cell replication and cell
!death(apoptosis).Carcinogenesis, 2000, 21(7):1411-1421.
!Male Wistar rats, 6-8wks old, were initiated with N-nitrosomorpholine. With day 14 a watershed, the
!minifoci (including single cell foci) number increased before day 14 and declined afterwards. The labeling
!index (LI) of the single GSTP cells was less than that of normal cells and which, in turn, was less than that
!of the cells in multicell foci. Two possibilities:(1) the single initiated cells are homogeneous in terms of
!proliferation (very low rate), and once a single cell divides, the resultant two cells proliferate much faster;
!(2) the single initiated cells are heterogeneous in terms of proliferation, one subpopulation dividing much
!slower than the other. Once the faster dividing single cells become two cells, they keep proliferating at a
!high rate.
!Assumption 3:
!There are four kinds of foci in term of growth kinetics: single cell, mini-, multicell-, and big foci.

!Single cell number and volume percentage level off 1 week after DEN dosing.
  constant pdenmutfolda0 = 350     !mutation rate for A 350-fold higher
  constant pdenmutfoldb0 = 35      !mutation rate for B 35-fold higher
  constant pdencba0single = 0.03   !DEN birth rate for single A cell
  constant pdencbb0single = 0.03   !DEN birth rate for single B cell
  constant pdencda0single =8e-4    !DEN death rate for single A cell
  constant pdencdb0single =8e-5    !DEN death rate for single B cell
  constant pdencba0mini = 0.3      !DEN birth rate for mini A foci
  constant pdencbb0mini = 0.3      !DEN birth rate for mini B foci
  constant pdencda0mini = 8e-4     !DEN birth rate for mini A foci
  constant pdencdb0mini = 8e-5     !DEN birth rate for mini B foci
```

```
  constant pdencba0multi =0.41    !DEN birth rate for A cell
  constant pdencbb0multi =0.41    !DEN birth rate for B cell
  constant pdencda0multi =8e-4    !DEN death rate for A cell
  constant pdencdb0multi =8e-5    !DEN death rate for B cell
  constant pdencba0big =0.42      !DEN birth rate for A cell
  constant pdencbb0big =0.42      !DEN birth rate for B cell
  constant pdencda0big =8e-4      !DEN death rate for A cell
  constant pdencdb0big =8e-5      !DEN death rate for B cell

  pmuta = pmutac*pdenmutfolda0
  pmutb = pmutbc*pdenmutfoldb0
  rbn1asingle=pdencba0single
  rdn1asingle=pdencda0single
  rbn1bsingle=pdencbb0single
  rdn1bsingle=pdencdb0single
  rbn1amini=pdencba0mini
  rdn1amini=pdencda0mini
  rbn1bmini=pdencbb0mini
  rdn1bmini=pdencdb0mini
  rbn1amulti=pdencba0multi
  rdn1amulti=pdencda0multi
  rbn1bmulti=pdencbb0multi
  rdn1bmulti=pdencdb0multi
  rbn1abig=pdencba0big
  rdn1abig=pdencda0big
  rbn1bbig=pdencbb0big
  rdn1bbig=pdencdb0big

END !of DENON
!--------1---------2---------3---------4---------5---------6---------7---------8

DISCRETE DENOFF1                  !reduce DEN effects

  constant pdenmutfolda1 = 20     !mutation rate for A 20-fold higher
  constant pdenmutfoldb1 = 2      !mutation rate for B 2-fold higher
  constant pdencba1single =0.012  !DEN birth rate for single A cell
  constant pdencbb1single =0.012  !DEN birth rate for single B cell
  constant pdencda1single =8e-4   !DEN death rate for single A cell
  constant pdencdb1single =8e-5   !DEN death rate for single B cell
  constant pdencba1mini =0.22     !DEN birth rate for mini A foci
  constant pdencbb1mini =0.22     !DEN birth rate for mini B foci
  constant pdencda1mini =8e-4     !DEN death rate for mini A foci
  constant pdencdb1mini =8e-5     !DEN death rate for mini B foci
  constant pdencba1multi =0.35    !DEN birth rate for A cell
  constant pdencbb1multi =0.35    !DEN birth rate for B cell
  constant pdencda1multi =0.05    !DEN death rate for A cell
  constant pdencdb1multi =8e-4    !DEN death rate for B cell
  constant pdencba1big =0.42      !DEN birth rate for A cell
  constant pdencbb1big =0.42      !DEN birth rate for B cell
  constant pdencda1big =0.01      !DEN death rate for A cell
  constant pdencdb1big =8e-4      !DEN death rate for B cell

  pmuta = pmutac*pdenmutfolda1
  pmutb = pmutbc*pdenmutfoldb1
  rbn1asingle=pdencba1single
  rdn1asingle=pdencda1single
```

```
  rbn1bsingle=pdencbb1single
  rdn1bsingle=pdencdb1single
  rbn1amini=pdencba1mini
  rdn1amini=pdencda1mini
  rbn1bmini=pdencbb1mini
  rdn1bmini=pdencdb1mini
  rbn1amulti=pdencba1multi
  rdn1amulti=pdencda1multi
  rbn1bmulti=pdencbb1multi
  rdn1bmulti=pdencdb1multi
  rbn1abig=pdencba1big
  rdn1abig=pdencda1big
  rbn1bbig=pdencbb1big
  rdn1bbig=pdencdb1big

end !of DENOFF1
!--------1---------2---------3---------4---------5---------6---------7---------8

DISCRETE DENOFF2                !further reduce DEN effects
!Promoter treatment starts on day14. In the treated rats, the numbers of foci in the low size classes (1-4)
!are larger than their counterpart in the control rats. So it is likely HCB+PCB126 has different effects on
!the growth kinetics dependent on focal size.

  constant pdenmutfolda2 = 1            !mutation rate for A to background
  constant pdenmutfoldb2 = 1            !mutation rate for B to background
  constant pdencba2single =0.02         !DEN birth rate for single A cell
     pdencbb2single =pdencba2single     !DEN birth rate for single B cell
  constant pdencda2single =8e-4         !DEN death rate for single A cell
  constant pdencdb2single =8e-5         !DEN death rate for single B cell
  constant pdencba2mini =0.11           !DEN birth rate for mini A foci
     pdencbb2mini =pdencba2mini         !DEN birth rate for mini B foci
  constant pdencda2mini =0.0015         !DEN death rate for mini A foci
  constant pdencdb2mini =8e-5           !DEN death rate for mini B foci
  constant pdencba2multi =0.20          !DEN birth rate for A cell
     pdencbb2multi =pdencba2multi       !DEN birth rate for B cell
  constant pdencda2multi =0.04          !DEN death rate for A cell
  constant pdencdb2multi =8e-4          !DEN death rate for B cell
  constant pdencba2big =0.42            !DEN birth rate for A cell
     pdencbb2big =pdencba2big
  constant pdencda2big =0.01            !DEN death rate for A cell
  constant pdencdb2big =8e-4            !DEN death rate for B cell
  constant pdenfoldba2lowsingle=1.0
  constant pdenfoldbb2lowsingle=1.0
  constant pdenfoldda2lowsingle=1.0
  constant pdenfolddb2lowsingle=1.0
  constant pdenfoldba2lowmini=1.0
  constant pdenfoldbb2lowmini=1.0
  constant pdenfoldda2lowmini=1.0
  constant pdenfolddb2lowmini=1.0
  constant pdenfoldba2lowmulti=1.0
  constant pdenfoldbb2lowmulti=1.0
  constant pdenfoldda2lowmulti=1.0
  constant pdenfolddb2lowmulti=1.0
  constant pdenfoldba2lowbig=1.0
  constant pdenfoldbb2lowbig=1.0
  constant pdenfoldda2lowbig=1.0
```

```
constant pdenfolddb2lowbig=1.0
constant pdenfoldba2hisingle=1.0
constant pdenfoldbb2hisingle=1.0
constant pdenfoldda2hisingle=1.0
constant pdenfolddb2hisingle=1.0
constant pdenfoldba2himini=0.5
constant pdenfoldbb2himini=0.5
constant pdenfoldda2himini=2.2
constant pdenfolddb2himini=1.0
constant pdenfoldba2himulti=1.0
constant pdenfoldbb2himulti=1.0
constant pdenfoldda2himulti=1.8
constant pdenfolddb2himulti=1.0
constant pdenfoldba2hibig=1.0
constant pdenfoldbb2hibig=1.0
constant pdenfoldda2hibig=1.0
constant pdenfolddb2hibig=1.0

pmuta = pmutac*pdenmutfolda2
pmutb = pmutbc*pdenmutfoldb2

if (promodose.eq.0) then
  rbn1asingle=pdencba2single
  rdn1asingle=pdencda2single
  rbn1bsingle=pdencbb2single
  rdn1bsingle=pdencdb2single
  rbn1amini=pdencba2mini
  rdn1amini=pdencda2mini
  rbn1bmini=pdencbb2mini
  rdn1bmini=pdencdb2mini
  rbn1amulti=pdencba2multi
  rdn1amulti=pdencda2multi
  rbn1bmulti=pdencbb2multi
  rdn1bmulti=pdencdb2multi
  rbn1abig=pdencba2big
  rdn1abig=pdencda2big
  rbn1bbig=pdencbb2big
  rdn1bbig=pdencdb2big
 else if (promodose.eq.1) then
  rbn1asingle=pdencba2single*pdenfoldba2lowsingle
  rdn1asingle=pdencda2single*pdenfoldda2lowsingle
  rbn1bsingle=pdencbb2single*pdenfoldbb2lowsingle
  rdn1bsingle=pdencdb2single*pdenfolddb2lowsingle
  rbn1amini=pdencba2mini*pdenfoldba2lowmini
  rdn1amini=pdencda2mini*pdenfoldda2lowmini
  rbn1bmini=pdencbb2mini*pdenfoldbb2lowmini
  rdn1bmini=pdencdb2mini*pdenfolddb2lowmini
  rbn1amulti=pdencba2multi*pdenfoldba2lowmulti
  rdn1amulti=pdencda2multi*pdenfoldda2lowmulti
  rbn1bmulti=pdencbb2multi*pdenfoldbb2lowmulti
  rdn1bmulti=pdencdb2multi*pdenfolddb2lowmulti
  rbn1abig=pdencba2big*pdenfoldba2lowbig
  rdn1abig=pdencda2big*pdenfoldda2lowbig
  rbn1bbig=pdencbb2big*pdenfoldbb2lowbig
  rdn1bbig=pdencdb2big*pdenfolddb2lowbig
 else if (promodose.eq.2) then
```

```
    rbn1asingle=pdencba2single*pdenfoldba2hisingle
    rdn1asingle=pdencda2single*pdenfoldda2hisingle
    rbn1bsingle=pdencbb2single*pdenfoldbb2hisingle
    rdn1bsingle=pdencdb2single*pdenfolddb2hisingle
    rbn1amini=pdencba2mini*pdenfoldba2himini
    rdn1amini=pdencda2mini*pdenfoldda2himini
    rbn1bmini=pdencbb2mini*pdenfoldbb2himini
    rdn1bmini=pdencdb2mini*pdenfolddb2himini
    rbn1amulti=pdencba2multi*pdenfoldba2himulti
    rdn1amulti=pdencda2multi*pdenfoldda2himulti
    rbn1bmulti=pdencbb2multi*pdenfoldbb2himulti
    rdn1bmulti=pdencdb2multi*pdenfolddb2himulti
    rbn1abig=pdencba2big*pdenfoldba2hibig
    rdn1abig=pdencda2big*pdenfoldda2hibig
    rbn1bbig=pdencbb2big*pdenfoldbb2hibig
    rdn1bbig=pdencdb2big*pdenfolddb2hibig
  end if

end !of DENOFF2
!--------1---------2---------3---------4---------5---------6---------7---------8

DISCRETE PHepON                 !turn on the PH effects on initiated cells

constant phmutation=5           !mutation prob. 5-fold higher
constant phba0single=0.004      !birth rate,single cell
   phbb0single=phba0single      !birth rate,single cell
constant phda0single=0.002      !death rate,single cell
constant phdb0single=0.001      !death rate,single cell
constant phba0mini=0.09         !birth rate,minifoci
   phbb0mini=phba0mini          !birth rate,minifoci
constant phda0mini=0.07         !death rate,minifoci
constant phdb0mini=0.02         !death rate,minifoci
constant phba0multi=0.17        !birth rate
   phbb0multi=phba0multi
constant phda0multi=0.06        !death rate
constant phdb0multi=0.02
constant phba0big=0.4           !birth rate
   phbb0big=phba0big
constant phda0big=0.01          !death rate
constant phdb0big=0.01
constant phfoldba0lowsingle=1.0
constant phfoldbb0lowsingle=1.0
constant phfoldda0lowsingle=1.0
constant phfolddb0lowsingle=1.0
constant phfoldba0lowmini=1.1
constant phfoldbb0lowmini=1.1
constant phfoldda0lowmini=1.0
constant phfolddb0lowmini=1.0
constant phfoldba0lowmulti=1.0
constant phfoldbb0lowmulti=1.0
constant phfoldda0lowmulti=1.0
constant phfolddb0lowmulti=1.0
constant phfoldba0lowbig=1.0
constant phfoldbb0lowbig=1.0
constant phfoldda0lowbig=1.0
constant phfolddb0lowbig=1.0
```

```
constant phfoldba0hisingle=1.0
constant phfoldbb0hisingle=1.0
constant phfoldda0hisingle=1.0
constant phfolddb0hisingle=1.0
constant phfoldba0himini=3.0
constant phfoldbb0himini=3.0
constant phfoldda0himini=1.0
constant phfolddb0himini=1.0
constant phfoldba0himulti=2.8
constant phfoldbb0himulti=2.8
constant phfoldda0himulti=1.0
constant phfolddb0himulti=1.0
constant phfoldba0hibig=1.18
constant phfoldbb0hibig=1.18
constant phfoldda0hibig=1.0
constant phfolddb0hibig=1.0

  pmuta = pmutac*phmutation
  pmutb = pmutbc*phmutation

  if (promodose.eq.0) then
      rbn1asingle=phba0single
      rdn1asingle=phda0single
      rbn1bsingle=phbb0single
      rdn1bsingle=phdb0single
      rbn1amini=phba0mini
      rdn1amini=phda0mini
      rbn1bmini=phbb0mini
      rdn1bmini=phdb0mini
      rbn1amulti=phba0multi
      rdn1amulti=phda0multi
      rbn1bmulti=phbb0multi
      rdn1bmulti=phdb0multi
      rbn1abig=phba0big
      rdn1abig=phda0big
      rbn1bbig=phbb0big
      rdn1bbig=phdb0big
    else if (promodose.eq.1) then
      rbn1asingle=phba0single*phfoldba0lowsingle
      rdn1asingle=phda0single*phfoldda0lowsingle
      rbn1bsingle=phbb0single*phfoldbb0lowsingle
      rdn1bsingle=phdb0single*phfolddb0lowsingle
      rbn1amini=phba0mini*phfoldba0lowmini
      rdn1amini=phda0mini*phfoldda0lowmini
      rbn1bmini=phbb0mini*phfoldbb0lowmini
      rdn1bmini=phdb0mini*phfolddb0lowmini
      rbn1amulti=phba0multi*phfoldba0lowmulti
      rdn1amulti=phda0multi*phfoldda0lowmulti
      rbn1bmulti=phbb0multi*phfoldbb0lowmulti
      rdn1bmulti=phdb0multi*phfolddb0lowmulti
      rbn1abig=phba0big*phfoldba0lowbig
      rdn1abig=phda0big*phfoldda0lowbig
      rbn1bbig=phbb0big*phfoldbb0lowbig
      rdn1bbig=phdb0big*phfolddb0lowbig
    else if (promodose.eq.2) then
      rbn1asingle=phba0single*phfoldba0hisingle
```

```
      rdn1asingle=phda0single*phfoldda0hisingle
      rbn1bsingle=phbb0single*phfoldbb0hisingle
      rdn1bsingle=phdb0single*phfolddb0hisingle
      rbn1amini=phba0mini*phfoldba0himini
      rdn1amini=phda0mini*phfoldda0himini
      rbn1bmini=phbb0mini*phfoldbb0himini
      rdn1bmini=phdb0mini*phfolddb0himini
      rbn1amulti=phba0multi*phfoldba0himulti
      rdn1amulti=phda0multi*phfoldda0himulti
      rbn1bmulti=phbb0multi*phfoldbb0himulti
      rdn1bmulti=phdb0multi*phfolddb0himulti
      rbn1abig=phba0big*phfoldba0hibig
      rdn1abig=phda0big*phfoldda0hibig
      rbn1bbig=phbb0big*phfoldbb0hibig
      rdn1bbig=phdb0big*phfolddb0hibig
 end if

end !of PHepON
!--------1---------2---------3---------4---------5---------6---------7---------8

DISCRETE PHepOff1              !turn off the PH effects on initiated cells

constant phmutation1=2         !mutation prob. 2-fold higher
constant phba1single=0.001     !birth rate,single cell
   phbb1single=phba1single     !birth rate,single cell
constant phda1single=0.0005    !death rate,single cell
constant phdb1single=0.0005    !death rate,single cell
constant phba1mini=0.08        !birth rate,minifoci
   phbb1mini=phba1mini         !birth rate,minifoci
constant phda1mini=0.18        !death rate,minifoci
constant phdb1mini=0.13        !death rate,minifoci
constant phba1multi=0.17       !birth rate
   phbb1multi=phba1multi
constant phda1multi=0.28       !death rate
constant phdb1multi=0.23
constant phba1big=0.25         !birth rate
   phbb1big=phba1big
constant phda1big=0.20         !death rate
constant phdb1big=0.16
constant phfoldba1lowsingle=1.0
constant phfoldbb1lowsingle=1.0
constant phfoldda1lowsingle=1.0
constant phfolddb1lowsingle=1.0
constant phfoldba1lowmini=2.4
constant phfoldbb1lowmini=2.4
constant phfoldda1lowmini=0.25
constant phfolddb1lowmini=0.1
constant phfoldba1lowmulti=1.85
constant phfoldbb1lowmulti=1.85
constant phfoldda1lowmulti=0.8
constant phfolddb1lowmulti=0.6
constant phfoldba1lowbig=1.0
constant phfoldbb1lowbig=1.0
constant phfoldda1lowbig=1.1
constant phfolddb1lowbig=1.0
constant phfoldba1hisingle=1.0
```

```
constant phfoldbb1hisingle=1.0
constant phfoldda1hisingle=1.0
constant phfolddb1hisingle=1.0
constant phfoldba1himini=3.0
constant phfoldbb1himini=3.0
constant phfoldda1himini=0.7
constant phfolddb1himini=0.2
constant phfoldba1himulti=1.1
constant phfoldbb1himulti=1.1
constant phfoldda1himulti=1.0
constant phfolddb1himulti=1.0
constant phfoldba1hibig=1.0
constant phfoldbb1hibig=1.0
constant phfoldda1hibig=3.2
constant phfolddb1hibig=1.0

  pmuta = pmutac*phmutation1
  pmutb = pmutbc*phmutation1

   if (promodose.eq.0) then
       rbn1asingle=phba1single
       rdn1asingle=phda1single
       rbn1bsingle=phbb1single
       rdn1bsingle=phdb1single
       rbn1amini=phba1mini
       rdn1amini=phda1mini
       rbn1bmini=phbb1mini
       rdn1bmini=phdb1mini
       rbn1amulti=phba1multi
       rdn1amulti=phda1multi
       rbn1bmulti=phbb1multi
       rdn1bmulti=phdb1multi
       rbn1abig=phba1big
       rdn1abig=phda1big
       rbn1bbig=phbb1big
       rdn1bbig=phdb1big
    else if (promodose.eq.1) then
       rbn1asingle=phba1single*phfoldba1lowsingle
       rdn1asingle=phda1single*phfoldda1lowsingle
       rbn1bsingle=phbb1single*phfoldbb1lowsingle
       rdn1bsingle=phdb1single*phfolddb1lowsingle
       rbn1amini=phba1mini*phfoldba1lowmini
       rdn1amini=phda1mini*phfoldda1lowmini
       rbn1bmini=phbb1mini*phfoldbb1lowmini
       rdn1bmini=phdb1mini*phfolddb1lowmini
       rbn1amulti=phba1multi*phfoldba1lowmulti
       rdn1amulti=phda1multi*phfoldda1lowmulti
       rbn1bmulti=phbb1multi*phfoldbb1lowmulti
       rdn1bmulti=phdb1multi*phfolddb1lowmulti
       rbn1abig=phba1big*phfoldba1lowbig
       rdn1abig=phda1big*phfoldda1lowbig
       rbn1bbig=phbb1big*phfoldbb1lowbig
       rdn1bbig=phdb1big*phfolddb1lowbig
    else if (promodose.eq.2) then
       rbn1asingle=phba1single*phfoldba1hisingle
       rdn1asingle=phda1single*phfoldda1hisingle
```

```
      rbn1bsingle=phbb1single*phfoldbb1hisingle
      rdn1bsingle=phdb1single*phfolddb1hisingle
      rbn1amini=phba1mini*phfoldba1himini
      rdn1amini=phda1mini*phfoldda1himini
      rbn1bmini=phbb1mini*phfoldbb1himini
      rdn1bmini=phdb1mini*phfolddb1himini
      rbn1amulti=phba1multi*phfoldba1himulti
      rdn1amulti=phda1multi*phfoldda1himulti
      rbn1bmulti=phbb1multi*phfoldbb1himulti
      rdn1bmulti=phdb1multi*phfolddb1himulti
      rbn1abig=phba1big*phfoldba1hibig
      rdn1abig=phda1big*phfoldda1hibig
      rbn1bbig=phbb1big*phfoldbb1hibig
      rdn1bbig=phdb1big*phfolddb1hibig
 end if

end !of PHepOff1
!--------1---------2---------3---------4---------5---------6---------7---------8

DISCRETE PHepOff2              !further turn off the PH effects on initiated cells
constant phmutation2=1         !mutation prob. to background
constant phba2single=0.001     !birth rate,single cell
   phbb2single=phba2single     !birth rate,single cell
constant phda2single=0.0001    !death rate,single cell
constant phdb2single=0.0001    !death rate,single cell
constant phba2mini=0.1         !birth rate,minifoci
   phbb2mini=phba2mini         !birth rate,minifoci
constant phda2mini=0.18        !death rate,minifoci
constant phdb2mini=0.15        !death rate,minifoci
constant phba2multi=0.10       !birth rate
   phbb2multi=phba2multi
constant phda2multi=0.12       !death rate
constant phdb2multi=0.06
constant phba2big=0.10         !birth rate
   phbb2big=phba2big
constant phda2big=0.09         !death rate
constant phdb2big=0.04
constant phfoldba2lowsingle=1.0
constant phfoldbb2lowsingle=1.0
constant phfoldda2lowsingle=1.0
constant phfolddb2lowsingle=1.0
constant phfoldba2lowmini=1.75
constant phfoldbb2lowmini=1.75
constant phfoldda2lowmini=1.2
constant phfolddb2lowmini=0.6
constant phfoldba2lowmulti=1.38
constant phfoldbb2lowmulti=1.38
constant phfoldda2lowmulti=1.53
constant phfolddb2lowmulti=0.95
constant phfoldba2lowbig=0.95
constant phfoldbb2lowbig=0.95
constant phfoldda2lowbig=2.2
constant phfolddb2lowbig=2.05
constant phfoldba2hisingle=1.0
constant phfoldbb2hisingle=1.0
constant phfoldda2hisingle=1.0
```

```
constant phfolddb2hisingle=1.0
constant phfoldba2himini=1.7
constant phfoldbb2himini=1.7
constant phfoldda2himini=1.0
constant phfolddb2himini=0.5
constant phfoldba2himulti=1.2
constant phfoldbb2himulti=1.2
constant phfoldda2himulti=1.2
constant phfolddb2himulti=0.4
constant phfoldba2hibig=0.7
constant phfoldbb2hibig=0.7
constant phfoldda2hibig=3.0
constant phfolddb2hibig=1.15

  pmuta = pmutac*phmutation2
  pmutb = pmutbc*phmutation2

  if (promodose.eq.0) then
       rbn1asingle=phba2single
       rdn1asingle=phda2single
       rbn1bsingle=phbb2single
       rdn1bsingle=phdb2single
       rbn1amini=phba2mini
       rdn1amini=phda2mini
       rbn1bmini=phbb2mini
       rdn1bmini=phdb2mini
       rbn1amulti=phba2multi
       rdn1amulti=phda2multi
       rbn1bmulti=phbb2multi
       rdn1bmulti=phdb2multi
       rbn1abig=phba2big
       rdn1abig=phda2big
       rbn1bbig=phbb2big
       rdn1bbig=phdb2big
    else if (promodose.eq.1) then
       rbn1asingle=phba2single*phfoldba2lowsingle
       rdn1asingle=phda2single*phfoldda2lowsingle
       rbn1bsingle=phbb2single*phfoldbb2lowsingle
       rdn1bsingle=phdb2single*phfolddb2lowsingle
       rbn1amini=phba2mini*phfoldba2lowmini
       rdn1amini=phda2mini*phfoldda2lowmini
       rbn1bmini=phbb2mini*phfoldbb2lowmini
       rdn1bmini=phdb2mini*phfolddb2lowmini
       rbn1amulti=phba2multi*phfoldba2lowmulti
       rdn1amulti=phda2multi*phfoldda2lowmulti
       rbn1bmulti=phbb2multi*phfoldbb2lowmulti
       rdn1bmulti=phdb2multi*phfolddb2lowmulti
       rbn1abig=phba2big*phfoldba2lowbig
       rdn1abig=phda2big*phfoldda2lowbig
       rbn1bbig=phbb2big*phfoldbb2lowbig
       rdn1bbig=phdb2big*phfolddb2lowbig
    else if (promodose.eq.2) then
       rbn1asingle=phba2single*phfoldba2hisingle
       rdn1asingle=phda2single*phfoldda2hisingle
       rbn1bsingle=phbb2single*phfoldbb2hisingle
       rdn1bsingle=phdb2single*phfolddb2hisingle
```

```
      rbn1amini=phba2mini*phfoldba2himini
      rdn1amini=phda2mini*phfoldda2himini
      rbn1bmini=phbb2mini*phfoldbb2himini
      rdn1bmini=phdb2mini*phfolddb2himini
      rbn1amulti=phba2multi*phfoldba2himulti
      rdn1amulti=phda2multi*phfoldda2himulti
      rbn1bmulti=phbb2multi*phfoldbb2himulti
      rdn1bmulti=phdb2multi*phfolddb2himulti
      rbn1abig=phba2big*phfoldba2hibig
      rdn1abig=phda2big*phfoldda2hibig
      rbn1bbig=phbb2big*phfoldbb2hibig
      rdn1bbig=phdb2big*phfolddb2hibig
 end if

end !of PHepOff2

!--------1---------2---------3---------4---------5---------6---------7---------8
DISCRETE SIZE_CLASS
! CALCULATION OF SIZE DISTIRBUTION OF FOCI
if (dist) then
  do 605 w = 1,100                !sample 100 times, then take the average
    do 17 i = 1,cmaxx
      clones(i,1) = -1            !Initial
      clones(i,2) = -1.           !Initial
    17: continue

    !Copy clones in dimension "clonesa" to dimension "clones"
    k = 0
    do 300 i = 1,cmax
      if(clonesa(i,1).eq.-1) goto 305
           !If this element is never occupied (-1),so are the followings. Skip out.
      if(clonesa(i,1).eq.0) goto 300
      if(clonesa(i,1).gt.0) then
        k = k+1
        clones(k,1) = clonesa(i,1)
      endif
    300: continue
    305: continue

    !After the data in dimension clonesa are copied, copy the data in dimension "clonesb" to dimension
     !"clones"
    do 310 i = 1,cmax
      if (clonesb(i,1).eq.-1) goto 315
      if (clonesb(i,1).eq.0) goto 310
      if (clonesb(i,1).gt.0) then
        k = k+1
        clones(k,1) = clonesb(i,1)
       else
        goto 315
      endif
    310: continue
    315: continue

    !Convert the cell numbers to volumes and store in clones(i,2)
    !Once in subroutine, this part was moved here because I do not know how to handle subroutines.
     do 410 i=1,cmaxx
```

```
 if (clones(i,1).eq.-1) goto 415
 if (clones(i,1).eq.0) goto 410
 if (clones(i,1).gt.0) clones(i,2) = clones(i,1)/hepsdt
410: continue
415: continue

!Bin the detectable clones into individual classes
!Once in subroutine, this part was moved here because I do not know how to handle subroutines.
 do 30 i = 1,cmaxx
    if (clones(i,2).lt.cutoffvolum) then
     goto 30
    else if(clones(i,2).le.volclass1) then
      bin3d(1,w) = bin3d(1,w) + 1
     goto 30
    else if (clones(i,2).le.volclass2) then
      bin3d(2,w) = bin3d(2,w) + 1
     goto 30
    else if(clones(i,2).le.volclass3) then
      bin3d(3,w) = bin3d(3,w) + 1
     goto 30
    else if(clones(i,2).le.volclass4) then
      bin3d(4,w) = bin3d(4,w) + 1
     goto 30
    else if(clones(i,2).le.volclass5) then
      bin3d(5,w) = bin3d(5,w) + 1
     goto 30
    else if(clones(i,2).le.volclass6) then
      bin3d(6,w) = bin3d(6,w) + 1
     goto 30
    else if(clones(i,2).le.volclass7) then
      bin3d(7,w) = bin3d(7,w) + 1
     goto 30
    else if(clones(i,2).le.volclass8) then
      bin3d(8,w) = bin3d(8,w) + 1
     goto 30
    else if(clones(i,2).le.volclass9) then
      bin3d(9,w) = bin3d(9,w) + 1
     goto 30
    else if(clones(i,2).le.volclass10) then
      bin3d(10,w) = bin3d(10,w) + 1
     goto 30
    else if(clones(i,2).le.volclass11) then
      bin3d(11,w) = bin3d(11,w) + 1
     goto 30
    else if(clones(i,2).le.volclass12) then
      bin3d(12,w) = bin3d(12,w) + 1
     goto 30
    else if(clones(i,2).le.volclass13) then
      bin3d(13,w) = bin3d(13,w) + 1
     goto 30
    else if(clones(i,2).le.volclass14) then
      bin3d(14,w) = bin3d(14,w) + 1
     goto 30
    else if(clones(i,2).le.volclass15) then
      bin3d(15,w) = bin3d(15,w) + 1
     goto 30
```

```
      else if(clones(i,2).le.volclass16) then
        bin3d(16,w) = bin3d(16,w) + 1
       goto 30
      else if(clones(i,2).le.volclass17) then
        bin3d(17,w) = bin3d(17,w) + 1
       goto 30
      else if(clones(i,2).le.volclass18) then
        bin3d(18,w) = bin3d(18,w) + 1
       goto 30
      else if(clones(i,2).le.volclass19) then
        bin3d(19,w) = bin3d(19,w) + 1
       goto 30
      else if(clones(i,2).le.volclass20) then
        bin3d(20,w) = bin3d(20,w) + 1
       goto 30
      else if(clones(i,2).le.volclass21) then
        bin3d(21,w) = bin3d(21,w) + 1
       goto 30
      else if(clones(i,2).le.volclass22) then
        bin3d(22,w) = bin3d(22,w) + 1
       goto 30
      else if(clones(i,2).le.volclass23) then
        bin3d(23,w) = bin3d(23,w) + 1
       goto 30
      else if(clones(i,2).le.volclass24) then
        bin3d(24,w) = bin3d(24,w) + 1
       goto 30
      else
        bin3d(25,w) = bin3d(25,w) + 1
       goto 30
     endif
   30: continue
   605: continue

    !Result of size classes
    !Once in subroutine, this part was moved here because I do not know how to handle subroutines.
     do 208 i = 1,25
       numsum = 0
       do 108 w = 1,100
         numsum = numsum + bin3d(i,w)
     108: continue
       bin3d(i,101) = numsum/100
    !Transfer the result of each run into repeatsizedayXX(25,50)
     if(days.eq.7)  repeatsizeday7(i,count)  = bin3d(i,101)
     if(days.eq.14) repeatsizeday14(i,count) = bin3d(i,101)
     if(days.eq.20) repeatsizeday20(i,count) = bin3d(i,101)
     if(days.eq.24) repeatsizeday24(i,count) = bin3d(i,101)
     if(days.eq.28) repeatsizeday28(i,count) = bin3d(i,101)
     if(days.eq.47) repeatsizeday47(i,count) = bin3d(i,101)
     if(days.eq.56) repeatsizeday56(i,count) = bin3d(i,101)
    208: continue
endif

!Size distribution is a little confusing here because of the change in hepsdt. For the control group and the
!early stage (prior to day28) of treated groups, the cutoffvolum is 6.59222e-8 (50.12 um), and the class1 is
!6.59222e-8-1.31549e-7 cm^3, and the class2 is 1.31549-2.62393e-7 cm^3. However, for the late stage
```

```
!(day 28-56) of the treated groups,the cutoffvolum is increased to 1.31549e-7 (63.1 um) because of cell
!enlargement. Hence the class1 under this situation is 1.31549-2.62393e-7 cm^3. That is, the class(N+1) of
!the situation with 50.12 um cutoff is corresponding to the classN of the situation with 63.1 um. If we set
!the class demarcations with "cell numbers", there is no such change. But in fact, we set them with
!"volume", and such change is necessary because cell volume is increased by the chemical treatment.

!The code here is not explicitly modified to reflect such change. The 'cutoffvolum' is switched b/t
!6.59222e-8 and 1.31549e-7 at the beginning of DYNAMIC. When the 'cutoffvolum' is 1.31549e-7 cm^3,
!it is equal to volclass1, and hence there is no class1 output.

!The 2D data of days 28,47,and 56 of the low and high dose groups need to be reprocessed with a cutoff of
!63.1 um.

END !of SIZE_CLASS
!--------1---------2---------3---------4---------5---------6---------7---------8
DISCRETE AVE_SIZE
  write(buffer,*) 'Average size distribution of foci at day ',days
  call disstr(buffer)
    if (repeatsize(1,50).gt.0.) then
      write(buffer,*) 'Soltykov size class 1 = ',repeatsize(1,50)
      call disstr(buffer)
    endif
    if (repeatsize(2,50).gt.0.) then
      write(buffer,*) 'Soltykov size class 2 = ',repeatsize(2,50)
      call disstr(buffer)
    endif
    if (repeatsize(3,50).gt.0.) then
      write(buffer,*) 'Soltykov size class 3 = ',repeatsize(3,50)
      call disstr(buffer)
    endif
    if (repeatsize(4,50).gt.0.) then
      write(buffer,*) 'Soltykov size class 4 = ',repeatsize(4,50)
      call disstr(buffer)
    endif
    if (repeatsize(5,50).gt.0.) then
      write(buffer,*) 'Soltykov size class 5 = ',repeatsize(5,50)
      call disstr(buffer)
    endif
    if (repeatsize(6,50).gt.0.) then
      write(buffer,*) 'Soltykov size class 6 = ',repeatsize(6,50)
      call disstr(buffer)
    endif
    if (repeatsize(7,50).gt.0.) then
      write(buffer,*) 'Soltykov size class 7 = ',repeatsize(7,50)
      call disstr(buffer)
    endif
    if (repeatsize(8,50).gt.0.) then
      write(buffer,*) 'Soltykov size class 8 = ',repeatsize(8,50)
      call disstr(buffer)
    endif
    if (repeatsize(9,50).gt.0.) then
      write(buffer,*) 'Soltykov size class 9 = ',repeatsize(9,50)
      call disstr(buffer)
    endif
    if (repeatsize(10,50).gt.0.) then
      write(buffer,*) 'Soltykov size class 10 = ',repeatsize(10,50)
```

```
  call disstr(buffer)
endif
if (repeatsize(11,50).gt.0.) then
  write(buffer,*) 'Soltykov size class 11 = ',repeatsize(11,50)
  call disstr(buffer)
endif
if (repeatsize(12,50).gt.0.) then
  write(buffer,*) 'Soltykov size class 12 = ',repeatsize(12,50)
  call disstr(buffer)
endif
if (repeatsize(13,50).gt.0.) then
  write(buffer,*) 'Soltykov size class 13 = ',repeatsize(13,50)
  call disstr(buffer)
endif
if (repeatsize(14,50).gt.0.) then
  write(buffer,*) 'Soltykov size class 14 = ',repeatsize(14,50)
  call disstr(buffer)
endif
if (repeatsize(15,50).gt.0.) then
  write(buffer,*) 'Soltykov size class 15 = ',repeatsize(15,50)
  call disstr(buffer)
endif
if (repeatsize(16,50).gt.0.) then
  write(buffer,*) 'Soltykov size class 16 = ',repeatsize(16,50)
  call disstr(buffer)
endif
if (repeatsize(17,50).gt.0.) then
  write(buffer,*) 'Soltykov size class 17 = ',repeatsize(17,50)
  call disstr(buffer)
endif
if (repeatsize(18,50).gt.0.) then
  write(buffer,*) 'Soltykov size class 18 = ',repeatsize(18,50)
  call disstr(buffer)
endif
if (repeatsize(19,50).gt.0.) then
  write(buffer,*) 'Soltykov size class 19 = ',repeatsize(19,50)
  call disstr(buffer)
endif
if (repeatsize(20,50).gt.0.) then
  write(buffer,*) 'Soltykov size class 20 = ',repeatsize(20,50)
  call disstr(buffer)
endif
if (repeatsize(21,50).gt.0.) then
  write(buffer,*) 'Soltykov size class 21 = ',repeatsize(21,50)
  call disstr(buffer)
endif
if (repeatsize(22,50).gt.0.) then
  write(buffer,*) 'Soltykov size class 22 = ',repeatsize(22,50)
  call disstr(buffer)
endif
if (repeatsize(23,50).gt.0.) then
  write(buffer,*) 'Soltykov size class 23 = ',repeatsize(23,50)
  call disstr(buffer)
endif
if (repeatsize(24,50).gt.0.) then
  write(buffer,*) 'Soltykov size class 24 = ',repeatsize(24,50)
```

```
      call disstr(buffer)
    endif
    if (repeatsize(25,50).gt.0.) then
      write(buffer,*) 'Soltykov size class 25 = ',repeatsize(25,50)
      call disstr(buffer)
    endif
  write(buffer,*) 'Done.'
  call disstr(buffer)
END                              !of AVE_SIZE

!--------1---------2---------3---------4---------5---------6---------7---------8
!CALCULATE DATA DESCRIBING CLONE GROWTH

!^^^^^^^^^^^^^^^^^^^^^^^^^^^^^^^^^^^^^^^^^^^^^^^^^^^^^^^^^^^^^^^^^^^^^^^^^^^^^^^^^^^^^^^^^^^^
!(YC Ou) The code was adjusted to account for a reduction in the number of foci which will fall within 1
!cm3 space when the density of hepatocytes decreases. Reported values of cnumdetecta, cnumdetectb
!which have not been adjusted will be incorrect when there is a modeled change in hepatocyte density (YC
!Ou).
!voladetect =(100*detectcellnoa/hepsdt(days))*(hepsdt(days)/hepsdt(0))
!volbdetect = (100*detectcellnob/hepsdt(days))*(hepsdt(days)/hepsdt(0))
!cnumdetectaadj=cnumdetecta*hepsdt(days)/hepsdt(0) !Rory
!cnumdetectbadj=cnumdetectb*hepsdt(days)/hepsdt(0)
!cnumdetect = cnumdetectaadj + cnumdetectbadj
!cnumtaadj=cnumta*hepsdt(days)/hepsdt(0) !Rory
!cnumtbadj=cnumtb*hepsdt(days)/hepsdt(0)
!cnumt = cnumtaadj + cnumtbadj
!^^^^^^^^^^^^^^^^^^^^^^^^^^^^^^^^^^^^^^^^^^^^^^^^^^^^^^^^^^^^^^^^^^^^^^^^^^^^^^^^^^^^^^^^^^^^

!Here the values are not adjusted by hepatocyte density because the data for comparison are not adjusted
!accordingly. (Yasong Lu)
! "A" CELLS
call report1(allcellnoa,detectcellnoa,cnumdetecta,cnumta,avga,&
fatboya,cutoffcellno,clonesa,invisa,singlea)
vola =100*allcellnoa/hepsdt
voladetect =100*detectcellnoa/hepsdt         !detectable as volume percent of liver
!Other available results: cnuma, allcellnoa, singlea, invisa, fatboya, cnumdetecta, detectcellnoa, avga, losta

! "B" CELLS
call report1(allcellnob,detectcellnob,cnumdetectb,cnumtb,avgb,&
fatboyb,cutoffcellno,clonesb,invisb,singleb)
volb =100*allcellnob/hepsdt
volbdetect = 100*detectcellnob/hepsdt        !detectable as volume percent of liver
!Other available results: cnumb, allcellnob, singleb, invisb, fatboyb, cnumdetectb, detectcellnob, avgb,lostb

! "A" AND "B" CELLS COMBINED
voltot = vola + volb
voltotdetect = voladetect + volbdetect !volume percentage of detectable
percentavol = voladetect/(voltotdetect+1d-30)*100    !vol percentage of A foci
percentbvol = volbdetect/(voltotdetect+1d-30)*100    !vol percentage of B foci
cnumt = cnumta + cnumtb
cnumdetect = cnumdetecta + cnumdetectb
percentano = cnumdetecta/(cnumdetect+1d-30)*100  !No percentage of A foci
percentbno = cnumdetectb/(cnumdetect+1d-30)*100  !No percentage of B foci
single = singlea + singleb
invis=invisa+invisb
allcellno=allcellnoa+allcellnob
```

```
detectcellno=detectcellnoa+detectcellnob
avg=detectcellno/(cnumdetect+1)          !avg cell no per focus
volsingle=100*single/hepsdt              !volume percentage of single cells
fatboy = max(fatboya,fatboyb)
lost=losta+lostb

if (days.eq.7) then
    schedule size_class .at. days
 else if (days.eq.14) then
      do 289 i = 1,25
       do 189 w = 1,101
       numsum = 0
       bin3d(i,w)=0
   189: continue
   289: continue
 !Reset the element values to avoid accumulation of the results
  schedule size_class .at. days
 else if (days.eq.20) then
      do 279 i = 1,25
       do 179 w = 1,101
       numsum = 0
       bin3d(i,w)=0
   179: continue
   279: continue
  schedule size_class .at. days
 else if (days.eq.24) then
      do 219 i = 1,25
       do 119 w = 1,101
       numsum = 0
       bin3d(i,w)=0
   119: continue
   219: continue
  schedule size_class .at. days
 else if (days.eq.28) then
      do 229 i = 1,25
       do 129 w = 1,101
       numsum = 0
       bin3d(i,w)=0
   129: continue
   229: continue
  schedule size_class .at. days
 else if (days.eq.47) then
      do 239 i = 1,25
       do 139 w = 1,101
       numsum = 0
       bin3d(i,w)=0
   139: continue
   239: continue
  schedule size_class .at. days
 else if (days.eq.56) then
      do 249 i = 1,25
       do 149 w = 1,101
       numsum = 0
       bin3d(i,w)=0
   149: continue
   249: continue
```

```
   schedule size_class .at. days
end if

!To calculate average size distribution of multiple runs. It seems to me the last run result is not accounted
!for in the calculation. If use repeat instead of repeat-1, the result is wrong. Why?
if(count.ge.repeat) then
 if(dist) then
   if(days.eq.7) then
    do 1013 i = 1,25
      repeatsizesum=0
     do 1014 k = 1,count
      repeatsizesum=repeatsizesum+repeatsizeday7(i,k)
     1014: continue
      repeatsizeday7(i,50)=repeatsizesum/(repeat-1)
      repeatsize(i,50)=repeatsizeday7(i,50)
    1013: continue
   schedule AVE_SIZE .at. days
   endif
   if(days.eq.14) then
    do 1003 i = 1,25
      repeatsizesum=0
     do 1004 k = 1,count
      repeatsizesum=repeatsizesum+repeatsizeday14(i,k)
     1004: continue
      repeatsizeday14(i,50)=repeatsizesum/(repeat-1)
      repeatsize(i,50)=repeatsizeday14(i,50)
    1003: continue
   schedule AVE_SIZE .at. days
   endif
   if(days.eq.20) then
    do 1113 i = 1,25
      repeatsizesum=0
     do 1114 k = 1,count
      repeatsizesum=repeatsizesum+repeatsizeday20(i,k)
     1114: continue
      repeatsizeday20(i,50)=repeatsizesum/(repeat-1)
      repeatsize(i,50)=repeatsizeday20(i,50)
    1113: continue
   do 3130 i=1,15
      sizedist20(i)=repeatsize(i,50)
   3130: continue
         sizeclass1=sizedist20(1)
         sizeclass2=sizedist20(2)
         sizeclass3=sizedist20(3)
         sizeclass4=sizedist20(4)
         sizeclass5=sizedist20(5)
         sizeclass6=sizedist20(6)
         sizeclass7=sizedist20(7)
         sizeclass8=sizedist20(8)
         sizeclass9=sizedist20(9)
         sizeclass10=sizedist20(10)
         sizeclass11=sizedist20(11)
         sizeclass12=sizedist20(12)
         sizeclass13=sizedist20(13)
         sizeclass14=sizedist20(14)
         sizeclass15=sizedist20(15)
```

```
schedule AVE_SIZE .at. days
endif
if(days.eq.24) then
 do 1513 i = 1,25
   repeatsizesum=0
  do 1514 k = 1,count
   repeatsizesum=repeatsizesum+repeatsizeday24(i,k)
  1514: continue
   repeatsizeday24(i,50)=repeatsizesum/(repeat-1)
   repeatsize(i,50)=repeatsizeday24(i,50)
 1513: continue
do 3131 i=1,15
   sizedist24(i)=repeatsize(i,50)
3131: continue
       sizeclass1=sizedist24(1)
       sizeclass1=sizedist24(1)
       sizeclass2=sizedist24(2)
       sizeclass3=sizedist24(3)
       sizeclass4=sizedist24(4)
       sizeclass5=sizedist24(5)
       sizeclass6=sizedist24(6)
       sizeclass7=sizedist24(7)
       sizeclass8=sizedist24(8)
       sizeclass9=sizedist24(9)
       sizeclass10=sizedist24(10)
       sizeclass11=sizedist24(11)
       sizeclass12=sizedist24(12)
       sizeclass13=sizedist24(13)
       sizeclass14=sizedist24(14)
       sizeclass15=sizedist24(15)
schedule AVE_SIZE .at. days
endif
if(days.eq.28) then
 do 1313 i = 1,25
   repeatsizesum=0
  do 1314 k = 1,count
   repeatsizesum=repeatsizesum+repeatsizeday28(i,k)
  1314: continue
   repeatsizeday28(i,50)=repeatsizesum/(repeat-1)
   repeatsize(i,50)=repeatsizeday28(i,50)
 1313: continue
do 3132 i=1,15
   sizedist28(i)=repeatsize(i,50)
3132: continue
       sizeclass1=sizedist28(1)
       sizeclass1=sizedist28(1)
       sizeclass2=sizedist28(2)
       sizeclass3=sizedist28(3)
       sizeclass4=sizedist28(4)
       sizeclass5=sizedist28(5)
       sizeclass6=sizedist28(6)
       sizeclass7=sizedist28(7)
       sizeclass8=sizedist28(8)
       sizeclass9=sizedist28(9)
       sizeclass10=sizedist28(10)
       sizeclass11=sizedist28(11)
```

```
        sizeclass12=sizedist28(12)
        sizeclass13=sizedist28(13)
        sizeclass14=sizedist28(14)
        sizeclass15=sizedist28(15)
schedule AVE_SIZE .at. days
endif
if(days.eq.47) then
 do 1213 i = 1,25
   repeatsizesum=0
  do 1214 k = 1,count
   repeatsizesum=repeatsizesum+repeatsizeday47(i,k)
   1214: continue
   repeatsizeday47(i,50)=repeatsizesum/(repeat-1)
   repeatsize(i,50)=repeatsizeday47(i,50)
 1213: continue
do 3133 i=1,15
   sizedist47(i)=repeatsize(i,50)
3133: continue
        sizeclass1=sizedist47(1)
        sizeclass1=sizedist47(1)
        sizeclass2=sizedist47(2)
        sizeclass3=sizedist47(3)
        sizeclass4=sizedist47(4)
        sizeclass5=sizedist47(5)
        sizeclass6=sizedist47(6)
        sizeclass7=sizedist47(7)
        sizeclass8=sizedist47(8)
        sizeclass9=sizedist47(9)
        sizeclass10=sizedist47(10)
        sizeclass11=sizedist47(11)
        sizeclass12=sizedist47(12)
        sizeclass13=sizedist47(13)
        sizeclass14=sizedist47(14)
        sizeclass15=sizedist47(15)
schedule AVE_SIZE .at. days
endif
if(days.eq.56) then
 do 1913 i = 1,25
   repeatsizesum=0
  do 1914 k = 1,count
   repeatsizesum=repeatsizesum+repeatsizeday56(i,k)
   1914: continue
   repeatsizeday56(i,50)=repeatsizesum/(repeat-1)
   repeatsize(i,50)=repeatsizeday56(i,50)
 1913: continue
do 3134 i=1,15
   sizedist56(i)=repeatsize(i,50)
3134: continue
        sizeclass1=sizedist56(1)
        sizeclass1=sizedist56(1)
        sizeclass2=sizedist56(2)
        sizeclass3=sizedist56(3)
        sizeclass4=sizedist56(4)
        sizeclass5=sizedist56(5)
        sizeclass6=sizedist56(6)
        sizeclass7=sizedist56(7)
```

```
        sizeclass8=sizedist56(8)
        sizeclass9=sizedist56(9)
        sizeclass10=sizedist56(10)
        sizeclass11=sizedist56(11)
        sizeclass12=sizedist56(12)
        sizeclass13=sizedist56(13)
        sizeclass14=sizedist56(14)
        sizeclass15=sizedist56(15)
   schedule AVE_SIZE .at. days
   endif
  endif
endif

END !of DYNAMIC section
!--------1---------2---------3---------4---------5---------6---------7---------8
TERMINAL

!REPEAT RUNS
if (count.le.repeat) then
  multisumclonedata(1,1)=multisumclonedata(1,1)+clonedata(1,1)
  multisumclonedata(2,1)=multisumclonedata(2,1)+clonedata(2,1)
  multisumclonedata(3,1)=multisumclonedata(3,1)+clonedata(3,1)
  multisumclonedata(4,1)=multisumclonedata(4,1)+clonedata(4,1)
  multisumclonedata(5,1)=multisumclonedata(5,1)+clonedata(5,1)

  multisumclonedata(1,2)=multisumclonedata(1,2)+clonedata(1,2)
  multisumclonedata(2,2)=multisumclonedata(2,2)+clonedata(2,2)
  multisumclonedata(3,2)=multisumclonedata(3,2)+clonedata(3,2)
  multisumclonedata(4,2)=multisumclonedata(4,2)+clonedata(4,2)
  multisumclonedata(5,2)=multisumclonedata(5,2)+clonedata(5,2)

  sumsqclonedata(1,1)=sumsqclonedata(1,1)+clonedata(1,1)**2
  sumsqclonedata(2,1)=sumsqclonedata(2,1)+clonedata(2,1)**2
  sumsqclonedata(3,1)=sumsqclonedata(3,1)+clonedata(3,1)**2
  sumsqclonedata(4,1)=sumsqclonedata(4,1)+clonedata(4,1)**2
  sumsqclonedata(5,1)=sumsqclonedata(5,1)+clonedata(5,1)**2

  sumsqclonedata(1,2)=sumsqclonedata(1,2)+clonedata(1,2)**2
  sumsqclonedata(2,2)=sumsqclonedata(2,2)+clonedata(2,2)**2
  sumsqclonedata(3,2)=sumsqclonedata(3,2)+clonedata(3,2)**2
  sumsqclonedata(4,2)=sumsqclonedata(4,2)+clonedata(4,2)**2
  sumsqclonedata(5,2)=sumsqclonedata(5,2)+clonedata(5,2)**2
 endif

 if(count.lt.repeat) then
   call initd
   goto begin    !for multiple runs
 endif

 !Calculate averages
  meanclonedata(1,1)=multisumclonedata(1,1)/repeat
  meanclonedata(2,1)=multisumclonedata(2,1)/repeat
  meanclonedata(3,1)=multisumclonedata(3,1)/repeat
  meanclonedata(4,1)=multisumclonedata(4,1)/repeat
  meanclonedata(5,1)=multisumclonedata(5,1)/repeat
  meanclonedata(1,2)=multisumclonedata(1,2)/repeat
```

```
 meanclonedata(2,2)=multisumclonedata(2,2)/repeat
 meanclonedata(3,2)=multisumclonedata(3,2)/repeat
 meanclonedata(4,2)=multisumclonedata(4,2)/repeat
 meanclonedata(5,2)=multisumclonedata(5,2)/repeat

!Calculate standard deviations
 sdterm1_clonedata(1,1)=sumsqclonedata(1,1)/repeat
 sdterm1_clonedata(2,1)=sumsqclonedata(2,1)/repeat
 sdterm1_clonedata(3,1)=sumsqclonedata(3,1)/repeat
 sdterm1_clonedata(4,1)=sumsqclonedata(4,1)/repeat
 sdterm1_clonedata(5,1)=sumsqclonedata(5,1)/repeat
 sdterm1_clonedata(1,2)=sumsqclonedata(1,2)/repeat
 sdterm1_clonedata(2,2)=sumsqclonedata(2,2)/repeat
 sdterm1_clonedata(3,2)=sumsqclonedata(3,2)/repeat
 sdterm1_clonedata(4,2)=sumsqclonedata(4,2)/repeat
 sdterm1_clonedata(5,2)=sumsqclonedata(5,2)/repeat

 sdclonedata(1,1)=(sdterm1_clonedata(1,1)-meanclonedata(1,1)**2)**0.5
 sdclonedata(2,1)=(sdterm1_clonedata(2,1)-meanclonedata(2,1)**2)**0.5
 sdclonedata(3,1)=(sdterm1_clonedata(3,1)-meanclonedata(3,1)**2)**0.5
 sdclonedata(4,1)=(sdterm1_clonedata(4,1)-meanclonedata(4,1)**2)**0.5
 sdclonedata(5,1)=(sdterm1_clonedata(5,1)-meanclonedata(5,1)**2)**0.5
 sdclonedata(1,2)=(sdterm1_clonedata(1,2)-meanclonedata(1,2)**2)**0.5
 sdclonedata(2,2)=(sdterm1_clonedata(2,2)-meanclonedata(2,2)**2)**0.5
 sdclonedata(3,2)=(sdterm1_clonedata(3,2)-meanclonedata(3,2)**2)**0.5
 sdclonedata(4,2)=(sdterm1_clonedata(4,2)-meanclonedata(4,2)**2)**0.5
 sdclonedata(5,2)=(sdterm1_clonedata(5,2)-meanclonedata(5,2)**2)**0.5

600: continue
write(buffer,*) ' *****NORMAL END OF SIMULATION**********'
call disstr(buffer)

if(messa) then
  write(buffer,*) ' WARNING:Fraction of "A" cells in cell cycle was > 1.'
  call disstr(buffer)
endif
if(messb) then
  write(buffer,*) ' WARNING:Fraction of "B" cells in cell cycle was > 1.'
  call disstr(buffer)
endif

 END                !of TERMINAL section
!--------1---------2---------3---------4---------5---------6---------7---------8
 END
     SUBROUTINE BD(j,lost,pbn1,pdn1,pbd,clone)
     implicit real*8(a-z)
     integer*4 j(3),lost

 !Binomial distribution for stochastic clone growth
     bd1 = bnldev(pbd,clone,j)        !# divisions + # deaths
     if(nint(bd1).eq.0) return        !nothing happens
     pbx = pbn1/(pbn1+pdn1)
  !Conditioning on something happening, the probability of birth is pbn1/(pbn1+pdn1) or rbn1/(rbn1+rdn1)
     if(pbx.lt.1.) then
       divs = bnldev(pbx,bd1,j)
      else
```

```
      divs = bd1
    endif
    deaths = bd1-divs
    clone = clone + divs – deaths    !clone size changed
    if(nint(clone).lt.1) lost = lost+1  !clone disappears

    return
    end
!--------1---------2---------3---------4---------5---------6---------7---------8
    SUBROUTINE REPORT1(allcellno,detectcellno,cnumdetect,cnumt,avg
   *,fatboy,cutoffcellno,clon,invis,single)
    implicit real*8(a-z)
    integer*4 i,cnumdetect,cnumt,invis,cmax
    parameter (cmax = 50000, cmaxx=100000)
    dimension clon(cmax,1)

!bookkeeping on 3D clones
    cnumdetect = 0          !number of detectable clones
    cnumt = 0               !number of all clones
    single = 0              !number of single cells
    allcellno = 0           !number of cells in all clones
    detectcellno = 0        !number of cells in detectable clones
    avg =0.                 !average cell number of detectable clones
    fatboy = 0              !size of the biggest clone
    invis = 0               !number of undetectable clones
    do i = 1,cmax
     if(clon(i,1).eq.-1.) return
     if(clon(i,1).gt.0.) then
       cnumt = cnumt + 1
       allcellno = allcellno + clon(i,1)
     endif
     if(clon(i,1).eq.1) single = single + 1
     if(clon(i,1).gt.0..and.clon(i,1).lt.cutoffcellno) invis=invis+1
     if(clon(i,1).gt.fatboy) fatboy = clon(i,1)
     if(clon(i,1).ge.cutoffcellno) then
       cnumdetect = cnumdetect + 1
       detectcellno = detectcellno + clon(i,1)
       avg = detectcellno/cnumdetect
     endif
    enddo

    return
    end
c--------1---------2---------3---------4---------5---------6---------7---------8
    real*8 FUNCTION UNIFL(jx)
    integer*4 jx(3),k

c inputs for random number generator
c   j(2), j(3) = 2 random integers with:
c   j(2) < 2147483563
c   j(3) < 2147483399
c outputs:
c   jx(1) = pseudo random integer, 0 < jx(1) < 2147483563
c jx(1) should be a high quality random integer
c period of jx(1) is about 2.30584e18.
c   jx(2) = pseudo random integer, 0 < jx(2) < 2147483563
```

```
c  jx(3) = pseudo random integer, 0 < jx(3) < 2147483399
c  unifl = pseudo random real, 0. < unifl < 1.

c for any given seed for stream 1, i.e. jx(2), the following seeds
c  for stream 2, i.e. jx(3), will give nonoverlapping
c  sequences of length 2147483562 for the output stream, jx(1):
c  1, 1408222472, 905932980, 1185805228, 1749585844, 563802022,
c  1147463446, 1209938334, 155409276, 617052445, etc.,
c  i.e. every 164th term from stream jx(3).

c get next term in the first stream = 40014*jx(2) mod 2147483563
    k=jx(2)/53668
    jx(2)=40014*(jx(2)-k*53668)-k*12211
    if (jx(2).lt.0) jx(2)=jx(2)+2147483563

c get next term in the second stream = 40692*jx(3) mod 2147483399
    k=jx(3)/52774
    jx(3)=40692*(jx(3)-k*52774)-k*3791
    if(jx(3).lt.0) jx(3)=jx(3)+2147483399

c set jx(1)=((jx(3)+2147483562-jx(2)) mod 2147483562) + 1

    k=jx(3)-jx(2)
    if(k.le.0) k=k+2147483562

c put the combination back into jx(1)
    jx(1)=k

c put it on the interval (0,1)
    unifl=k*4.656613e-10

    return
    end
!--------1---------2---------3---------4---------5---------6---------7--
    FUNCTION BNLDEV(PP,NX,IDUM)
!Returns as a floating-point number (an integer value?? In here in the original Ou code. Typo?) that is a
!random deviate drawn from a binomial distribution of N trials each of probability PP, using UNIFL(IDUM)
!as a source of uniform random deviates.

    real*8 nx,bnldev,pp,pi
    integer*4 idum(3),n,nold
    parameter (pi=3.141592654)
    real*8 am,em,en,g,oldg,p,pc,pclog,plog,pold,sq,t,y,gammln,unifl
    save nold,pold,pc,plog,pclog,en,oldg
    data nold /-1/, pold /-1./

    n = nint(nx)
    if (pp.le.0.5) then      !The binomial distribution is invariant
      p = pp                 ! under changing pp to 1.-pp, if also
    else                     ! change the answer to N minus
      p = 1. – pp            ! itself; we'll remember to do this
    endif                    ! below.
    am = n*p                 !Mean of the deviate to be produced.
    if (n.lt.25) then        !Use the direct method when n is not
      bnldev = 0.            ! too large. This can require up to
      do j = 1,n             ! 25 calls to UNIFL.
```

```
        if (unifl(idum).lt.p) bnldev=bnldev+1.
      enddo
    else if (am.lt.1.) then   !If fewer than one event is expected
      g = exp(-am)            ! out of 25 or more trials, then the
      t = 1.                  ! distribution is quite accurately
      do j = 0,n              ! Poisson.  Use direct Poisson
        t = t*unifl(idum)     ! method.
        if (t.lt.g) goto 1
      enddo
      j = n
1     bnldev = j
    else                      !Use the rejection method.
      if (n.ne.nold) then     !If N has changed, then compute useful
        en = n                ! quantities.
        oldg = gammln(en+1.)
        nold = n
      endif
      if (p.ne.pold) then     !If P has changed, then compute useful
        pc = 1.-p             ! quantities.
        plog = log(p)
        pclog = log(pc)
        pold = p
      endif
      sq = sqrt(2.*am*pc)             !Rejection method with a Lorentzian
2     y = tan(pi*unifl(idum))         ! comparison function.
      em = sq*y+am
      if (em.lt.0..or.em.ge.en+1.) goto 2 !Reject.
      em = int(em)                    !Trick for integer-valued distribution.
      t = 1.2*sq*(1.+y**2)*exp(oldg-gammln(em+1.)
     *  -gammln(en-em+1.)+em*plog+(en-em)*pclog)
      if (unifl(idum).gt.t) goto 2    !Reject.  This happens about 1.5
      bnldev = em                     ! times per deviate, on average.
    endif
    if (p.ne.pp) bnldev = n-bnldev    !Remember to undo symmetry
                                      !transformation
    return
    end
!--------1---------2---------3---------4---------5---------6---------7---------8
    FUNCTION GAMMLN(XX)

    real*8 gammln,xx,ser,stp,tmp,x,y,cof(6)
    integer*4 j

    save cof,stp
    cof(1)=76.18009172947146d0
    cof(2)=-86.50532032941677d0
    cof(3)=24.01409824083091d0
    cof(4)=-1.231739572450155d0
    cof(5)=0.1208650973866179d-2
    cof(6)=-0.5395239384953d-5
    stp=2.5066282746310005d0

    x = xx
    y=x
    tmp = x+5.5d0
    tmp = (x+0.5d0)*log(tmp)-tmp
```

```
      ser = 1.000000000190015d0
      do j=1,6
        y=y+1.d0
        ser=ser+cof(j)/y
      enddo
      gammln=tmp+log(stp*ser/x)

      return
      end
!--------1---------2---------3---------4---------5---------6---------7---------8
      FUNCTION POIDEV(XM,J)
!Returns as a floating-point number an integer value that is a random deviate drawn from a Poisson
!distribution of mean XM using UNIFL(J) as a source of uniform random deviates

      real*8 poidev,xm,pi
      parameter (pi = 3.141592654)
      integer*4 j(3)
      real*8 alxm,em,g,oldm,sq,t,y,gammln,unifl
      save alxm,g,oldm,sq
      data oldm /-1./

      if (xm.lt.12.) then
        if(xm.ne.oldm) then
          oldm = xm
          g = exp(-xm)
        endif
        em = -1.
        t = 1.
2       em = em+1.
        t = t*unifl(j)
        if (t.gt.g) goto 2
      else
        if (xm.ne.oldm) then
          oldm = xm
          sq = sqrt(2.*xm)
          alxm = log(xm)
          g = xm*alxm-gammln(xm+1.)
        endif
1       y = tan(pi*unifl(j))
        em = sq*y+xm
        if (em.lt.0.) goto 1
        em = int(em)
        t = 0.9*(1.+y**2)*exp(em*alxm-gammln(em+1.)-g)
        if (unifl(j).gt.t) goto 1
      endif
      poidev = em

      return
      end
```

```
!FILE BinaryMixtureLu.CMD
!Yasong Lu, starting from 9/1/04
!This code is to simulate the GST-P foci formation following DEN/Binary Mixture (HCB+PCB 126)
!treatment in male F344 rats. The study was run by Y.Lu and M.Lohitnavy et al. in 2003.
!This code is based on Ying Ou's code (for HCB). ACSL tox 11.8. For printout, Font Courier New, size 10
!is good.
!The treatment-specific parameters are set in this file.

s grdcpl=.f.       !no grid on line plots
s hvdprn=.f.       !high volume output on display
s dpnplt=.f.
s symcpl=.f.
s ftsplt=.t.
s satcpl=.f.
s nciout=100
s dscplt=1         !octagon for default symbol for data plotting
s ltfcpl=.f.       !draw line type fragment - doesn't character in line as it should
!s xincpl=5.0      !X axis length in inches
!s xticpl=1.0      !X axis tick increment
!s yincpl=5.0      !Y axis length in inches
!s yticpl=1.0      !Y axis length in inches
s dcvprn=.t.       !display old and new values of changed variable

prepar days,weeks,months                      !time
prepar rbn0,rdn0,lwc,an0,an0c,divs            !normal hepatocytes
 !Diterministic calculation
 !prepar n0n1a,n0n1b,ica,icb,numad,numbd,numtotd,volad,volbd,voltotd
 !Stochastic calculation
prepar xma,n0a,mutota,cnumdetecta,cnumta,voladetect,fatboya
prepar allcellnoa,detectcellnoa,vola,singlea,avga,losta,invisa,pmuta
prepar faincycle,fasingleincycle,faminiincycle,famultiincycle,fabigincycle
                              !A cell related parameters & results
prepar xmb,n0b,mutotb,cnumdetectb,cnumtb,volbdetect,fatboyb
prepar allcellnob,detectcellnob,volb,singleb,avgb,lostb,invisb,pmutb
prepar fbincycle,fbsingleincycle,fbminiincycle,fbmultiincycle,fbbigincycle,
                              !B cell related parameters & results
prepar cnumdetect,cnumt,voltotdetect,voltot,single,volsingle
prepar detectcellno,allcellno,avg,fatboy,lost,invis
                              !Size-related focal growth parameters
prepar rbn1asingle,rbn1amini,rbn1amulti,rbn1abig
prepar rdn1asingle,rdn1amini,rdn1amulti,rdn1abig
prepar rbn1bsingle,rbn1bmini,rbn1bmulti,rbn1bbig
prepar rdn1bsingle,rdn1bmini,rdn1bmulti,rdn1bbig
prepar deltaasingle,deltaamini,deltaamulti,deltaabig
prepar deltabsingle,deltabmini,deltabmulti,deltabbig
prepar cutoffcellno,cutoffvolum,hepsdt
prepar percentavol,percentbvol,percentano,percentbno

prepar repeatsizesum
prepar sizedist20,sizedist24,sizedist28,sizedist47,sizedist56
prepar sizeclass1,sizeclass2,sizeclass3,sizeclass4,sizeclass5,sizeclass6
prepar sizeclass7,sizeclass8,sizeclass9,sizeclass10,sizeclass11
prepar sizeclass12,sizeclass13,sizeclass14,sizeclass15

!!!!!!!!!!!!!!!!!!!!!!!!!!!!!!!!!!!!!!!!!!!!!!!!!!!!!!!!!!!!!!!!!!!
!Part I: calibrate hepatocyte growth & death rate constants after DEN
```

```
!Only DEN, no other treatment. Data from Kato et al. 1993, Fundam Appl Toxicol. 20:155-62.

PROCED test
s tstop=20.
s phtime=60.                !no partial hepatectomy effects considered
s lw=8.2
s promodose=-1
s hepsdtdays=1.20e8,1.20e8,1.20e8,1.20e8,1.20e8,1.20e8,1.20e8
start
END

PROCED ptest                !plot test results
SET TITLE='  Simulated VS Measured Values '
set TITLE(41)='     Liver weight     '
set TITLE(81)='  Calibrating liver growth after DEN    '
  !Number 41 indicates where the string starts
plot /data=liverTest /lo=0 lwc
set TITLE(41)='    Cell birth rate constant    '
plot /data=TestDENbr rbn0
set TITLE(41)='    Cell death rate constant    '
plot rdn0
END

!Liver weight DEN only, no other treatment
DATA liverTest(days, lwc)
0       8.2             !3.5% of 235g body weight
2       6.3
4       5.7
6       6.7
7       6.8
8       6.7
10      7.0
14      7.3
21      8.1
28      8.3
END

!Birth rate constant DEN only, no other treatment.
!Data from Kato et al. 1993, Fundam Appl Toxicol. 20:155-62.
DATA TestDENbr(days, rbn0)
0       0.002512584
2       0.012823324
4       0.075276273
6       0.060517890
8       0.020845402
10      0.011510985
14      0.010205499
21      0.005050676
28      0.003778409
END

!!!!!!!!!!!!!!!!!!!!!!!!!!!!!!!!!!!!!!!!!!!!!!!!!!!!!!!!!!!!!!!!!!!!!!!
!Part II: DEN+corn oil control group
!Study run by Lu et al at CETT,CSU,2003

PROCED con              !control
```

```
s phtime=21.                !day
s dist=.t.
s promodose=0
s repeat=20                 !change repeat run numbers
s tstop=60.
s lw=7.0
s hepsdtdays=1.20e8,1.20e8,1.14e8,1.20e8,1.10e8,1.16e8,1.01e8
!start
END

PROCEDURE pconliver   !plot liver growth parameters
SET TITLE='       Simulated VS Measured Values '
SET TITLE(41)='    Liver weight (g) '
SET TITLE(81)='     DEN control '
plot /data=DENliver /xhi=70 lwc
SET TITLE(41)='   Normal birth rate constant    '
SET TITLE(81)='     DEN control '
plot /data=DENbr /xhi=70 rbn0
SET TITLE(41)='   Normal Death rate constant    '
SET TITLE(81)='     DEN control '
plot /xhi=70 rdn0
SET TITLE(41)='   Hepatocyte numerical density   '
SET TITLE(81)='     DEN control '
plot /xhi=70 hepsdt
END

PROCEDURE pconfoci              !plot focal growth parameters
SET TITLE='       Focal growth parameters '
SET TITLE(41)='    Birth rate constant A and B '
SET TITLE(81)='     DEN control '
plot /xhi=70 rbn1asingle,rbn1bsingle
plot /xhi=70 rbn1amini,rbn1bmini
plot /xhi=70 rbn1amulti,rbn1bmulti
plot /xhi=70 rbn1abig,rbn1bbig
SET TITLE(41)='    Death rate constant A and B '
SET TITLE(81)='     DEN control '
plot /xhi=70 rdn1asingle,rdn1bsingle
plot /xhi=70 rdn1amini,rdn1bmini
plot /xhi=70 rdn1amulti,rdn1bmulti
plot /xhi=70 rdn1abig,rdn1bbig
SET TITLE(41)='    Birth - Death rate constant A  '
SET TITLE(81)='     DEN control '
plot /xhi=70 deltaasingle,deltaamini,deltaamulti,deltaabig
SET TITLE(41)='    Birth - Death rate constant B  '
SET TITLE(81)='     DEN control '
plot /xhi=70 deltabsingle,deltabmini,deltabmulti,deltabbig
SET TITLE(41)='    Probability of mutation to A and B  '
SET TITLE(81)='     DEN control '
plot /xhi=70 pmuta,pmutb
SET TITLE(41)='   Cell fraction in cell cycle and death   '
SET TITLE(81)='     DEN control '
plot /xhi=70 fasingleincycle,faminiincycle,famultiincycle,fabigincycle
plot /xhi=70 fbsingleincycle,fbminiincycle,fbmultiincycle,fbbigincycle
END

PROCEDURE pconresult
```

```
SET TITLE='      Simulated VS Measured Values '
SET TITLE(41)='      Volume Percent (%) '
SET TITLE(81)='       DEN Control     '
plot /data=DEN /xhi=70 /character=2 voltotdetect
SET TITLE(41)='     Number of Foci/cm^3 '
SET TITLE(81)='       DEN Control '
plot /data=DEN /xhi=70 /character=2 cnumdetect
plot /character=2 sizeclass1,sizeclass2,sizeclass3
d meanclonedata
d sdclonedata
d sizedist20,sizedist24,sizedist28,sizedist47,sizedist56
END

PROCEDURE pconallresult
SET TITLE='      Simulated VS Measured Values '
SET TITLE(41)='      Volume Percent (%) '
SET TITLE(81)='       DEN Control     '
plot /data=DEN /xhi=70 /character=2 voltotdetect,voltot
plot /data=DEN /xhi=70 /character=2 voladetect,volbdetect
SET TITLE(41)='     Number of Foci/cm^3 '
SET TITLE(81)='       DEN Control '
plot /data=DEN /xhi=70 /character=2 cnumdetect,cnumt
plot /data=DEN /xhi=70 /character=2 cnumdetecta,cnumdetectb
plot /xhi=70 /character=2 single,singlea,singleb
plot /data=DENvolsingle /xhi=70 /character=2 volsingle
plot /xhi=70 /character=2 lost,losta,lostb
plot /xhi=70 /character=2 invis,invisa,invisb
plot /xhi=70 /character=2 fatboy,fatboya,fatboyb
plot /xhi=70 /character=2 avg,avga,avgb
d meanclonedata
d sdclonedata
END

PROCEDURE pconab
SET TITLE='      Simulated Values of A and B'
SET TITLE(41)='      Volume Percent (%) '
SET TITLE(81)='       DEN Control     '
plot /character=2 /xhi=70 voladetect,volbdetect
SET TITLE(41)='     Number of Foci/cm^3 '
SET TITLE(81)='       DEN Control '
plot /character=2 /xhi=70 cnumdetecta,cnumdetectb
plot /character=2 /xhi=70 singlea,singleb
plot /character=2 /xhi=70 losta,lostb
plot /character=2 /xhi=70 invisa,invisb
plot /character=2 /xhi=70 avga,avgb
plot /character=2 /xhi=70 percentavol,percentbvol
plot /character=2 /xhi=70 percentano,percentbno
END

!Foci formation following DEN+Corn oil.
DATA DEN(days,voltotdetect,cnumdetect)
20      0.0915  1746
24      0.1615  1775
28      0.1455  1610
47      0.1991  1360
56      0.2946  1148
```

```
END

!Kato,T.1993, Jpn J Cancer Res 84:1252-7. Cannot trust these data; but the trend may be instructive.
!It takes 1 week to level off, might be severely overestimated
DATA DENsingle(days,single)
0.25    3000
4       12000
7       300000
14      330000
21      180000
22      120000
24      100000
28      100000
42      65000
56      65000
END

!Cannot trust these data; but the trend may be instructive. might be underestimated.
DATA DENvolsingle(days,volsingle)
0.25    0
4       0.00005
7       0.00012
14      0.00011
21      0.00010
22      0.00007
24      0.00005
28      0.00007
42      0.00005
56      0.00007
END

DATA DENliver(days,lwc)
0       7.00
20      7.39
21      2.22
24      4.92
28      5.03
47      6.81
56      7.70
end

!Birth rate constant DEN+corn oil
!Data of day 0-14 from Kato et al. 1993, Fundam Appl Toxicol. 20:155-62; the other from our study.
DATA DENbr(days, rbn0)
0       0.00227519
2       0.012823324
4       0.075276273
6       0.060517890
8       0.020845402
10      0.011510985
14      0.010205499
20      0.00227519
24      0.11344521
28      0.00725342
47      0.00086275
56      0.00108723
```

```
end

!!!!!!!!!!!!!!!!!!!!!!!!!!!!!!!!!!!!!!!!!!!!!!!!!!!!!!!!!!!!
!Part III:DEN+low dose mixture treatment
!Study run by Lu et al at CETT, CSU, 2003

proced Lo
s Mixtime=14.            !after 2 weeks of initiation, (day)
s phtime=21.
s dist=.t.
s promodose=1
s repeat=20              !set repeat run numbers
s tstop=60.
s lw=7.0
S hepsdtdays=1.20e8,1.20e8,9.92e7,9.89e7,8.25e7,5.69e7,6.43e7
start
end

PROCEDURE ploliver    !plot liver growth parameters
SET TITLE='     Simulated VS Measured Values '
SET TITLE(41)='    Liver weight (g) '
SET TITLE(81)='    Low dose group '
plot /data=lowliver /xhi=70 lwc
SET TITLE(41)='    Normal birth rate constant    '
SET TITLE(81)='    Low dose group '
plot /data=mixlowbr /xhi=70 rbn0
SET TITLE(41)='    Normal Death rate constant    '
SET TITLE(81)='    Low dose group '
plot /xhi=70 rdn0
SET TITLE(41)='    Hepatocyte numerical density    '
SET TITLE(81)='    Low dose group '
plot /xhi=70 hepsdt
END

PROCEDURE plofoci     !plot focal growth parameters
SET TITLE='     Focal growth parameters '
SET TITLE(41)='    Birth rate constant A and B '
SET TITLE(81)='    DEN-MixLow '
plot /xhi=70 rbn1asingle,rbn1bsingle
plot /xhi=70 rbn1amini,rbn1bmini
plot /xhi=70 rbn1amulti,rbn1bmulti
plot /xhi=70 rbn1abig,rbn1bbig
SET TITLE(41)='    Death rate constant A and B '
SET TITLE(81)='    DEN-MixLow '
plot /xhi=70 rdn1asingle,rdn1bsingle
plot /xhi=70 rdn1amini,rdn1bmini
plot /xhi=70 rdn1amulti,rdn1bmulti
plot /xhi=70 rdn1abig,rdn1bbig
SET TITLE(41)='    Birth - Death rate constant A  '
SET TITLE(81)='    DEN-MixLow '
plot /xhi=70 deltaasingle,deltaamini,deltaamulti,deltaabig
SET TITLE(41)='    Birth - Death rate constant B  '
SET TITLE(81)='    DEN-MixLow '
plot /xhi=70 deltabsingle,deltabmini,deltabmulti,deltabbig
SET TITLE(41)='    Probability of mutation to A and B  '
SET TITLE(81)='    DEN-MixLow '
```

```
plot /xhi=70 pmuta,pmutb
SET TITLE(41)='   Cell fraction in cell cycle and death   '
SET TITLE(81)='     DEN-MixLow '
plot /xhi=70 fasingleincycle,faminiincycle,famultiincycle,fabigincycle
plot /xhi=70 fbsingleincycle,fbminiincycle,fbmultiincycle,fbbigincycle
END

PROCEDURE ploresult
SET TITLE='      Simulated VS Measured Values '
SET TITLE(41)='        Volume Percent (%) '
SET TITLE(81)='         DEN-MixLow '
plot /data=LowFoci /xhi=70 /character=2 voltotdetect
SET TITLE='      Simulated VS Measured Values '
SET TITLE(41)='      Number of Foci/cm^3 '
Set TITLE(81)='         DEN-MixLow '
plot /data=LowFoci /xhi=70 /character=2 cnumdetect
d meanclonedata
d sdclonedata
END

PROCEDURE ploab
SET TITLE='      Simulated Values A and B  '
SET TITLE(41)='      Volume Percent (%) '
SET TITLE(81)='        DEN-MixLow '
plot /character=2 /xhi=70 voladetect,volbdetect
SET TITLE(41)='      Number of Foci/cm^3 '
SET TITLE(81)='        DEN-MixLow '
plot /character=2 /xhi=70 cnumdetecta,cnumdetectb
plot /character=2 /xhi=70 percentavol,percentbvol
plot /character=2 /xhi=70 percentano,percentbno
END

!Foci formation following DEN+MixLow.
DATA LowFoci(days,voltotdetect,cnumdetect)
20        0.1076   2158
24        0.1737   2053
28        0.3403   2665
47        0.2917   2201
56        0.3302   1487
END

!Liver weight following DEN+MixLow
DATA LowLiver(days,lwc)
0.        7.00
20.       7.52
21.       2.26
24.       4.94
28.       7.43
47.       13.13
56.       12.73
END

!Hepatocyte birth rate following DEN+MixLow
!Data of day 0-14 from Kato et al. 1993, Fundam Appl Toxicol. 20:155-62; the other from our study.
DATA MixLowbr(days,rbn0)
0         0.00227519
```

```
2       0.012823324
4       0.075276273
6       0.060517890
8       0.020845402
10      0.011510985
14      0.010205499
20.     0.00241327
24.     0.12998477
28      0.01494874
47      0.00076182
56      0.00366414
end

!!!!!!!!!!!!!!!!!!!!!!!!!!!!!!!!!!!!!!!!!!!!!!!!!!!!!!!!!!!!!!!!!!!!!!!!
!Part IV:DEN+Mixture high dose treatment
!Study by Lu et al at CETT,CSU,2003

proced Hi
s Mixtime=14.           !after 2 weeks of initiation, (day)
s phtime=21.
s dist=.t.
s promodose=2
s repeat=20             !set repeat run times
s tstop=60.
s lw=7.0
S hepsdtdays=1.20e8,1.20e8,9.69e7,1.07e8,8.12e7,6.01e7,6.43e7
start
end

PROCEDURE philiver    !plot liver growth parameters
SET TITLE='     Simulated VS Measured Values '
SET TITLE(41)='   Liver weight (g) '
SET TITLE(81)='   High dose group '
plot /data=highliver /xhi=70 lwc
SET TITLE(41)='   Normal birth rate constant   '
SET TITLE(81)='   High dose group '
plot /data=mixhighbr /xhi=70 rbn0
SET TITLE(41)='   Normal Death rate constant   '
SET TITLE(81)='   High dose group '
plot /xhi=70 rdn0
SET TITLE(41)='   Hepatocyte numerical density   '
SET TITLE(81)='   High dose group '
plot /xhi=70 hepsdt
END

PROCEDURE phifoci     !plot focal growth parameters
SET TITLE='     Focal growth parameters '
SET TITLE(41)='   Birth rate constant A and B '
SET TITLE(81)='   DEN-MixHigh '
plot /xhi=70 rbn1asingle,rbn1bsingle
plot /xhi=70 rbn1amini,rbn1bmini
plot /xhi=70 rbn1amulti,rbn1bmulti
plot /xhi=70 rbn1abig,rbn1bbig
SET TITLE(41)='   Death rate constant A and B '
SET TITLE(81)='   DEN-MixHigh '
plot /xhi=70 rdn1asingle,rdn1bsingle
```

```
plot /xhi=70 rdn1amini,rdn1bmini
plot /xhi=70 rdn1amulti,rdn1bmulti
plot /xhi=70 rdn1abig,rdn1bbig
SET TITLE(41)='    Birth - Death rate constant A  '
SET TITLE(81)='     DEN-MixHigh '
plot /xhi=70 deltaasingle,deltaamini,deltaamulti,deltaabig
SET TITLE(41)='    Birth - Death rate constant B  '
SET TITLE(81)='     DEN-MixHigh '
plot /xhi=70 deltabsingle,deltabmini,deltabmulti,deltabbig
SET TITLE(41)='    Probability of mutation to A and B  '
SET TITLE(81)='     DEN-MixHigh '
plot /xhi=70 pmuta,pmutb
SET TITLE(41)='   Cell fraction in cell cycle and death   '
SET TITLE(81)='     DEN-MixHigh '
plot /xhi=70 fasingleincycle,faminiincycle,famultiincycle,fabigincycle
plot /xhi=70 fbsingleincycle,fbminiincycle,fbmultiincycle,fbbigincycle
END

PROCEDURE Phiresult
SET TITLE='      Simulated VS Measured Values '
SET TITLE(41)='       Volume Percent (%) '
SET TITLE(81)='       DEN-MixHigh '
plot /data=HighFoci /xhi=70 /character=2 voltotdetect
SET TITLE='      Simulated VS Measured Values '
SET TITLE(41)='       Number of Foci/cm^3 '
Set TITLE(81)='       DEN-MixHigh '
plot /data=HighFoci /xhi=70 /character=2 cnumdetect
!plot /character=2 cnumdetecta,cnumdetectb
!plot /character=2 voladetect,volbdetect
d meanclonedata
d sdclonedata
END

PROCEDURE phiab
SET TITLE='      Simulated Values A and B  '
SET TITLE(41)='      Volume Percent (%) '
SET TITLE(81)='       DEN-MixHigh '
plot /character=2 /xhi=70 voladetect,volbdetect
SET TITLE(41)='      Number of Foci/cm^3 '
SET TITLE(81)='       DEN-MixHigh '
plot /character=2 /xhi=70 cnumdetecta,cnumdetectb
plot /character=2 /xhi=70 percentavol,percentbvol
plot /character=2 /xhi=70 percentano,percentbno
END

!Foci formation following DEN+MixHigh.
DATA HighFoci(days,voltotdetect,cnumdetect)
20      0.0753  1450
24      0.2849  2307
28      0.2886  2959
47      0.3784  2285
56      0.4342  2526
END

!Liver weight following DEN+MixHigh
DATA HighLiver(days,lwc)
```

```
0.        7.00
20.       7.60
21.       2.28
24.       5.36
28.       7.84
47.       12.17
56.       11.93
END

!Hepatocyte birth rate following DEN+MixHigh
!Data of day 0-14 from Kato et al. 1993, Fundam Appl Toxicol. 20:155-62; the other from our study.
DATA MixHighbr(days,rbn0)
0         0.00227519
2         0.012823324
4         0.075276273
6         0.060517890
8         0.020845402
10        0.011510985
14        0.010205499
20.       0.00254062
24.       0.12635120
28        0.02773255
47        0.00347246
56        0.01422274
end

!!!!!!!!!!!!!!!!!!!!!!!!!!!!!!!!!!!!!!!!!!!!!!!!!!!!!!!!!!!!!!!!!!
!Place results of three groups in the same plots.
proced allvoldetect
s dist=.f.
s phtime=21.                    !day
s promodose=0
s tstop=60.
s lw=7.0
s hepsdtdays=1.20e8,1.20e8,1.14e8,1.20e8,1.10e8,1.16e8,1.01e8
start
s defplt=.t.
SET TITLE='       Simulated VS Measured Values '
SET TITLE(41)='       Volume Percent (%) '
plot /data=DEN /xhi=70 /hi=0.65 /character=2 voltotdetect
s Mixtime=14. ! after 2 weeks of initiation, (day)
s promodose=1
S hepsdtdays=1.20e8,1.20e8,9.92e7,9.89e7,8.25e7,5.69e7,6.43e7
start
s defplt=.t.
plot /data=LowFoci /xhi=70 /hi=0.65 /character=3 voltotdetect
s promodose=2
S hepsdtdays=1.20e8,1.20e8,9.69e7,1.07e8,8.12e7,6.01e7,6.43e7
start
s defplt=.f.
plot /data=HighFoci /xhi=70 /hi=0.65 /character=4 voltotdetect
end

proced allcnumdetect
s dist=.f.
s phtime=21.                    !day
```

```
s promodose=0
s tstop=60.
s lw=7.0
s hepsdtdays=1.20e8,1.20e8,1.14e8,1.20e8,1.10e8,1.16e8,1.01e8
start
s defplt=.t.
SET TITLE='       Simulated VS Measured Values '
SET TITLE(41)='       Number of Foci/cm^3 '
plot /data=DEN /xhi=70 /hi=4000 /character=2 cnumdetect
s Mixtime=14. ! after 2 weeks of initiation, (day)
s promodose=1
S hepsdtdays=1.20e8,1.20e8,9.92e7,9.89e7,8.25e7,5.69e7,6.43e7
start
s defplt=.t.
plot /data=LowFoci /xhi=70 /hi=4000 /character=3 cnumdetect
s promodose=2
S hepsdtdays=1.20e8,1.20e8,9.69e7,1.07e8,8.12e7,6.01e7,6.43e7
start
s defplt=.f.
plot /data=HighFoci /xhi=70 /hi=4000 /character=4 cnumdetect
end
```